Neural network connectivity and response latency modeled by stochastic processes

PhD thesis by

MASSIMILIANO TAMBORRINO

Department of Mathematical Sciences
University of Copenhagen
Denmark

Massimiliano Tamborrino
Department of Mathematical Sciences
University of Copenhagen
Universitetsparken 5
DK-2100 Købehavn Ø
Denmark

mt@math.ku.dk
htpp://www.math.ku.dk/~mt

Preface

This dissertation is submitted in partial fulfillment of the requirements for the Ph.D. degree at the Faculty of Science, University of Copenhagen, Denmark. The work was carried out at the Department of Mathematical Sciences, University of Copenhagen, from December 2009 to November 2012. It was financed by the Department of Mathematical Sciences, the Program of Excellence and The Danish Council for Independent Research (DFF).

First and foremost I wish to thank my advisor Susanne Ditlevsen, for all her continuous encouragements, useful feedbacks, help and support, inspiring discussions and talks. Her willingness to give her time whenever I needed was simply amazing. Also thanks to my co-authors Martin Jacobsen, who patiently answered to my questions and gave me so many useful feedbacks, Petr Lansky, for inviting me to Prague and giving me stimulating critiques, Laura Sacerdote, for having firstly introduced me to the fascinating worlds of stochastic processes and neuroscience, and Cristina Zucca, who makes collaboration a pleasant event.

To everyone at the Department of Mathematics, thank you for creating a scientifically exciting environment. Special thanks are due to Jessica Kasza, Emanuele Dotto and Anders Christian Jensen (who I am also grateful for helping me with the Dansk Resumé), thank for having been and being such good Friends aside from colleagues.

Furthermore, thanks also to those new and old friends who I met on my way and made Copenhagen a second joyful home.

To my family, thank you for having always encouraged me to follow my dreams. Your continuous support and presence canceled thousands of kilometers of distance.

Last, but certainly not least, I would like to thank Francesca for all her love and sweetness, for all experiences and travels that we had along these years and for those that are waiting us.

Summary

One-dimensional diffusion models have been widely used to describe membrane potential dynamics of single neurons. Moreover, first passage times of stochastic processes have been chosen for modeling neural action potentials, called spikes. A spike is observed whenever the membrane potential exceeds a certain threshold. Nowadays, data from simultaneous recordings of groups of neurons detect the existence of *temporal patterns*, which are precise temporal relations in sequences of spike intervals. Several experimental observations support the hypothesis of the existence of dynamical cell assemblies as an organizational principle of higher brain activity. The cell assembly is formed by a population of neurons that spontaneously organizes on the basis of a sequence of input patterns of spikes. The same temporal activity is reproduced whenever the same input pattern is presented. For this reason, it is of paramount interest to understand the dynamics of neural networks and detect dependencies between simultaneously recorded spike trains. This has been investigated in Paper I, II and III.

In Paper I, a multidimensional stochastic model for describing the spontaneous firing activity of a neural network is proposed. To reflect the biology correctly, each firing is followed by a refractory period, where a second spike cannot occur. The dynamics of each single neuron are modeled as unidimensional Stein models, while the dependencies between neurons are assumed to be determined by the existence of common inputs acting on clusters of neurons. In particular, a generalized Stein model is proposed. Being a multivariate jump process, its first passage time problem yields several mathematical difficulties. For this reason, a diffusion approximation of the Stein process is performed and the limit process is shown to be a multivariate Ornstein-Uhlenbeck. The covariance matrix is non-diagonal and it encodes the cluster dependence of the network.
Consider a point process with events given by all the passage times of a process. Then weak and strong convergence results for the point process of a generic jump process to that of its diffusion approximation are proved. This allows the switching from the Stein to the Ornstein-Uhlenbeck model. Such process can be used to model experimentally observed phenomena, e.g. inhibition, excitation, synchronism and silencing of neurons. The bivariate version of this model has been used in Paper II and III.

In Paper II, a non-parametric method to investigate dependence structures of neural networks analyzing simultaneously recorded spike trains, is proposed. The method is based on copulas and allows to discern dependencies determined by the surrounding network from those due to direct interactions between neurons. Moreover, it also recognizes delays

in the spike propagation. The proposed method and two of the other existing techniques, i.e. cross-correlograms and the Cox-method, are compared on simulated data. The dependence structures between neurons are modeled as determined by either direct interactions or cluster dependencies. The first scenario is reproduced by describing the membrane potential as a jump diffusion process, with jumps of the non-firing component whenever the other fires. For the second scenario, the bivariate Ornstein-Uhlenbeck described in Paper I is considered.

In Paper III, the joint distribution of the exit times of a bivariate Gauss-Markov process from a bidimensional strip in presence of absorbing boundaries is determined. Explicit expressions are provided for a bivariate Wiener process with drift and non-diagonal covariance matrix. For more general processes, a numerical algorithm is given and the convergence of its error is proved. Theoretical and numerical results for the Wiener cases are compared. Numerical investigations of the joint distribution of the bivariate Ornstein-Uhlenbeck proposed in Paper I are provided. This work represents a first step toward the theoretical analysis of dependencies between point processes, e.g. spike trains.

The other main topic of this dissertation is the investigation of the response latency. In many biological systems there is a time delay before a stimulation has an impact on the response. The quantification of this delay is particularly relevant in neuroscience, as hereby presented. Neurons are commonly characterized by spontaneous firing, which is not due to any apparent or controlled stimulation. In presence of a stimulus, the spontaneous firing may prevail and hamper identification of the effect of the stimulus. Therefore, for analyzing the evoked neuronal activity, the presence of spontaneous firing has to be taken into account. If the background signal is ignored, then estimation of the response latency will be wrong, and the error will persist even when sample size is increasing. The interesting question is: what is the response latency to the stimulus? Answering this question becomes even more difficult if the latency is of a complex nature, for example composed of a biologically implied deterministic part and a stochastic part. This scenario is considered in Paper IV and V, where the response time is a sum of two components; the delay and the relative latency.

In Paper IV, a unified concept of response latency identification in presence of a background noise is proposed. The (parametric and non-parametric) estimators of the time delay are compared on simulated data and the most suitable for specific situations are recommended.

In Paper V, parametric estimators for the time delay and the response latency are derived and compared on simulated data. Their properties are also discussed, e.g. the mean of the response latency is always satisfactorily estimated, even assuming a wrong distribution for the response latency.

Short abstract

Stochastic processes and their first passage times have been widely used to describe the membrane potential dynamics of single neurons and to reproduce neuronal spikes, respectively. However, cerebral cortex in human brains is estimated to contain 10-20 billions of neurons and each of them is connected to thousands of other neurons. The first question is: how to model neural networks through stochastic processes? A multivariate Ornstein-Uhlenbeck process, obtained as a diffusion approximation of a jump process, is the proposed answer. Obviously, dependencies between neurons imply dependencies between their spike times. Therefore, the second question is: how to detect neural network connectivity from simultaneously recorded spike trains? Answering this question corresponds to investigate the joint distribution of sequences of first passage times. A non-parametric method based on copulas is proposed. As a first step toward a theoretical analysis, a simplified framework with two neurons and their first spikes is considered. For computing the joint distribution of the passage times, theoretical and numerical results are provided.

Now imagine to observe neurons characterized by spontaneous generation of spikes. When a stimulus is applied to the network, the spontaneous firings may prevail and hamper detection of the effects of the stimulus. Therefore, the spontaneous firings cannot be ignored and the response latency has to be detected on top of a background signal. Everything becomes more difficult if the latencies are expressed as a sum of deterministic (absolute response latency) and stochastic (relative response latency) parts. The third question is: what is the response latency to the stimulus? Non-parametric and parametric estimators of the two components are proposed in a single neuron framework.

Dansk resumé

Stokastiske processer og deres førstepassagetider er ofte blevet brugt til henholdsvis at beskrive dynamikken af membranpotentialet og til at reproducere fyringsdynamikken i neuroner. Hjernebarken i den menneskelig hjerne indeholder omkring 10-20 milliarder neuroner og hver af disse er forbundet til tusindvis af andre neuroner. Et vigtigt spørgsmål er: Hvordan kan man på fornuftig vis modellere neuronnetværk ved stokastiske processer? En mulighed er en flerdimensional Ornstein-Uhlenbeck proces, fremkommet som en diffusionsapproksimation til en springproces. Det er klart at afhængigheder mellem neuroner medfører afhængighed mellem deres fyringstider. Et andet spørgsmål er derfor: Hvordan kan man detektere sammenhænge i neuronnetværk fra simultant målte fyringssekvenser? Dette svarer til at undersøge den simultane fordeling af følger af førstepassagetider. Her foreslåes en ikke-parametrisk metode baseret på copulaer. Som et første skridt i en teoretisk analyse betragtes et simplificeret setup med to neuroner og ventetiden til deres første fyring undersøges. Både teoretiske og numeriske resultater gives for den simultane fordeling af passagetiderne.

Neuroner er ofte karakteriseret ved spontan fyringsaktivitet. Når et netværk stimuleres vil den spontane aktivitet potentielt forstærke eller dæmpe effekten af stimulationen. Derfor kan den spontane aktivitet ikke ignoreres og detekteringen af responslatensen vanskeliggøres af baggrundssignalet. Dette kompliceres yderligere hvis latensen er en sum af en deterministisk del (absolut responslatens) og af en stokastisk del (relativ responslatens). Et tredie spørgsmål er: Hvad er responslatensen for stimulationen? Ikke-parametriske og parametriske estimatorer for de to komponenter præsenteres i et enkelt neuron setup.

Contents

Bibliography

Papers

1

Introduction

Neuronal dynamics represent a fascinating and complicated topic which is far from being understood. Interestingly, mathematics and statistics can help neuroscientists to get a better understanding of neuronal processes. Indeed, the firing mechanism, which is responsible for the temporal coding, can be satisfactorily defined with mathematical models, e.g. renewal diffusion processes. Then, theoretical models can be used to extract neuronal information from experimental data. Moreover, simulations from models may be performed to obtain features which are difficult or expensive to reproduce through experiments. Obviously, this is only possible if these models reflect the biology correctly and this can be checked through experiments. Besides that, a close collaboration with neuroscientists would be useful for both mathematician and statistician. Indeed, there are several neuronal problems leading to scenarios which are extremely challenging from a theoretical point of view. Some of these unknown questions have been investigated in this dissertation.

The objective of this dissertation is dual. First, I want to understand how neural networks can be modeled and how dependencies between neurons can be detected. Second, how a neuron with spontaneous firing activity reacts to an incoming stimulus. This thesis can, hopefully, answer some of these questions and give an indication of what can be done in the future.

1.1   Thesis objective and structure

The thesis is structured as follows. Chapter 2 provides the mathematical background of Paper I-III. In particular, diffusion processes, convergence results of jump processes, first passage times and copulas are shortly introduced. Some key references for a detailed reading are also given. Paper IV and V are self-explanatory from a mathematical and statistical point of view, such that further descriptions are not needed.

Chapter 3 gives an overview of the neuronal background of the papers. In particular, a brief review of stochastic neural models for the description of single neuronal dynamics is presented, together with the motivations for considering neural networks. Moreover, response latency and the character of experimental data used in Paper IV and V are shortly presented.

Chapter 4 presents a detailed overview of the papers, while some interesting perspectives are discussed in Chapter 5, which precedes the bibliography, where the list of references

of these introductory chapters is collected.

The papers contain my contributions and are attached in the format of the journal where they have been either submitted for publication (Paper I and III) or published (Paper II, IV and V).

2

Stochastic processes

2.1 Stochastic differential equations

Modeling of neuronal phenomena through deterministic ordinary differential equations is an oversimplification. Indeed, neuronal dynamics evolve in presence of forces that we can neither predict nor understand. To take them into account, stochastic differential equations (SDEs) can be used. A typical SDE driven by Gaussian noise is of the form

$$d\mathbf{X}(t) = A\left(\mathbf{X}(t); t\right) dt + B\left(\mathbf{X}(t); t\right) d\mathbf{W}(t), \tag{2.1}$$

where $\mathbf{X}$ is a k-dimensional stochastic process assuming values in $I^k \subset \mathbb{R}^k$ and $\mathbf{W}$ is a k-dimensional standard Wiener process, also called Brownian motion. Here $A(\cdot)$ and $B(\cdot)$ are functions representing the deterministic and the stochastic component of the SDE, respectively. If they are measurable, Lipschitz in t and square integrable in x, then there exists a unique solution to (2.1), which has almost surely continuous paths and satisfies the strong Markov property. These processes are called diffusions, while A and B are known as drift and diffusion coefficients, respectively.

The simplest diffusion model is the Wiener process, which is solution of (2.1) with $A\left(\boldsymbol{X}(t); t\right) = \boldsymbol{\mu}$ and $B\left(\boldsymbol{X}(t); t\right) = \boldsymbol{\sigma}$, with drift $\boldsymbol{\mu} \in \mathbb{R}^k$ and positive-definite diffusion coefficient $\boldsymbol{\sigma} \in \mathbb{R}^k \times \mathbb{R}^k$.

Pearson diffusions are a flexible class of one-dimensional diffusions defined by having linear drift and quadratic square diffusion coefficient [25]. A Pearson diffusion is a stationary solution to a SDE of the form

$$dX(t) = -\theta(X(t) - \mu)dt + \sqrt{2\theta\left(aX^2(t) + bX(t) + c\right)}dW(t),$$

where $\theta > 0$, a, b, c are such that the square root is well defined when $X(t)$ is in the state space. A widely used Pearson diffusion is the unidimensional Ornstein-Uhlenbeck (OU) process, which is solution of the following SDE

$$dX(t) = -\theta\left(X(t) - \mu\right) dt + \sigma dW(t), \tag{2.2}$$

for $\mu \in \mathbb{R}$, $\theta, \sigma > 0$. Another example, which is mentioned in Paper I, is the Feller process, which solves

$$dX(t) = -\theta\left(X(t) - \mu\right) dt + \sigma\sqrt{X(t)}dW(t). \tag{2.3}$$

It has been proposed as a model of population growth [23], but is also commonly used in finance, where is referred to as the Cox-Ingersoll-Ross model [13].

Besides diffusion processes, jump processes represent another well known and used class of stochastic processes. A typical example of SDEs driven by Poisson noise is of the form

$$dX(t) = A(\mathbf{X}(t); t)\, dt + \sum_{l=1}^{m} B_l(\mathbf{X}(t); t)\, d\mathbf{N}^{(l)}(t), \tag{2.4}$$

where $B_l(\cdot)$ is a function, $\mathbf{N}^{(l)}$ is a k-dimensional Poisson process with independent components, intensity $\lambda_i^{(l)} > 0$ and is independent of $\mathbf{N}^{(r)}$, for $r \neq l, i = 1, \ldots, k, l = 1, \ldots, m$. The Stein model [73] is one of the first jump processes which has been used in neuroscience for modeling the membrane potential dynamics of a neuron. It is a one-dimensional process, which is solution of (2.4) with $A(X(t), t) = -X(t)/\theta$, $m = 2$ and $B_1 = a > 0, B_2 = b < 0$, i.e.

$$dX(t) = -\frac{X(t)dt}{\theta} + adN^{(1)}(t) + bdN^{(2)}(t). \tag{2.5}$$

In Paper I, a generalization of the Stein model to the k-dimensional case is proposed, and its weak convergence to a suitable multivariate OU process is proved.

Some key references on stochastic processes and their applications are [1, 3, 12, 24, 37, 76, 44, 45, 46, 53, 59, 61, 75].

Kolmogorov forward equation

A quantity of interest is the so-called transition probability density of $\boldsymbol{X}$, denoted by $f_{\boldsymbol{X}}$, which can be obtained as a solution of

$$\frac{\partial f(\boldsymbol{x}, t)}{\partial t} = -\sum_{i=1}^{k} \frac{\partial}{\partial x_i}[A(\boldsymbol{x}; t)f_{\boldsymbol{X}}(\boldsymbol{x}, t)] + \frac{1}{2}\sum_{i=1}^{k}\sum_{j=1}^{k} \frac{\partial^2}{\partial x_i \partial x_j}[C_{ij}(\boldsymbol{x}; t)f_{\boldsymbol{X}}(\boldsymbol{x}, t)]. \tag{2.6}$$

This equation is called k-dimensional Kolmogorov forward equation, also known as Fokker-Planck equation. Here $C_{ij}(\boldsymbol{x}; t) = \sum_{l=1}^{k} B_{il}(\boldsymbol{x}; t)B_{lj}(\boldsymbol{x}; t)$. In Paper II, a bidimensional Kolmogorov diffusion equation is considered for describing the behavior of a bivariate Wiener process under absorbing boundary conditions.

A key reference for methods of solution of a Kolmogorov forward equation is [64]. For the purposes of Paper II, refer to [21], which contains a step-by-step method for solving (2.6) for a bidimensional Wiener process.

2.2   Convergence of stochastic processes

Limit theorems for probability measures and stochastic processes have been widely investigated in the literature [4, 5, 40, 43, 80]. The reasons are several. First, convergences are

challenging and exciting from a theoretical point of view. Second, they allow to switch from more complicated processes to their diffusion approximations, which are mathematically more tractable. The most famous example is the Wiener process, which can be shown to be the limit of a random walk [19]. Other known examples are the OU, which is obtained from the Stein [7, 43, 47, 61], or the Feller, which is obtained from a branching process [23]. In the following, meaning and conditions for diffusion approximations are explained.

The weak convergence (also referred to as convergence in law or in distribution) is denoted by $X_n \xrightarrow{\mathcal{L}} X$ or $X_n \xrightarrow{d} X$, meaning that there is a sequence of processes, denoted by $(X_n)_{n \geq 1}$ and defined on the probability spaces $(\Omega^n, \mathcal{F}^n, P^n)$, assuming values in E, which converges in law to the process X. Citing Jacod and Shiryaev [40], "since the famous paper [58] of Prokhorov, the traditional mode of convergence is the weak convergence of the laws of the processes, considered as random elements of some functional space". Therefore, the convergence of processes deals with the convergence of some suitable random elements. Using the method proposed by Prokhorov [58], X_n converges weakly to X if the following three conditions hold:

  i. tightness of the sequence $(X_n)_{n \geq 1}$: for every $\epsilon > 0$ there is a compact subset K of E such that $P^n(X_n \notin K) \leq \epsilon$ for all n;

  ii. convergence of the finite-dimensional distributions:

$$(X_n(t_1), \ldots, X_n(t_k)) \xrightarrow{\mathcal{L}} (X(t_1), \ldots, X(t_k)), \quad \forall t_i \in D, k \geq 1,$$

  where D is a subset of $[0, \infty[$.

  iii. characterization of X by finite-dimensional distributions (which is basically trivial): X can be rewritten in terms of $(X(t_1), \ldots, X(t_k)), \forall t_i \in D, k \geq 1$

For proving tightness, different criteria were proposed, e.g. [5, 31]. Since condition ii. is often difficult to show, an alternative approach for semimartingales was proposed by Jacod and Shiryaev [40]. Semimartingales are processes that can be decomposed into a sum of a local martingale and a Cadlag adapted process of locally bounded variation [22, 32, 40]. Therefore, they belong to the Cadlag space, denoted by $\mathcal{D}^1 = \mathcal{D}([0, \infty[, \mathbb{R})$, which includes all functions that are right-continuous with left-hand limit. Obviously, the functional space of continuous functions, denoted by $\mathcal{C}^1 = \mathcal{C}([0, \infty[, \mathbb{R})$, is included in $\mathcal{D}^1$. The choice of only considering semimartingales is not a shortcoming. Indeed, examples of semimartingales are discrete-time processes, diffusion processes, point processes, solutions of SDEs, Lévy processes and many Markov processes. For the weak convergence, Jacod and Shiryaev [40] replaced condition ii. with the convergence of triplets of characteristics, and condition iii. with the characterization of X by the triplet of characteristics. The notion of characteristic has been introduced by them to generalize the drift, the variance of the Gaussian part, and the Lévy measure characterizing the distribution of a process with independent increments.

The notation $X_n \to X$ a.s. is used for the almost sure convergence of a sequence of processes $(X_n)_{n \geq 1}$ to X. It is also known as strong convergence and it represents the analogous of

the pointwise convergence in analysis theory [14]. It can be thought of as the convergence of the trajectories of the processes, i.e. the path of X_n is getting closer and closer to that of X, as n increases. Also in this case, the strong convergence can be proved by showing the convergence of some suitable random elements. Moreover, as happens for convergence of random variables, strong convergence implies weak convergence. The other implication is generally not true. However, if X_n is a semimartingale, then it belongs to the Cadlag space, which is shown to be a Polish space with the Skorohod's topology [48, 72]. Therefore, for the Skorohod's representation theorem, there exists a probability space and random elements $\widetilde{X}_n$ and $\widetilde{X}$ defined on a new probability space such that $\widetilde{X}_n \overset{d}{=} X_n$, $\widetilde{X} \overset{d}{=} X$ and $\widetilde{X}_n \to \widetilde{X}$ a.s. [72]. Here $\overset{d}{=}$ denotes identically distributed random variables.
Convergence of triplets of characteristics, Skorohod's theorem and strong convergence of random functions have been used in Paper II.

2.3   Integral equations

The expression *integral equation* is used for those equations where an unknown function appears under an integral sign. Then, integral and differential equations are two formulations of the same problem. Linear integral equations are called of Fredholm or Volterra type, depending on whether the limits of integration are both fixed or variable, respectively. The domain where the function is defined does not necessarily have to be bounded. If the unknown function only appears in the integral, then the equation is called of the first kind. If it appears both inside and outside the integral, then is called of the second kind. If the unknown function is bivariate, we may have a combination of Volterra and Fredholm types. A Volterra-Fredholm integral equation of the first kind defined on an unbounded spatial domain is of the form

$$f(t,x) = \int_{t_0}^{t} \int_{-\infty}^{a} k(t - s, x, \xi) u(s, \xi) d\xi ds. \tag{2.7}$$

Here u is the unknown function defined on $(t, x) \in [0, T] \times (-\infty, a]$, f is a given function and k is a function called a kernel. If f is identically null, then the equation is called homogeneous, otherwise it is called inhomogeneous.

Different methods for the analytical solutions of integral equations have been proposed, see e.g. [51, 74], while a collection of solutions to some specific integral equations can be found in [57]. Numerical methods can be applied if the equation cannot be explicitly solved [2, 17, 33, 49]. For the purpose of Paper III, it is sufficient to refer to [8], which contains a quadratic method based on a time and spatial discretization procedure of (2.7). Indeed, a system of two homogeneous Volterra-Fredholm integral equations of the first kind on an unbounded spatial domain is investigated in Paper III.

2.4 The first passage time problem

When does a stochastic process reach a boundary level for the first time? Answering this question would solve the so-called first passage time (FPT) problem, which has been widely investigated in the literature [39, 60, 62, 63]. For any given random function $\mathbb{X} \in \mathcal{D}^1$ starting in x_0, the FPT of $\mathbb{X}$ through a boundary $B > x_0$ is defined by

$$T_B(\mathbb{X}) = \inf\{t > 0 : \mathbb{X}(t) > B\}.$$

The distribution of $T_B(\mathbb{X})$ is explicitly known only for a few processes, e.g. Wiener and a special case of the OU process [18, 65]. As an alternative approach, numerical algorithms can be applied [65].

Besides the mathematical interest, the derivation of the FPT distribution is useful in several applications. In neuroscience, FPTs are used to model the epochs when the neuron releases an electrical impulse, called spike, which is believed to encode neuronal information (see Chapter 3). In finance, FPTs model the epochs when a stock reaches a certain value and it is convenient to sell or buy. In reliability theory, FPTs describe the times when a crash of an object happens.
Connections between neurons, dependencies between stocks in the same portfolio or common crash epochs suggest the presence of dependencies between FPTs. Thus it is relevant to extend the FPT problem to more general scenarios.

2.4.1 The multivariate first passage time problem

Let $\mathbb{X} \in \mathcal{D}^1$ be reset to its starting value whenever a FPT is observed, and the evolution of $\mathbb{X}$ does not depend on the previous time intervals, i.e. $\mathbb{X}$ is a renewal process. In Paper II and III, two different scenarios for the multivariate FPT problem has been analyzed. First, consider the sequence of passage times. Formally, the ith passage time of $\mathbb{X} \in \mathcal{D}^1$ is defined by

$$T_B^{(i)}(\mathbb{X}) = \inf\{t > T_B^{(i-1)} : \mathbb{X}(t) > B\}.$$

The sequence of FPTs can be interpreted as a point process where the events are the crossings of the boundary. For renewal processes, intertimes between two consecutive FPTs are independent and identically distributed. In particular, if they are exponentially distributed, then $\mathbb{X}$ is a Poisson process [10]. In Papers IV and V, a Poisson process is chosen for modeling the spontaneous neural activity. Note that if the underlying process is not renewal, then the intertimes might be autocorrelated. Therefore, in the non-renewal case, the autocorrelation has to be taken into account for computing the FPT density of $T_B^{(i)}(\mathbb{X})$ (see Section 2.5.1).

A different scenario can be the following. Imagine a multivariate process $\mathbb{X} \in \mathcal{D}^k$ and define the ith passage time of the component j through a boundary B_j by

$$T_{B_j}^{(i)}(\mathbb{X}_j) = \inf\{t > T_{B_j}^{(i-1)}(\mathbb{X}_j) : \mathbb{X}_j(t) > B_j\}.$$

If $\mathbb{X}$ has independent components, then the passage times of the lth and jth components are independent too, for $j \neq l$, and then this scenario is analogous to the previous one. The interesting case is when the coordinates of $\mathbb{X}$ are dependent, implying dependent FPTs. A challenging task is to solve the two proposed multivariate FPT problems. This is the purpose of Paper II and III.

2.5 Measures for the dependence between point processes

Different techniques have been proposed to detect dependencies between point processes. A review can be found in [34], where the analysis is carried out in a neuronal framework. Then spike trains, which are collections of spikes, can be modeled by point processes with events given by FPTs. In Paper II, the proposed copula method is compared with crosscorrelograms and with the Cox method [11] revised by Masud and Borisyuk [50]. A description of this method is presented in Section 5.1.1 of Paper II, and therefore is not reported here. Auto and crosscorrelations are shortly described in the following.

2.5.1 Auto and crosscorrelation

Since the pioneering work of [56], crosscorrelation histograms, known as crosscorrelograms, represent the most used tool for detecting dependencies between pairs of spike trains (i.e. point processes with events given by releases of action potentials) in neuroscience. Referring to [9], a detailed analysis is pursued as follows. First, check whether each point process is renewal, e.g. perform a test based on sample serial correlation coefficients. If the processes are renewal, then the distribution of the intervals between two events completely characterizes the point process. Therefore, the investigation of this distribution is of paramount interest. Second take an arbitrary event in the renewal point process and consider the sequence of successive kth order intervals, defined as the sum of k consecutive intervals between events after the arbitrary event. That is, if X_i denotes the ith intertime interval following the arbitrary event, then the kth-order interval is given by $X_1 + \cdots + X_k$. Denote f_k the density of the kth-order interval and consider the so-called *intensity function* $h(\tau)$, given by

$$h(\tau) = \sum_{k=1}^{\infty} f_k(\tau),$$

for any $\tau > 0$. Then $h(\tau)\Delta\tau$ can be interpreted as the probability of an event in a small time interval $(\tau, \tau + \Delta\tau]$ given an event happened at time 0, i.e.

$$h(\tau) = \lim_{\Delta\tau \to 0} \frac{\mathbb{P}(\text{ an event in}(\tau, \tau + \Delta\tau]|\text{ an event at } 0)}{\Delta\tau}.$$

A study of the renewal density gives information about the behavior of the single point process, e.g. it is constant for a Poisson process.

Third, consider two point processes A and B. Take an arbitrary event in A. Define the forward (resp. backward) waiting times of order i as the interval between the event in A to the ith subsequent (resp. previous) in B. Denote $\eta_i(\tau)$ the corresponding densities of order i. Then consider the so-called cross-intensity function $\xi_{AB}(\tau)$ given by

$$\xi_{AB}(\tau) = \sum_{i=-\infty; i \neq 0}^{i=\infty} \eta_i(\tau),$$

for any $\tau > 0$. Then $\xi_{AB}(\tau)\Delta\tau$ can be interpreted as the probability of any event in B before or after an event in A. The study of ξ_{AB} allows to understand dependencies between point processes [11]. For a complete analysis, the role of A and B has to be switched, leading to also compute ξ_{BA}.

In spike train analysis, the renewal and cross-intensity densities are called *auto and cross-correlations*, respectively. Neuroscientists estimate these functions for different τ from pairs of simultaneously recorded spike trains [55, 56]. Histograms of the estimated auto and crosscorrelations are called auto and crosscorrelograms, respectively. Each process, i.e. spike train, has independent and identically distributed intertime intervals if the estimated autocorrelation lies inside a suitable confidence region. Similarly, the two point processes are independent if the estimated crosscorrelation is inside a suitable confidence region [6]. Peaks or troughs outside the confidence interval evidence dependent point processes. Dealing with neuronal spike trains, peaks far from 0 indicate excitatory effects between pairs of neurons, while peaks around 0 indicate a tendency to simultaneous firings. Moreover, troughs far from zero indicate inhibition between the two neurons.

Cross-correlograms are easy to compute and for this reason, they are widely used by neuroscientists. However, there are several drawbacks on their use, as argued in [66, 67]. First, they merge marginal and joint behaviors, making it difficult to distinguish between coupling or marginal phenomena. Moreover, they strongly depend on the choice of the bin-size of the histogram and may fail to recognize weak dependencies. Finally, they exclusively catch pairwise dependencies, and cannot be used for detecting dependencies between more than two neurons.

2.6 Copulas

A k-dimensional copula is defined as a function $C : [0,1]^k \to \mathbb{R}$ such that

i. $C(u_1, \ldots, u_{i-1}, 0, u_{i+1}, \ldots, u_k) = 0$;

ii. $C(1, \ldots, 1, u, 1, \ldots, 1) = u$;

iii. C is k-increasing, i.e. for each hyperrectangle $B = \prod_{i=1}^{k}[a_i, b_i] \in [0,1]^k$, the C-volume of B, defined as $\int_B dC(u)$, is not negative.

Besides this formal definition, a key theorem for the understanding of copulas is Sklar's theorem [71], which establishes a correspondence between joint distributions and copulas. Denote $X_1, \ldots, X_k$ random variables with marginal distributions $F_1, \ldots, F_k$ and joint distribution H. Then, there exists a k-copula, denoted by $C_{X_1, \ldots, X_k}$ or simply C, such that

$$H(x_1, \ldots, x_k) = C_{X_1, \ldots, X_k}(F_1(x_1), \ldots, F_k(x_k)),$$

which is unique if the marginals are continuous. The other implication is also true. Therefore, copulas are joint distributions with uniform marginals.

There are several advantages for using copulas instead of joint distributions. First, copulas are scale free. Therefore they catch the dependence due to the joint behavior, ignoring the effect of the marginals. Definitions and properties of distribution functions can be easily rewritten in terms of copulas. Archimedean copulas are the most known and used class of copulas, since they have several nice properties and are easy to construct. Archimedean copulas are of the form

$$C(u_1, \ldots, u_k) = \phi^{[-1]}\left(\sum_{i=1}^{k} \phi(u_i)\right),$$

where ϕ is called a generator of the copula. It is a continuous, strictly decreasing function from $[0, 1]$ to $[0, \infty]$, such that $\phi(1) = 0$. Here $\phi^{[-1]}$ is the pseudo-inverse of ϕ, defined such that $\phi^{[-1]}(t)$ is equal to $\phi^{(-1)}(t)$ if $t \in [0, \phi(0)]$ or 0 otherwise.
Dependencies between random variables can be investigated using the Spearman's rho, the Kendall's tau or the Pearson's rho, which all belong to $[-1, 1]$. However, only the Kendall's tau, denoted by τ_C, detects non-linear dependencies. It is defined by

$$\tau_C = 2^k \int_{[0,1]^k} C(u_1, \ldots, u_k) dC(u_1, \ldots, u_k) - 1 = 2^k \mathbf{E}[C(u_1, \ldots, u_k)] - 1. \qquad (2.8)$$

For Archimedean copulas, it can be expressed as a function of the generating function ϕ by $\tau_C = 1 + 4 \int_0^1 \phi(t)/\phi'(t) dt$, where $\phi'(t)$ denotes the derivate of ϕ with respect to t. If the random variables are independent, then $C(u_1, \ldots, u_k) = \prod_{i=1}^{k} u_i$ and C is called product copula. Since $F_i(X_i)$ are uniform in $[0, 1]$, then $\mathbb{E}[\prod_{i=1}^{k} u_i] = 1/(2^k)$ and thus $\tau_C = 0$. That is, the Kendall's tau is null for independent random variables.
Copulas can also be used to express the mutual information of two random variables as follows. Denote c the density function of the copula, i.e.

$$c(u_1, \ldots, u_k) = \frac{\partial^k C(u_1, \ldots, u_k)}{\partial u_1 \cdots \partial u_k},$$

and define the copula entropy, denoted by H_C, by

$$H_C(u_1, \ldots, u_k) = -\int_{[0,1]^k} c(u_1, \ldots, u_k) \log c(u_1, \ldots, u_k) d\mathbf{u},$$

for $\mathbf{u} = (u_1, \ldots, u_k)$. Then, the mutual information is equal to the negative of the copula entropy [41].

Copulas also play an interesting role in the characterization of stochastic processes. Indeed, the transition density of a stochastic process can be rewritten as a product of copulas [15]. In particular, copulas for the Brownian motion, the Ornstein-Uhlenbeck and other known processes have been calculated [68]. Note that since the geometric Brownian motion can be expressed as an increasing transformation of the Brownian motion, the two processes have the same copula. Indeed, copulas are invariant under increasing transformations: if α and β are increasing functions on the range of X and Y respectively, then $C_{\alpha(X),\beta(Y)} = C_{X,Y}$. Refer to [16, 20, 26, 27, 28, 42, 52, 71, 81] for a detailed overview on copulas and their applications.

3

Neuronal Background

The brain is a highly interconnected network of nerve cells, called *neurons*. Each neuron is composed of three parts: *soma*, *dendrites* and *axon*. A schematic illustration is in Fig. 3.1. The dendrites (which branch several times determining the dendritic tree) represent input devices and they collect electro-stimulations from other neurons to the soma. The soma is a processing unit which collects incoming inputs and generates an output whenever the total inputs exceed a specific threshold. Such output is then carried out by the axon, working as an output device. Interconnections between neurons are ensured by synapses.

The difference of potential across the cell membrane is called *membrane potential*. When the membrane potential attains a certain threshold value, an active mechanism produces a sudden hyperpolarization. Then the neuron releases a short-duration electrical signal, which is called *action potential*, *spike* or *firing*. After a spike, there is a time interval, called *absolute refractory period*, during which a second action potential cannot be generated, even in presence of a strong input. After that, there is a time interval, called *relative refractory period*, during which spikes are unusually difficult to evoke. The sum of these two periods represent the time needed for a neuron to rest after a spike.

The collection of spike epochs of a neuron is called a spike train, and raster displays are a common way to visualize sets of spike trains of groups of neurons. Data from simultaneous recordings of groups of neurons make possible to detect the existence of precise temporal relations in sequences of spike intervals, referred to as temporal patterns. Several experimental observations support the hypothesis of the existence of dynamical cell assemblies as an organizational principle of higher brain activity [78, 79]. A cell assembly is formed by a population of neurons that spontaneously organizes on the basis of a sequence of input patterns of spikes. Moreover, it reproduces the same temporal activity whenever the same input pattern is presented [77]. It is believed that such patterns encode the neural information [55]. It is also known that dependencies between neurons are due either to direct interactions, e.g. a neuron excites or inhibits the others, or to common sources, i.e. a cluster of neurons receives the same stimulus. Refer to [69] for an overview of features and problems involved in neural coding.
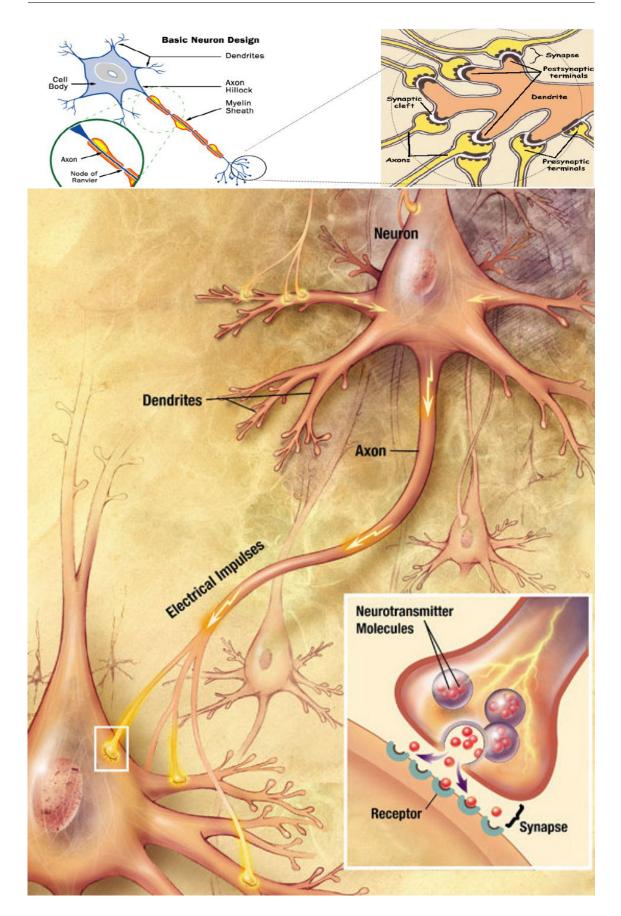
3.1   Mathematical modeling of neural phenomena

There is a strong connection between mathematics and neuroscience. Indeed, from a mathematical point of view, a spike train is a sequence of events, i.e. neuronal spikes, and can be modeled as a point process. Moreover, mathematical models of single neuronal units are used to reproduce the neural coding mechanisms. In 1952, Hodgkin and Huxley proposed to model the membrane potential evolution through a set of nonlinear ordinary differential equations [36]. An alternative approach makes use of stochastic models. It has been proposed by Gerstein and Mandelbrot [29] in 1964, and Stein [73] in 1965. Gerstein and Mandelbrot considered a Wiener process, also known as perfect integrator neuronal model, due to its simplicity among other diffusions. The model proposed by Stein, called Stein model, belongs to the class of jump processes. It takes into account neuronal features, e.g. the exponential decay of the membrane potential to a resting value after a spike. A shortcoming of one-dimensional diffusion processes is that they ignore the structure of the neuron, describing it as a single point. However, this oversimplification is necessary to be able to analyze such models. A good compromise between mathematical tractability and neuronal features has been reached by the so called leaky-integrate-and-fire models, which represent a large and widely used class of processes [65]. Conversely, there have been few attempts to develop mathematical models to describe small or large neuronal networks and the existing results are mainly of simulation type.

Neuronal spikes have been modeled as FPTs of a process through a suitable boundary. It is commonly assumed that the membrane potential is instantaneously reset to its resting value whenever it fires and then it evolves independently from before. Thus, for simplifying the mathematics, the refractory period is often not taken into account. The resulting process is renewal and the intertimes between two consecutive spikes, called interspike intervals (ISIs), are independent and identically distributed random variables.

3.2   Background of Paper IV and V: response latency

Neurons release spikes even without any controlled or apparent stimulation, usually with a low firing rate. That is the so-called spontaneous firing activity, which can be described by a Poisson process, as often supported by experimental data [30, 75]. If a stimulus is applied to the neuron, then a change in the firing activity is expected. In particular, if the stimulus is excitatory, then the firing rate increases, otherwise it decreases. A spike due to the stimulus onset is called evoked spike. The response latency is defined as the time to the first evoked spike after the stimulus onset. In presence of spontaneous activity, the response is observed on top of an indistinguishable background signal. That is, an observer cannot distinguish whether a spike is spontaneous or evoked. It is also believed that the response to the stimulus is not instantaneous, but appears with a time delay called *absolute response latency.* Then, the response latency can be described as a sum

of two components, namely the absolute and the *relative response latency*, defined as the time to the first evoked spike following the absolute response latency.

Basic Neuron Design

Dendrites

Cell Body

Axon Hillock

Myelin Sheath

Axon

Node of Ranvier

Synapse

Postsynaptic terminals

Synaptic cleft

Dendrite

Axons

Presynaptic terminals

Neuron

Dendrites

Axon

Electrical Impulses

Neurotransmitter Molecules

Receptor

Synapse

4

Overview of the results

An overview of the papers in this thesis in relation to existing results is shortly presented here. In particular, inspiring papers, key ideas, neuronal and mathematical motivations and main results are emphasized.

4.1 Overview of Paper I

Membrane potential dynamics of single neurons are commonly described by unidimensional OU processes. Besides a reasonable mathematical tractability, the parameters of the OU can be biologically interpreted. Indeed, this process can be obtained as a diffusion approximation of a Stein model, which has parameters with a biological interpretation, as discussed in Section 2.2. Therefore, a multivariate OU represents a natural choice for describing neural network activity. How should dependencies between neurons be taken into account? And is it still possible to obtain the multivariate OU as a limit of a multivariate Stein model? Answering these questions is the first aim of Paper I.

A generalized Stein model with cluster dependencies is proposed for modeling neural network dynamics. Cluster dependencies mean that the neurons within group (cluster) of neurons are dependent if there are common inputs impinging on them. In the univariate Stein (2.5), incoming inputs are modeled by Poisson processes. If neurons share the same input, then the same Poisson process appears in their SDEs.
Weak convergence criteria (given in [40] and shortly presented in Section 2.2) are used to prove a diffusion approximation of sequences of generalized Stein processes. As expected, the resulting limit process is a multivariate OU process satisfying the SDE

$$d\boldsymbol{Y}(t) = \int_0^t \left(\frac{-\boldsymbol{Y}(s)}{\theta} + \boldsymbol{\Gamma} \right) ds + \boldsymbol{W}(t), \tag{4.1}$$

where $\boldsymbol{\Gamma}$ denotes the drift vector and $\boldsymbol{W}$ is a multivariate Wiener process with positive-definite covariance matrix denoted by $\boldsymbol{\Psi}$. All parameters in $\boldsymbol{\Gamma}$ and $\boldsymbol{\Psi}$ are obtained as limits of frequency rates of the Poisson processes underlying the Stein model. In particular, ψ_{ij}, an element of $\boldsymbol{\Psi}$, is a function of parameters coming from the Poisson processes common to the ith and jth component, for $1 \leq i, j \leq k$. Thus, the covariance matrix is not diagonal.

The obtained OU inherits the biological meaning and dependence structure of the Stein. Since the information is encoded by spike trains, it is relevant to check whether there exists

17

a correspondence between the passage times of the jump process and those of the diffusion. If this happens, then the information is carried over from the Stein to the OU model. Therefore, the jump process can be replaced by its diffusion approximation. This is the second aim of the paper. To achieve it, the firing mechanism of a network has to be defined, as well as the meaning of "convergence of spike trains". When a neuron $j, 1 \leq j \leq k$ fires at time τ, its membrane potential is reset to its resting potential and then it is restarted. Thanks to the reset and since dependencies between processes are described through either stationary Poisson processes (for the Stein model) or correlated Gaussian noise (for the OU model), the ISIs of each neuron are independent and identically distributed. Thus, marginally each process is renewal. Meanwhile, the non firing components Y_i, for $i \neq j$, continue their evolution, starting at time τ in a random position $Y_i(\tau)$. Hence, the multivariate process is not renewal. A formal construction of a new process $\boldsymbol{Y}^*$ describing the firing neural network mechanism is given. In particular, $\boldsymbol{Y}^*$ is iteratively defined in each ISI of the process. On $[\tau_i, \tau_{i+1}[$, the process $\boldsymbol{Y}^*$ is obtained by conditional independence from $\boldsymbol{Y}^*$ on $[\tau_{i-1}, \tau_i[$, with initial value $\boldsymbol{Y}^*(\tau_i)$. Hence, each ISI depends on a triplet of random variables: starting position, firing component and passage time. It is shown that the convergence of the spike trains corresponds to the convergence of the triplets of all the ISIs. Since the FPT is not a continuous function, the convergence does not follow applying the continuous mapping theorem on the processes. The result is proved iteratively, following the construction of $\boldsymbol{Y}^*$, and using two key ideas. The first is to apply the Skorohod's representation theorem for switching from weak to strong convergences on a suitable probability space. The second is to apply the convergence properties on a product topology on $\mathcal{D}^k$: $\boldsymbol{X}_n \to \boldsymbol{X}$ a.s. if $X_{in} \to X_i$ a.s. for each component $i = 1, \ldots, n$. Interestingly, these convergence results hold for any multivariate jump process $\mathbb{X} \in \mathcal{D}^k$ converging weakly to its diffusion approximation $\mathbb{Y}$. Indeed, the proof only depends on the equality between FPTs and hitting times (defined as the first times when a process reaches a threshold, for the process $\boldsymbol{Y}$) and it is well known that diffusion processes satisfy this condition.

Among the convergence results shown in Paper I, the following lemma deserves to be mentioned.

Lemma 2. *Let x_n° belong to $\mathcal{D}^1$ for $n \geq 1$, and $y^\circ \in H$ with $y^\circ(0) < B$. If $x_n^\circ \to y^\circ$ in $\mathcal{D}^1$, then $T_B(x_n^\circ) \to T_B(y^\circ)$,*

where $T_B(\cdot)$ denotes the FPT through B and H is the space of continuous functional having equal crossing and hitting times. Thus, the convergence of the FPTs follows from the convergence of the processes. The result itself is not surprising. Indeed, it seems obvious that two processes having the same asymptotic trajectories, will also have the same FPTs. However, it is particularly useful because then the weak convergence of a unidimensional FPT follows straightforwardly from the Skorohod's representation theorem and Lemma 2. Moreover, using also the product topology on $\mathcal{D}^k$, the weak convergence of the minimum of the FPTs of a multivariate process is proved. Thanks to these convergence results, the generalized Stein can be replaced by the multivariate OU model, which is less complicated from a mathematical point of view.
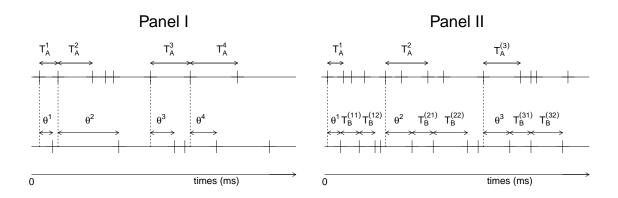
Figure 4.1: Different pairs of random variables extracted from two spike trains. Select A as target neuron. Panel I: Pairs (T_A^i, θ_i), obtained considering the FPT in A and the time up to the first spike following it in B. Panel II: Pairs $(T_A^i, \theta_i + \sum_{l=1}^{m} T_B^{(il)})$, with $m = 2$, obtained considering a FPT in A and the FPTs up to the $(m+1)$th spike following it in B.

To propose a model reflecting the neuronal features, absolute refractory periods Δ are also considered. The new firing mechanism is more complicated than before. Indeed, the reset of the firing component is now shifted a time Δ, during which the other components can fire. However, the previous convergence results on the spike trains are still valid.

To conclude, the multivariate OU model can be a good candidate for describing neural networks with refractory periods. In particular, it reproduces inhibition, excitation, synchronism and silencing of neurons, as shown through simulations. Several generalizations can be done, according to the neural features of the network that is of interest.

4.2   Overview of Paper II

Since temporal patterns are believed to encode information, their study is of paramount interest to understand connectivity between simultaneously recorded spike trains. Crosscorrelograms, i.e. histograms of the crosscorrelation functions, are the most used tool to detect pairwise connections [56]. However, they may fail to detect non-linearities, as shortly mentioned in Section 2.5 and shown in [66]. As an alternative approach, the parametric Cox method [50] or any of the techniques proposed in [34] can be applied. The aim of Paper II is to propose a new non-parametric method. To simplify the description, the technique is illustrated for two neurons A and B, but can be easily extended to larger networks. The key idea is to express the two spike trains through two suitable random variables, and then investigate their joint distribution. Throughout the paper, three different scenarios have been studied:

   i. Consider pairs of FPTs (T_A^i, T_B^i) such that T_A^i are iid, T_B^j are iid and (T_A^i, T_B^j) are

independent for $i \neq j$, $1 \leq i, j \leq n$. This case is mainly introduced for helping the understanding of the method, but biological interpretations can also be given. First, these pairs can be obtained as the first ISIs in A and B following synchronous spikes (see left panel in Fig. 1 of Paper II). Second, imagine to apply the same stimulus to two dependent neurons and being interested in determining their response latencies from the analysis of the first spikes following the stimulus onset. This gives the first pair (T_A^1, T_B^1). The sample is then obtained repeating this procedure n times, waiting for a time interval large enough to ensure that the neurons are at rest.

ii. Select A as target neuron, denote S_A^i the ith spike epoch, and T_A^i the ISI between the ith and the $(i+1)$th spike in A. Define θ_i as the intertime between S_A^i and the first spike following it in B. Then, dependencies between (T_A^i, θ_i) can be investigated. A sample is constructed such that two consecutive random variables θ_i and θ_{i+1} are not overlapped. This is done to avoid autocorrelation between the θ variables. A schematic illustration is reported in Panel I in Fig. 4.1.

iii. Select A as target neuron and consider dependencies between $(T_A^i, \theta_i + \sum_{l=1}^m T_B^{(il)})$, for $1 \leq i \leq n$. Here T_B^{il} denotes the lth spike following θ_i in neuron B. This allows to study the duration (that we also call memory) of the dependence between two spike trains, i.e. the number of spikes m necessary for neuron B to forget the firing activity of neuron A. The $(i+1)$th pair is chosen such that it does not overlap with the ith, allowing to avoid autocorrelated random variables. A schematic illustration for $m = 2$ is reported in Panel II in Fig. 4.1.

Fig. 4.1 improves the right panel in Fig. 1 of Paper II. In cases ii and iii, the pairs are not symmetric and therefore the procedure has to be repeated selecting B as target neuron. This allows to detect uni-directional dependencies, since it may happen that neuron A influences neuron B but not the reverse.

The joint distributions of the described pairs of random variables are studied through copulas, which are joint distributions with uniform marginals. Besides the practical advantages (e.g. several implemented goodness-of-fit tests, flexibility of the parameter choice, R package available for simulations), the main reason for using copulas is that they capture the joint properties, ignoring the marginal features. It is well known that, if F_X denotes the distribution of a random variable X, then $F_X(X)$ is uniformly distributed. Empirical cumulative distribution functions, denoted by $\hat{F}_X$, have been used to estimate the unknown F_X. An illustration of the relation between (X, Y) can be obtained looking at the so-called *copula scatterplots*, i.e. scatterplot of $(\hat{F}_X(X), \hat{F}_Y(Y))$. A particular effort is put on what we call *curve of monotony*. It consists of the set of points such that $F_X(X) = F_Y(Y)$. If the marginal distributions are the same, then the curve of monotony is the main diagonal of the square $[0, 1]^2$. To test the presence of dependencies between X and Y (and hence between neurons A and B), a statistical test for the null hypothesis $H_0 : \tau = 0$ is considered. Here τ denotes the Kendall's tau given by (2.8).

The proposed method is illustrated on simulated data. Two alternative firing mechanisms are considered:

a) The sub-threshold membrane potential dynamics is modeled by a bivariate OU process with independent components. Whenever a neuron fires, its membrane potential is reset to its resting value, while the other membrane potential has a jump of amplitude $h > 0$. This reproduces a *direct connection* between neurons, that we call *local*, to pinpoint that the dependence is localized to the jumps.

b) The sub-threshold membrane potential evolutions are modeled by the bivariate OU process with correlated components proposed in Paper I. The firing component is instantaneously reset, while the other component does not jump. Such model considers *global connections* between neurons, since the neuronal dynamics are characterized by a continuous coupling effect.

Here the refractory period is not taken into account. The features of the copula scatterplots change according to the considered pairs of random variables and firing mechanism. The proposed method has also been applied on simulated data from the special LIF model proposed in [50]. The neural connectivity, even in presence of delays in the coupling, is correctly detected by the copula method, which may however fail for small dependencies. A comparison with other techniques, i.e. crosscorrelograms and the Cox method, is also performed, highlighting advantages and drawbacks of the different tools.

4.3 Overview of Paper III

The FPT problem for univariate processes has been widely investigated in the literature. Conversely, few results are available for joint distributions of FPTs of multivariate processes. This is due to several reasons. First of all, explicit expressions of the FPT density are available only for few unidimensional processes, e.g. Wiener. This discouraged an extension to the multivariate case. Moreover, the multivariate FPT problem can often be traced back to the univariate scenario. The simplest example is a multivariate process with independent components. Then the joint distribution of the FPT is equal to the product of the marginal distributions. A more interesting scenario is a bivariate process with a jump of the non-firing component whenever the other fires. Then, conditioning on the passage times of the first firing components, the problem can be described as the FPT problem of a univariate process which has one (or multiple) jumps at a given time.

As previously discussed, a challenging task is the detection of dependencies between point processes. A (very) preliminary step toward this direction is given in [38], where the joint distribution of the exit times from a bidimensional strip of a bivariate Wiener process without drift has been calculated. Denote $\boldsymbol{X} = (X_1, X_2)$ the bivariate process, T_i the FPT of X_i through the boundary $B_i, i = 1, 2$ and $(-\infty, B_1) \times (-\infty, B_2)$ the bivariate strip. What they compute is the density of $\min(T_1, T_2)$. Some mistakes have been found and corrected by Domine and Pieper [21]. Moreover, they solve a two dimensional Kolmogorov forward equation for the unknown bivariate density $f_{\boldsymbol{X}}$ of $\boldsymbol{X}$ under absorbing boundary conditions. Such density has then been used to explicitly compute the joint density of

$\min(T_1, T_2)$, when $\boldsymbol{X}$ is a Wiener process with drift $\boldsymbol{\mu} = (\mu_1, 0), \mu_1 \neq 0$ under absorbing boundary conditions.

These works have inspired Paper III. The aim is to compute the joint distribution of the exit times $\boldsymbol{T} = (T_1, T_2)$ from a bidimensional strip of a bivariate Gauss-Markov process under absorbing boundary conditions. That is, the process is bivariate in $[0, \min(T_1, T_2)]$ and then only the non-firing component evolves as a univariate process in $[\min(T_1, T_2), \max(T_1, T_2)]$. Thanks to the Markov property, the dynamics after the first spike are independent of what happens before, conditioned on the random initial position at time $\min(T_1, T_2)$. Then, the distribution of $\boldsymbol{T}$ can be expressed as a function of the marginal FPT densities of each component and of the transition density of the slower component under the boundary. In particular, the following density needs to be calculated:

$$
\begin{aligned}
f_{(X_j^a, T_i)}(x_j, t | y_j, s) &= \frac{partial^2}{\partial x_j \partial t} \mathbb{P}\left(X_j^a(T_i) < x_j, T_i < t | X_j^a(s) = y_j\right) \\
&= f_{X_j^a | T_i}(x_j | s_i) g_{T_i}(s_i),
\end{aligned}
$$

for $i, j = 1, 2, i \neq j$. Here X_j^a denotes the jth component of the process inside the strip, i.e.

$$
\boldsymbol{X}^a = \{\boldsymbol{X}(t); \ t \in [0, \min(T_1, T_2)]\}.
$$

In Theorem 3.3, it is shown that $f_{(X_j^a, T_i)}$ can be obtained as solution of a system of Volterra-Fredholm first kind integral equations for boundaries which are not necessarily absorbing. In general, the system cannot be explicitly solved. For this reason, a numerical method is proposed. The algorithm is based on a discretization of both the time and the state spaces and the convergence of its error is proved in Theorem 5.2, mimicking and extending the proof in [8]. Then, the approximated density can be used to compute the desired joint distribution of $\boldsymbol{T}$.

If $\boldsymbol{X}$ is a bivariate Wiener process with constant drifts and non-diagonal covariance matrix, the unknown density $f_{(X_j^a, T_i)}$ can be explicitly calculated, extending and correcting the results in [21].

Finally, theoretical and numerical results for the bivariate Wiener process are compared; numerical approximations of the joint FPT density for the bivariate OU processes proposed in Paper I, are shown.

4.4   Overview of Paper IV and V

Imagine to measure the spontaneous firing activity of a neuron. When a stimulus is applied at time t_s, the spikes due to the stimulus onset, called evoked, are recorded on top of an undistinguished background signal, representing the pre-existing spontaneous activity. This scenario becomes even more complex when the response to the stimulus is not instantaneous, but happens with a delay $\theta > 0$. For neuroscientists, it is of paramount interest both the detection of θ [35] and the investigation of the response latency (denoted by R), i.e. the intertime between the delivery of the stimulus and the first evoked spike. Most

of the standard techniques ignore the spontaneous activity after stimulation, assuming it negligible with respect to the evoked. Then, they consider evoked the first spike following t_s, denoted by T. The minimum of the observations of T is used as a naive estimator of the delay θ. However, when $\theta = 0$, the estimation of the response latency is biased if the spontaneous activity is not taken into account [54]. Motivated by this paper, a unified concept of response latency identification in event data corrupted by a background signal is proposed. As previously described, the response latency is defined as a sum of two components, namely the absolute and relative response latencies, denoted by θ and Z respectively. During θ, only spontaneous spikes can be observed. Here Z is defined as the intertime between $t_s + \theta$ and the first evoked spike. The key assumption of Paper IV and V is that the spontaneous activity is not affected by the stimulus up to the first evoked spike. Whatever happens after t_s is outside the scope of the work. Then, since neither the spontaneous (denoted by W) nor the evoked spikes can be distinguished after t_s, the estimation of the response latency is entirely based on T, which is the minimum between W and R.

4.4.1 Paper IV

The primary aim is the investigation of the absolute response latency θ, the second is the understanding of the role of the spontaneous activity. The distribution of the ISIs before the stimulus onset is estimated under different assumptions:

A1. the spontaneous firing activity follows a renewal process model, i.e. the ISIs before the stimulus onset are independent and identically distributed;

A2. stationarity of the data, i.e. the time from the last spike prior the stimulation to t_s is identically distributed with the time up to the first spontaneous spike following t_s;

A3. the spontaneous firing activity follows a renewal Poisson process.

In particular, in presence of Poissonian activity, it is shown that

- the nth moment of T is

$$\mathbb{E}[T^n] = \mathbb{E}[W^n]\left\{1 - e^{-\lambda\theta}\sum_{j=0}^{n-1}\frac{\lambda^j}{j!}\sum_{h=0}^{j}\binom{j-h}{h}\theta^h\mathcal{L}_Z^{(j-h)}(\lambda)\right\},$$

where $\mathcal{L}_Z(s)$ denotes the Laplace transform of f_Z, which is defined by $\mathcal{L}_Z(s) = \mathbb{E}[e^{-sZ}] = \int_0^\infty e^{-st}f_Z(t)dt$, and $\mathcal{L}_Z^{(k)}(\cdot)$ denotes its kth derivative;

- the probability p that the first observed spike after t_s is spontaneous is

$$p := \mathbb{P}(T = W) = \frac{\mathbb{E}[T]}{\mathbb{E}[W]}.$$

The probability p can be used to calculate the risk of failure when the first observed spike is assumed to be evoked, i.e. $T = R$, when in fact is spontaneous, i.e. $T = W$. Thus, its estimation is of primary interest to understand experimental data. Indeed, it gives an overview of the strength of the background activity in the measurements. Such probability can be easily estimated from data, with a good performance even in a non-parametric approach.

Six estimators of θ have been proposed under different assumptions for the spontaneous, i.e. A1–A3, and evoked activity, i.e. model free or distribution of the response latency known. These estimators are based on the following ideas:

- $\hat{\theta}_1$ ignores the presence of the spontaneous activity, being defined as the minimum of the observations of T;

- $\hat{\theta}_2$ is based on the average number of first observed spikes which are spontaneous (hence is related to p);

- $\hat{\theta}_3$ uses the assumption that no evoked spikes can be observed in $[t_s, t_s + \theta]$;

- $\hat{\theta}_4$ is the maximum likelihood estimator (parametric estimator);

- $\hat{\theta}_5$ is based on the moment estimator (parametric estimator);

- $\hat{\theta}_6$ is the maximum likelihood estimator when assuming a wrong distribution family for the response latency.

It is interesting to remark that the estimator $\hat{\theta}_1$ is shown to go to zero as the number of observations increases, suggesting the importance of taking the spontaneous activity into account.

4.4.2 Paper V

The absolute response latency θ is deeply investigated in Paper IV. The aim of Paper V is the investigation of the relative response latency Z. This can only be done under a parametric approach, i.e. both the distribution families of the spontaneous and the evoked activity are known. Paper IV shows that the MLE provides the best estimate of θ. Therefore, the MLE represents the natural approach for inference about the parameters of Z. Throughout the paper, the spontaneous activity is Poissonian, while the relative response latency is assumed to be exponential, gamma or inverse Gaussian distributed. The error in the estimation of the distribution of R is measured by the relative integrate absolute error. It is defined as the integral of the absolute difference between the distribution of R and its estimation, divided by the mean of R. If the spontaneous activity is ignored, i.e. R is estimated as T, then the error is given by $1 - \mathbb{E}[T]/\mathbb{E}[R]$. Since $\mathbb{E}[T] \leq \mathbb{E}[R]$ by definition of T, this error is null only if the spontaneous activity is not present.

The authors are aware that no experimental evidence is available about the distribution

of the response latency. To supply this lack of information, model control or model selection can be applied. Interestingly, mean and variance of R are always well estimated, even when a wrong distribution family for R is assumed. This happens because there exists an infinite number of suitable sets of parameter values of the distribution of R yielding the same mean and variance. This is particularly important, since those quantities, together with the value of p, can give useful information to neuroscientists about the response of neurons to the stimulus.

5

Perspective

Throughout this dissertation, neural network connectivity and response latency are discussed, and different models and statistical analyses are proposed. Some of the open problems arising from my work are here shortly discussed.

5.1 Future work suggested by Paper I-III

5.1.1 From Paper I

In Paper I, a multivariate jump process is proposed as a model for describing the neural network connectivity and an opportune firing scheme is introduced. The shown convergence results have allowed to switch to its limiting process, which is a multivariate OU process. A preliminary description of the model and an illustration of its features have been given. A relevant future work would be a detailed characterization of the process, e.g. investigating the relation between the dependence structure of spike trains and the choice of the parameter values of the OU. This could be done applying the copula method proposed in Paper II.
Another interesting work would be to propose a model with also direct connections between neurons, e.g. jumps of the membrane potentials in presence of spikes.

5.1.2 From Paper II

In Paper II, a non-parametric method for catching dependencies between pairs of neurons in a neural network with k neurons is proposed. A preliminary illustration on different sets of simulated data is discussed. At the moment, a statistical analysis of the method is missing. In particular, it would be relevant to improve the analysis of its reliability. That is, to understand how often the method does not recognize dependencies or independence on simulated data. This could be done simulating pairs of spike trains with a given dependence structure, performing the statistical test $H_0 : \tau = 0$, checking whether the test result agrees with the structure and repeating this procedure several times. Once that the method has been validated, it would be useful to apply on experimental data.

It would also be interesting to perform a statistical comparison with other existing techniques, i.e. crosscorrelograms, Cox method and those described in [34], to highlight their advantages and drawbacks. To help neuroscientists in the analysis of real data, it would be of paramount importance to implement a software with all the techniques.

Finally, since neurons belong to cell assemblies with thousands of other neurons, a natural extension of the proposed method would be to consider d-dimensional copulas, for $2 < d \leq k$, for the detection of dependencies between groups of d neurons in a neural network with k neurons.

5.1.3   From Paper III

In Paper III, the bivariate FPT problem for a bivariate Wiener process with constant drifts and non-diagonal covariance matrix in presence of absorbing boundaries is solved. For other Gauss-Markov processes, the joint FPT distribution is not explicitly available and a numerical method is then proposed. An illustration of the approximated joint FPT distribution for a bivariate OU process is given. First, it would be interesting to characterize this scenario, investigating the relation between the approximated joint FPT distribution and the parameter values of the OU. Second, it would be relevant to extend the bivariate FPT problem to the case of non-absorbing boundary conditions, considering e.g. diffusion processes or models where each component is a renewal process.

5.2   Future work suggested by Paper IV-V

5.2.1   Use of the entire spike train

In Paper IV and V, a shortcoming of the analysis is the use of only the first spike after the stimulus onset, ignoring the further information carried out by the following spikes. It would be relevant to extend the developed methods for considering the entire spike train. It can be discussed if it is biologically correct to assume that the spontaneous and the evoked activities are independent and can be distinguished once the stimulus is applied. Consider two independent neurons A and B, with A spontaneously firing and B silent, and apply a stimulus on B. Then, B reacts to the stimulus and an evoked firing activity is observed. If the spike trains are simultaneously recorded from two neurons which are located very close in the cortex, it may be difficult to distinguish whether a recorded spike comes from A or B. What is observed is a pooled spike train, obtained overlapping the two single spike trains, as illustrated in Fig. 5.1. In this experimental set up, the spontaneous activity can be estimated through the spikes before the stimulus onset. Then, the response latency may be investigated considering all spikes following the stimulation, filtering out the spontaneous firing from the pooled train. The next step would be to apply the resulting method on real data.
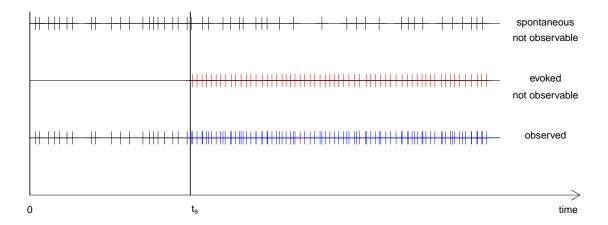
Figure 5.1: Schematic description of the experimental trial with two neurons A and B. Spikes are indicated with vertical dashes. At time 0 the measurement starts and the spontaneous spikes from neuron A are recorded. Neuron B is silent up to time t_s, when a stimulus is applied to it. For an observer, the two spike trains cannot be distinguished. What is observed is their pooled version, obtained by the overlapping of the two trains.

5.2.2   Statistical test $H_0 : \theta = 0$

Besides the estimation of the absolute response latency θ, it is biologically relevant to perform a statistical test to decide whether the response to the stimulus is or not instantaneous. This represents a challenging task, since $\theta = 0$ belongs to the boundary of the parameter space where the delay θ is defined. Therefore, suitable asymptotic properties for the test statistics must be investigated, following [70]. A natural choice may be to consider a parametric likelihood ratio-test. As a further step, since there are no experimental evidence about the distribution of the response latency, it would be extremely useful for neuroscientists to provide a non-parametric test. The method must be validated on simulated data and thereafter applied on experimental data.

5.2.3   Response latency for IF models

Model the spontaneous firing activity of a neuron through a renewal Wiener process X with constant drift $\mu_1 > 0$ and coefficient diffusion σ_1^2, with $\sigma_1 > 0$. After a spike, the reset of the membrane potential can be either instantaneous or shifted. At a given time t_s, a stimulus is applied. Then, the membrane potential is described as a Wiener process Y with drift $\mu_2 > 0$ and coefficient diffusion σ_2^2, with $\sigma_2 > 0$. What is the distribution of the first spike following t_s? Is it possible to estimate μ_2 and σ_2^2, assuming μ_1 and σ_1^2 previously estimated from the spontaneous activity up to the stimulus onset? A schematic representation is reported in Fig. 5.2.
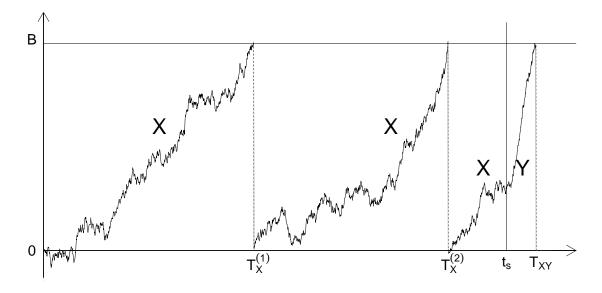
Figure 5.2: Schematic illustration of the single experimental trial. At time 0, the measurement starts. The membrane potential is described as a renewal Wiener process X with drift $\mu_1 > 0$ and diffusion coefficient σ_1^2, with $\sigma_1 > 0$. The ith FPT of X through a boundary B is denoted by $T_X^{(i)}$. At time t_s, a stimulus is applied. The membrane potential is now described as a Wiener process Y with drift $\mu_2 > 0$ and diffusion coefficient σ_2^2, with $\sigma_2 > 0$. Here T_{XY} denotes the FPT of the mixture process of X and Y following the stimulus onset.

Bibliography

[1] L. Arnold. *Stochastic Differential Equations: Theory and Applications*. John Wiley & Sons, New York, 1974.

[2] K.E. Atkinson. *A Survey of Numerical Method for the Solution of Fredholm Integral Equation of the Second Kind*. SIAM, Philadelphia, 1976.

[3] M. Bachar, J. Batzel, and S. Ditlevsen, editors. *Stochastic Biomathematical Models with Applications to Neuronal Models*, volume 2058 of *Lecture notes in Mathematics*. Springer, 2013.

[4] P. Billingsley. *Probability and Measure*. Probability and Mathematical Statisticis. Wiley Interscience, New York, second edition, 1995.

[5] P. Billingsley. *Convergence of Probability Measures*, volume 493 of *Wiley Series in Probability and Mathematical Statisticis*. John Wiley & Sons, New York, second edition, 1999.

[6] D.R. Brillinger. Confidence intervals for the cross-covariance function. *Selecta Statist. Canadiana*, V:1–16, 1979.

[7] R.M. Capocelli and L.M. Ricciardi. Diffusion approximation and first passage time problem for a model neuron. *Kybernetik*, 8:214–223, 1971.

[8] A. Cardone, E. Messina, and A. Vecchio. An adaptive method for Volterra-Fredholm integral equations on the half line. *J. Comput. Appl. Math.*, 228(2):538–547, 2009.

[9] D. R. Cox and P. A. W. Lewis. *The Statistical Analysis of Series of Events*. Methuen & Co. Ltd., London, 1966.

[10] D.R. Cox. *Renewal Theory*. Methuen & Co. Ltd., London, 1962.

[11] D.R. Cox. *The Statistical Analysis of Dependencies in Point Processes*. Stochastic point processes, New York, 1972.

[12] D.R. Cox and H.D. Miller. *The Theory of Stochastic Processes*. John Wiley & Sons, New York, 1977.

[13] J.C. Cox, J.E. Ingersoll, and S.A. Ross. A theory of the term structure of interest rates. *Econometrica*, 53:385–407, 1985.

[14] M. Csörgö and Révész. *Strong Approximation in Probability and Statistics*. Academic Press, New York–London, 1981.

[15] W.F. Darsow, B. Nguyen, and E.T. Olsen. Copulas and Markov processes. *Illinois J. Math.*, 36:600–642, 1992.

[16] V. H. De la Pẽna, R. Ibragimov, and S. Sharakhmetov. Characterizations of joint distributions, copulas, information, dependence and decoupling, with applications to time series. In *Optimality. Lecture Notes - Monograph Series*, volume 49, pages 183–209. IMS, 2006.

[17] L.M. Delves and J.L. Mohamed. *Computational Methods for Integral Equations*. Cambridge University Press, Cambridge, 1985.

[18] S. Ditlevsen and P. Lansky. Estimation of the input parameters in the Ornstein-Uhlenbeck neuronal model. *Physical Review E*, 71(011907), 2005.

[19] S. Ditlevsen and A. Samson. Introduction to Stochastic models in biology. In *Stochastic Biomathematical Models with Application to Neuronal Modeling*, volume 2058 of *Lecture notes in Mathematics*. Springer, 2013.

[20] J. Dobric and F. Schimd. A goodness of fit test for copulas based on Rosenblatt's transformation. *Comput. Statist. Data Anal.*, 51(9):4633–4642, 2007.

[21] M. Dominé and V. Pieper. First passage time distribution of a two-dimensional Wiener process with drift. *Prob. Eng. Inf. Sci.*, 7:545–555, 1993.

[22] J.L. Doob. *Stochastic processes*. John Wiley & Sons, New York, 1954.

[23] W. Feller. Diffusion processes in genetics. In *Proceedings of the second Berkeley symposium on mathematical statistics and probability*, pages 227–246. University of California Press, Berkeley and Los Angeles, 1951.

[24] W. Feller. Diffusion processes in one dimension. *Trans. Amer. Math. Soc.*, 77:1–31, 1954.

[25] J.L. Forman and M. Sørensen. The Pearson diffusion: a class of statistically tractable diffusion processes. *Scand. J. Statist.*, 53(3):438–465, 2008.

[26] E. W. Frees and E. A. Valdez. Understanding relationships using copulas. *N. Am. Actuar. J.*, 2(1):1–25, 1998.

[27] C. Genest and A.C. Favre. Everything you always wanted to know about copula modeling but were afraid to ask. *J. Hydrol. Eng.*, 12:347–368, 2007.

[28] C. Genest, B. Remillard, and D. Beaudoin. Goodness-of-fit tests for copulas: A review and a power study. *Insurance Math. Econom.*, 44(2):199–213, 2009.

[29] G.L. Gerstein and B. Mandelbrot. Random walk models for the spike activity of a single neuron. *Biophys. J.*, 4:41–68, 1964.

[30] W. Gerstner and W. M. Kistler. *Spiking Neuron Models*. Cambridge University Press, 2002.

[31] I.I. Gikhman and A.V. Skorohod. *The Theory of Stochastic Processes. I.* Springer–Verlag, Berlin, 2004.

[32] I.I. Gikhman and A.V. Skorohod. *The Theory of Stochastic Processes. III.* Springer–Verlag, Berlin, 2007.

[33] M.A. Golberg. *Numerical Solution of Integral Equation*. Plenum Press, New York, 1990.

[34] S. Grün and S. Rotter. *Analysis of parallel spike trains*. Springer, New York, first edition, 2010.

[35] D. Hampel and P. Lansky. On the estimation of refractory period. *J. Neurosci. Meth.*, 171(2):288–295, 2008.

[36] A. Hodgkin and A. Huxley. A quantitative description of membrane current and its application to conduction and excitation in nerve. *J. Physiol.*, 117:500–544, 1952.

[37] S. M. Iacus. *Simulation and Inference for Stochastic Differential Equations (with R examples)*. Springer Series in Statistics. Springer, New York, first edition, 2008.

[38] S. Iyengar. Hitting line with two–dimensional Brownian motion. *SIAM J. Appl. Math.*, 45(6):983–989, 1985.

[39] M. Jacobsen. One-dimensional homogeneous diffusions. In *Stochastic Biomathematical Models with Application to Neuronal Modeling*, volume 2058 of *Lecture notes in Mathematics*. Springer, 2013.

[40] J. Jacod and A.N. Shiryaev. *Limit Theorem for Stochastic Processes*. Springer–Verlag, Berlin, second edition, 2002.

[41] R.L. Jenison and R.A. Reale. The shape of neural dependence. *Neural Comput.*, 16(4):665–672, 2004.

[42] H. Joe. *Multivariate Models and Dependence Concepts*. Chapman & Hall, London, 1997.

[43] G. Kallianpur and R. L. Wolpert. *Weak convergence of stochastic neuronal models*. Springer–Verlag, New York, 1987. Proceedings of a workshop on Stochastic methods in biology.

[44] I. Karatzas and S.E. Shreve. *Brownian Motion and Stochastic Calculus.* Springer–Verlag, New York, second edition, 1991.

[45] S. Karlin and H.M. Taylor. *A first course in stochastic processes.* Academic Press, New York–London, second edition, 1975.

[46] S. Karlin and H.M. Taylor. *A second course in stochastic processes.* Academic Press, New York–London, second edition, 1981.

[47] P. Lansky. On approximations of Stein's neuronal model. *J. Theoret. Biol,* 107:631–647, 1984.

[48] T. Lindvall. *Lectures on the Coupling Method.* Wiley Series in Probability and Mathematical Statistics. John Wiley & Sons, New York, 2002.

[49] P. Linz. *Analytical and numerical methods for Volterra equations.* Number 7 in SIAM Studies in Applied Mathematics. SIAM, Philadelphia, PA, 1985.

[50] M.S. Masud and R. Borisyuk. Statistical technique for analyzing functional connectivity of multiple spike trains. *J. Neurosci. Methods,* 196(1):201–219, 2011.

[51] N.I. Muskhelishvili. *Singular Integral Equations: Boundary Problems of Function Theory and Their Application to Mathematical Physic.* Dover publications, Mineola, New York, second edition, 1988.

[52] R.B. Nelsen. *An introduction to copulas.* Springer Series in Statistics. Springer, New York, 2006.

[53] B.K. Øksendal. *Stochastic Differential Equations: An introduction with Applications.* Springer–Verlag, Berlin, fifth edition, 2002.

[54] Z. Pawlas, L. B. Klebanov, V. Beneš, M. Prokešová, J. Popelář, and P. Lánský. First-spike latency in the presence of spontaneous activity. *Neural Comput.,* 22(7):1675–1697, 2010.

[55] D.H. Perkel, G.L. Gernstein, and G.P. Moore. Neuronal spike trains and stochastic point processes. I. The Single Spike Train. *Biophys. J.,* 7:391–418, 1967.

[56] D.H. Perkel, G.L. Gernstein, and G.P. Moore. Neuronal spike trains and stochastic point processes. II. Simultaneous Spike Trains. *Biophys. J.,* 7:419–440, 1967.

[57] A. D. Polyanin and A. V. Manzhirov. *Handbook of Integral Equations.* CRC Press, Boca Raton, 1988.

[58] Yu. V. Prokhorov. Convergence of stochastic processes and limit theorems in probability theory. *Theory Probab. Appl.,* 1(2):157–214, 1956.

[59] P.E. Protter. *Stochastic integration and differential equations.* Springer–Verlag, Berlin, second edition, 2005.

[60] S. Redner. *A Guide to First-Passage Processes.* Cambridge University Press, Cambridge, 2001.

[61] L.M. Ricciardi. *Diffusion Processes and Related Topics in Biology*, volume 14 of *Lecture notes in Biomathematics.* Springer–Verlag, Berlin, 1977.

[62] L.M. Ricciardi, A. Di Crescenzo, V. Giorno, and A. Nobile. An outline of theoretical and algorithmic approaches to first passage time problems with applications to biological modeling. *Math. Japon.*, 50:247–321, 1999.

[63] L.M. Ricciardi and S. Sato. Diffusion processes and first-passage-time problems. In *Lectures in Applied Mathematics and Informatics*, chapter 5, pages 206–285. Manchester University Press, Manchester, 1990.

[64] H. Risken. *The Fokker-Planck Equation. Methods of Solution and Applications.* Springer Series in Synergetics. Springer–Verlag, Berlin, 1989.

[65] L. Sacerdote and M.T. Giraudo. Leaky Integrate and Fire models: a review on mathematical methods and their applications. In *Stochastic biomathematical models with applications to neuronal modeling*, volume 2058 of *Lecture Notes in Mathematics*, pages 95 –148. Springer, 2013.

[66] L. Sacerdote and M. Tamborrino. Leaky integrate and fire models coupled through copulas: association properties of the interspike intervals. *Chin. J. Physiol.*, 53(6):396–406, 2010.

[67] L. Sacerdote, M. Tamborrino, and C. Zucca. Detecting dependences between spike trains of pairs of neurons through copulas. *Brain Res.*, 1434:243–256, 2012.

[68] V. Schmitz. *Copulas and Stochastic Processes.* PhD dissertation, Rheinisch-Westfälische Technische Hochschule Aachen. Fakultät für Mathematik. Informatik und Naturwissenschaften, Germany, 2003.

[69] J. P. Segundo. Some thoughts about neural coding and spike trains. *BioSystems*, 58:3–7, 2000.

[70] S.G. Self and K.Y. Liang. Asymptotic properties of maximum likelihood estimators and likelihood ratio tests under nonstandard conditions. *J. Am. Stat. Ass.*, pages 605–610, 1987.

[71] A. Sklar. Fonctions de répartition à n dimensions et leurs marges. *Publ. Inst. Statist. Univ. Paris*, 8:229–231, 1959.

[72] A.V. Skorohod. Limit Theorems for Stochastic Processes. *Theory Probab. Appl.*, 1(3):261–290, 1956.

[73] R.B. Stein. A theoretical analysis of neuronal variability. *Biophys. J.*, 5:173–194, 1965.

[74] F.G. Tricomi. *Integral Equations.* Dover Publications, New York, 1985.

[75] H. C. Tuckwell. *Introduction to theoretical neurobiology. Vol.2: Nonlinear and stochastic theories.* Cambridge Univ. Press, Cambridge, 1988.

[76] N. G. Van Kampen. *Stochastic Processes in Physics and Chemistry.* North-Holland, Amsterdam, 2007.

[77] A.E.P. Villa. Empirical Evidence about Temporal Structure in Multi-Unit Recordings. In *Time and the Brain*, pages 1–51. Harwood Acad, 2000.

[78] A.E.P. Villa and M. Abeles. Evidence for spatiotemporal firing patterns within the auditory thalamus of the cat. *Brain Res.*, 509:325–327, 1990.

[79] A.E.P. Villa, A. Najem, J. Iglesias, I.V. Tetko, and J.L. Eriksson. Spatio-temporal patterns of spike occurrences in freely-moving rats associated to perception of human vowels. *Soc. Neurosci. Abstr.*, 27:166–18, 2001.

[80] W. Whitt. *Stochastic Processes Limits.* Springer-Verlag, New York, 2002.

[81] J. Yan. Enjoy the joy of copulas: with a package copula. *J. Stat. Soft.*, 21(4):1–21, 2007.

Papers

I

The multivariate Ornstein-Uhlenbeck process as a model for neural network activity with refractory periods

Massimiliano Tamborrino
Department of Mathematical Sciences
University of Copenhagen

Laura Sacerdote
Department of Mathematics
University of Turin

Martin Jacobsen
Department of Mathematical Sciences
University of Copenhagen

The multivariate Ornstein-Uhlenbeck process as a model for neural network activity with refractory periods

Massimiliano Tamborrino · Laura Sacerdote · Martin Jacobsen

Abstract We propose a multivariate extension of the Stein Leaky Integrate and Fire model to describe the spontaneous activity of a neural network. The model accounts for the existence of inputs shared by groups of neurons and considers the existence of a refractory period following each spike. The dynamics of the network are described through a multivariate process, whose components evolve according to one-dimensional renewal Stein models, with reset after each spike. To make the model mathematically tractable, a diffusion limit is performed. We prove that the limit process is a multivariate process with dependent components evolving as one-dimensional renewal Ornstein-Uhlenbeck processes. Moreover, we show that the marked point process determined by the exit times of a multivariate jump process with reset, converges weakly to the marked point process determined by the exit times of its diffusion approximation. Examples of neural networks described through the proposed Ornstein-Uhlenbeck process are discussed, showing the ability of the model in reproducing experimental features, such as inhibition, excitation, silencing and synchronization of neurons.

M. Tamborrino
Department of Mathematical Sciences
Universitetsparken 5, DK 2100, Copenhagen, Denmark
Tel.: +45 3532 0732
Fax: +45 3532 0704
E-mail: mt@math.ku.dk

L. Sacerdote
Department of Mathematics
V. Carlo Alberto 8, 10123, Turin, Italy

M. Jacobsen
Department of Mathematical Sciences
Universitetsparken 5, DK 2100, Copenhagen, Denmark

Mathematics Subject Classification (2000) 60B10 · 92B20 · 60J60 · 60G40

1 Introduction

Membrane potential (MP) dynamics of neurons are determined by the arrival of excitatory and inhibitory inputs that increase or decrease the membrane polarization. An action potential, or spike, is a short-lasting event in which the electrical MP of a cell rapidly rises and falls. This is commonly modeled assuming that a spike is generated whenever the MP exceeds a threshold level. After a spike, there is a time interval, called absolute refractory period, during which the neuron cannot fire, even in presence of strong stimulation (Tuckwell, 1988). The neuronal code is related to the times when each neuron fires. The collection of spike epochs of a neuron defines a spike train, and the set of spike trains of groups of neurons is commonly visualized through raster displays.
Mathematical models of single neuron dynamics have played an important role for the understanding of neural coding. Different models account for different levels of complexity in the description of the neuronal MP dynamics. A reasonable compromise between mathematical tractability and biological realism characterizes leaky-integrate-and-fire models. They extend the integrate-and-fire model, proposed by Gerstein and Mandelbrot (1964). They modeled the MP of a neuron through a random walk converging to a Wiener process through a diffusion limit. The intertimes between two consecutive spikes, called Interspike Intervals (ISIs), were modeled as first passage times (FPTs) of the Wiener process through a suitable threshold. Whenever a neuron fired, its MP was reset to its resting potential and the process restarted. This allowed to obtain a renewal process with independent and identically distributed ISIs. For modeling of the MP dynamics, Stein (1965) proposed to use a a birth and death process. The novelty of his model was to account for the spontaneous decay of the MP toward its resting value in absence of incoming inputs. Due to the presence of a leakage constant, this was the first LIF model. However, the study of the FPT properties for birth and death processes presents mathematical difficulties. For this reason, diffusion approximations of the jump processes were proved (Capocelli and Ricciardi, 1971; Kallianpur and Wolpert, 1987; Lansky, 1984; Ricciardi, 1977). Then the resulting models were used for different studies, e.g. the analysis of the role of the noise in neural transmission, the investigation of stochastic resonance phenomena or problems related with the estimation of the response of a neuron (Burkitt, 2006a,b; Lansky and Ditlevsen, 2008; Sacerdote and Giraudo, 2013; Segundo, 2000).

Nowadays simultaneous recordings from many neurons are possible. However, there have been few attempts for developing mathematical models for the description of neural networks. Moreover, the existing ones either are of simulation type, e.g. Izhikevich and Edelman (2007), or oversimplify the features of the single units, to focus on the interactions in the networks, e.g. Alberverio and Cebulla (2008); Watts and Strogatz (1998).

In absence of external inputs, neurons are characterized by spontaneous generation of spikes. The aim of this paper is to propose a multivariate stochastic LIF model to describe the spontaneous activity of neural networks. The model avoids oversimplifications of the single neuron dynamics, considers refractory periods of each component and is able to reproduce different features of neural networks. Analytical methods can be developed for its study, opening interesting mathematical problems, as already happened for one-dimensional models.

Mimicking LIF models for the description of single neurons dynamics, in Section 2 we propose a multivariate generalization of the Stein model for the sub-threshold dynamics of the neurons. The presence of common inputs between clusters of neurons determines dependencies between their dynamics. To reduce the mathematical complexity of the proposed jump processes, in Section 3 we prove its convergence to a multivariate Ornstein-Uhlenbeck (OU) diffusion process. This limit procedure is biologically meaningful when the neuron receives frequent inputs of very small amplitude.

In Section 4, we describe the firing mechanism for the neural network, both ignoring and considering the refractory periods. In Section 5, the weak convergence of the marked point process determined by the crossing times of the multivariate firing Stein model to that determined by the crossing times of its diffusion approximation is shown. More generally, we prove that this result holds for any underlying jump process which converges weakly to a diffusion process.

Due to the presence of common inputs between neurons, both the jump and the diffusion limit processes have dependent components, which determine dependent spike trains, i.e. point processes. Here we limit our study to the multivariate OU model, describing its features and the role of the refractory period, in Section 6. Using simulated data, we show that the proposed model reproduces inhibition, excitation, synchronism or silencing of neurons. Future studies may allow the introduction of analytical tools to complete the analysis of the model.

The mathematical (Sections 3 and 5) and the biological modeling parts (Section 2 and 4) can be read independently from each other, depending on the interest and the scientific background of the reader.

2 Non-firing neural network model

We propose a model for the spontaneous activity of a neural network with k neurons, for $k \in \mathbb{N}$. Their MP dynamics are determined by the arrival of excitatory or inhibitory postsynaptic potentials (PSPs). We model these inputs of constant amplitude $a > 0, b < 0$ through Poisson processes N_j^+, N_j^-, for $1 \leq j \leq k$ and M_A^+, M_A^-, for $A \in \mathcal{A}$. The inputs N_j^+ (intensity α_j) and N_j^- (intensity β_j) are specific for neuron j, while M_A^+ (intensity λ_A) and M_A^- (intensity ω_A) are common to clusters of neurons belonging to a set A. Here $\mathcal{A}$ denotes the set of all subsets of $\{1, \ldots, k\}$ consisting of at least two elements.

In absence of incoming inputs, the MP of each neuron decays spontaneously with time constant $\theta > 0$. For simplifying the notation, throughout the paper we assume θ to be the same in all neurons. This is a common hypothesis since the resistance properties of the neuronal membrane are similar for different neurons (Tuckwell, 1988).

To model the dynamics of the MPs of the neurons of the network, we introduce the process $\mathbf{X} = \{(X_1, \ldots, X_k)(t); t \geq 0\}$, originated in the starting position $x_{0j} \in \mathbb{R}, 1 \leq j \leq k$. Each component X_j, and hence each MP, verifies

$$X_j(t) = x_{0j} - \int_0^t \frac{X_j(s)}{\theta} \, ds + \delta_j \left[a N_j^+(t) + b N_j^-(t) \right]$$
$$+ \sum_{A \in \mathcal{A}} \mathbb{1}_{\{j \in A\}} \delta_{j, A \setminus j} \left[a M_A^+(t) + b M_A^-(t) \right], \tag{1}$$

for $1 \leq j \leq k, \delta_j, \delta_{j, A \setminus j} \in \{-1, 0, 1\}$. When $k = 1$, X is a Stein model. For this reason, we call $\mathbf{X}$ *multivariate* Stein model and eq. (1) Stein equation of the jth component.

The different sign of a and b allows to distinguish between excitatory and inhibitory PSPs. The apexes $+$ and $-$ denote excitatory and inhibitory inputs, respectively. However, an input may also have opposite or no effects on specific neurons. This is modeled as follows.We choose $\delta_{j, A \setminus j} = 0$ if the input has no effect on neurons in A or $\delta_{j, A \setminus j} = -1$ if the same input has opposite effect on neuron $j \in A$. We similarly proceed for δ_j, which only acts on neuron j. The presence of M^+ (or M^-) allows simultaneous jumps for the corresponding set of neurons A, and determines a dependence between their MP evolutions. We call *cluster dynamics* this kind of structure and we limit our paper to this type of dependence between neurons. An example of a neural network with four neurons and dependence due to cluster dynamics is reported in Fig. 1. Note that (1) might be rewritten in a more compact way, summing the Poisson processes with the same jump amplitudes. However, we prefer to distinguish between N and M, to highlight their different role in determining the dependence structure.

3 Weak convergence of the multivariate Stein to the OU process

In the literature (Kallianpur and Wolpert, 1987; Lansky, 1984; Ricciardi, 1977), continuous limits of the univariate Stein process have been proposed to model single neurons receiving frequent and small inputs, e.g. the Purkinje cells. This allowed to replace the Stein with its unidimensional diffusion approximation. Lansky (1984) proved that a sequence of Stein processes converges weakly to an OU process when the input amplitudes decrease to zero and their frequencies diverge in a suitable way. Mimicking the one-dimensional case, we introduce a sequence of multivariate Stein processes $(\mathbf{X}_n)_{n \geq 1}$, with $\mathbf{X}_n = \{(X_{1;n}, \ldots, X_{k;n})(t); t \geq 0\}$ originated in the starting position $\boldsymbol{x}_{0;n} = (x_{01;n}, \ldots, x_{0k;n})$. To do that, we consider a sequence of independent Poisson
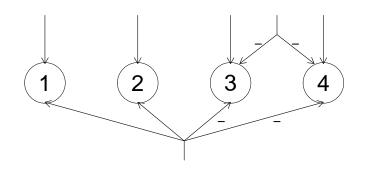
Fig. 1 Schematic representation of a neural network with four neurons. Excitatory inputs act on each neuron, i.e. $\delta_j = 1$, for $1 \leq j \leq 4$. Moreover, common inputs act on two clusters of neurons: $\{1, 2, 3, 4\}$ and $\{3, 4\}$ On cluster $A = \{1, 2, 3, 4\}$, inputs are excitatory on neurons 1 and 2, i.e. $\delta_{1,234} = \delta_{2,134} = 1$, and inhibitory on neurons 3 and 4 (represented by a $-$), i.e $\delta_{3,124} = \delta_{4,123} = -1$. On cluster $A = \{3, 4\}$, inputs are inhibitory on both neurons, i.e. $\delta_{3,4} = \delta_{4,3} = -1$.

processes $N_{j;n}^+$ (intensity $\alpha_{j;n}$), $N_{j;n}^-$ (intensity $\beta_{j;n}$) for $1 \leq j \leq k$, $M_{A;n}^+$ (intensity $\lambda_{A;n}$), $M_{A;n}^-$ (intensity $\omega_{A;n}$) for $A \in \mathcal{A}$. Then, for each $1 \leq j \leq k$, we define $X_{j;n}(t)$ as

$$X_{j;n}(t) = x_{0j;n} - \int_0^t \frac{X_{j;n}(s)}{\theta} \, ds + \delta_j \left[a_n N_{j;n}^+(t) + b_n N_{j;n}^-(t) \right]$$

$$+ \sum_{A \in \mathcal{A}} \mathbb{1}_{\{j \in A\}} \delta_{j, A \setminus j} \left[a_n M_{A;n}^+(t) + b_n M_{A;n}^-(t) \right]. \tag{2}$$

For each $A \in \mathcal{A}$ and

$$\alpha_{j;n} \to \infty, \qquad \beta_{j;n} \to \infty, \qquad \lambda_{A;n} \to \infty, \qquad \omega_{A;n} \to \infty, \tag{3}$$

$$a_n \to 0, \qquad b_n \to 0, \tag{4}$$

we assume that the rates of the Poisson processes fulfill

$$\mu_{j;n} = \alpha_{j;n} a_n + \beta_{j;n} b_n \to \mu_j, \qquad \mu_{A;n} = \lambda_{A;n} a_n + \omega_{A;n} b_n \to \mu_A, \tag{5}$$

$$\sigma_{j;n}^2 = \alpha_{j;n} a_n^2 + \beta_{j;n} b_n^2 \to \sigma_j^2, \qquad \sigma_{A;n}^2 = \lambda_{A;n} a_n^2 + \omega_{A;n} b_n^2 \to \sigma_A^2, \tag{6}$$

as $n \to \infty$. A possible parameter choice satisfying these conditions is

$$a_n = -b_n = \frac{1}{n} \tag{7}$$

$$\alpha_{j;n} = (\mu_j + \frac{\sigma_j^2}{2} n) n, \qquad \beta_{j;n} = \frac{\sigma_j^2}{2} n^2, \qquad 1 \leq j \leq k \tag{8}$$

$$\lambda_{A;n} = (\mu_A + \frac{\sigma_A^2}{2} n) n, \qquad \omega_{A;n} = \frac{\sigma_A^2}{2} n^2, \qquad A \in \mathcal{A}. \tag{9}$$

To prove the weak convergence of $\mathbf{X}_n$, we first define a new process $\mathbf{Z}_n = \{(Z_{1;n}, \ldots, Z_{k;n})(t); t \geq 0\}$, simpler than $\mathbf{X}_n$, which converges to a Wiener process $\mathbf{W} = \{(W_1, \ldots, W_n)(t); t \geq 0\}$, such that $\mathbf{X}_n$ is a continuous functional of $\mathbf{Z}_n$. Each component $Z_{j;n}$, for $1 \leq j \leq k$, is defined by

$$Z_{j;n}(t) = -\Gamma_{j;n} t + \delta_j \left[a_n N_{j;n}^+(t) + b_n N_{j;n}^-(t) \right]$$
$$+ \sum_{A \in \mathcal{A}} \mathbb{1}_{\{j \in A\}} \delta_{j, A \backslash j} \left[a_n M_{A;n}^+(t) + b_n M_{A;n}^-(t) \right],$$

where $\Gamma_{j;n}$ is given by

$$\Gamma_{j;n} = \delta_j \mu_{j;n} + \sum_{A \in \mathcal{A}} \mathbb{1}_{\{j \in A\}} \delta_{j, A \backslash j} \mu_{A;n}, \qquad 1 \leq j \leq k.$$

The characteristic function of $\mathbf{Z}_n(t)$, is:

$$\phi_{\mathbf{Z}_n(t)}(\mathbf{u}) = \mathbb{E} \left[i \exp \left\{ \sum_{j=1}^{k} u_j Z_{j;n}(t) \right\} \right], \qquad (10)$$

where $\mathbf{u} = (u_1, \ldots, u_k) \in \mathbb{R}^k$. We can write:

$$\sum_{j=1}^{k} u_j Z_{j;n}(t) = \sum_{j=1}^{k} u_j \left[-\Gamma_{j;n} t + \delta_j \left(a_n N_{j;n}^+(t) + b_n N_{j;n}^-(t) \right) \right]$$
$$+ \sum_{A \in \mathcal{A}} G_A \left(a_n M_{A;n}^+(t) + b_n M_{A;n}^-(t) \right), \qquad (11)$$

where

$$G_A = \sum_{j \in A} u_j \delta_{j, A \backslash j}.$$

Plugging (11) in (10) and since the processes in (11) are independent and Poisson distributed for each n, we get the characteristic function

$$\phi_{\mathbf{Z}_n(t)}(\mathbf{u}) = \exp\{t \rho_n(\mathbf{u})\},$$

where

$$\rho_n(\mathbf{u}) = -i \sum_{j=1}^{k} u_j \Gamma_{j;n} + \sum_{j=1}^{k} \alpha_{j;n} \left(e^{i u_j \delta_j a_n} - 1 \right) + \sum_{j=1}^{k} \beta_{j;n} \left(e^{i u_j \delta_j b_n} - 1 \right)$$
$$+ \sum_{A \in \mathcal{A}} \lambda_{A;n} \left(e^{i G_A a_n} - 1 \right) + \sum_{A \in \mathcal{A}} \omega_{A;n} \left(e^{i G_A b_n} - 1 \right).$$

In Jacod and Shiryaev (2002), convergence results are proved for $\rho_n(\mathbf{u})$ given by

$$\rho_n(\mathbf{u}) = i \mathbf{u} \cdot \mathbf{b}_n - \frac{1}{2} \mathbf{u} \cdot \mathbf{c}_n \cdot \mathbf{u} + \int_{\mathbb{R}^k \backslash 0} \left(e^{i \mathbf{u} \cdot \mathbf{x}} - 1 - i \mathbf{u} \cdot \mathbf{h}(\mathbf{x}) \right) \nu_n(d\mathbf{x}),$$

(see Corollary II.4.19 in Jacod and Shiryaev (2002)), where $\mathbf{u} \cdot \mathbf{v} = \sum_{j=1}^{k} u_j v_j$ and $\mathbf{u} \cdot \mathbf{d} \cdot \mathbf{v} = \sum_{j,l=1}^{k} u_j d_{jl} v_l$. The vector $\boldsymbol{b}_n$, the matrix $\boldsymbol{c}_n$ and the Lévy measure ν_n are known as characteristic triplet of the process. Here $\mathbf{h} : \mathbb{R}^k \to \mathbb{R}^k$ is an arbitrary truncation function that is the same for all n, is bounded with compact support and satisfies $\mathbf{h}(\mathbf{x}) = \mathbf{x}$ in a neighborhood of $\mathbf{0}$. In our case, the triplet is

1. ν_n: finite measure concentrated on finitely many points,

$$\nu_n\left(\{\mathbf{x} : x_j = \delta_j a_n\}\right) = \alpha_{j;n}, \quad (1 \leq j \leq k, \delta_j \neq 0);$$
$$\nu_n\left(\{\mathbf{x} : x_j = \delta_j b_n\}\right) = \beta_{j;n}, \quad (1 \leq j \leq k, \delta_j \neq 0);$$
$$\nu_n\left(\{\mathbf{x} : x_j = \delta_{j,A\setminus j} a_n\} \text{ for } j \in A\right) = \lambda_{A;n}, \quad \left(A \in \mathcal{A}, \delta_{j,A\setminus j} \neq 0\right);$$
$$\nu_n\left(\{\mathbf{x} : x_j = \delta_{j,A\setminus j} b_n\} \text{ for } j \in A\right) = \omega_{A;n}, \quad \left(A \in \mathcal{A}, \delta_{j,A\setminus j} \neq 0\right).$$

All the non-specified x_j are set to 0, i.e. $\{\mathbf{x} : x_j = \delta_j a_n\} = \{\mathbf{x} : x_j = \delta_j a_n, x_l = 0 \text{ for } l \neq j\}$. Since $a_n \to 0$ and $b_n \to 0$ when n is sufficiently large, ν_n is concentrated on a finite subset of the neighborhood of $\mathbf{0}$, where $\mathbf{h}(\mathbf{x}) = \mathbf{x}$. Without loss of generality, we may therefore, and shall, assume that $\mathbf{h}(\mathbf{x}) = \mathbf{x}$.

2. $\mathbf{c}_n = \mathbf{0}$.

3. $\mathbf{b}_n = -\boldsymbol{\Gamma}_n + \int \mathbf{h}(\mathbf{x})\, \nu_n(d\mathbf{x}) = 0$. Indeed, using $\mathbf{h}(\mathbf{x}) = \mathbf{x}$, we have

$$\begin{aligned}
b_{j;n} &= -\Gamma_{j;n} + (\alpha_{j;n}\delta_j a_n + \beta_{j;n}\delta_j b_n) \\
&\quad + \sum_{A \in \mathcal{A}} \mathbb{1}_{\{j \in A\}}\left(\lambda_{A;n}\delta_{j,A\setminus j} a_n + \omega_{A;n}\delta_{j,A\setminus j} b_n\right) \\
&= 0.
\end{aligned}$$

Having provided the triplet $(\mathbf{b}_n, \mathbf{c}_n, \nu_n)$, we are able to prove the following

Lemma 1 *Under conditions* $(3),(4),(5),(6)$, $\mathbf{Z}_n$ *converges weakly to a multivariate Wiener process* $\mathbf{W}$ *with mean* $\mathbf{0}$ *and covariance matrix* $\boldsymbol{\Psi}$, *with elements*

$$\psi_{jl} = \mathbb{1}_{\{j=l\}}\delta_j^2 \sigma_j^2 + \sum_{A \in \mathcal{A}} \mathbb{1}_{\{j,l \in A\}}\delta_{j,A\setminus j}\delta_{l,A\setminus l}\sigma_A^2, \qquad 1 \leq j,l \leq k \quad (12)$$

Proof Use Theorem VII.3.4 in Jacod and Shiryaev (2002). In our case, the weak convergence of $\mathbf{Z}_n$ to $\mathbf{W}$ follows if

i. $\mathbf{b}_n \to \mathbf{0}$;

ii. $\widetilde{c}_{jl;n} := \int x_j x_l\, \nu_n(d\mathbf{x}) \to \psi_{jl}$ for $1 \leq j,l \leq k$;

iii. $\int g\, d\nu_n \to 0$ for all $g \in C_1\left(\mathbb{R}^k\right)$;

iv. $\mathbf{B}_t^n = t\boldsymbol{b}_n$ and $\tilde{\mathbf{C}}_t^n = t\widetilde{\boldsymbol{c}}_n$ converge uniformly to $\mathbf{B}_t$ and $\tilde{\mathbf{C}}_t$ respectively, on any compact interval $[0,t]$.

Here $C_1\left(\mathbb{R}^k\right)$ is defined in VII.2.7 in Jacod and Shiryaev (2002). Since $\boldsymbol{B}_t^n = t\mathbf{b}_n$, the uniform convergence is evident. Furthermore, $\widetilde{\boldsymbol{C}}_t^n = t\widetilde{\mathbf{c}}_n$ converges uniformly provided that condition [ii] holds.

To prove [ii], we note that

$$
\begin{aligned}
\widetilde{c}_{jl;n} &= \sum_{i=1}^{k} \left(\mathbb{1}_{\{i=l=j\}} \alpha_{j;n} \delta_j^2 a_n^2 + \mathbb{1}_{\{i=l=j\}} \beta_{j;n} \delta_j^2 b_n^2 \right) \\
&+ \sum_{A \in \mathcal{A}} \mathbb{1}_{\{j,l \in A\}} \left(\lambda_{A;n} \delta_{j,A \setminus j} \delta_{l,A \setminus l} a_n^2 + \omega_{A;n} \delta_{j,A \setminus j} \delta_{l,A \setminus l} b_n^2 \right) \\
&= \mathbb{1}_{\{j=l\}} \delta_j^2 \sigma_{j;n}^2 + \sum_{A \in \mathcal{A}} \mathbb{1}_{\{j,l \in A\}} \delta_{j,A \setminus j} \delta_{l,A \setminus l} \sigma_{A;n}^2.
\end{aligned}
\tag{13}
$$

Then, $\widetilde{c}_{jl;n} \to \psi_{jl}$ follows from the convergence assumptions $(3), (4), (5), (6)$. Using Theorem VII.2.8 in Jacod and Shiryaev (2002), we may show [iv] considering $g \in C_3\left(\mathbb{R}^k\right)$, i.e. the space of bounded and continuous function $g : \mathbb{R}^k \to \mathbb{R}$ such that $g(\mathbf{x}) = o\left(|\mathbf{x}|^2\right)$ as $\mathbf{x} \to 0$. Here, $|\mathbf{x}|$ is the Euclidean norm. For $g \in C_3\left(\mathbb{R}^k\right)$ and $\varepsilon > 0$, we have $|g(\mathbf{x})| \leq \varepsilon |\mathbf{x}|^2$ for $|\mathbf{x}|$ sufficiently small. Then

$$
\left| \int g \, d\nu_n \right| \leq \varepsilon \int |\mathbf{x}|^2 \, d\nu_n \to \varepsilon \sum_{i=1}^{k} \psi_{ii}
$$

by (13), and $\int g \, d\nu_n \to 0$ follows. Indeed, since $\mathbf{W}$ is continuous, the Lévy measure ν for $\mathbf{W}$ is the null measure.

We are now able to prove the following

Theorem 1 *Let $\boldsymbol{x}_{0;n}$ be a sequence in $\mathbb{R}^k$ converging to $\boldsymbol{y}_0 = (y_{01}, \ldots, y_{0k})$. Then, the sequence of processes $\mathbf{X}_n$ defined by (2) with rates fulfilling $(5), (6)$, under conditions $(3), (4)$, converges weakly to the multivariate OU diffusion process $\mathbf{Y}$ given by*

$$
Y_j(t) = y_{0j} + \int_0^t \left[-\frac{Y_j(s)}{\theta} + \Gamma_j \right] ds + W_j(t), \qquad 1 \leq j \leq k, \tag{14}
$$

where Γ_j is defined by

$$
\Gamma_j = \delta_j \mu_j + \sum_{A \in \mathcal{A}} \delta_{j,A \setminus j} \mu_A, \qquad 1 \leq j \leq k, \tag{15}
$$

and $\mathbf{W}$ is the k-dimensional Wiener process with mean $\mathbf{0}$ and covariance matrix $\boldsymbol{\Psi}$ defined in (12).

Proof The jth component of $\mathbf{X}_n$ can be rewritten in terms of the j-th component of $\mathbf{Z}_n$ as

$$
X_{j;n}(t) = x_{0j;n} + \int_0^t \left[-\frac{X_{j;n}(s)}{\theta} + \Gamma_{j;n} \right] ds + Z_{j;n}(t), \qquad 1 \leq j \leq k. \tag{16}
$$

Solving it, we get

$$X_{j;n}(t) = x_{0j;n}e^{-\frac{t}{\theta}} + Z_{j;n}(t) - \frac{1}{\theta}\int_0^t e^{-(t-s)/\theta}Z_{j;n}(s)ds, \qquad 1 \le j \le k.$$

Hence, $\mathbf{X}_n$ is a continuous functional of both $\boldsymbol{x}_{0;n}$ and $\mathbf{Z}_n$. Therefore, due to the continuous mapping theorem (Lindvall, 2002), the weak convergence of $\boldsymbol{x}_{0;n}$ (for hypothesis) and $\mathbf{Z}_n$ (from Lemma 1) implies the weak convergence of $\mathbf{X}_n$. Moreover, (16) guarantees that the limiting process of $\mathbf{X}_n$ is that defined by (14).

Remark 1 Theorem 1 also holds when $(\boldsymbol{x}_{0;n})_{n\ge 1}$ is a random sequence converging to a random vector $\boldsymbol{y}_0$.

Denote $E \overset{d}{=} F$ two random variables that are identically distributed and consider the space $\mathcal{D}^k = \mathcal{D}\left([0,\infty[,\mathbb{R}^k\right)$, i.e. the space of functions $f : [0,\infty) \to \mathbb{R}^k$ that are right continuous and have a left limit at each $t \ge 0$. The following corollary can be introduced:

Corollary 1 *If $\boldsymbol{X}_n$ converges weakly to $\boldsymbol{Y}$, there exists a probability space $(\Omega, \mathcal{F}, \mathbf{P})$ and random elements $\left(\widetilde{\boldsymbol{X}}_n\right)_{n=1}^{\infty}$, $\widetilde{\boldsymbol{Y}}$ in the Polish space $\mathcal{D}^k$, defined on $(\Omega, \mathcal{F}, \mathbf{P})$ such that $\mathbf{X}_n \overset{d}{=} \widetilde{\mathbf{X}}_n, \mathbf{X} \overset{d}{=} \widetilde{\mathbf{Y}}$ and $\widetilde{\mathbf{X}}_n \to \widetilde{\mathbf{Y}}$ a.s. as $n \to \infty$.*

Proof From its definition, $\mathbf{X}_n$ belongs to $\mathcal{D}^k$. This space is a Polish space with the Skorohod topology (Lindvall, 2002). Then, the corollary follows from the previous theorem, applying the Skorohod's representation theorem.

4 Firing neural network model

The spiking mechanism of a single neuron is modeled with the introduction of a firing threshold B: a neuron releases a spike when its MP attains the threshold value. In absence of refractory period, the MP is instantaneously reset to its resting value $r_0 \in (-\infty, B)$ and the dynamics restarts. The ISIs are modeled as FPTs of the process through the boundary. Since the ISIs of the single neuron are independent and identically distributed, the underlying process is renewal. The firing mechanism for single neurons has also been defined in presence of absolute refractory periods $\Delta > 0$. The MP is reset to its resting value r_0 after a time delay Δ and then the MP evolution restarts. During the absolute refractory period, spikes cannot occur. The underlying process describing the MP evolution is still renewal and then the intertimes between two consecutive resets are independent and identically distributed.

Here we extend the single neuron firing mechanism, defining a firing mechanism of networks of k neurons, both ignoring the absolute refractory period, i.e. $\Delta = 0$, or taking it into account, i.e. $\Delta > 0$. In both cases, we denote $r_{0j} < B_j$ the resting potential of the jth neuron of the network and we use the multivariate Stein model to describe the MP dynamics. A schematic illustration is reported in Fig. 2.

Firing mechanism of neural networks for $\Delta = 0$. Consider a neural network described through a multivariate Stein model. A neuron j, $1 \leq j \leq k$ releases a spike when the MP attains its boundary level B_j. Whenever it fires, its MP is instantaneously reset to its resting potential r_{0j} and then its dynamics restart. Meanwhile, the other components are not reset but continue their evolutions. Since the inputs are modeled by stationary Poisson processes, the ISIs within each neuron are independent and identically distributed. Thus the firing single neuron mechanism holds for each component, which is described as a one-dimensional renewal Stein model. The firing neural network model is described by a multivariate process of MPs behaving as a multivariate Stein process between two consecutive FPTs. For this reason, we call this model, *firing multivariate Stein model.* Note that the ISIs of the multivariate processes are neither independent nor identically distributed. We identify the spike epochs of the jth component of the Stein process, as the FPT of $X_{j,n}$ through the boundary B_j, with $B_j > r_{0j}$. The set of spike trains of all neurons corresponds to a multivariate point process with events given by the spikes and we call it *multivariate Stein point process.* An alternative way of considering the simultaneously recorded spike trains is to overlap them, marking each spike with the component which generates it. Thus, we obtain a univariate point process with marked events, that we call *marked Stein point process.*
Note that the multivariate Stein model allow the presence of simultaneous firings. They may happen when common inputs determine the simultaneous crossings of the respective boundaries of two or more components of the multivariate firing Stein model.

Firing mechanism of neural networks for $\Delta > 0$. The only difference with respect to the previous case is that whenever a neuron $j, 1 \leq j \leq k$ fires, its MP returns to a given resting potential r_{0j} after a time Δ. That is, the reset is not instantaneous but shifted a delay Δ, during which neuron j cannot fire. During the absolute refractory period of neuron j, the other neurons can fire. Also in this case, simultaneous spikes of two or more neurons can be observed.

5 Weak convergence of the marked point processes

In Section 3 we performed a diffusion limit on a sequence of multivariate Stein models to obtain a multivariate OU model describing the dynamics of a neural network in absence of spiking mechanism. This procedure was motivated by the difficulty in developing mathematical tools for the study of multivariate jump processes. The same problem arises for the study of the firing multivariate Stein model, which is denoted by $\boldsymbol{X}_n^*$ and is a k-dimensional Markov process, when $\Delta = 0$, and the related marked Stein point process. For this reason, we introduce the firing multivariate OU model, denoted by $\boldsymbol{Y}^*$, which is determined by the multivariate OU process as done in Section 4 for the Stein process. Similarly, we call *multivariate OU point process* and *marked*
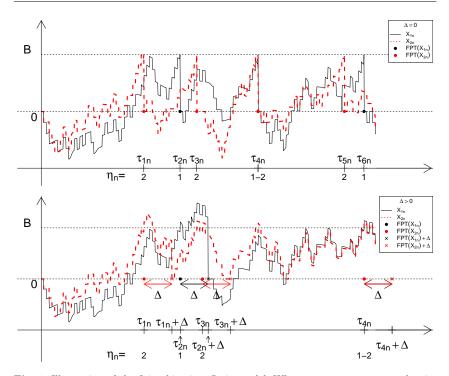
Fig. 2 Illustration of the firing bivariate Stein model. Whenever a component reaches its threshold, it is reset to its resting value, either istantaneously (Top figure) or with a time delay Δ (Bottom figure), called refractory period, during which that component cannot have a second spike. Here $\tau_{i,n}$ denotes the ith FPT of the process, obtained in the component $\eta_{i,n}$. Note that simultaneous spikes are observed in $\tau_{4,n}$.

OU point process the processes whose events are the crossings of $\boldsymbol{Y}^*$ through the boundary $\boldsymbol{B}$. Note that also $\boldsymbol{Y}^*$ is a k-dimensional Markov process. The aims of this section are to show the convergence of a sequence of multivariate firing Stein models to a multivariate firing OU model and the convergence of the corresponding univariate marked point processes. Four main difficulties arise:

- due to the reset of the firing component, the multivariate firing OU is not a diffusion because it is not continuous;
- the ISIs of each component are independent and identically distributed, but they depend on the ISIs of other components;
- after a spike, the firing component j is reset to r_{0j} and restarts its evolution, while the other components start from random positions;
- assume $\Delta > 0$. During the absolute refractory period of neuron j, the other neurons may release spikes.

These problems suggest to prove the convergence results in suitable time windows, which change depending on whether $\Delta = 0$ or $\Delta > 0$. For mathematical

convenience, the convergence of the point processes is proved for the marked
point process instead of those multivariate.

5.1 Definition of the involved processes

We define $\boldsymbol{X}_n^*$ introducing a sequence $\left(\mathbf{X}_n^{(m)}\right)_{m\geq 1}$ of multivariate Stein pro-
cesses, with $\mathbf{X}_n^{(m)}$ defined on the mth time window. Set $\mathbf{X}_n^{(1)} \equiv \mathbf{X}_n$. Condition-
ally on $\left(\mathbf{X}_n^{(1)}, \ldots, \mathbf{X}_n^{(m)}\right)$, $\mathbf{X}_n^{(m+1)}$ is given by (2) with $x_{0j;n}$ random value de-
termined by $\left(\mathbf{X}_n^{(1)}, \ldots, \mathbf{X}_n^{(m)}\right)$ and with the Poisson processes $\mathbf{N}_{j;n}^{\pm}$ and $\mathbf{M}_{A;n}^{\pm}$
stochastically independent of $\left(\mathbf{X}_n^{(1)}, \ldots, \mathbf{X}_n^{(m)}\right)$, for $m \geq 1$. Similarly, we define
$\mathbf{Y}^*$ by introducing a sequence $\left(\mathbf{Y}^{(m)}\right)_{m\geq 1}$ of multivariate OU processes. Set
$\mathbf{Y}^{(1)} \equiv \mathbf{Y}$. Conditionally on $\left(\mathbf{Y}^{(1)}, \ldots, \mathbf{Y}^{(m)}\right)$, $\mathbf{Y}^{(m+1)}$ is given by (13) with
y_{0j} random value determined by $\left(\mathbf{Y}^{(1)}, \ldots, \mathbf{Y}^{(m)}\right)$ and with the k-dimensional
Brownian motion $(\mathbf{W}_1, \ldots, \mathbf{W}_k)$ independent of $\left(\mathbf{Y}^{(1)}, \ldots, \mathbf{Y}^{(m)}\right)$, for $m \geq 1$.
Below we shall briefly say that $\mathbf{X}_n^{(m+1)}$ (or $\mathbf{Y}^{(m+1)}$) is obtained by conditional
independence and then specify the initial value $x_{0j;n}$ (or y_{0j}).

We denote $T_{j,n}$ the spike epoch of the jth component of the Stein process,
and we identify it with the FPT of $X_{j;n}$ through the boundary B_j, with
$B_j > x_{0j;n}$. That is

$$T_{j,n} = T_{B_j}(X_{j;n}) = \inf\{t > 0 : X_{j;n}(t) > B_j\}.$$

Furthermore, we denote $\tau_{1,n}$ the minimum of the FPTs of the multivariate
Stein process $\boldsymbol{X}_n$, i.e.

$$\tau_{1,n} = \min\left(T_{1,n}, \ldots, T_{k,n}\right).$$

Finally we denote $\eta_{1,n} \in \{1, \ldots, k\}$ the discrete random variable specifying
which component of the Stein process reaches the boundary at time $\tau_{1,n}$.
Similarly, we define T_j, τ_1, η_1 for the process $\boldsymbol{Y}$.
Now we are able to define recursively $\boldsymbol{X}_n^*$ and $\boldsymbol{Y}^*$ on the successive time
windows $m \geq 1$, and to formally define the multivariate firing mechanism. A
schematic illustration of the involved random variables is given in Fig. 2.

Firing mechanism of neural networks for $\Delta = 0$

Step $m = 1$. Define $\boldsymbol{X}_n^*(t) = \boldsymbol{X}_n(t)$ on the interval $[0, \tau_{1,n}[$ and $\boldsymbol{Y}^*(t) = \boldsymbol{Y}(t)$ on $[0, \tau_1[$,
with resting potential $\boldsymbol{X}_n^*(0) = \boldsymbol{r}_0 = \boldsymbol{Y}^*(0)$. It is assumed that only one
neuron fires at time $\tau_{1,n}$ which is sufficient for the asymptotic $n \to \infty$.
Then, if $\eta_{1,n} = j$, define $X_{i,n}^*(\tau_{1,n}) = X_{i,n}(\tau_{1,n})$ if $i \neq j$ or r_{0j} if $i = j$. If
$\eta_1 = j$, define $Y_i^*(\tau_1) = Y_i(\tau_1)$ if $i \neq j$ or r_{0j} if $i = j$.

Step $m = 2$. If $\eta_{1,n} = j$, obtain $\mathbf{X}_n^{(2)}$ by conditional independence from $\mathbf{X}_n^{(1)}$, with initial value $\boldsymbol{x}_{0;n} = \mathbf{X}_n^*(\tau_{1,n})$. Similarly, if $\eta_1 = j$, obtain $\mathbf{Y}^{(2)}$ by conditional independence from $\mathbf{Y}^{(1)}$, with initial value $\boldsymbol{y}_0 = \mathbf{Y}^*(\tau_1)$. Then, define $T_{j,n}^{(2)}, \tau_{2,n}, \eta_{2,n}$ from $\mathbf{X}_n^{(2)}$ and $T_j^{(2)}, \tau_2, \eta_2$ from $\mathbf{Y}^{(2)}$, for $m = 1$. Define $\mathbf{X}_n^*(t) = X_n^{(2)}(t - \tau_{1,n})$ on the interval $[\tau_{1,n}, \tau_{1,n} + \tau_{2,n}[$ and $\mathbf{Y}^*(t) = \mathbf{Y}(t - \tau_1)$ on $[\tau_1, \tau_1 + \tau_2[$. Then, if $\eta_{2,n} = j$, define $X_{i,n}^*(\tau_{1,n} + \tau_{2,n}) = X_{i,n}^{(2)}(\tau_{2,n})$ if $i \neq j$ or r_{0j} if $i = j$. Similarly, if $\eta_2 = j$, define $Y_i^*(\tau_1 + \tau_2) = Y_i^{(2)}(\tau_2)$ if $i \neq j$ or r_{0j} if $i = j$.

Step $m > 2$. If $\eta_{m,n} = j$, obtain $\mathbf{X}_n^{(m)}$ by conditional independence from $\mathbf{X}^{(m-1)}$, with initial value $\boldsymbol{x}_{0;n} = \mathbf{X}_n^*(\sum_{l=1}^{m-1} \tau_{l,n})$. Similarly, if $\eta_m = j$, obtain $\mathbf{Y}^{(m)}$ by conditional independence from $\mathbf{Y}^{(m-1)}$, with initial value $\boldsymbol{y}_0 = \mathbf{Y}^*(\sum_{l=1}^{m-1} \tau_l)$. Define, $T_{j,n}^{(m)}, \tau_{m,n}, \eta_{m,n}$ from $\mathbf{X}_n^{(m)}$ and $T_j^{(m)}, \tau_m, \eta_m$ from $\mathbf{Y}^{(m)}$ as above. Define $\mathbf{X}_n^*(t) = \mathbf{X}_n^{(m)}(t - \sum_{l=1}^{m-1} \tau_{l,n})$ for $t \in [\sum_{l=1}^{m-1} \tau_{l,n}, \sum_{l=1}^{m} \tau_{l,n}[$ and $\mathbf{Y}^*(t) = \mathbf{Y}^{(m)}(t - \sum_{l=1}^{m-1} \tau_l)$ for $t \in [\sum_{l=1}^{m-1} \tau_l, \sum_{l=1}^{m} \tau_l[$. Then, if $\eta_{m,n} = j$, define $\mathbf{X}_{i,n}^*(\sum_{l=1}^{m} \tau_{l,n}) = X_{i,n}^{(r)}(\tau_{m,n})$ if $i \neq j$ or r_{0j} if $i = j$. Similarly, if $\eta_m = j$, define $Y_i^*(\sum_{l=1}^{m} \tau_l) = Y_i^{(m)}(\tau_m)$ if $i \neq j$ or r_{0j} if $i = j$.

Firing mechanism of neural networks for $\Delta > 0$. Also in this scenario, the construction of $\mathbf{X}_n^*$ and $\mathbf{Y}^*$ is recursive, even if more complicated for the shifted reset of the firing component $j, 1 \leq j \leq k$. During the absolute refractory period, neuron j cannot fire, while several spikes from the other neurons can be observed. The process $\mathbf{X}_n^*$ needs to be specified on three different time windows, namely $[\tau_{i,n}, \tau_{i+1i,n}[, [\tau_{j,n}, \tau_{i,n} + \Delta[, [\tau_{i,n} + \Delta, \tau_{j,n}[$, with $i \leq j$ and likewise for $\mathbf{Y}^*$. Then $\mathbf{X}_n^*$ ($\mathbf{Y}*$) is constructed considering which component is firing, i.e. $\eta_{i,n}$ (η_i), when is firing, i.e. $\tau_{i,n}$ (τ_i), what is the type of time interval where the process is observed and what is the corresponding starting position.

As previously observed, for simplifying the notation, the refractory period Δ is considered fixed and equal for all neurons. But this choice is not a shortcoming, since the proofs can be extended to the case refractory periods to depend on the neurons, e.g. considering $\Delta_{\eta_{i,n}}$ and Δ_{η_i}.

5.2 Main results

To show the weak convergence of the multivariate firing processes and their related marked point processes, proceed as follows. Consider the spaces $\mathcal{D}^1$ and $\mathcal{C}^1 = \mathcal{C}([0, \infty[, \mathbb{R})$ and for $y^\circ \in \mathcal{C}^1$, define the hitting time

$$\widetilde{T}_B(y^\circ) = \inf\{t > 0 : y^\circ(t) = B\},$$

and introduce the sets

$$H = \left\{y^\circ \in \mathcal{C}^1 : T_B(y^\circ) = \widetilde{T}_B(y^\circ)\right\},$$

and
$$H^k = \left\{ \boldsymbol{y}^\circ \in \mathcal{C}^k : T_{B_j}\left(y_j^\circ\right) = \widetilde{T}_{B_j}\left(y_j^\circ\right) \text{ for all } 1 \le j \le k \right\}.$$

The weak convergence of the multivariate models and their point processes corresponds to the weak convergence of the finite dimensional distributions of $(\boldsymbol{\tau}_n; \mathbf{X}_n^*(\boldsymbol{\tau}_n), \boldsymbol{\eta}_n)$ to $(\boldsymbol{\tau}; \mathbf{Y}^*(\boldsymbol{\tau}), \boldsymbol{\eta})$, where $\boldsymbol{\tau}_n = (\tau_{1,n}, \ldots, \tau_{l,n}), \mathbf{X}_n^*(\boldsymbol{\tau}_n) = (\mathbf{X}_n^*(\tau_{1,n}), \ldots, \mathbf{X}_n^*(\tau_{l,n})), \boldsymbol{\eta}_n = (\eta_{1,n}, \ldots, \eta_{l,n}), \boldsymbol{\tau} = (\tau_1, \ldots, \tau_l),$
$\mathbf{Y}^*(\boldsymbol{\tau}) = (\mathbf{Y}^*(\tau_1), \ldots, \mathbf{Y}^*(\tau_l))$ and $\boldsymbol{\eta} = (\eta_1, \ldots, \eta_l)$, for any $l \in \mathbb{N}$. The convergence does not follow directly from the convergence of the processes. Indeed, the FPT is not a continuous function of the process. Remember that, due to the reset of the firing components, the process $\mathbf{Y}^*$ is neither continuous nor a diffusion.

To prove the main theorem, we need some lemmas.

Lemma 2 *Let x_n° belong to $\mathcal{D}^1$ for $n \ge 1$, and $y^\circ \in H$ with $y^\circ(0) < B$. If $x_n^\circ \to y^\circ$ in $\mathcal{D}^1$, then $T_B\left(x_n^\circ\right) \to T_B\left(y^\circ\right)$.*

Proof For each $s < T_B\left(y^\circ\right)$, $\sup_{t \le s} y^\circ(t) < B$ and since $x_n^\circ \to y^\circ$ uniformly on $[0, s]$, also $\sup_{t \le s} x_n^\circ(t) < B$ for n sufficiently large. This implies

$$\lim_{n \to \infty} \inf T_B\left(x_n^\circ\right) \ge s \text{ for all } s < T_B\left(y^\circ\right)$$
$$\Rightarrow \lim_{n \to \infty} \inf T_B\left(x_n^\circ\right) \ge T_B\left(y^\circ\right).$$

Because $y^\circ \in H$ we can find a sequence t_k such that $t_k \downarrow T_B\left(y^\circ\right) = \widetilde{T}_B\left(y^\circ\right)$ (with $y^\circ\left(\widetilde{T}_B\left(y^\circ\right)\right) = B$) and $y^\circ\left(t_k\right) > B$ for all k. Since $x_n^\circ\left(t_k\right) \to y^\circ\left(t_k\right)$ for all k, it follows that $T_B\left(x_n^\circ\right) \le t_k$ for n sufficiently large and therefore

$$\forall k, \; \lim_{n \to \infty} \sup T_B\left(x_n^\circ\right) \le t_k$$
$$\Rightarrow \lim_{n \to \infty} \sup T_B\left(x_n^\circ\right) \le T_B\left(y^\circ\right).$$

Lemma 3 *Let $\boldsymbol{x}_n^\circ$ belong to $\mathcal{D}^k$ for $n \ge 1$, $\boldsymbol{y}^\circ \in H^k$ with $\boldsymbol{y}^\circ(0) < \boldsymbol{B}$. If $\boldsymbol{x}_n^\circ \to \boldsymbol{y}^\circ$ in $\mathcal{D}^k$, then*

$$(\tau_{1,n}^\circ; \boldsymbol{x}_n^\circ(\tau_{1,n}^\circ); \eta_{1,n}^\circ) \to (\tau_1^\circ; \boldsymbol{y}^\circ(\tau_1^\circ); \eta_1^\circ). \tag{17}$$

Proof If $\eta_1^\circ = j$, then $\eta_{1,n}^\circ = j$ for n large enough, since marginally $x_{i;n}^\circ \to y_{i;n}^\circ$ for each component $1 \le i \le k$. By Lemma 2 and since $y_j^\circ(0) < B_j$ by assumption, it follows

$$\tau_{1,n}^\circ = T_{B_j}\left(x_{j,n}^\circ\right) \to T_{B_j}\left(y_j^\circ\right) = \tau_1^\circ. \tag{18}$$

Moreover, it holds

$$|x_{i,n}^\circ(\tau_{1,n}^\circ) - y_i^\circ(\tau_1^\circ)| \le |x_{i,n}^\circ(\tau_{1,n}^\circ) - y_i^\circ(\tau_{1,n}^\circ)| + |y_i^\circ(\tau_{1,n}^\circ) - y_i^\circ(\tau_1^\circ)|, \tag{19}$$

which goes to zero when $n \to \infty$, for any $1 \le i \le k$. Indeed, for each $s < \tau_1^\circ$, the strong convergence of $x_{i,n}^\circ$ to y_i° on a compact time interval $[0, s]$ implies

the uniform convergence of $x_{i,n}^\circ$ to y_i° on $[0, s]$. Thus $x_{i,n}^\circ(\tau_{1,n}^\circ) - y_i^\circ(\tau_{i,n}^\circ) \to 0$. From (18) and since y_i° is continuous, the second addend on the right hand side of (19) goes to zero when $n \to \infty$ for the continuous mapping theorem. Using the product topology on $\mathcal{D}^k$, we have that $\boldsymbol{x}_n^\circ \to \boldsymbol{y}^\circ$ in $\mathcal{D}^k$ if $x_{j;n}^\circ \to y_{j;n}^\circ$ in $\mathcal{D}^1$, for each $1 \leq j \leq k$ (Whitt, 2002), implying the thesis.

Note that the firing component has not been reset. Now, we are able to prove the main result on the weak convergence of the marked point process of $\boldsymbol{X}_n^*$ to that of $\boldsymbol{Y}^*$ in absence of refractory period:

Theorem 2 *The finite dimensional distributions of $(\boldsymbol{\tau}_n; \mathbf{X}_n^*(\boldsymbol{\tau}_n), \boldsymbol{\eta}_n)$ converge weakly to those of $(\boldsymbol{\tau}; \mathbf{Y}^*(\boldsymbol{\tau}), \boldsymbol{\eta})$.*

Proof By definition of the multivariate firing Stein and OU models, we can apply Theorem 1 and Corollary 1 in any of the time intervals between two consecutive FPTs. Therefore, between two consecutive passage times, there exist $\widetilde{\boldsymbol{X}}_n^*$ and $\widehat{\boldsymbol{Y}}^*$ such that $\widetilde{\boldsymbol{X}}_n^* \stackrel{d}{=} \boldsymbol{X}_n^*$ and $\widehat{\boldsymbol{Y}}^* \stackrel{d}{=} \boldsymbol{Y}^*$ and $\widetilde{\boldsymbol{X}}_n^*$ converges strongly to $\widetilde{\boldsymbol{Y}}^*$. Define $\widetilde{\eta}_{j;n}, \widetilde{\tau}_{j;n}$ from $\widetilde{\boldsymbol{X}}_n^*$ and $\widetilde{\eta}_j, \widetilde{\tau}_j$ from $\widetilde{\boldsymbol{Y}}^*$ as done in Section 4. The theorem is proved if

$$(\widetilde{\boldsymbol{\tau}}_n; \widetilde{\mathbf{X}}_n^*(\widetilde{\boldsymbol{\tau}}_n), \widetilde{\boldsymbol{\eta}}_n) \to (\widetilde{\boldsymbol{\tau}}; \widetilde{\mathbf{Y}}^*(\widetilde{\boldsymbol{\tau}}), \widetilde{\boldsymbol{\eta}}) \text{ a.s.} \tag{20}$$

holds. Assume that $\widetilde{\eta}_m = j$ and thus $\widetilde{\eta}_{m,n} = j$ for n sufficiently large, due to the strong convergence of the processes. If (20) is true, we would have

$$\widetilde{\tau}_{m,n} = T_{B_j}\left(\widetilde{X}_{j,n}^*\right) \stackrel{d}{=} T_{B_j}\left(X_{j,n}^*\right) = \tau_{m,n}, \quad \widetilde{\tau}_m = T_{B_j}\left(\widetilde{Y}_j^*\right) \stackrel{d}{=} T_{B_j}\left(Y_j^*\right) = \tau_m,$$

since $\widetilde{\mathbf{X}}_n^* \stackrel{d}{=} \mathbf{X}_n^*$ and $\widetilde{\mathbf{Y}}^* \stackrel{d}{=} \mathbf{Y}^*$ between two successive FPTs, which would also imply $\widetilde{\mathbf{X}}_n^*(\widetilde{\tau}_{m,n}) \stackrel{d}{=} \mathbf{X}_n^*(\tau_{m,n})$ and $\widetilde{\mathbf{Y}}^*(\widetilde{\tau}_m) \stackrel{d}{=} \mathbf{Y}^*(\tau_m)$, for any $1 \leq m \leq l$ and $l \in \mathbb{N}$, and thus the thesis.

To prove (20), we proceed recursively in each time window between two consecutive passage times:

Step $m = 1$. Since $\widetilde{\boldsymbol{Y}}^*(0) < \boldsymbol{B}$ by assumption, Lemma 3 holds if we show that $\widetilde{\boldsymbol{Y}}^* \in H^k$. By definition, $\widetilde{\boldsymbol{Y}}^*$ behaves like the multivariate OU diffusion $\boldsymbol{Y}$ in $[0, \widetilde{\tau}_1[$. It is well known that each one-dimensional diffusion component $\widetilde{Y}_j$ will cross the level B_j infinitely often immediately after $\widetilde{T}_B(\widetilde{Y}_j)$, so that indeed $T_{B_j}(\widetilde{Y}_j) = \widetilde{T}_{B_j}(\widetilde{Y}_j)$, for all $1 \leq j \leq k$. Hence $\widetilde{\boldsymbol{Y}}^* \in H^k$. Then it holds the convergence of the triplets (17) with not-reset firing components. This convergence also holds if we reset the firing components. Indeed, assume $\widetilde{\eta}_1 = j$ and then $\widetilde{\eta}_{1,n} = j$ for n large enough. Then

$$\widetilde{X}_{j;n}^*(\widetilde{\tau}_{1,n}) = r_{0,\widetilde{\eta}_{1,n}} = \widetilde{Y}_j^*(\widetilde{\tau}_1), \tag{21}$$

and thus $\widetilde{\boldsymbol{X}}_n^*(\widetilde{\tau}_{1,n}) \to \widetilde{\boldsymbol{Y}}^*(\widetilde{\tau}_1)$, implying (20).

Step $m = 2$. On $[\widetilde{\tau}_{1,n}, \widetilde{\tau}_{1,n} + \widetilde{\tau}_{2,n}[$, $\widetilde{\boldsymbol{X}}_n^*$ is obtained by conditionally independence from $\widetilde{\boldsymbol{X}}_n^*$ on $[0, \widetilde{\tau}_{1,n}[$, with initial value $\widetilde{\boldsymbol{x}}_{0;n} = \widetilde{\boldsymbol{X}}^*(\tau_{1,n})$. Similarly, on $[\widetilde{\tau}_1, \widetilde{\tau}_1 + \widetilde{\tau}_2[$, $\widehat{\boldsymbol{Y}}^*$ in obtained by conditionally independence from $\widehat{\boldsymbol{Y}}^*$ on $[\widetilde{\tau}_1, \widetilde{\tau}_1 + \widetilde{\tau}_2[$, with initial value $\widetilde{\boldsymbol{y}}_0 = \widehat{\boldsymbol{Y}}^*(\widetilde{\tau}_1)$. From Step $m = 1$, $\widetilde{\boldsymbol{X}}^*(\widetilde{\tau}_{1,n}) \to \widetilde{\boldsymbol{Y}}^*(\widetilde{\tau}_1)$; since $\widetilde{\boldsymbol{Y}}^*(\widetilde{\tau}_1) < \boldsymbol{B}$ and $\widetilde{\boldsymbol{Y}}^* \in H^k$, Lemma 3 can be applied. Then, (20) follows noting that (17) also holds if we reset the firing components $\widetilde{\eta}_{2,n}$ and $\widetilde{\eta}_2$, as done in (21).

Step $m > 2$ It follows mimicking Step 2.

Corollary 2 *The weak convergence of the marked point processes hold in presence of refractory periods $\Delta > 0$.*

Proof (Sketch) It can be proved mimicking the proof of Theorem 2. However, two new mathematical difficulties arise. First, during the refractory period of a component, there may happen several crossings of the other components. Second, one has to show that $\boldsymbol{X}_n^*(\boldsymbol{\tau}_n + \Delta)$ converges weakly to $\boldsymbol{Y}^*(\boldsymbol{\tau} + \Delta)$, i.e. there is a convergence of the processes with shifted reset. The first problem is solved applying Lemma 3 in all the time windows, resetting the firing component with a delay Δ from its spike epoch. The second is solved replacing τ. with $\tau. + \Delta$ in (19) and using the continuous mapping theorem on $\tau. + \Delta$.

Remark 2 The results in this Section are not built ad-hoc for the multivariate Stein and the OU models, but hold for any k-dimensional jump process $\mathbb{X}_n$ which converges weakly to a diffusion process $\mathbb{Y}$.

Denote $\mathbb{X}^*$ ($\mathbb{Y}^*$) the process constructed recursively from $\mathbb{X}_n$ ($\mathbb{Y}$), as done in Section 4. Then, it holds

Corollary 3 *The finite dimensional distributions of $(\boldsymbol{\tau}_n, \mathbb{X}_n^*, \boldsymbol{\eta}_n)$ converge weakly to those of $(\boldsymbol{\tau}, \mathbb{Y}^*, \boldsymbol{\eta})$, both when $\Delta = 0$ and $\Delta > 0$.*

Proof The thesis follows noting that the proof of Theorem 2 holds for any limiting process belonging to H^k, between two consecutive spikes. But this is true for $\mathbb{Y}^*$, since it behaves as a multivariate diffusion process in each of the considered time windows.

6 Discussion

In absence of spiking activity and when the neurons are characterized by a large number of synapses, e.g. for the Purkinjie cells, Theorem 1 allows to replace the multivariate Stein model with its diffusion approximation. Using Theorem 2, the ISIs can be modeled as FPTs of the diffusion process instead of the jump process. Thus, neural networks can be studied through the proposed multivariate firing OU model. Here we first describe some general features of the model and then we illustrate them on simulated data, considering a small network with four neurons.

6.1 Description of the spiking neural network model

Being the diffusion limit of the multivariate Stein model, the OU given by (14) inherits both its dependence structure and biological meaning. In particular, both processes have the same membrane time constant θ, which is responsible for the exponential decay of the MP. If some neurons belong to the same cluster A, their dynamics are related. This dependence is caught in the drift vector by $\delta_{j,A\setminus j}\mu_A$ and in the covariance matrix by $\delta_{j,A\setminus j}\delta_{l,A\setminus l}\sigma_A^2$, with $l \in A, l \neq j$. Also for the OU, $\delta_.$ specifies whether two or more neurons are affected by the same excitatory ($\delta_. > 0$) and inhibitory ($\delta_. < 0$) inputs or are independent ($\delta_. = 0$). Since $\mu_.$ and $\sigma_.$ are given by (5) and (6) respectively, they incorporate both frequencies and amplitudes of the jumps of the Poisson processes underlying the multivariate Stein model. Common inputs impinging on neurons of a specific cluster cause simultaneous jumps of the MPs of the multivariate Stein. This feature is not inherited by the OU model, since the FPTs of continuous processes can never be simultaneous. However, in neuroscience the definition of simultaneous spikes is less restrictive. Indeed, two firings are considered simultaneous if their distance cannot be detected by standard measurement tools. Under this definition, the OU process is able to reproduce simultaneous spikes.

Finally, using the covariance matrix (12), the correlation of the Gaussian noise of the jth and lth components is

$$\rho_{jl} = \frac{\sum\limits_{A\in\mathcal{A}} \mathbb{1}_{\{j,l\in A\}}\delta_{j,A\setminus j}\delta_{l,A\setminus l}\sigma_A^2}{\sqrt{\left(\delta_j^2\sigma_j^2 + \sum\limits_{A\in\mathcal{A}} \mathbb{1}_{\{j,l\in A\}}\delta_{j,A\setminus j}\delta_{l,A\setminus l}\sigma_A^2\right)\left(\delta_l^2\sigma_l^2 + \sum\limits_{A\in\mathcal{A}} \mathbb{1}_{\{j,l\in A\}}\delta_{j,A\setminus j}\delta_{l,A\setminus l}\sigma_A^2\right)}}.$$
(22)

6.1.1 Features of the multivariate firing OU model

The proposed OU model (14) can be studied in two different regimes:

- sub-threshold regime: the asymptotic mean of the MP, i.e. $\Gamma_j\theta$ is smaller than the threshold value; the regime is characterized by long ISIs. In this case, choose Γ_j, θ and B_j such that $\Gamma_j\theta < B_j$;
- supra-threshold regime: the asymptotic mean of the MP is larger than the threshold value; the regime is characterized by short ISIs. In this case, choose Γ_j, θ and B_j such that $\Gamma_j\theta > B_j$.

This model can reproduce a set of experimentally observed behaviors of a neural network with a suitable tuning of its parameter values.

1. *Excitation of neurons*: choose $\psi_{jl} > 0$. The strength of excitation increases with ρ_{jl}.
2. *Inhibition of neurons*: choose $\psi_{jl} < 0$.
3. *"Simultaneous"spikes*: choose $\rho_{jl} \approx 1$ in the supra-threshold regime.
4. *Silencing of neuron j*: choose $\psi_{jl} < 0$ and Γ_j such that $\Gamma_j\theta \ll B_j$.

Since ψ_{jl} is a sum of components, the condition $\delta_{jl} = \delta_{lj} \neq 0$ does not ensure $\psi_{jl} > 0$. Note that ψ_{jl} measures the concordance between j and l. Indeed, inhibitory inputs acting on both j and l, e.g. $\delta_{j,l} = \delta_{l,j} = -1$ give a positive term in the covariance ψ_{jl}. From (22), it follows that highly correlated neurons, which exhibit simultaneous spikes, can be obtained by choosing $\sigma_j^2, \sigma_l^2 \ll \sigma_A^2$. In particular, $\rho_{jl} = 1$ can be obtained choosing $\delta_j = \delta_l = 0$, and $\delta_{j,A \setminus j} = 0$ for any A such that $l \notin A$. In the fourth feature, the neuron is inhibited and evolves in a strong sub-threshold regime. Therefore, the probability of observing a spike during a recorded experiment is very low. Except for the last scenario, the processes should be either in supra-threshold or slightly sub-threshold (possibly with a large variance) regimes to exhibit firing activity. A network can be studied for different choices of the value of the refractory period, depending on the purposes of the analysis or the features of the neurons:

– For slow neurons, the refractory period is negligible with respect to the average ISI. Therefore, the choice $\Delta = 0$ can be performed.
– When the spikes are frequent or in the presence of clusters of spikes, the refractory period cannot be ignored. Thus $\Delta > 0$.
– In some networks, the refractory period may change from neuron to neuron. Therefore, choose $\Delta_j \geq 0$, for $i \leq j \leq k$.

This last scenario could be studied with both the proposed multivariate firing OU model and its corresponding marked point process, since Theorem 2 can be easily extended to the case of neurons with different refractory periods, as observed in Section 4.

6.2 Examples

Here we consider a small network with four neurons in a time interval $[0, 2000]$ ms. The firing activity of the network is modeled through the multivariate firing OU model and we show that it reproduces the experimental features 2-4. Moreover, we discuss the role of the absolute refractory period Δ, comparing two multivariate OU point processes, generated as follows. Until time $t = 1000$ms, the MP dynamics are modeled assuming that each neuron receives only its own inputs, i.e. we ignore the presence of shared inputs. Therefore, the covariance matrix $\boldsymbol{\Psi}$ given by (12) is diagonal. At time $t = 1000$ms, those common inputs are taken into account and therefore non-null dependencies between neurons are modeled. For $k = 4$, the drift vector (15) of the proposed OU model becomes

$$\boldsymbol{\Gamma} = \begin{pmatrix} \delta_1\mu_1 + \delta_{1,2}\mu_{12} + \delta_{1,3}\mu_{13} + \delta_{1,4}\mu_{14} + \delta_{1,23}\mu_{123} + \delta_{1,24}\mu_{124} + \delta_{1,34}\mu_{134} + \delta_{1,234}\mu_{1234} \\ \delta_2\mu_2 + \delta_{2,1}\mu_{12} + \delta_{2,3}\mu_{23} + \delta_{2,4}\mu_{24} + \delta_{2,13}\mu_{123} + \delta_{2,14}\mu_{124} + \delta_{2,34}\mu_{234} + \delta_{2,134}\mu_{1234} \\ \delta_3\mu_3 + \delta_{3,1}\mu_{13} + \delta_{3,2}\mu_{23} + \delta_{3,4}\mu_{34} + \delta_{3,12}\mu_{123} + \delta_{3,14}\mu_{134} + \delta_{3,24}\mu_{234} + \delta_{3,124}\mu_{1234} \\ \delta_4\mu_4 + \delta_{4,1}\mu_{14} + \delta_{4,2}\mu_{24} + \delta_{4,3}\mu_{34} + \delta_{4,12}\mu_{124} + \delta_{4,13}\mu_{134} + \delta_{4,23}\mu_{234} + \delta_{4,123}\mu_{1234} \end{pmatrix},$$

(23)

while the covariance matrix is (12). For example, the terms ψ_{11} and ψ_{12} are

$$\psi_{11}=\delta_1^2\sigma_1^2+\delta_{1,2}^2\sigma_{12}^2+\delta_{1,3}^2\sigma_{13}^2+\delta_{1,4}^2\sigma_{14}^2+\delta_{1,23}^2\sigma_{123}^2+\delta_{1,24}^2\sigma_{124}^2+\delta_{1,34}^2\sigma_{134}^2+\delta_{1,234}^2\sigma_{1234}^2,$$

$$\psi_{12}=\delta_{1,2}\delta_{2,1}\sigma_{12}^2+\delta_{1,23}\delta_{2,13}\sigma_{123}^2+\delta_{1,24}\delta_{2,14}\sigma_{124}^2+\delta_{1,234}\delta_{2,134}\sigma_{1234}^2.$$

Parameters of the model. We set $\theta = 10$ms and $B_j = 10$mV for $1 \leq j \leq k$, according to the standard choices for the one-dimensional case. The parameter values specific of each component are $\mu_1 = 0.9, \mu_2 = 1, \mu_3 = 1.5, \mu_4 = 1.1$mV ms^{-1}, $\sigma_1^2 = \sigma_2^2 = 0.01, \sigma_3^2 = \sigma_4^2 = 0.6$mV^{2}ms^{-1} and $\delta_j = 1$, for $j = 1, \ldots, 4$. Therefore in $[0, 1000]$ms, the multivariate OU has drift $\Gamma_j = \mu_j$ and a diagonal covariance matrix $\psi_{jj} = \sigma_{jj}^2, 1 \leq j \leq 4$.

The parameter values due to common inputs are $\mu_{1234} = 0.4, \mu_{34} = 0.2$mVms^{-1} and $\sigma_{1234}^2 = 0.5, \sigma_{34}^2 = 0.1$mV^{2}ms^{-1}, $\delta_{1234} = \delta_{2134} = 1$ and $\delta_{3124} = \delta_{4123} = \delta_{34} = \delta_{43} = -1$. Thus, we are considering a network with inputs acting on two clusters, namely $\{1, 2, 3, 4\}$ and $\{3, 4\}$. On cluster $\{1, 2, 3, 4\}$, inputs are excitatory on neurons 1 and 2 and inhibitory on 3 and 4. On cluster $\{3, 4\}$, they are inhibitory on both neurons, implying a positive resulting effect in the covariance ψ_{34}. A schematic representation of the described dependence structure when common inputs are taken into account is reported in Fig. 1. Then, in $[1000, 2000]$ms, the drift vector and covariance matrix of the OU with dependent component are

$$\boldsymbol{\Gamma} = \begin{pmatrix} 1.3 \\ 1.4 \\ 0.9 \\ 0.5 \end{pmatrix}, \qquad \boldsymbol{\Psi} = \begin{pmatrix} 0.51 & 0.5 & -0.5 & -0.5 \\ 0.5 & 0.51 & -0.5 & -0.5 \\ -0.5 & -0.5 & 1.2 & 0.6 \\ -0.5 & -0.5 & 0.6 & 1.2 \end{pmatrix}, \tag{24}$$

with correlation matrix

$$\rho = \begin{pmatrix} 1 & 0.980 & -0.639 & -0.639 \\ 0.980 & 1 & -0.639 & 0.639 \\ -0.639 & -0.639 & 1 & 0.5 \\ -0.639 & -0.639 & 0.5 & 1 \end{pmatrix},$$

as follows from (23), (24) and (22), respectively. Simulations are performed both with $\Delta = 0$ and $\Delta = 5$ms.

Results In Fig. 3 we report the raster displays of four simulated spike trains, both ignoring and considering the refractory period. If the common inputs are taken into account, which happens in $[1000, 2000]$ms, the firing activity of neurons 1 and 2 increases, that of neuron 3 decreases, while neuron 4 is silenced. In particular, there are several simultaneous firings in the first two spike trains, suggesting a high positive dependence between those neurons. Hence neurons 1 and 2 are excited, 3 is inhibited and 4 silenced. Finally, the presence of $\Delta > 0$ does not change the main features of the spike trains in the raster display but highlights the simultaneous spikes between neurons 1 and 2. As expected, the difference between the mean of the ISIs when $\Delta > 0$ and that of the ISIs with $\Delta = 0$ is about Δ (values not shown).
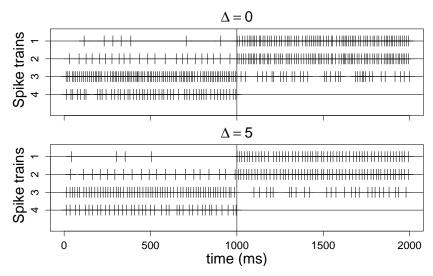
Fig. 3 Raster displays of the firing activity of a neural network with four neurons modeled by the multivariate firing OU model described in Section 4. Different cluster dynamics and values of the refractory periods are considered. In [0,1000]ms, common inputs between neurons are not taken into account, i.e. the MPs of the neurons are independent. In [1000, 2000]ms, common inputs are taken into account, with a dependent structure given in Fig. 1. Top figure: $\Delta = 0$ms. Bottom figure: $\Delta = 5$ms.

6.3 Conclusion

To model the spontaneous firing activity of neural networks, we introduce a multivariate firing Stein process, identifying the spikes as FPTs of the components of the process through a boundary. The model also accounts for the presence of absolute refractory periods. Dependences between neurons are modeled through cluster dynamics, i.e. there are inputs impinging on groups of neurons. To avoid the mathematical difficulties related with the study of jump processes and their FPTs, a diffusion approximation of the multivariate Stein to the OU is proved, as well the convergence of their marked point processes. This allows us to focus on the limit process, which inherits the biological features of the Stein model. We are aware that for reporting the biology correctly, a model should also take into account direct interactions between neurons or other types of indirect interactions (e.g. dependence structure in the drift term). The first case can be for example modeled introducing jumps in the MP of a neuron every time that the MP of a connected neuron crosses its boundary. However, new mathematical difficulties arise with the analysis of these models. Therefore, we suggest to start focusing on the proposed diffusion process and its FPT problem, developing suitable mathematical tools.
Note that a LIF paradigm for each component is considered. Therefore, we can use the existing literature to get ideas on how to develop analytical, numerical and statistical methods for the multivariate OU and its FPT problem,

as done by Sacerdote et al (2012b). It would be also interesting to provide a statistical study of the proposed model. Mimicking the techniques for unidimensional LIF model, we may estimate the total drift Γ_j and variance ψ_{jj} of each component $j, 1 \leq j \leq k$. However, the singular terms yielding them are not identifiable. Thus, we cannot distinguish between terms due to common and specific inputs. The estimation of the covariance matrix $\boldsymbol{\Psi}$, and thus of the dependencies between processes, is a more difficult task.

We have explained how to choose the parameters of the firing OU model for reproducing excitation, inhibition, silencing of neurons, as well as simultaneous spikes. These features are observed on simulated data from a small network with four neurons. To understand the reason leading to such phenomena, one may detect the dependence structure of the network from the analysis of the simultaneously recorded spike trains. Different statistical techniques are available (Borisyuk et al, 1985; Eldawlatly et al, 2009; Grün and Rotter, 2010; Perkel et al, 1967; Roudi and Hertz, 2011; Sacerdote et al, 2012a; Shimazaki et al, 2012). It would be interesting to compare them on simulated data from our proposed OU model.

Our analytical results show that the multivariate firing model and marked point process with underlying jumps processes converge weakly to analogous processes with underlying diffusions, obtained as limit of the jump processes. Therefore, the procedure presented here can be extended to other instances. For example, as underlying process for the single dynamics, we may consider a one-dimensional branching process which is proved to converge to a Feller diffusion process (Feller, 1951), also known as the Cox-Ingersoll–Ross process in finance (Cox et al, 1985).

Finally, note that our mathematical results are presented in the neuroscience framework, but can be used in other fields, such as reliability theory, finance or epidemiology. In reliability theory, FPTs represent crashing epochs and the refractory period corresponds to the time needed to repair or replace the broken component. In finance, FPTs identify the epochs when stocks reach an assigned value and the refractory period is typically null. In epidemiology, FPTs model the epochs when an epidemic is below a certain threshold level representing its quiescence state, while the refractory period describes the time needed to recover from that state.

References

Alberverio S, Cebulla C (2008) Synchronizability of stochastic network ensembles in a model of interacting dynamical units. Physica A 386:503–512

Borisyuk G, Borisyuk R, Kovalenko E, Kryukov V (1985) A new statistical method for identifying interconnections between neuronal network elements. Biol Cybern 52:301–306

Burkitt A (2006a) A review of the integrate-and-fire neuron model: I. homogeneous synaptic input. Biol Cybern 95(1):1–19

Burkitt A (2006b) A review of the integrate-and-fire neuron model: Ii. inhomogeneous synaptic input and network properties. Biol Cybern 95:97–112

Capocelli R, Ricciardi L (1971) Diffusion approximation and first passage time problem for a model neuron. Kybernetik 8:214–223

Cox J, Ingersoll J, Ross S (1985) A theory of the term structure of interest rates. Econometrica 53:385–407

Eldawlatly S, Jin R, Oweiss K (2009) Identifying functional connectivity in large-scale neural ensemble recordings: a multiscale data mining approach. Neural Comput 21:450–477

Feller W (1951) Diffusion processes in genetics. In: Proceedings of the second Berkeley symposium on mathematical statistics and probability, University of California Press, Berkeley and Los Angeles, pp 227–246

Gerstein G, Mandelbrot B (1964) Random walk models for the spike activity of a single neuron. Biophys J 4:41–68

Grün S, Rotter S (2010) Analysis of parallel spike trains, 1st edn. Springer, New York

Izhikevich E, Edelman G (2007) Large-scale model of mammalian thalamo-cortical systems. PNAS 105(9):3593–3598

Jacod J, Shiryaev A (2002) Limit Theorem for Stochastic Processes, 2nd edn. Springer–Verlag, Berlin

Kallianpur G, Wolpert RL (1987) Weak convergence of stochastic neuronal models. Springer–Verlag, New York, proceedings of a workshop on Stochastic methods in biology

Lansky P (1984) On approximations of Stein's neuronal model. J Theoret Biol 107:631–647

Lansky P, Ditlevsen S (2008) A review of the methods for signal estimation in stochastic diffusion leaky integrate-and-fire neuronal models. Biol Cybern 99:253–262

Lindvall T (2002) Lectures on the Coupling Method. Wiley Series in Probability and Mathematical Statistics, John Wiley & Sons, New York

Perkel D, Gernstein G, Moore G (1967) Neuronal spike trains and stochastic point processes. II. Simultaneous Spike Trains. Biophys J 7:419–440

Ricciardi L (1977) Diffusion Processes and Related Topics in Biology, Lecture notes in Biomathematics, vol 14. Springer–Verlag, Berlin

Roudi Y, Hertz J (2011) Mean field theory for nonequilibrium network reconstruction. Phys Rev Let 106:048,702

Sacerdote L, Giraudo M (2013) Leaky Integrate and Fire models: a review on mathematical methods and their applications. In: Stochastic biomathematical models with applications to neuronal modeling, Lecture Notes in Mathematics, vol 2058, Springer, pp 95 –148

Sacerdote L, Tamborrino M, Zucca C (2012a) Detecting dependences between spike trains of pairs of neurons through copulas. Brain Res 1434:243–256

Sacerdote L, Tamborrino M, Zucca C (2012b) First passage time for bivariate processes, submitted

Segundo JP (2000) Some thoughts about neural coding and spike trains. BioSystems 58:3–7

Shimazaki H, Amari S, Brown EN, Gruen S (2012) State-space analysis of time-varying higher-order spike correlation for multiple neural spike train data. PLoS Comput Biol 8:e1002,385

Stein R (1965) A theoretical analysis of neuronal variability. Biophys J 5:173–194

Tuckwell HC (1988) Introduction to theoretical neurobiology. Vol.2: Nonlinear and stochastic theories. Cambridge Univ. Press, Cambridge

Watts D, Strogatz S (1998) Collective dynamics of small-world network. NATURE 393:440–442

Whitt W (2002) Stochastic Processes Limits. Springer-Verlag, New York

II

Detecting dependencies between spike trains of pairs of neurons through copulas

Laura Sacerdote
Department of Mathematics
University of Turin

Massimiliano Tamborrino
Department of Mathematical Sciences
University of Copenhagen

Cristina Zucca
Department of Mathematics
University of Turin

List of typos in Paper II

- Section 2.1, line 7: ignore the rectangle

- Section 2.2, line 4: replace tn with n

- Section 2.2, line 19: ignore fleft

- Page 245, 2nd column, line 1: replace C_n with c_n

- Page 245, 2nd column, line 6 from the bottom. A bracket parenthesis $\}$ is missing

- Page 246, eq. 3: replace θ with ω

- Page 246, 1 line below eq. 3: replace τ with ω

- Page 247, 2nd column, line 5: replace τ with ω

- Page 253, 2n column, line 13 and 15 from the bottom: replace $\beta - 0$ with $\beta = 0$

- Caption of Fig. 4: replace $\hat{\tau}_1 - 0.84$ with $\hat{\tau}_1 = 0.84$

- Page 254, 1st column, line 2: replace $\tau_s = \frac{1}{100}\tau_r$ with $\tau_r = 1/100\tau_s$

- Section 5.1.2, line 2: replace $\tau_s = \theta$ and $\tau_s = \theta$ with $\tau_s = \omega$ and $\tau_r = 0$

Research Report

Detecting dependencies between spike trains of pairs of neurons through copulas

Laura Sacerdote[a,b], Massimiliano Tamborrino[c,], Cristina Zucca[a,b]*

[a]*Department of Mathematics "G. Peano", University of Turin, Via Carlo Alberto 10, Turin, Italy*
[b]*Neuroscience Institute of Turin (NIT), University of Turin, Regione Gonzole 10, Orbassano (Turin), Italy*
[c]*Department of Mathematical Sciences, University of Copenhagen, Universitetsparken 5, Copenhagen, Denmark*

ARTICLE INFO

ABSTRACT

The dynamics of a neuron are influenced by the connections with the network where it lies. Recorded spike trains exhibit patterns due to the interactions between neurons. However, the structure of the network is not known. A challenging task is to investigate it from the analysis of simultaneously recorded spike trains. We develop a non-parametric method based on copulas, that we apply to simulated data according to different bivariate Leaky Integrate and Fire models. The method discerns dependencies determined by the surrounding network, from those determined by direct interactions between the two neurons. Furthermore, the method recognizes the presence of delays in the spike propagation. This article is part of a Special Issue entitled "Neural Coding".

© 2011 Elsevier B.V. All rights reserved.

1. Introduction

The knowledge of the structure of a network is helpful to understand principles of its organization. Unfortunately, the connections between neurons belonging to a specific or different areas of the brain are generally unknown. Experimental techniques will not allow to get such information in an immediate future. However, the analysis of recorded spike trains may suggest possible connections and help neuroscientists to reconstruct the structure of networks.

Raster displays might reveal the presence of dependencies between the interspike intervals (ISIs) of the observed neurons, reflecting the existence of connections in the network. To study its structure, one should first establish the depen-

dencies between the recorded neurons, and then investigate the nature and the strength of these dependencies.

Since the pioneering work of Perkel et al. (1967), large efforts have been devoted to analyze simultaneously recorded data coming from several neurons. In the last thirty years, different techniques have been proposed; limits and difficulties are known, allowing their use in laboratories. There exists a lot of fundamental work on this subject. An exhaustive list of references can be found in a recent book (Grün and Rotter, 2010), where the available methods are collected, explained and discussed.

The most used methods to detect connections between neurons are based on the study of the crosscorrelation function (Perkel et al., 1967). Unfortunately, crosscorrelation de-

scribes linear dependencies and it might fail to detect non-linearities (Sacerdote and Tamborrino, 2010).

Other techniques include Generalized Linear Models (GLMs) (Brillinger, 1988) with their variants (Stevenson et al., 2009). However, these methods present difficulties too. A typical problem is the dependence of the results upon the size of the testing window (Eldawlatly et al., 2009).

Updating an older paper (Borisyuk et al., 1985), Masud and Borisyuk (2011) propose to use the Cox method as a statistical method to analyze functional connectivity of simultaneously recorded multiple spike trains. It is based on the theory of modulated renewal processes (Cox, 1972). This method detects bivariate dependencies between multiple spike trains in a neural network, providing statistical estimates of the strengths of influence and their confidence intervals. Moreover, it presents a set of advantages with respect to the others, e.g. it does not depend on the window amplitude, it detects weak dependencies and it succeeds in the presence of spurious connection due to common source or indirect connections. However, it requests a preliminary estimation of a set of parameters that is a very difficult task if the underlying model is unknown. Therefore, the results may become unreliable.

We propose the use of the copula notion to detect possible dependencies between ISIs. Copulas are joint probability distributions with uniform marginal distributions (Nelsen, 2006). Therefore, they catch dependencies between random variables (rvs), and they can be easily used for modeling purposes, being scale-free.

In neuroscience, the use of copulas is not a novelty. Jenison and Reale (2004) show how to couple probability densities to get flexibility in the construction of a multivariate neural population. Furthermore, they express the mutual information between two ISIs in terms of the copula distribution. More recently, Onken et al. (2009) inferred the connectivity between neurons by fitting the spike counts through the copulas of a given family. In particular, they provide a method to estimate the parameters of the prescribed copula. Sacerdote and Sirovich (2010) propose to use copulas to model the coupling of two or more neurons, while Sacerdote and Tamborrino (2010) investigate the reliability of crosscorrelograms analysis to detect dependencies in spike trains with known connections, being simulated through copula models.

A spike train is a collection of spike times and it can be considered as a vector of rvs. Therefore, a copula between two spike trains can be determined. Different types of dependency correspond to different shapes of the copula.

The aim of this work is to illustrate the ability of copulas to recognize dependencies between spike trains coming from different underlying models. To do this, we propose a non-parametric method.

A detailed study on simulated data could allow to classify shapes of copulas corresponding to different kinds of connections. However, in this paper, our main goal is to detect dependencies, instead of classifying their nature. Indeed, it represents a long task, since it corresponds to determine the joint distribution, i.e. the copula, that fits the data.

Furthermore, we limit ourselves to the study of two spike trains. The extension to multiple dependencies arising in the case of a larger number of spike trains requests further mathematical effort. Indeed, in a network of n neurons, it would correspond to investigate dependencies in groups of k neurons, $k=2,…,n$, i.e. to investigate k dimensional copulas for groups of k spike trains. However, our method can be applied immediately to the case of n spike trains, if the interest is focused on pairwise dependencies, as it happens in Masud and Borisyuk (2011). To do this, it is enough to select a target and a reference neuron, and then consider all the possible combinations.

In Section 2, we describe our method to catch dependencies between spike trains through copulas. In Section 3, we introduce the different Leaky Integrate and Fire (LIF) models used to generate coupled spike trains. In Section 4, we test the proposed method on those data. In Section 5, we discuss the results of our approach, providing a comparison with other methods, in particular with the Cox method. Finally, in Section 6, we describe conclusions, open problems and possible developments.

2. The copula method

2.1. A mathematical tool: copulas

A copula is a mathematical object that catches dependencies between rvs. In (Nelsen, 2006), it is defined as

Definition 1. A two-dimensional copula is a function C: $[0,1]^2 \rightarrow [0,1]$ with the following properties:

$$C(u;0) = C(0;v) = 0 \text{ and } C(u;1) = u; C(1;v) = v \text{ for every } u,v \in [0;1]; \tag{1}$$

$$C \text{ is } 2-\text{increasing, i.e. for every } u_1,u_2,v_1,v_2 \in [0;1] \text{ such that } u_1 \leq u_2, v_1 \leq v_2, \tag{2}$$

$$C(u_1,v_1) + C(u_2,v_2) - C(u_1,v_2) - C(u_2,v_1) \geq 0.$$

Let X and Y be two rvs with marginal cumulative distribution functions (cdfs) F and G, respectively. Let $H(x, y)$ be the joint cdf of (X,Y). Due to the Sklar's theorem, a two dimensional copula C satisfies:

$$H(x,y) = C(F(x), G(y)) \, x,y \in \mathbb{R}. \tag{1}$$

This theorem holds also in the multivariate case (Nelsen, 2006).

From Eq. (1), it follows that a copula is a joint cdf with two standard uniform marginals. Therefore, copulas are scale-free and capture all the information related to the joint behavior, and do not involve the marginal distributions. Hence, the study of a bivariate distribution can be split in two parts: the marginal behaviors caught by the marginal cdfs and the dependencies contained in the copula structure.

Copulas have other properties, as for instance the invariance under strictly increasing transformations, or the possibility to model several joint distribution functions.

In the literature, there exists a list of families of copulas, e.g. the Archimedean and the Euclidean families. Given a sample, we may perform a goodness-of-fit test to test if the data could belong to a certain family (Genest et al., 2009).

After that, we may estimate the involved parameters as done by Genest and Favre (2007) or Onken et al. (2009).

To measure the strength of dependencies, we consider the Kendall's tau τ. It is a rank correlation index assuming values in $[-1,1]$ and it measures the concordance for bivariate random vectors.

Given a data sample of size n, an estimator $\hat{\tau}$ of the Kendall's tau is given by:

$$\hat{\tau} = \frac{n_c - n_d}{\frac{1}{2}n(n-1)},$$

Here, n_c and n_d denote the number of concordant and discordant pairs in the sample. A pair of observations (x_i, y_i) and (x_j, y_j) is said to be concordant if $(x_i - x_j)(y_i - y_j) > 0$, otherwise it is called discordant (Nelsen, 2006).

A rank correlation test verifies if $\hat{\tau}$ is statistically different from zero, i.e. if data are dependent. This index detects non linear dependencies, while the common Pearson's and Spearman's rho detect linear dependencies (Nelsen, 2006).

In the next Subsection, we explain how to obtain empirical copulas starting from data belonging to samples of first passage times (FPTs) or spike trains.

2.2. Detect dependencies between ISIs through copulas

Copulas are multivariate joint distributions. For this reason, they can be used to investigate dependencies in a neural network with n neurons. However, their use is more intuitive for $n=2$. The extension to the pairwise analysis for tn neurons is immediate, while the study of k dimensional dependencies, for $k=3,\ldots,n$, is computationally not trivial, although it is theoretically analogous.

Given a sample $\{(X_1, Y_1), \ldots, (X_n, Y_n)\}$, we calculate the empirical cdfs $\hat{F}$ and $\hat{G}$ as

$$\hat{F}(x) = \frac{1}{n}\sum_{i=1}^{n} 1_{\{X_i \leq x\}}, \quad \hat{G}(y) = \frac{1}{n}\sum_{i=1}^{n} 1_{\{Y_i \leq y\}}, \quad x, y \in \mathbb{R}. \quad (2)$$

Then, we define the pseudo-observations from the copula as $\hat{U}_i = \left(\hat{F}(X_i), \hat{G}(Y_i)\right)$, $i=1,\ldots,n$. A scatterplot of $\hat{U}$, called "copula scatterplot", helps to understand dependencies between the involved rvs.

From the theory of copulas, we know that the points lying on the main diagonal (i.e. the diagonal which runs from the bottom left corner to the top right corner) correspond to times related by a strictly increasing function f such that $F(X) = f \circ \text{left}(G(Y))$. If $X \sim Y$, then f becomes the identity function, otherwise a new curve appears. Indeed, if the marginal distributions are different, then a straight line on the time scatterplot is transformed into a curve on the copula scatterplot. We call it *curve of monotony*. If X and Y are times, then the synchrony is caught by a straight line along the diagonal on the time scatterplot. These points are mapped into points lying on the main diagonal or on a curve on the copula scatterplot, depending on whether X and Y are identically distributed.

For independent rvs, characterized by the independent copula $C(u,v) = uv$, the scatterplot presents a uniform distribution of points on the square $[0,1]^2$. On the contrary, the presence of clusters of points reveals a specific dependency. Furthermore, we have considered the empirical cdf C_n and

the empirical probability density function (pdf) $\tilde{C}_n$ of the copula (Nelsen, 2006). Their study, together with the estimation of the Kendall's tau, gives further information about the dependencies between X and Y.

To illustrate how to apply copulas to neuronal data, we first assume to have a sample of FPTs $T = \{(T_A^1, T_B^1), \ldots, (T_A^n, T_B^n)\}$, where (T_A^i, T_B^i) and (T_A^j, T_B^j) are independent for $i \neq j$ and $(T_A^i, T_B^i) \sim (T_A^j, T_B^j)$, where $\sim$ denotes rvs with the same distributions. In this case, we can calculate the pseudo-observations as described before.

Then, to deal with pairs of spike trains, we need to define how to extract a sample of two-dimensional rvs, representative of the dependencies between the spike trains. Denote S_A^i and S_B^j the epochs of the i-th and the j-th events in the spike trains A and B, and T_A^i and T_B^j the i-th and j-th ISIs, for $i=1,\ldots,$ n; $j=1,\ldots,l$. On a fixed time, the number of spikes of two neurons is different, i.e. $n \neq l$. We assume that the ISIs T_A^i (resp. T_B^j) in A (B) are independent and identically distributed and we denote them T_A (T_B).

To pursue the analysis, we select A as target neuron. To each spike time S_A^i, we associate the time θ^i, defined as the intertime between S_A^i and the first spike in B following it (Fig. 1, Panel I). The pairs $(T_A^1, \theta^1), \ldots, (T_A^N, \theta^N)$ determine a sample (T_A, θ) for the study of the relationships between the spike trains. If the corresponding copula is not the independent copula, then there is a connection between the two neurons. We investigate it comparing the two scatterplots and testing if τ is statistically different from zero. Moreover, the copula scatterplot allows to make hypotheses on the dynamics driving the membrane potential (MP) evolutions of the two neurons, as explained in Section 4.

Another interesting task is the investigation of the duration (or "memory") of the dependency between spike trains. After a certain time M, neuron B may forget the activity of neuron A, if no new phenomena coupling their dynamics are present. The time M may be short, corresponding to instantaneous effect, or long, implying a durable effect in the coupling.

To investigate it, we consider the sample $\left(T_A, \theta + \sum_{k=1}^{m} T_B^{(k)}\right)$ $= \left\{\left(T_A^1, \theta^1 + \sum_{k=1}^{m} T_B^{(1k)}\right), \ldots, \left(T_A^{\tilde{N}}, \theta^{\tilde{N}} + \sum_{k=1}^{m} T_B^{(\tilde{N}k)}\right)\right\}$, as shown in Fig. 1, Panel I. Here, $T_B^{(ik)}$ corresponds to the k-th ISI following θ_i, while $\tilde{N}$ denotes the sample size that might change with m. In particular, we are interested in the value m such that the corresponding copula approaches the independent one, i.e. $\tau = 0$. If the dependence disappears for small (large) m,
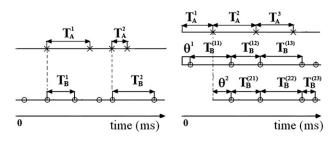

Fig. 1 – Samples of FPTs and of spike trains. Let A be the target neuron. Panel I: sample of FPTs, obtained considering only the first ISIs in A and B following synchronous spikes. Panel II: rvs involved in a sample of spike trains. For each T_A^i in A, we show the corresponding θ^i and the following $T_B^{(ik)}$ in B for i=1, 2 and m=3.

then the coupling has an instantaneous (long) effect. Furthermore, we study the optimal value m maximizing the coupling. It can be detected as the value of m that maximizes $\hat{\tau}$. Note that $m=0$ leads to the previous sample (T_A, θ).

To study the presence of delayed dependencies, we analyze the sample $(T_A, T_B^{(k)}) = \{(T_A^1, T_B^{(1k)}), \ldots, (T_A^n, T_B^{(nk)})\}$. Indeed, it might happen that a spike in A influences the k-th spike in B. Therefore, the delay can be estimated as $\theta + \sum_{j=1}^k T_B^{(ij)} - T_A^i$, where k is the first index such that the Kendall's tau for $(T_A, T_B^{(k)})$ is statistically different from zero.

These properties of memory and delayed dependencies hold when $\mathbb{E}[\theta + \sum_{i=1}^k T_B^{(i)}] - \mathbb{E}[T_A] > \mathbb{E}[T_B^{(k)}]$, i.e. the projection of $T_B^{(k)}$ on A does not overlap with T_A on average, otherwise such phenomena are due to the slower nature of A.

To conclude the analysis, we select B as target neuron and we repeat the procedure. Note that this is not necessary if T_A and T_B are identically distributed, since this leads to the same results, the study being symmetric.

3.   Models for data generation

The samples were generated from two bivariate LIF models. Both of them describe the spike times of each neuron as the FPT of their MP evolution through a boundary, where the MPs are coupled through different rules.

3.1.   Model of the MP evolution through jump diffusion processes

Musila and Lansky (1991) proposed to use jump diffusion processes to describe the MP evolution of a single neuron to account for the effects of the postsynaptic potentials (PSPs) impinging on the membrane near the trigger zone. Deco and Schürmann (1998) studied resonance phenomena for central neurons described by Ornstein Uhlenbeck (OU) processes with jumps modeling a discrete input spike train. In Sirovich (2003), jump processes are associated to the arrival of a spike, but the model is not a diffusion. Recently, Sirovich

(2006) and Sirovich et al. (2007) proposed to use these processes to describe interactions in a small network.

Here, we describe the MP evolutions through a two dimensional jump diffusion process $\mathbf{X}(t) = \{(X_1, X_2)(t); t \geq t_0\}$. Each component evolves independently from the other, until the time when one of them attains a threshold value C for the first time. Then, that neuron releases a spike, its MP is reset to its resting value and the evolution restarts anew. Meanwhile, the MP of the other neuron has a jump of amplitude h (Fig. 2, Panel I) and then it pursues its evolution. In the absence of jumps, the MP of each neuron is modeled as an OU process given by

$$dX_i(t) = \left(-\frac{1}{\theta} X_i(t) + \mu_i\right) dt + \sigma_i dW_i(t), \tag{3}$$

with $t_0 = 0$ and $X_i(0) = x_{0i}$, for $i = 1, 2$. Here, τ, μ_i, σ_i denote the membrane constant (or decay time), the input and the noise intensity respectively. Moreover, $W_1(t)$ and $W_2(t)$ are two standard Wiener processes. Hence, the Brownian increments are independent.

We say that this corresponds to a local connection between neurons, since the dependency between spikes is direct, being determined only by the jumps.

To simulate a sample of FPTs T, we proceed as follows. When both neurons release a spike, the MPs are reset to their resting values and a new simulation starts. This type of sample reproduces the interspike times following synchronous spikes of the two neurons (Fig. 1, Panel I).

To generate two coupled spike trains, we collect the crossing times of the two MPs up to a maximum observed time $t_{\max}$.

3.2.   Model of the MP evolution through correlated diffusion processes

The Stein process for the spiking activity of a single neuron was introduced by Stein (1965). However, the study of the FPT problem for jump processes is mathematically intractable. Assuming the high frequency and the small amplitude of the jumps, diffusion limits have been proposed for instance by Capocelli and Ricciardi (1971) and Lansky (1984). From a
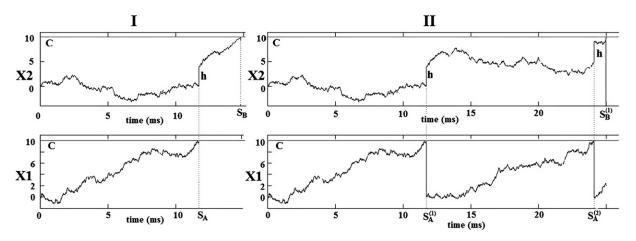

Fig. 2 – MP evolution through jump diffusion processes. Description of the MP evolution of two coupled neurons through a two dimensional jump process. The MP evolution of A (B) is reset to its resting value after that it spikes, meanwhile the MP evolution of B (A) has a jump of amplitude h. These dynamics are stopped when both neurons have released a spike (Panel I) or after a maximum time $t_{\max}$ (Panel II).

biological view point, when the neuron receives a huge number of inputs from the surrounding network, the continuous limit is a good approximation of the original process. A multivariate extension of these models has been recently proposed (Tamborrino et al., submitted for publication). There, the PSPs impinging on each neuron correspond to two kinds of input: those influencing a specific neuron and those simultaneously acting on a collection of at least two neurons.

Here, the MP evolutions of the two neurons are described by a bivariate diffusion process $\mathbf{X}(t)$ with correlated components. The sub-threshold MP evolutions are still described by Eq. (3), but now the Brownian increments are not independent anymore. Indeed, we assume $Cov(W_1(t), W_2(t)) = \sigma_{12}t$, with $\sigma_{12}\epsilon$ (0,1). Therefore, the evolutions proceed jointly in all the observed time intervals, due to the presence of a common noise. We say that this situation corresponds to a global kind of dependence, since the dependencies are determined by the surrounding network.

To obtain a sample of FPTs T, we stop the MP evolution of the fastest neuron after it fires. Meanwhile, the slowest one continues its evolution until its MP reaches the boundary (Fig. 3, Panel I). After that, the dynamics restarts anew. These neural dynamics are characterized by a continuous coupling effect up to the first spike.

To generate two coupled spike trains, we reset the MP of the firing neuron to its resting potential and then restart it. Meanwhile, the other neuron continues its evolution until it spikes (Fig. 3, Panel II). This procedure continues up to t_{max}, coupling the dynamics of the two neurons.

4. Results

In this Section, we apply our method on samples of FPTs and pairs of spike trains simulated from the jump and the covariance models. In Subsection 4.3, we enlighten the differences observed in the corresponding copula scatterplots. Performing the data analysis, we ignore the knowledge of the models and we infer coupling properties directly from copula scatterplots

and Kendall's tau (values reported in the captions of the figures). The goodness of fit of the results is finally checked.

The parameter values of the models agree with those used for one dimensional LIF models in the literature. In particular, we choose membrane constant $\tau = 10\ ms$, threshold value for the MP $C = 10\ mV$, jump amplitude $h = 3\ mV$, covariances 0.5; 0.8; 0.91 mV^2ms^{-1}, drifts and noise intensities are reported in Table 1. Examples of negative covariances, implying negative dependencies between spike trains, have been also analyzed, obtaining correct results. Also in this case, our method detects them. Unfortunately, the simulation of data from the jump model requests long computational times when we have negative jump amplitudes. For this reason, we do not illustrate these examples.

4.1. Data from the jump model

4.1.1. Samples of FPTs
The biological interpretation of samples of FPTs is not intuitive, since they do not correspond to time series. However, they can be interpreted as the intertimes after synchronous spikes (Fig. 1, Panel I) and their analysis helps to understand the use of copula scatterplots.

In Fig. 4, we report the copula scatterplots for different samples of T, obtained from the jump model, using the parameters reported in Table 1, with $h = 3\ mV$. We first test the null hypothesis $H_0 : T_A \sim T_B$ through a Kolmogorov–Smirnov (KS) test. Since the p-values $\hat{P}$ are 1, 0.998, 0.901 and 0 respectively, we reject $H_0 : T_A \sim T_B$ only for the fourth sample, in agreement with how they were sampled.

We start considering the first three samples. The distribution of T_A (and hence of T_B) changes in each sample. Indeed, their means and variances are different (values not reported).

From the scatterplots and the values of $\hat{\tau}$ in Fig. 4, Panels I–III, we observe the following features:

1. Panels are characterized by decreasing values of $\hat{\tau}$, all statistically different from 0.
2. many points lie on the main diagonal, drawing its shape;
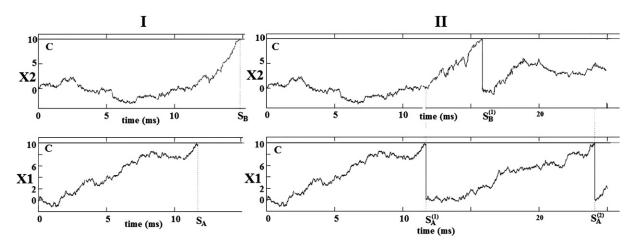

Fig. 3 – MP evolution through correlated diffusion processes. Example of MP evolution of two neurons coupled through a two dimensional correlated diffusion process. The MP evolution of A (B) is reset to its resting value after it spikes, while the MP evolution of B (A) is not influenced by the spike. These dynamics are stopped after both neurons have released a spike (Panel I) or after a maximum time t_{max} (Panel II).

Table 1 – Drifts μ and noise intensities σ^2 used to simulate spike data. Units are: $mVms^{-1}$ and mV^2ms^{-1}, respectively.				
Case	μ_A	μ_B	σ_A^2	σ_B^2
I	1.2	1.2	0.3	0.3
II	1.2	1.2	0.5	0.5
III	1.2	1.2	1.1	1.1
IV	1.0	1.5	0.5	0.5

3. scatterplots exhibit similar features, although with different densities of the points. Moving from the left to the right side, the density of the points not on the diagonal increases;

4. there is a lack of points around the main diagonal.

Due to feature 1, a dependency is caught by the method in each sample. The analogies between the plots suggest the presence of a similar coupling phenomenon acting with different strengths, as suggested also by the first feature. The coupling phenomenon acts only to determine the synchrony, while the other intertimes are scarcely dependent. Indeed, feature 4 and the lack of clusters do not reveal further dependencies. That means that specific phenomenon might determine synchronous spikes or have no effect if the instantaneous coupling is not strong enough. A local connection is compatible with this kind of behavior. These remarks agree with the underlying model used to generate the samples.

Now, consider Panel IV. Also in this case, a positive $\hat{\tau}$ is observed, but the copula scatterplot is not symmetric anymore. In the time scatterplots (figures not reported), we observe many points lying on the main diagonal. Therefore, the curve in Panel IV corresponds to the curve of synchrony. Moreover, a high density of points is observed on the curve that is surrounded by a lack of points. Hence, we can hypothesize a similar dynamics to that observed in Panels I–III, but with different marginals.

4.1.2. Samples of spike trains

We consider two spike trains generated according to the jump model with parameters given by case III in Table 1. We cannot reject $H_0: T_A \sim T_B$, since $\hat{p} = 0.998$. Therefore, the analysis does not change inverting the roles of target and reference neurons. Thus, we choose A as target neuron.

The pairs $(T_A, T_B^{(k)})$ are characterized by Kendall's tau statistically equal to zero (e.g. $\hat{p} = 0.71, 0.70, 0.79$ for $k = 1, 2, 3$). Hence, the samples do not present delayed coupling phenomena.

In Fig. 5, we report the copula scatterplots of $(T_A, \theta + \sum_{k=1}^{m} T_B^{(k)})$ for $m = 0, 1, 2, 3, 5, 10$. From these plots and the values of $\hat{\tau}$, we observe that increasing the value of m, the copula scatterplots approach the independent copula.

In Panel I, the curve with the highest density of points is well approximated by a straight line. Moreover, T_A and θ have a similar distribution (histograms not shown). Since $T_A \sim T_B$, θ, and T_B have a similar distribution too. Therefore, the spiking dynamics are characterized by the presence of synchronous spikes. Moreover, we observe a lack of points around the diagonal, as in Fig. 4. Therefore, we can hypothesize a local coupling.

In the remaining panels, new curves catch the dependency between T_A and $\theta + \sum_{k=1}^{m} T_B^{(k)}$. Since these rvs have different distributions (p-values not reported), these curves correspond to curves of monotony.

Now, we consider two spike trains obtained with parameters of case IV in Table 1. We reject $H_0: T_A \sim T_B$ and $H_0: T_A \sim \theta$, since both p-values are null. The Kendall's tau for $(T_A, T_B^{(k)})$ is statistically different from zero only when $k = 1$, since $\hat{p} \approx 0$ for $H_0: \tau = 0$. However, it does not represent a delayed dependency, since $\mathbb{E}[T_A] = 17.92$, $\mathbb{E}[\theta + T_B^{(1)}] = 20.40$ and $\mathbb{E}[T_B^{(1)}] = 10.32$.

In Fig. 6, we plot the copulas for $(T_A, \theta + \sum_{k=1}^{m} T_B^{(k)})$. Here, $m = 1$ maximizes $\hat{\tau}$. This figure presents some similarities to Fig. 5. Indeed, for m greater than the optimal one, the dependency decreases and the copula scatterplots look like the independent copula. Moreover, in both figures, we observe a lack of points around the curve of monotony for $m = 0$ and 1 as well as the presence of clusters. Finally, in Fig. 6, these curves can be detected up to $m = 5$.

The analogies between samples of Figs. 5 and 6 allow to hypothesize dynamics for the spike trains driven by similar kinds of dependencies, even if with different marginal behaviors.

Since T_A and T_B are not identically distributed, we repeat the analysis considering B as target neuron. In Fig. 7, we report the copula scatterplots for $m = 0, 1, 2$. The shapes of these scatterplots and the strength of the dependencies caught by $\hat{\tau}$ are different from those in Fig. 6. Also in this case, $\hat{\tau}$ is statistically different from 0. Furthermore, a curve of monotony is
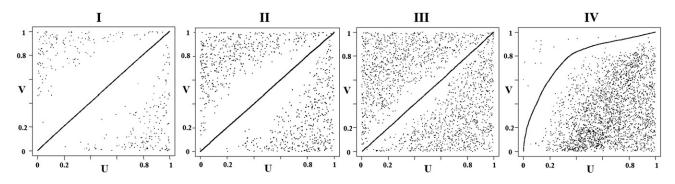

Fig. 4 – Samples of FPTs from the jump model. Copula scatterplots corresponding to four samples of ISIs (T_A, T_B), where $T_A \sim T_B$ for the first three pairs. The estimated Kendall's tau are $\hat{\tau}_I$–0.84, $\hat{\tau}_{II} = 0.69$, $\hat{\tau}_{III} = 0.41$ and $\hat{\tau}_{IV} = 0.18$, respectively. They are statistically different from zero, since all the corresponding p-values are smaller than 0.05.
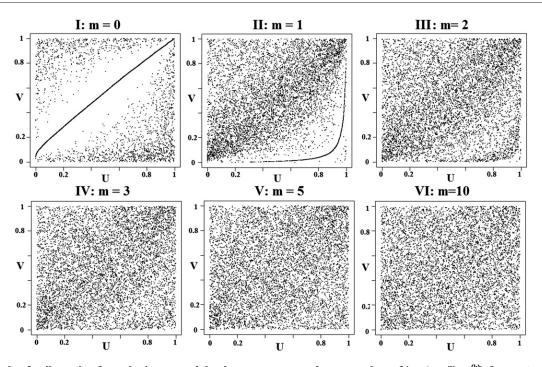
Fig. 5 – Sample of spike trains from the jump model, where $T_A \sim T_B$. Copula scatterplots of $(T_A, \theta + \sum_{k=1}^{m} T_B^{(k)})$, for m = 0, 1, 2, 3, 5, 10, where T_A and T_B have the same distribution. The estimated Kendall's tau are statistically different from zero, with values $\hat{\tau}_I = 0.42, \hat{\tau}_{II} = 0.20, \hat{\tau}_{III} = 0.15, \hat{\tau}_{IV} = 0.12, \hat{\tau}_V = 0.10$ and $\hat{\tau}_{VI} = 0.07$, respectively. Note that $m = 0$ represents the optimal value maximizing the dependency between the involved times.

recognized only for $m = 0$. This is related to the slower nature of neuron A. Note that we have detected dependencies alternating A and B as target neurons. Therefore, there exists a bi-directional influence connection between the two neurons.

The results obtained applying our method are coherent with the features of the models used to simulate data. In particular, we were able to detect bi-directional connections, such as those determined by the jump dynamics of the
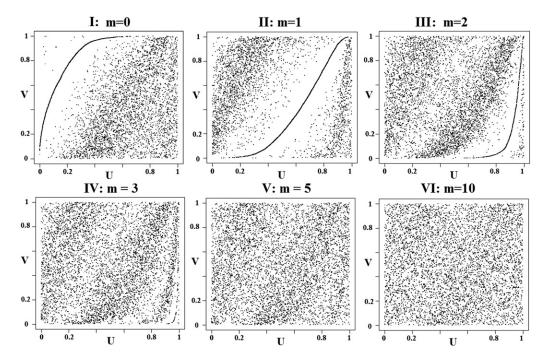

Fig. 6 – Sample of spike trains from the jump model with different distributions of T_A and T_B. Copula scatterplots of $(T_A, \theta + \sum_{k=1}^{m} T_B^{(m)})$, for m = 0, 1, 2, 3, 5, 10, where T_A and T_B have different distributions. The estimated Kendall's tau are statistically different from zero and equal to $\hat{\tau}_I = 0.04, \hat{\tau}_{II} = 0.12, \hat{\tau}_{III} = 0.06, \hat{\tau}_{IV} = 0.04, \hat{\tau}_V = 0.02, \hat{\tau}_{VI} = 0.01$, where $m = 1$ represents the optimal value maximizing $\hat{\tau}$.
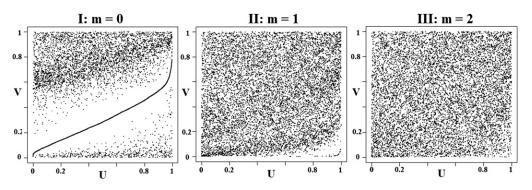
Fig. 7 – Choice of B as target neuron. Copula scatterplots of $(T_B, \theta + \sum_{k=1}^{m} T_A^{(k)})$, for $m = 0, 1, 2$, obtained considering B as target neuron in the spike trains analyzed in Fig. 6. The estimated Kendall's tau are $\hat{\tau}_I = 0.23, \hat{\tau}_{II} = 0.08, \hat{\tau}_{III} = 0.06$, respectively. The maximum dependence is observed for $m = 0$.

considered model, as well as to hypothesize a correct local coupling. As previously remarked, we have ignored the knowledge of the underlying models during the analysis phase.

4.2. Data from the covariance model

Here, we consider data generated from the covariance model with parameters reported in Table 1 and covariances equal to 0.5, 0.8, 0.91, 0.8 $mV^2 ms^{-1}$, respectively.

4.2.1. Samples of FPTs
In Fig. 8, we report the copula scatterplots coming for the four samples of FPTs. Testing H_0: $T_A \sim T_B$, we obtain $\hat{p} = 0.69$, 0.95, 0.89 and 0, respectively. We start considering the first three pairs, characterized by identically distributed ISIs.

Looking at Fig. 8, Panels I–III and the corresponding $\hat{\tau}$, we observe the following features:

1. Panels are characterized by increasing values of $\hat{\tau}$, all statistically different from 0.
2. many points lie on the main diagonal and around it;
3. scatterplots exhibit similar features, although with different densities of the points. Moving from the left to the right side, the density of the points far from the diagonal decreases.

Positive dependencies are caught in all samples. Furthermore, the numerous points lying on the diagonal (indicator

of synchrony) are surrounded by a cloud of other points. This suggests the presence of a noise that continuously perturbs the coupling phenomenon, destroying the synchrony. A global connection is compatible with this kind of behavior.

Now, consider Panel IV. In the time scatter plot, not reported, (resp. copula scatterplot) no points lie on or above the main diagonal (the curve of synchrony), due to the fact that $\mathbb{E}[T_A] = 24.98$, $\mathbb{E}[T_B] = 10.65$. Therefore, no synchrony is observed. For the similarity with Panel I, we hypothesize a similar dynamics characterized by different marginals.

4.2.2. Samples of spike trains
We consider two spike trains generated with drifts and variances given by case III in Table 1, and covariance 0.91 $mV^2 ms^{-1}$. We cannot reject $T_A \sim T_B$, since $\hat{p} = 0.94$. Therefore, it is sufficient to consider A as target neuron.

In Fig. 9, we report the copula scatterplots of $(T_A, \theta + \sum_{k=1}^{m} T_B^{(k)})$ for $m = 0, 1, 2, 3, 5, 10$. From these plots and the values of $\hat{\tau}$, we note that the copula scatterplots approach the independent copula as m increases.

In Panel I, T_A and θ have different distributions since $\hat{p} = 0$ for the hypothesis H_0: $T_A \sim \theta$. Therefore, the monotone dependency is caught by a curve and the largest part of the points lays on and under it. This behavior may be explained admitting the existence of a noise that perturbs the system and destroys the deterministic relationship. Furthermore, the dependencies seem to be determined by a continuous phenomenon that tunes the activity of the two neurons, despite
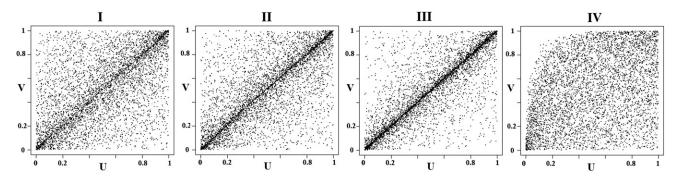

Fig. 8 – Samples of FPTs from the covariance model. Copula scatterplots corresponding to four pairs of ISIs (T_A, T_B), with $T_A \sim T_B$ for the first three pairs. The estimated Kendall's tau are $\hat{\tau}_I = 0.41, \hat{\tau}_{II} = 0.53, \hat{\tau}_{III} = 0.67$, respectively. They are statistically different from zero, since the corresponding p-values are smaller than 0.05.
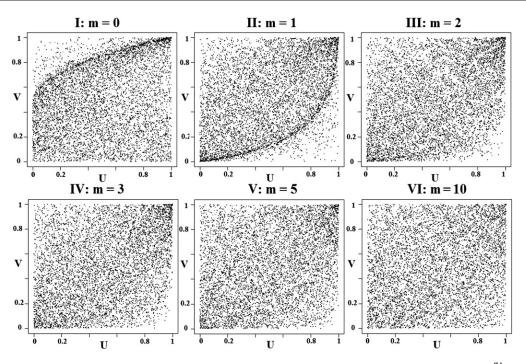
Fig. 9 – Sample of spike trains from the covariance model, where $T_A \sim T_B$. Copula scatterplots of $(T_A, \theta + \sum_{k=1}^m T_B^{(k)})$, for $m = 0, 1, 2, 3$, 5, 10, where T_A and T_B have the same distribution. The estimated Kendall's tau are statistically different from zero, with values $\hat{\tau}_I = 0.16, \hat{\tau}_{II} = 0.30, \hat{\tau}_{III} = 0.25, \hat{\tau}_{IV} = 0.22, \hat{\tau}_V = 0.18$, and $\hat{\tau}_{VI} = 0.14$, respectively. Note that $m = 0$ represents the optimal value maximizing the dependency between the involved times.

the noise. Therefore, a global coupling might be hypothesized. This is supported by the fact that $(T_A, \sum_{k=1}^m T_B^{(k)})$ becomes statistically independent for $m \geq 409$. That means that we are observing a long memory phenomenon.

In the remaining panels, new curves of monotony catch the synchrony between T_A and $\theta + \sum_{k=1}^m T_B^{(k)}$. In particular, in Panel *II*, the number of points lying on this curve is greater than those in Panel *I*.

Finally, we consider two spike trains generated using the parameters given by case *IV* in Table 1, and covariance $0.8\ mV^2 ms^{-1}$. We reject $H_0: T_A \sim T_B$, since $\hat{p} \approx 0$. In Fig. 10, we plot the copulas for $(T_A, \theta + \sum_{k=1}^m T_B^{(k)})$. Here, $m = 2$ maximizes $\hat{\tau}$ for the considered samples and curve of monotony can be detected up to $m = 5$. This figure presents some similarities to Fig. 9. Indeed, for m greater than the optimal value, the dependence decreases and the copula scatterplots look like the independent copula. These analogies allow to hypothesize dynamics for the spike trains driven by similar kinds of dependencies, even with different marginal behaviors.

Due to the different roles of neurons A and B, we repeat the analysis considering B as target neuron. The copula scatterplots for $m = 0, 1, 2$ are plotted in Fig. 11. The shapes are obviously different from those in Fig. 10, but also in this case, $\hat{\tau}$ is statistically different from 0. Therefore, we have detected a bi-directional connection between the two neurons.

In both samples, no delayed phenomena are detected. Indeed, no p-values statistically different from zero are observed for $(T_A, T_B^{(k)})$ such that $\mathbb{E}[\theta + \sum_{i=1}^k T_B^{(i)}] - \mathbb{E}[T_A] > \mathbb{E}[T_B^{(k)}]$.

The results agree with those expected, determined by the structure of the used model.

4.3. Comparison between data from the two models

Data used in Figs. 4–8, 5–9, 6–10, 7–11 came from two OU processes with the same parameters, but coupled according to different rules, i.e. jumps or positive covariances. The different coupling leads to different shapes in the copula scatterplots, as well as to different properties. For instance, copula scatterplots related to the jump model are characterized by a lack of points around the main diagonals, while a cluster of points is observed in those coming from the covariance model. This allows us to hypothesize different coupling phenomena for those scatterplots presenting different features.

Furthermore, we may observe different shapes of scatterplots even with a similar $\hat{\tau}$. Look for instance at Fig. 4, Panel *II* and Fig. 8, Panel *III*, with $\hat{\tau} = 0.69$ and $\hat{\tau} = 0.67$, respectively. Therefore, the study of correlation or rank correlation indexes, such as the Pearson's rho or the Kendall's tau, is useful to recognize the presence of dependencies, but it cannot be used to investigate their nature.

5. Discussion

The use of copulas allows a new approach to analyze dependencies between spike trains. The discussed examples illustrate some features highlighted by means of this technique. Suitable statistical tests and further developments of the mathematical tools will allow to determine families of copulas able to fit data. Furthermore, a classification of the
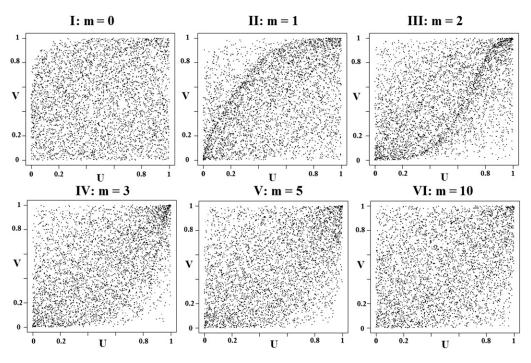
Fig. 10 – Sample of spike trains from the covariance model, with different distributions of T_A and T_B. Copula scatterplots of $(T_A, \theta + \sum_{k=1}^{m} T_B^{(m)})$, for $m = 0, 1, 2, 3, 5, 10$, where T_A and T_B have different distributions. The estimated Kendall's tau are statistically different from zero and equal to $\hat{\tau}_I = 0.07, \hat{\tau}_{II} = 0.27, \hat{\tau}_{III} = 0.33, \hat{\tau}_{IV} = 0.31, \hat{\tau}_V = 0.26, \hat{\tau}_{VI} = 0.20$, where $m = 2$ represents the optimal value maximizing τ.

different copulas corresponding to different kinds of coupling may help to interpret the structure of the network.

In this Section, we compare some of our results with those obtained through classical tools. At first, we consider cross-correlograms and time scatterplots. Then, we briefly discuss some features of the GLMs and finally we perform a detailed comparison with the Cox method.

Crosscorrelograms are one of the most used techniques to analyze spike trains. They detect synchronous and delayed activities but they are often unable to recognize other kinds of dependencies. Reversely, in copula scatterplots, the layout of the points out of the curve of synchrony discloses the presence of other kinds of dependencies. Moreover, it helps to hypothesize

the underlying coupling effects. A common feature between crosscorrelograms and the proposed approach is the necessity to fix a target neuron. Usually, the analysis is repeated, exchanging the roles of the two neurons.

The analysis of crosscorrelograms requests the simultaneous study of the autocorrelograms. Indeed, oscillations in the crosscorrelogram might be due to marginal behaviors, as described by Sacerdote and Tamborrino (2010) and Tetzlaff et al. (2008). Thus, it is not always possible to distinguish between the two cases. Furthermore, the duration of the dependencies is hidden in crosscorrelograms. Indeed, this information depends on the presence of several peaks or troughs and by their width. Unfortunately, these features
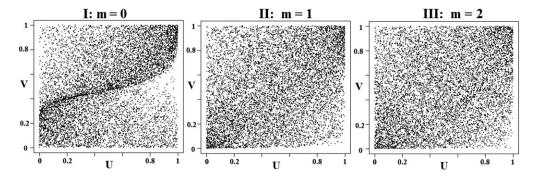

Fig. 11 – Choice of B as target neuron. Copula scatterplots of $(T_B, \theta + \sum_{k=1}^{m} T_A^{(k)})$, for $m = 0, 1, 2$, obtained considering B as target neuron, in the spike trains analyzed in Fig. 10. The estimated Kendall's tau are $\hat{\tau}_I = 0.27, \hat{\tau}_{II} = 0.22, \hat{\tau}_{III} = 0.18$ and $m = 0$ maximizes the dependency.

change according to the used bin. On the contrary, copulas allow to determine the value of m such that the two considered random times become independent, disclosing memory properties. In Fig. 12, we show autocorrelograms and crosscorrelograms corresponding to samples analyzed in Figs. 5 and 9. For each sample, we only plot one autocorrelogram, since $T_A \sim T_B$. In the crosscorrelograms, peaks and troughs far from zero are due to the marginal behaviors, as explained by the autocorrelograms. Hence, these oscillations do not represent two neurons firing with a delay, i.e. the only statistically meaningful peaks are those in 0.

One might wonder why to use copula scatterplots instead of time scatterplots. In a time scatterplot, one can easily recognize synchronous spikes from the presence of a straight line. Furthermore, such plot gives information on the marginal behavior, allowing to recognize the range of the involved times. However, the merge of marginal and joint behaviors represents the main limit of this tool. Indeed, it is hard to distinguish meaningful clusters, observing clouds of points (Fig. 13, Panels I and IV). Hence, any classification of the observed kinds of dependencies becomes difficult. Reversely, copula scatterplots (Fig. 13, Insets I' and IV') solve this problem, catching only the joint behavior, since the marginal distributions are uniform. The same considerations hold when one plots the 3-D histograms for the times (Fig. 13, Panels II and V) and for the copulas (Fig. 13, Panels III and VI).

GLMs, as well as correlation indices, privilege linear dependencies, while copulas and the Kendall's τ deal with any kind of dependency. For instance, correlation indices assume value 1 when the rvs are related by a linear relationship. On the contrary, the Kendall's tau is equal to 1 if there exists a strictly increasing transformation between the rvs. Furthermore, GLMs are sensible to the amplitude of the test window. In our approach, this problem becomes relevant only plotting a 3-D histogram for the copula, to perform a fit of data to a specific family of copulas.

The recent upgrading of the Cox method makes it a useful approach for the detection of dependencies in a neural network (Masud and Borisyuk, 2011). They study the dependency of a target neuron A on the other $(n-1)$ reference neurons, considering pairwise dependencies. For this reason, we focus on the comparison of the two methods for the case $n-2$, reporting the main advantages of each method.

5.1. Copula method versus Cox method

5.1.1. The Cox method

The Cox method makes use of the hazard function, that is defined as the occurrence rate at time t conditional on survival time until time t or later:

$$\varphi(t) = \lim_{\Delta t \to 0} \frac{P(t \leq T \leq t + \Delta t | T > t)}{\Delta t} = \frac{f(t)}{1 - F(t)}.$$

Here, $F(t)$ is the cdf of the ISIs and $f(t)$ is their density.

In (Masud and Borisyuk, 2011), modulated renewal processes (refer to Cox (1972) and Borisyuk et al. (1985)) have been considered to introduce the dependency between spike trains. They suppose that the hazard function ϕ of the target neuron A is a product of two multipliers. The first term is the hazard function φ of the renewal process A without influence from the reference neuron B, and the second term describes the influence of neuron B on A. In particular, they introduce an influence function $Z_B(t)$ that determines how the reference neuron influences the target. They propose to use a hazard function given by

$$\varphi(t) = \varphi_A(U_A(t)) \exp(\beta Z_B(t)). \tag{4}$$

Here, $U_A(t)$ is the backward recurrence time of the process A at time t and β is the parameter that has to be estimated (Perkel et al., 1967). It gives the strength of influence from train B to A: if $\beta - 0$, no influence is observed. Their method provides an estimation of β and a confidence interval for the test hypothesis $H_0 : \beta - 0$.

As influence function Z_B, they choose the alpha function proposed by Gerstner and Kistler (2002) to describe the synaptic connectivity between neurons. This choice implies the necessity to estimate a set of parameters: the delay time Δ due to spike propagation from neuron B to A and the characteristic decay and rise times of the postsynaptic potential (PSP), denoted by τ_s and τ_r, respectively.

The estimation of Δ can be properly done using using a pairwise Cox method or considering the time shift to the right side of zero corresponding to the highest value of the crosscorrelation function exceeding the upper boundary. If the MP evolution is described by a Stein's model, the decay time can be estimated
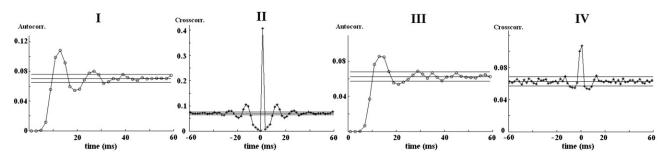

Fig. 12 – Autocorrelograms and crosscorrelograms. Panels I and III: autocorrelograms of TA for the samples analyzed in Figs. 5 and 9, respectively. The line with circles represents the estimated autocorrelation. The two straight lines limit the confidence interval at 0.05 for $\frac{1}{\mathbb{E}[T_A]}$. Panels II and IV: crosscorrelograms for the considered samples. The line with stars (dotted line) denotes the empirical (theoretical) crosscorrelation, while the two straight lines delimit a confidence interval for the hypothesis of independence between T_A and T_B.
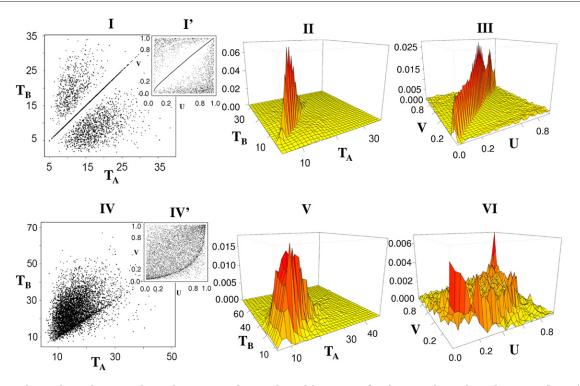
Fig. 13 – Analyses through ISIs and copulas. Scatterplots and 3-D histograms for times and copulas. The upper (lower) panels correspond to the samples analyzed in Fig. 5 (Fig. 9). Panels I, IV: ISI scatterplots of (T_A, T_B). Inset I′: copula scatterplot corresponding to (T_A, θ) (previously shown in Fig. 5, Panel I). Panel IV′: copula scatterplot corresponding to $(T_A, \theta + T_B^{(1)})$ (already shown in Fig. 9, Panel II). Panels II and V: 3-D time histograms. Panels III and VI: 3-D copula histograms.

from the ISI data using the algorithm in Tuckwell and Richter (1978), while the rise time is assumed to satisfy $\tau_s = \frac{1}{100}\tau_r$.

In general, the estimation of τ_s and τ_r from the ISI data is an unsolved task. Indeed, it requires the knowledge of the underlying model and the measurement of the PSP. Therefore, the results from the method may become unreliable. A solution might be to change the influence function Z_B, choosing a more general expression.

In the sequel, we consider a set of examples analyzed with the two methods.

5.1.2.   Examples

We apply the Cox method to the data sample used in Section 4. For an OU process, $\tau_s = \theta$, while $\tau_s = \theta$. However, to perform the analysis, we assume $\tau_r = 0.1$, as in Masud and Borisyuk (2011). The delay Δ is estimated using crosscorrelograms. To estimate β from Eq. (4) and its confidence interval, we use the software provided kindly to us by Borisyuk and Masud.

Using data from the covariance model, we obtain $\Delta = 0$ or $\Delta = 1$. With these estimates, the Cox method correctly catches the bi-directional dependencies, providing statistically positive estimates of β (analysis not reported).

However, the method does not succeed using data from the jump model. Choosing A as target neuron, we investigate β_{BA}, i.e. the influence from B to A. Here, we report the study of the Cox method on the spike trains analyzed in Fig. 5, with crosscorrelogram in Fig. 12, Panel II. Looking to the right side of Fig. 12, two peaks are observed at times 0 and 10. However, the second one is due to the autocorrelation and therefore, we choose $\Delta = 0$. This leads to $\beta_{BA} = -5.89$ with confidence interval $(-6.22; -5.59)$.

Therefore, a wrong negative dependency is caught. Vice versa, choosing the wrong delay $\Delta = 10$, we got a correct positive dependency $\beta_{BA} = 0.71$, with confidence interval $(0.46; 0.97)$. Choosing B as target neuron, similar features follow (data not reported).

Hence, the goodness of the results depends highly on the underlying model and on the ability of the experimenter to estimate the parameters correctly, when this can be done, i.e. when we can measure the PSP or we know τ_r and τ_s in advance.

As a second check, we have generated two spike trains according to the enhanced LIF model described in (Borisyuk, 2004), using the software from the website www.tech. plymouth.ac.uk/infovis. This model considers different biological parameters, e.g. the already mentioned Δ and τ_s, but also the absolute refractory period r, defined as the interval following a spike where the neuron is unable to spike again. Furthermore, the software allows to specify the connection scheme between the two neurons.

Here, we test the Copula method on two spike trains generated choosing $\Delta = 7, \tau_s = 2.78, \tau_r = 0.1, r = 5$ and uni-directional connection $\beta_{BA} = 12.18$, i.e. B influences A. Choosing A as target neuron, no delayed phenomena are observed. Indeed, the Kendall's tau for the pairs $(T_A, T_B^{(k)})$ are statistically equal to zero (refer to Table 2, for $k = 1, 2$). Reversely, we obtain a positive Kendall's tau for $m = 0$, i.e. for the pair (T_A, θ). Furthermore, the pairs $(T_A, \theta + \sum_{k=1}^{m} T_B^{(k)})$ are independent for $m > 1$, having a p-value larger than 0.05 (values not reported). Therefore, these data are characterized by an instantaneous effect. Choosing B as target neuron, no dependencies are caught, as shown in Table 2. Hence, as the Cox method, our method catches the connection scheme correctly.

Table 2 – Kendall's tau from different pairs of rvs extracted from spike trains generated via the enhanced LIF model. The choice of A as target neuron leads to a positive dependence between (T_A, θ). Vice versa, selecting B as target neuron, no dependencies are observed. Therefore, a uni-directional connection is found.

A as target neuron			B as target neuron		
Case	$\hat{\tau}$	p-value	Case	$\hat{\tau}$	p-value
$(T_A, T_B^{(1)})$	−0.0094	0.4862	$(T_A, T_B^{(1)})$	0.0307	0.0538
$(T_A, T_B^{(2)})$	−0.0038	0.7807	$(T_B, T_A^{(2)})$	0.0074	0.6407
(T_A, θ)	0.0527	0.0001	(T_B, θ)	0.0092	0.5672

5.1.3. Advantages of the two methods

Summarizing, each method presents some advantages and disadvantages, according to different situations.

The main advantages of the copula method are that:

- it is a non parametric method, only requesting the renewal assumptions, i.e. iid ISIs;
- it recognizes the duration of the effect of a coupling phenomenon through the investigation of m;
- it allows to recognize the presence of similar underlying dynamics for the MP, when the copula scatterplots or densities have similar shapes;
- it gives the possibility to fit the joint distribution for the examined ISIs, after a fit of the copula density. This allows a classification of different kinds of dependencies (not present in this paper);
- it might be extended to capture dependencies in triplets, quartets, etc.

A remark on the last feature. Our method can be already used to investigate dependencies of a neural network as done in Masud and Borisyuk (2011), i.e. considering pairs of spike trains and performing the aforementioned analysis on each pair. However, it would be interesting to investigate also the existence of triplets, quartets, etc. of dependencies. Using the copula method, this would request the investigation of k dimensional copulas, for $k > 2$, and the results may present difficulties of illustration, due to the impossibility to use scatterplots. Using the Cox method, this study would become even more difficult, since one should redefine the hazard function φ in a proper way, e.g. switching from φ_A to a function for the k involved neurons.

Two drawbacks of the Copula method are that sometimes this method does not catch small dependencies and it requests a large sample size to estimate the Kendall's tau properly.

The main advantages of the Cox method are that:

- it is reliable also for small sample size (i.e. 50 data for each train);
- it allows to ignore the "spurious"connection, distinguishing between direct and indirect connections and dealing correctly with connectivity due to common source
- it has been already tested in a network of 20 neurons, with satisfactory results.

The main drawback is its dependence on the goodness of the influence function Z_B for the considered data. Furthermore,

even choosing a good influence function, the estimation of its parameter, such as τ_s, τ_r for the alpha function, may represent a hard task.

Finally, both methods allow to detect the presence of a delay in the coupling.

Cox and Lewis (1972) underline the complementary role of the study of the occurrence rate of events (as done in the Cox method), and of the ISIs (as done in the copula method) for the theoretical study of point processes. This fact agrees with our results for the statistical study of dependencies between point processes. Hence, a reliable analysis should consider both methods.

6. Conclusions

We have proposed the use of the copula notion to analyze dependencies between two spike trains. This has allowed the development of a new non-parametric method based on the study of their scatterplots and densities, as well as association indexes, such as the Kendall's tau. This method allows to enlighten the effect of an interspike on the subsequent ones of the other neuron. This can be studied checking copula scatterplots and performing a test $H_0: \tau = 0$. Furthermore, the use of copulas helps to recognize the direction scheme of two neurons, exchanging the role of target and reference neurons. Finally, considering all this information, one might conjecture the nature of the phenomenon at the origin of the dependencies.

The proposed method can be also applied to experimental data, allowing to catch dependencies. However, it may happen to obtain copula scatterplots with shapes different from those discussed here. To interpret them, it is advisable to enlarge the set of examples, to include cases involving inhibition phenomena or spurious connections. The development of a specific software enclosing copulas and the previously mentioned methods, particularly Cox with a proper influence function Z_B, represents an important step toward a better comprehension of the structure of a network. Our future work will consider the possibility to fit data with suitable copula families.

Finally, a further step will be to consider k-dimensional copulas to investigate the dependencies in groups of k neurons, non pairwise.

REFERENCES

Borisyuk, R., 2004. Oscillatory activity in the neural networks of spiking elements. Biosystems 52, 301–306.
Borisyuk, G.N., Borisyuk, R.M., Kirillov, A.B., Kovalenko, E.I., 1985. A new statistical method for identifying interconnections between neuronal network elements. Biol. Cybern. 52, 301–306.

Brillinger, D.R., 1988. Maximum likelihood analysis of spike trains of interacting nerve cells. Biol. Cybern. 59, 189–200.

Capocelli, R.M., Ricciardi, L.M., 1971. Diffusion approximation and first passage time problem for a model neuron. Kybernetik 8, 214–223.

Cox, D.R., 1972. The statistical analysis of dependencies in point processes. In: Lewis, P.A. (Ed.), Stochastic Point Processes, pp. 55–66. New York.

Cox, D.R., Lewis, P.A.W., 1972. Multivariate point processes. Proceedings Sixth Berkeley Symposium on Probability and Mathematical Statistics, 3, pp. 401–448.

Deco, G., Schürmann, B., 1998. Stochastic resonance in the mutual information between input and output spike trains of noisy central neurons. Physica D. 117, 276–282.

Eldawlatly, S., Jin, R., Oweiss, K.G., 2009. Identifying functional connectivity in large-scale neural ensemble recordings: a multiscale data mining approach. Neural Comput. 21, 450–477.

Genest, C., Favre, A.C., 2007. Everything you always wanted to know about copula modeling but were afraid to ask. J. Hydrol. Eng. 12, 347–368.

Genest, C., Rémillard, B., Beaudoin, D., 2009. Goodness-of-fit tests for copulas: a review and a power study. Insurance: Math. Econ. 44 (2), 199–213.

Gerstner, W., Kistler, W.M., 2002. Spiking Neuron Models: Single Neurons, Populations, Plasticity. Cambridge University Press.

Grün, S., Rotter, S., 2010. Analysis of parallel spike trains, In: Grun, S., Rotter, S. (Eds.), 1st ed. Springer.

Jenison, R.L., Reale, R.A., 2004. The shape of neural dependence. Neural Comput. 16 (4), 665–672.

Lansky, P., 1984. On approximations of Stein's neuronal model. J. Theoret. Biol. 107, 631–647.

Masud, M.S., Borisyuk, R., 2011. Statistical technique for analyzing functional connectivity of multiple spike trains. J. Neurosci. Methods 196 (1), 201–219.

Musila, M., Lansky, P., 1991. Generalized Stein's model for anatomically complex neurons. Biosystems 25, 179–191.

Nelsen, R.B., 2006. An Introduction to Copulas. Springer, United States of America.

Onken, A., Grünewälder, S., Munk, M.H.J., Obermayer, K., 2009. Analyzing short-term noise dependencies of spike-counts in macaque prefrontal cortex using copulas and flashlight transformation. PLoS Comput. Biol. 5, e1000577.

Perkel, D.H., Gerstein, G.L., Moore, G.P., 1967. Neuronal spike trains and stochastic point processes II. Simultaneous spike trains. Biophys. J. 7, 419–440.

Sacerdote, L., Sirovich, R., 2010. A copulas approach to neuronal networks models. J. Physiol. Paris 104, 223–230.

Sacerdote, L., Tamborrino, M., 2010. Leaky Integrate and Fire models coupled through copulas: association properties of the Interspike Intervals. Chin. J. Physiol. 53 (6), 396–406.

Sirovich, L., 2003. Dynamics of neuronal populations: eigen function theory; some solvable cases. Comput. Neural Syst. 14, 249–272.

Sirovich, R., 2006. Mathematical models for the study of synchronization phenomena in neuronal networks. Ph.D. Thesis.

Sirovich, R., Sacerdote, L., Villa, A.E.P., 2007. Effect of increasing inhibitory inputs on information processing within a small network of spiking neurons. Lect. Notes Comput. Sci. 4507, 23–30.

Stein, R.B., 1965. A theoretical analysis of neuronal variability. Biophys. J. 5, 173–194.

Stevenson, I.H., Rebesco, J.M., Hatsopoulos, N.G., Haga, Z., Miller, L.E., Kording, K.P., 2009. Bayesian inference of functional connectivity and network structure from spikes. Brain Connectivity 17 (3), 203–213.

Tamborrino, M., Sacerdote, L. and Jacobsen, M., submitted for publication. Diffusion approximation and first passage time for multivariate jump processes.

Tetzlaff, T., Rotter, S., Stark, E., Abeles, M., Aertsen, A., Diesmann, M., 2008. Dependence of neuronal correlations on filter characteristics and marginal spike train statistics. Neural Comput. 20, 9.

Tuckwell, H.C., Richter, W., 1978. Neuronal interspike time distributions and the estimation of neurophysiological and neuroanatomical parameters. J. Theor. Biol. 71, 167–183.

III

First passage times for bivariate processes

Laura Sacerdote
Department of Mathematics
University of Turin

Massimiliano Tamborrino
Department of Mathematical Sciences
University of Copenhagen

Cristina Zucca
Department of Mathematics
University of Turin

Publication details

FIRST PASSAGE TIMES FOR BIVARIATE GAUSS-MARKOV PROCESSES

L. SACERDOTE[*], M. TAMBORRINO [†], AND C. ZUCCA [‡]

Abstract. We determine the joint distribution of the exit times of a bivariate Gauss-Markov process from a two-dimensional strip under absorbing boundary conditions. This distribution depends on the transition density of the process constrained to evolve under the boundary. Solving a two-dimensional Kolmogorov forward equation, we explicitly derive these two quantities for a bivariate Wiener process with drift and non-diagonal covariance matrix. Explicit expressions for other Gauss-Markov processes are not available. For this reason, we propose a numerical algorithm, which is shown to be convergent. A comparison between theoretical and numerical results for Wiener and an illustration of the numerical approximation for a bivariate Ornstein-Uhlenbeck process are carried out. Extensions to renewal and diffusion processes in presence of non-absorbing boundaries are also suggested.

Key words. Exit times, System of Volterra-Fredholm integral equations, Bivariate Kolmogorov forward equation, Bivariate Wiener process

AMS subject classifications. 60G40, 65R20, 60J65, 60J70

1. Introduction and motivation. The first passage time (FPT) problem for one-dimensional stochastic processes has been widely investigated through simulation, analytical and numerical methods [3, 6, 13, 17]. Besides its mathematical interest, the derivation of the FPT distribution is relevant in different fields, e.g. neuroscience, reliability theory, finance, epidemiology. In neuroscience, FPTs describe the times when the neuron releases an electrical impulse, called spike. In reliability theory, FPTs model the epochs when a crash of an object happens. In finance, FPTs describe the time when a bond or a stock reaches a certain value and it is profitable to sell or buy. In epidemiology, FPTs describe the times when an epidemic reaches a threshold level, exiting from its quiescence state. Connections between neurons, common shocks and direct interaction between objects, dependencies between stocks in the same portfolio or belonging to the same market and interactions between populations suggest the presence of dependencies between FPTs. Therefore, it is of interest to extend the FPT problem to more general scenarios.

This paper is inspired by [12], where the FPT of a two-dimensional Brownian motion without drift, in presence of absorbing boundary, was derived. The bivariate Wiener was proposed as an oversimplified model of a neural network. As a more realistic model to describe the dynamics of k neurons, we propose a multivariate Ornstein-Uhlenbeck (OU) process [23], which is shown to be the diffusion approximation of a multivariate Stein process [22]. The model is characterized by constant drifts and non-diagonal covariance matrix, implying dependent component. A bivariate version of this model is investigated through simulations in [21]. Motivated by these papers, we study multivariate FPT distributions in the framework of neural networks. In neuroscience, experimentalists measure the difference of potential between the internal and external parts of the membrane of a neuron. The arrival of inputs

---

[*]Department of Mathematics "G. Peano", University of Turin, Via Carlo Alberto 10, Turin, Italy, (`laura.sacerdote@unito.it`).

[†]Department of Mathematical Sciences, Copenhagen University, Universitetsparken 5, Copenhagen, Denmark, (`mt@math.ku.dk`).

[‡]Department of Mathematics "G. Peano", University of Turin, Via Carlo Alberto 10, Turin, Italy, (`cristina.zucca@unito.it`).

on the membrane causes changes of its membrane potential dynamics. When the membrane potential attains a certain threshold level, an active mechanism produces a sudden hyperpolarization and the neuron generates a spike. It is believed that inter-spike intervals encode the neural information [24, 25, 26] and therefore their investigation is of primary interest. Merging biological and mathematical tractability reasons, leaky-integrate-and-fire models represent a commonly used class of one-dimensional diffusion processes in neuroscience [20]. The interspike times are described as FPTs of the process through a boundary. Connections and interactions between neurons imply dependencies between their dynamics and thus also their epochs.

For one-dimensional processes, transition densities are known for Wiener [8], OU, Feller (also note as Cox-Ingersol-Ross or square root processes), and all those cases where an explicit solution of the Kolmogorov forward equation is available [18, 19]. The transition density of a process in presence of absorbing boundaries and the FPT density are generally unknown, except for Wiener [20] and a special case of the OU process [10]. As an alternative approach, numerical methods can be applied [20].

For multivariate processes, the transition density is known for Gauss-Markov processes [4]. However, neither the transition density in presence of absorbing boundaries, nor the joint FPT density are available. Our aim is to solve the two-dimensional FPT problem of a bivariate Gauss-Markov process in presence of absorbing boundaries. We assume that a component is absorbed on its boundary whenever it reaches it, while the other independently pursues its evolution till the epoch when it attains its boundary.

In §2 we introduce notations and mathematical background used throughout the paper. In §3 we express the joint distribution of the FPTs as a function of the marginal distributions of the FPTs, and of the conditional probability densities of a component given that the other has attained its boundary at a fixed time. We show that these unknown conditional densities solve a system of Volterra-Fredholm integral equations. In §4 we present a numerical algorithm to solve the system. The obtained numerical solution is then used to evaluate the joint distribution of the FPTs. In §5 we study the order the convergence of the error of the proposed algorithm. In §6 we determine explicit expressions of the joint distribution of the FPTs of a bivariate Wiener process with constant drifts and non-diagonal covariance matrix. In particular, the transition density of the bivariate Wiener process in presence of absorbing boundary conditions is explicitly derived as solution of a bivariate Kolmogorov forward equation. The results in §6 extend and correct those in [5, 11, 12]. Finally, in §7 we apply the numerical algorithm to evaluate the joint FPT density of bivariate Wiener and OU processes, comparing numerical and theoretical results for Wiener.

2. Mathematical background. Consider a two-dimensional time homogeneous Gauss-Markov process $\mathbf{X} = \{(X_1, X_2)(t); t > t_0\}$, originated at time t_0 in $\mathbf{X}(t_0) = \mathbf{x}_0 = (x_{01}, x_{02})$, solution of the stochastic differential equation

$$d\mathbf{X}(t) = \boldsymbol{\mu}(\mathbf{X}(t))dt + \boldsymbol{\Sigma}(t)d\mathbf{W}(t). \qquad (2.1)$$

Here $\boldsymbol{\mu}(\boldsymbol{X}(t)) = \boldsymbol{A}(t)\boldsymbol{X}(t) + \boldsymbol{a}(t)$, $\boldsymbol{A}(t)$ and $\boldsymbol{\Sigma}(t)$ are $\mathbb{R}^k \times \mathbb{R}^k$-matrix valued, $\boldsymbol{\Sigma}(t)$ is positive-definite, and $\mathbf{W}(t)$ is a k-dimensional standard Wiener process [4].

Let $\mathbf{B} = (B_1, B_2) \in \mathbb{R}^2$ be a two-dimensional boundary, with $B_i > x_{0i}, i = 1, 2$ and denote T_i the random variable FPT of X_i through the boundary B_i, defined by

$$T_i = \inf\{t > t_0 : X_i(t) > B_i\} \qquad i = 1, 2.$$

Before the first exit time from the strip $(-\infty, B_1) \times (-\infty, B_2)$, the process $\boldsymbol{X}$ evolves under the boundary $\boldsymbol{B}$, and we denote it as $\boldsymbol{X}^a$, i.e.

$$\mathbf{X}^a = \{\mathbf{X}(t); t \in [t_0, \min(T_1, T_2)]\}.$$

Similarly, we denote X_i^a the unidimensional process X_i evolving under the boundary B_i, before time T_i, i.e.

$$X_i^a = \{X_i(t); t \in (t_0, T_i)\}, \qquad i = 1, 2.$$

Whenever a component reaches its boundary, it is absorbed there, while the other component independently pursues its evolution. Throughout the paper, absorbing boundary conditions are assumed, whenever it is not differently specified.

If $\mathbf{Z}$ is a k-dimensional process, we denote its transition probability by $F_{\mathbf{Z}}(\mathbf{x}, t|\mathbf{y}, s) = \mathbb{P}(\mathbf{Z}(t) < \mathbf{x}|\mathbf{Z}(s) = \mathbf{y})$, its survival function by $\bar{F}_{\mathbf{Z}}(\mathbf{x}, t|\mathbf{y}, s)$ and the transition probability density function (pdf) by $f_{\mathbf{Z}}(\mathbf{x}, t|\mathbf{y}, s)$ for $s < t, \mathbf{x}, \mathbf{y} \in \mathbb{R}^k$. Throughout the paper, $\mathbf{Z} = \mathbf{X}$ or $\mathbf{Z} = \mathbf{X}^a$, for $k = 1$ or 2.

For $s < t$, we denote $f_{X_i^a|X_j^a}(x_i, t|x_j, t; \mathbf{y}, s)$ the conditional pdf of X_i^a given X_j^a, for $i, j = 1, 2, i \neq j$, defined by

$$f_{X_i^a|X_j^a}(x_i, t|x_j, t; \mathbf{y}, s)dx_i = \mathbb{P}(X_i^a(t) \in dx_i|X_j^a(t) = x_j, \mathbf{X}^a(s) = \mathbf{y}),$$

and $f_{X_i^a|T_j}(x_i|t; y_i, s)$ the transition pdf of X_i^a conditioned on T_j when X_i^a starts in y_i at time s, defined by

$$f_{X_i^a|T_j}(x_i|t; y_i, s) dx_i = \mathbb{P}(X_i^a(T_j) \in dx_i|T_j = t, X_i^a(s) = y_i). \qquad (2.2)$$

The joint pdf of T_j and $X_i^a(T_j)$, when X_i^a starts in y_i at time $s > T_j$, denoted by $f_{(X_i^a, T_j)}(x_i, t|y_i, s)$, is defined by

$$f_{(X_i^a, T_j)}(x_i, t|y_i, s) dx_i dt = \mathbb{P}(X_i^a(T_j) \in dx_i, T_j \in dt|X_i^a(s) = y_i). \qquad (2.3)$$

The pdf of T_i is defined by $g_{T_i}(t|y_i, s) = \mathbb{P}(T_i \in dt|X_i(s) = y_i)$. Our aim is to determine the joint cumulative distribution function $\mathbb{P}(T_1 < t_1, T_2 < t_2|\mathbf{X}(s) = \mathbf{y})$ or its pdf $\mathbb{P}(T_1 \in dt_1, T_2 \in dt_2|\mathbf{X}(s) = \mathbf{y})$, for a process $\mathbf{X}$ starting in $\mathbf{y} < \mathbf{B}$ at time $\mathbf{s} = (s_1, s_2)$ in presence of absorbing boundary $\mathbf{B}$.

To simplify the notation, throughout we omit the starting position when $\mathbf{y} = \mathbf{x}_0$ and the starting time s, when $s = t_0$.

3. Joint distribution of (T_1, T_2). The joint distribution of (T_1, T_2) can be expressed in terms of the marginal FPTs densities and of the transitions pdfs (2.2).

THEOREM 3.1. *Let* $\mathbf{X}$ *be a two-dimensional Gauss-Markov process with* $\mathbf{X}(t_0) = \mathbf{x}_0$ *and let* $\mathbf{B}$ *be a two-dimensional absorbing boundary with* $B_1 > x_{01}$ *and* $B_2 > x_{02}$. *The joint distribution of* (T_1, T_2) *is*

$$\mathbb{P}(T_1 < t_1, T_2 < t_2)$$
$$= \sum_{i,j=1; i \neq j}^{2} \int_{t_0}^{t_i} \int_{-\infty}^{B_j} \left(\int_{s_i}^{t_j} g_{T_j}(s_j|x_j, s_i)ds_j \right) f_{(X_j^a, T_i)}(x_j, s_i)dx_j ds_i. \qquad (3.1)$$

Proof.

$$\mathbb{P}(T_1 < t_1, T_2 < t_2) = \sum_{i,j=1; i \neq j}^{2} \int_{t_0}^{t_i} \mathbb{P}(T_1 < t_1, T_2 < t_2|T_i < T_j, T_i = s_i)\mathbb{P}(T_i \in ds_i, T_i < T_j).$$

Conditioning on the value of the component which has not yet reached its boundary, at the time when the other component crosses its boundary, we get

$$\mathbb{P}(T_1 < t_1, T_2 < t_2)$$

$$= \sum_{i,j=1;i\neq j}^{2} \int_{t_0}^{t_i} \int_{-\infty}^{B_j} \mathbb{P}(T_j < t_j | T_i = s_i, X_j^a(s_i) = x_j) \mathbb{P}(X_j^a(s_i) \in dx_j | T_i = s_i) \mathbb{P}(T_i \in ds_i, T_i < T_j)$$

$$= \sum_{i,j=1;i\neq j}^{2} \int_{t_0}^{t_i} \int_{-\infty}^{B_j} \mathbb{P}(T_j < t_j | X_j^a(s_i) = x_j) \mathbb{P}(X_j^a(s_i) \in dx_j, T_i \in ds_i),$$

where the last equality holds because $\mathbf{X}$ and thus $\mathbf{X}^a$ are Markov processes.   □

REMARK 1. *The expression*

$$f_{(X_j^a, T_i)}(x_j, s_i) dx_j ds_i = f_{X_j^a | T_i}(x_j | s_i) g_{T_i}(s_i) dx_j ds_i \tag{3.2}$$

can be plugged in into (3.1), *obtaining*

$$\mathbb{P}(T_1 < t_1, T_2 < t_2) \tag{3.3}$$
$$= \sum_{i,j=1;i\neq j}^{2} \int_{t_0}^{t_i} \int_{-\infty}^{B_j} \left(\int_{s_i}^{t_j} g_{T_j}(s_j | x_j, s_i) ds_j \right) f_{X_j^a | T_i}(x_j | s_i) g_{T_i}(s_i) dx_j ds_i.$$

This expression is useful when g_{T_i} is known, because it allows to rewrite (3.1) *in terms of the unknown function $f_{X_j^a | T_i}$.*

From Theorem 3.1, it follows

COROLLARY 3.2. *The joint density of (T_1, T_2) for a two-dimensional Gauss-Markov process in presence of an absorbing boundary $\mathbf{B}$ is given by*

$$\mathbb{P}(T_1 \in dt_1, T_2 \in dt_2) = \sum_{i,j=1;i\neq j}^{2} \int_{-\infty}^{B_j} g_{T_j}(t_j | x_j, t_i) f_{(X_j^a, T_i)}(x_j, t_i) dx_j dt_i dt_j \tag{3.4}$$

The distribution of (T_1, T_2) can be explicitly determined when the densities g_{T_j} and $f_{(X_j^a, T_i)}$ are known, e.g. for the Wiener case, as shown in §6. For other processes, the FPT density g_{T_j} can be approximated through numerical methods [16, 20, 27]. Here we focus on the unknown density $f_{(X_j^a, T_i)}$ and we show that it solves a system of Volterra-Fredholm integral equations [1]:

THEOREM 3.3. *Let $\mathbf{X}$ be a bivariate Gauss-Markov process with $\mathbf{X}(t_0) = \mathbf{x}_0$ and let $\mathbf{B}$ be a two-dimensional boundary with $B_1 > x_{01}$ and $B_2 > x_{02}$. The joint transition pdfs $f_{(X_i^a, T_j)}$, for $i, j = 1, 2; \; i \neq j$, are solutions of the following system of Volterra-Fredholm first kind integral equations*

$$\bar{F}_{\mathbf{X}}((x_1, B_2), t) = \int_{t_0}^{t} \int_{-\infty}^{B_2} \bar{F}_{\mathbf{X}}((x_1, B_2), t | (B_1, y), \tau) f_{(X_2^a, T_1)}(y, \tau) \, dy d\tau$$

$$+ \int_{t_0}^{t} \int_{-\infty}^{B_1} \bar{F}_{\mathbf{X}}((x_1, B_2), t | (y, B_2), \tau)] f_{(X_1^a, T_2)}(y, \tau) \, dy d\tau; \tag{3.5a}$$

$$\bar{F}_{\mathbf{X}}((B_1, x_2), t) = \int_{t_0}^{t} \int_{-\infty}^{B_2} \bar{F}_{\mathbf{X}}((B_1, x_2), t | (B_1, y), \tau) f_{(X_2^a, T_1)}(y, \tau) \, dy d\tau$$

$$+ \int_{t_0}^{t} \int_{-\infty}^{B_1} \bar{F}_{\mathbf{X}}((B_1, x_2), t | (y, B_2), \tau) f_{(X_1^a, T_2)}(y, \tau) \, dy d\tau, \tag{3.5b}$$

where $x_1 > B_1$ and $x_2 > B_2$.

Proof. Let us consider the exit times of the process $\mathbf{X}$. The survival distribution of $\mathbf{X}$, for $x_1 > B_1$ and $x_2 > B_2$, is given by

$$
\begin{aligned}
\bar{F}_{\mathbf{X}}(\mathbf{x}, t) &= \mathbb{P}\left(\mathbf{X}(t) \geq \mathbf{x}, T_1 < T_2\right) + \mathbb{P}\left(\mathbf{X}(t) \geq \mathbf{x}, T_1 > T_2\right) \\
&= \int_{t_0}^{t} \int_{-\infty}^{B_2} \mathbb{P}\left(\mathbf{X}(t) \geq \mathbf{x}, T_1 < T_2 | T_1 = \tau, X_2(T_1) = y\right) \\
&\quad \cdot \mathbb{P}\left(X_2(T_1) \in dy, T_1 \in d\tau, T_1 < T_2\right) \\
&\quad + \int_{t_0}^{t} \int_{-\infty}^{B_1} \mathbb{P}\left(\mathbf{X}(t) \geq \mathbf{x}, T_1 > T_2 | T_2 = \tau, X_1(T_2) = y\right) \\
&\quad \cdot \mathbb{P}\left(X_1(T_2) \in dy, T_2 \in d\tau, T_1 > T_2\right) \\
&= \int_{t_0}^{t} \int_{-\infty}^{B_2} \mathbb{P}\left(\mathbf{X}(t) \geq \mathbf{x} | \mathbf{X}(\tau) = (B_1, y)\right) f_{(X_2^a, T_1)}(y, \tau)\, dy d\tau \\
&\quad + \int_{t_0}^{t} \int_{-\infty}^{B_1} \mathbb{P}\left(\mathbf{X}(t) \geq \mathbf{x} | \mathbf{X}(\tau) = (y, B_2)\right) f_{(X_1^a, T_2)}(y, \tau)\, dy d\tau, \quad (3.6)
\end{aligned}
$$

where the last equality follows from the strong Markov property. Then, the thesis (3.5) follows by choosing $\mathbf{x} = (x_1, B_2)$ and $\mathbf{x} = (B_1, x_2)$ respectively. $\square$

COROLLARY 3.4. *Differentiating (3.6) with respect to $\mathbf{x}$ and since $\int_{t_0}^{t_i} \int_{-\infty}^{B_2} f_{(X_1^a, T_2)}(y, \tau) dy d\tau = 1$, it follows*

$$
\begin{aligned}
f_{\mathbf{X}}(\mathbf{x}, t) &= \int_{t_0}^{t} \int_{-\infty}^{B_2} f_{\mathbf{X}}\left(\mathbf{x}, t | (B_1, y), \tau\right) f_{(X_2^a, T_1)}(y, \tau)\, dy d\tau \\
&\quad + \int_{t_0}^{t} \int_{-\infty}^{B_1} f_{\mathbf{X}}\left(\mathbf{x}, t | (y, B_2), \tau\right) f_{(X_1^a, T_2)}(y, \tau)\, dy d\tau.
\end{aligned}
$$

REMARK 2. *When B_1 and B_2 are regular boundaries, the distribution of (T_1, T_2) can be similarly computed for other processes:*

- *For a diffusion process, the faster component pursues its evolution after the crossing time. Mimicking Theorem 3.1, the joint FPT distribution can be rewritten as a product of $f_{(X_i^a, T_j)}$ and $f_{(X^j, T_i)}$, with $\mathbf{X}(T_j) = (X_i^a(T_j), B_j)$, for $T_j < T_i, i, j = 1, 2, i \neq j$. The first factor describes the dynamics of the process up to time $\min(T_1, T_2) = T_j$: the component j reaches its threshold, and X_i is constrained to be under the boundary B_i. The second factor describes the evolution of the process in $(\min(T_1, T_2), \max(T_1, T_2))$, i.e. (T_j, T_i): the component j pursues its evolution starting from the boundary B_j at time T_j, while the component i starts in $X_i(T_j)$ and has its FPT at time T_i.*

- *Imagine that, whenever a component reaches its value, it is reset to a starting value and then pursues its evolution. The intertimes between two consecutive FPTs of the same component are independent and identically distributed and thus each component is marginally modeled by a renewal process. Then the joint FPT distribution can be rewritten as a product of $f_{(X_i^a, T_j)}$ and $f_{(X_j, T_i)}$, when $T_j < T_i, i, j = 1, 2, i \neq j$. The second factor describes the evolution of the process in $(\min(T_1, T_2), \max(T_1, T_2))$, i.e. (T_j, T_i): $\mathbf{X}$ starts in $\mathbf{X}(T_j) = (X_i^a(T_j), x_{0j})$, where the firing component X_j is reset to its initial value x_{0j}. Then the slower component i has its FPT at time T_i, while X_j evolves, possibly with further crossings of B_j (with corresponding reset) before T_i.*

In both cases, the joint FPT density depends on $f_{(X_i^a, T_j)}$, which can be obtained through Theorem 3.3.

4. Numerical method and its convergence property. For a Gauss-Markov process, the density $f_{(X_j^a, T_i)}$ is generally unknown. Therefore the system (3.5) cannot be analytically solved and the joint FPT distribution (3.1) cannot be explicitly derived. Here we propose a numerical method to solve (3.5) and therefore approximate $f_{(X_j^a, T_i)}$.

Consider an assigned two-dimensional time interval $[0, \Theta_1] \times [0, \Theta_2]$, with $\Theta_1, \Theta_2 \in \mathbb{R}^+$. For each component $i = 1, 2$, let h_i and r_i be the time and space discretization steps, respectively. On $\{[-\infty, B_1] \times [-\infty, B_2] \times [0, \Theta_1] \times [0, \Theta_2]\}$ we introduce the partition $\{(y_{u_1}, y_{u_2}); t_{k_1}, t_{k_2}\}$ where $t_{k_i} = k_i h_i$ is the time discretization and $y_{u_i} = B_i - u_i r_i$ is the space discretization for $k_i = 0, \ldots, N_i, N_i h_i = \Theta_i, u_i \in \mathbb{N}$, and $i = 1, 2$.

To simplify the notations, we consider $h_1 = h_2 = h$ and $\Theta_1 = \Theta_2 = \Theta$, implying $N_1 = N_2 = N$, $k_1 = k_2 = k$ and thus $t_{k_1} = t_{k_2} = t_k$, for $k = 0, \ldots, N$.

Let $\hat{f}_{(X_1^a, T_2)}(y, t_j)$ denote the approximation of $f_{(X_1^a, T_2)}(y, t_j)$ due to the time discretization procedure. We approximate the time integrals of (3.5) through the Euler method [14], obtaining a system of integral equations for $\hat{f}_{(X_i^a, T_j)}(y, t)$, $i = 1, 2$. For $x_1 < B_1$ and $x_2 < B_2$, we get

$$\bar{F}_{\mathbf{X}}((x_1, B_2), t_k) = h \sum_{\rho=0}^{k} \int_{-\infty}^{B_2} \bar{F}_{\mathbf{X}}((x_1, B_2), t_k | (B_1, y), t_\rho) \hat{f}_{(X_2^a, T_1)}(y, t_\rho) \, dy$$

$$+ h \sum_{\rho=0}^{k} \int_{-\infty}^{B_1} \bar{F}_{\mathbf{X}}((x_1, B_2), t_k | (y, B_2), t_\rho) \hat{f}_{(X_1^a, T_2)}(y, t_\rho) \, dy; \quad (4.1a)$$

$$\bar{F}_{\mathbf{X}}((B_1, x_2), t_k) = h \sum_{\rho=0}^{k} \int_{-\infty}^{B_2} \bar{F}_{\mathbf{X}}((B_1, x_2), t_k | (B_1, y), t_\rho) \hat{f}_{(X_2^a, T_1)}(y, t_\rho) \, dy$$

$$+ h \sum_{\rho=0}^{k} \int_{-\infty}^{B_1} \bar{F}_{\mathbf{X}}((B_1, x_2), t_k | (y, B_2), t_\rho) \hat{f}_{(X_1^a, T_2)}(y, t_\rho) dy. \quad (4.1b)$$

Let $\mathbb{1}_A$ denote the indicator function of the set A. Then

$$\bar{F}_{\mathbf{X}}((B_1, x_2), t_k | (B_1, y), t_k) = \mathbb{1}_{\{y > x_2\}}; \quad (4.2)$$
$$\bar{F}_{\mathbf{X}}((B_1, x_2), t_k | (y, B_2), t_k) = 0;$$
$$\bar{F}_{\mathbf{X}}((x_1, B_2), t_k | (B_1, y), t_k) = 0;$$
$$\bar{F}_{\mathbf{X}}((x_1, B_2), t_k | (y, B_2), t_k) = \mathbb{1}_{\{y > x_1\}}.$$

Plugging (4.2) into (4.1) and differentiating with respect to $x_j, j = 1, 2$, we get the

system

$$\frac{\partial \bar{F}_{\mathbf{X}}((x_1, B_2), t_k)}{\partial x_1} = h\hat{f}_{(X_1^a, T_2)}(x_1, t_k)$$

$$+ h\sum_{\rho=0}^{k-1}\int_{-\infty}^{B_2}\frac{\partial \bar{F}_{\mathbf{X}}((x_1, B_2), t_k | (B_1, y), t_\rho)}{\partial x_1}\hat{f}_{(X_2^a, T_1)}(y, t_\rho)\, dy$$

$$+ h\sum_{\rho=0}^{k-1}\int_{-\infty}^{B_1}\frac{\partial \bar{F}_{\mathbf{X}}((x_1, B_2), t_k | (y, B_2), t_\rho)}{\partial x_1}\hat{f}_{(X_1^a, T_2)}(y, t_\rho)\, dy;$$

$$(4.3a)$$

$$\frac{\partial \bar{F}_{\mathbf{X}}((B_1, x_2), t_k)}{\partial x_2} = h\hat{f}_{(X_2^a, T_1)}(x_2, t_k)$$

$$+ h\sum_{\rho=0}^{k-1}\int_{-\infty}^{B_2}\frac{\partial \bar{F}_{\mathbf{X}}((B_1, x_2), t_k | (B_1, y), t_\rho)}{\partial x_2}\hat{f}_{(X_2^a, T_1)}(y, t_\rho)\, dy$$

$$+ h\sum_{\rho=0}^{k-2}\int_{-\infty}^{B_1}\frac{\partial \bar{F}_{\mathbf{X}}((B_1, x_2), t_k | (y, B_2), t_\rho)}{\partial x_2}\hat{f}_{(X_1^a, T_2)}(y, t_\rho)dy. \quad (4.3b)$$

Discretizing the spatial integral and truncating the corresponding series with a finite sum, we obtain

$$\frac{\partial \bar{F}_{\mathbf{X}}((x_1, B_2), t_k)}{\partial x_1} = h\tilde{f}_{(X_1^a, T_2)}(x_1, t_k)$$

$$+ hr_2\sum_{\rho=0}^{k-1}\sum_{u_2=0}^{m_2}\frac{\partial \bar{F}_{\mathbf{X}}((x_1, B_2), t_k | (B_1, y_{u_2}), t_\rho)}{\partial x_1}\tilde{f}_{(X_2^a, T_1)}(y_{u_2}, t_\rho)$$

$$+ hr_1\sum_{\rho=0}^{k-1}\sum_{u_1=0}^{m_1}\frac{\partial \bar{F}_{\mathbf{X}}((x_1, B_2), t_k | (y_{u_1}, B_2), t_\rho)}{\partial x_1}\tilde{f}_{(X_1^a, T_2)}(y_{u_1}, t_\rho);$$

$$(4.4a)$$

$$\frac{\partial \bar{F}_{\mathbf{X}}((B_1, x_2), t_k)}{\partial x_2} = h\tilde{f}_{(X_2^a, T_1)}(x_2, t_k)$$

$$+ hr_2\sum_{\rho=0}^{k-1}\sum_{u_2=0}^{m_2}\frac{\partial \bar{F}_{\mathbf{X}}((B_1, x_2), t_k | (B_1, y_{u_2}), t_\rho)}{\partial x_2}\tilde{f}_{(X_2^a, T_1)}(y_{u_2}, t_\rho)$$

$$+ hr_1\sum_{\rho=0}^{k-1}\sum_{u_1=0}^{m_1}\frac{\partial \bar{F}_{\mathbf{X}}((B_1, x_2), t_k | (y_{u_1}, B_2), t_\rho)}{\partial x_2}\tilde{f}_{(X_1^a, T_2)}(y_{u_1}, t_\rho).$$

$$(4.4b)$$

Here $\tilde{f}_{(X_i^a, T_j)}(y, t)$ denotes the approximation of $f_{(X_i^a, T_j)}(y, t)$ due to the time and space discretization procedures and to the truncation of the infinite sums of the space discretization.

Since $f_{(X_i^a, T_j)}(y_{u_i}, t_0) = 0$, we set $\tilde{f}_{(X_i, T_j)}(y_{u_i}, t_0) = 0$. The following algorithm can be used to approximate $f_{(X_i^a, T_j)}$ in the knots $\{(y_{u_1}, y_{u_2}); t_k\}$:

Step 1

$$\tilde{f}_{(X_1^a, T_2)}(y_{u_1}, t_1) = \frac{1}{h} \left. \frac{\partial}{\partial x_1} \bar{F}_{\mathbf{X}}((x_1, B_2), t_1) \right|_{x_1 = y_{u_1}} \quad ;$$

$$\tilde{f}_{(X_2^a, T_1)}(y_{u_2}, t_1) = \frac{1}{h} \left. \frac{\partial}{\partial x_2} \bar{F}_{\mathbf{X}}((B_1, x_2), t_1) \right|_{x_2 = y_{u_2}} \quad .$$

Step $k \geq 2$

$$\tilde{f}_{(X_1^a, T_2)}(y_{u_1}, t_k) = \left[\frac{1}{h} \left. \frac{\partial}{\partial x_1} \bar{F}_{\mathbf{X}}((x_1, B_2), t_k) \right|_{x_1 = y_{u_1}} \right.$$

$$- r_2 \sum_{\rho=0}^{k-1} \sum_{v_2=0}^{m_2} \tilde{f}_{(X_2^a, T_1)}(y_{v_2}, t_\rho) \left. \frac{\partial}{\partial x_1} \left[\bar{F}_{\mathbf{X}}((x_1, B_2), t_k | (B_1, y_{v_2}), t_\rho) \right] \right|_{x_1 = y_{u_2}}$$

$$\left. - r_1 \sum_{\rho=0}^{k-1} \sum_{v_1=0}^{m_1} \tilde{f}_{(X_1^a, T_2)}(y_{v_1}, t_\rho) \left. \frac{\partial}{\partial x_1} \left[\bar{F}_{\mathbf{X}}((x_1, B_2), t_k | (y_{v_1}, B_2), t_\rho)) \right] \right|_{x_1 = y_{u_1}} \right] \quad ;$$

$$\tilde{f}_{(X_2^a, T_1)}(y_{u_2}, t_k) = \left[\frac{1}{h} \left. \frac{\partial}{\partial x_2} \bar{F}_{\mathbf{X}}((B_1, x_2), t_k) \right|_{x_2 = y_{u_2}} \right.$$

$$- r_2 \sum_{\rho=0}^{k-1} \sum_{v_2=0}^{m_2} \tilde{f}_{(X_2^a, T_1)}(y_{v_2}, t_\rho) \left. \frac{\partial}{\partial x_2} \bar{F}_{\mathbf{X}}((B_1, x_2), t_k | (B_1, y_{v_2}), t_\rho) \right|_{x_2 = y_{u_2}}$$

$$\left. - r_1 \sum_{\rho=0}^{k-1} \sum_{v_1=0}^{m_1} \tilde{f}_{(X_1^a, T_2)}(y_{v_1}, t_\rho) \left. \frac{\partial}{\partial x_2} \bar{F}_{\mathbf{X}}((B_1, x_2), t_k | (y_{v_1}, B_2), t_\rho)) \right|_{x_2 = y_{u_1}} \right] \quad .$$

Note that at time t_1, $\hat{f}_{(X_i^a, T_j)}(y, t_1) = \tilde{f}_{(X_i^a, T_j)}(y_{u_i}, t_1)$ in each knot y_{u_i}.

REMARK 3. *We choose the Euler method because it simplifies the notation and is easy to implement. More efficient schemas, e.g. trapezoidal formula, can be similarly applied, improving the rate of convergence error of the proposed algorithm.*

5. Convergence of the algorithm. Let $E^{(i)}(y_{u_i}, t_k)$ denote the error of the proposed algorithm evaluated in the mesh points (y_{u_i}, t_k), for $k = 0, \ldots, N, u_i = 0, 1, \ldots, m_i, i = 1, 2$. It is defined by

$$E^{(i)}(y_{u_i}, t_k) = f_{(X_i^a, T_j)}(y_{u_i}, t_k) - \tilde{f}_{(X_i^a, T_j)}(y_{u_i}, t_k), \qquad i, j = 1, 2, i \neq j. \quad (5.1)$$

Mimiking the analysis of the error in [7], we rewrite the error (5.1) as a sum of two errors. The first is given by $e_k^{(i)}(y_{u_i}) = f_{(X_i^a, T_j)}(y_{u_i}, t_k) - \hat{f}_{(X_i^a, T_j)}(y_{u_i}, t_k)$ and is due to the time discretization. The second is given by $E_{k, u_i}^{(i)} = \hat{f}_{(X_i^a, T_j)}(y_{u_i}, t_k) - \tilde{f}_{(X_i^a, T_j)}(y_{u_i}, t_k)$ and is determined by the spatial discretization and by the truncation introduced at steps $k \geq 2$. We start computing $E_{k, u_i}^{(i)}$ through the following

LEMMA 5.1. *It holds*

$$E_{k,u_1}^{(1)} = \sum_{\rho=0}^{k-1}\left[-\int_{-\infty}^{B_1} K_{1,k,\rho}((y_{u_1}, B_2), (y, B_2))\hat{f}_{(X_1^a, T_2)}(y, t_\rho)dy\right.$$

$$-\int_{-\infty}^{B_2} K_{1,k,\rho}((y_{u_1}, B_2), (B_1, y))\hat{f}_{(X_2^a, T_1)}(y, t_\rho)\, dy$$

$$+r_1\sum_{v_1=0}^{m_1} K_{1,k,\rho}((y_{u_1}, B_2), (y_{v_1}, B_2))\tilde{f}_{(X_1^a, T_2)}(y_{v_1}, t_\rho)$$

$$\left.+r_2\sum_{v_2=0}^{m_2} K_{1,k,\rho}((y_{u_1}, B_2), (B_1, y_{v_2}))\tilde{f}_{(X_2^a, T_1)}(y_{v_2}, t_\rho)\right]; \qquad (5.2a)$$

$$E_{k,u_2}^{(2)} = \sum_{\rho=0}^{k-1}\left[-\int_{-\infty}^{B_1} K_{2,k,\rho}((B_1, y_{u_2}), (y, B_2))\hat{f}_{(X_1^a, T_2)}(y, t_\rho)dy\right.$$

$$-\int_{-\infty}^{B_2} K_{2,k,\rho}((B_1, y_{u_2}), (B_1, y))\hat{f}_{(X_2^a, T_1)}(y, t_\rho)\, dy$$

$$+r_1\sum_{v_1=0}^{m_1} K_{2,k,\rho}((B_1, y_{u_2}), (y_{v_1}, B_2))\tilde{f}_{(X_1^a, T_2)}(y_{v_1}, t_\rho)$$

$$\left.+r_2\sum_{v_2=0}^{m_2} K_{2,k,\rho}((B_1, y_{u_2}), (B_1, y_{v_2}))\tilde{f}_{(X_2^a, T_1)}(y_{v_2}, t_\rho)\right], \qquad (5.2b)$$

where the kernels are

$$K_{1,k,t}((y_{u_1}, b), (c, d)) = \frac{\partial}{\partial x_1}\left[\bar{F}_{\mathbf{X}}((x_1, b), t_k|(c, d), t) - \bar{F}_{\mathbf{X}}((x_1, b), t_{k-1}|(c, d), t)\right]\Big|_{x_1=y_{u_1}} \qquad (5.3)$$

$$K_{2,k,t}((a, y_{u_2}), (c, d)) = \frac{\partial}{\partial x_2}\left[\bar{F}_{\mathbf{X}}((a, x_2), t_k|(c, d), t) - \bar{F}_{\mathbf{X}}((a, x_2), t_{k-1}|(c, d), t)\right]\Big|_{x_2=y_{u_2}}.$$

When $t = t_\rho$, we write $K_{i,k,\rho}$ instead of K_{i,k,t_ρ} to simplify the notation. Here $a, c \in (-\infty, B_1)$ and $b, d \in (-\infty, B_2)$.

Proof. Subtracting (4.4) from (4.3), we obtain

$$
\begin{aligned}
\hat{f}_{(X_1^a,T_2)}(x_1,t_k) - \tilde{f}_{(X_1^a,T_2)}(x_1,t_k) = \sum_{\rho=0}^{k-1} & \left[-\int_{-\infty}^{B_1} \frac{\partial \bar{F}_{\mathbf{X}}((x_1,B_2),t_k|(y,B_2),t_\rho)}{\partial x_1} \hat{f}_{(X_1^a,T_2)}(y,t_\rho)\, dy \right. \\
& - \int_{-\infty}^{B_2} \frac{\partial \bar{F}_{\mathbf{X}}((x_1,B_2),t_k|(B_1,y),t_\rho)}{\partial x_1} \hat{f}_{(X_2^a,T_1)}(y,t_\rho)\, dy \\
& + r_1 \sum_{u_1=0}^{m_1} \frac{\partial \bar{F}_{\mathbf{X}}((x_1,B_2),t_k|(y_{u_1},B_2),t_\rho)}{\partial x_1} \tilde{f}_{(X_1^a,T_2)}(y_{u_1},t_\rho) \\
& \left. + r_2 \sum_{u_2=0}^{m_2} \frac{\partial \bar{F}_{\mathbf{X}}((x_1,B_2),t_k|(B_1,y_{u_2}),t_\rho)}{\partial x_1} \tilde{f}_{(X_2^a,T_1)}(y_{u_2},t_\rho) \right]; \qquad (5.4a)
\end{aligned}
$$

$$
\begin{aligned}
\hat{f}_{(X_2^a,T_1)}(x_2,t_k) - \tilde{f}_{(X_2^a,T_1)}(x_2,t_k) = \sum_{\rho=0}^{k-1} & \left[-\int_{-\infty}^{B_1} \frac{\partial \bar{F}_{\mathbf{X}}((B_1,x_2),t_k|(y,B_2),t_\rho)}{\partial x_2} \hat{f}_{(X_1^a,T_2)}(y,t_\rho)\, dy \right. \\
& - \int_{-\infty}^{B_2} \frac{\partial \bar{F}_{\mathbf{X}}((B_1,x_2),t_k|(B_1,y),t_\rho)}{\partial x_2} \hat{f}_{(X_2^a,T_1)}(y,t_\rho)\, dy \\
& + r_1 \sum_{\rho=0}^{k} \sum_{u_1=0}^{m_1} \frac{\partial \bar{F}_{\mathbf{X}}((B_1,x_2),t_k|(y_{u_1},B_2),t_\rho)}{\partial x_2} \tilde{f}_{(X_1^a,T_2)}(y_{u_1},t_\rho) \\
& \left. + r_2 \sum_{u_2=0}^{m_2} \frac{\partial \bar{F}_{\mathbf{X}}((B_1,x_2),t_k|(B_1,y_{u_2}),t_\rho)}{\partial x_2} \tilde{f}_{(X_2^a,T_1)}(y_{u_2},t_\rho) \right]. \qquad (5.4b)
\end{aligned}
$$

If we rewrite (5.4) for $k-1$, without making the $(k-1)$th term explicit, we obtain

$$
\begin{aligned}
\sum_{\rho=0}^{k-1} & \left[-\int_{-\infty}^{B_1} \frac{\partial \bar{F}_{\mathbf{X}}((x_1,B_2),t_k|(y,B_2),t_\rho)}{\partial x_1} \hat{f}_{(X_1^a,T_2)}(y,t_\rho)\, dy \right. \\
& - \int_{-\infty}^{B_2} \frac{\partial \bar{F}_{\mathbf{X}}((x_1,B_2),t_k|(B_1,y),t_\rho)}{\partial x_1} \hat{f}_{(X_2^a,T_1)}(y,t_\rho)\, dy \\
& + r_1 \sum_{u_1=0}^{m_1} \frac{\partial \bar{F}_{\mathbf{X}}((x_1,B_2),t_k|(y_{u_1},B_2),t_\rho)}{\partial x_1} \tilde{f}_{(X_1^a,T_2)}(y_{u_1},t_\rho) \\
& \left. + r_2 \sum_{u_2=0}^{m_2} \frac{\partial \bar{F}_{\mathbf{X}}((x_1,B_2),t_k|(B_1,y_{u_2}),t_\rho)}{\partial x_1} \tilde{f}_{(X_2^a,T_1)}(y_{u_2},t_\rho) \right] = 0; \qquad (5.5a)
\end{aligned}
$$

$$
\begin{aligned}
\sum_{\rho=0}^{k-1} & \left[-\int_{-\infty}^{B_1} \frac{\partial \bar{F}_{\mathbf{X}}((B_1,x_2),t_k|(y,B_2),t_\rho)}{\partial x_2} \hat{f}_{(X_1^a,T_2)}(y,t_\rho)\, dy \right. \\
& - \int_{-\infty}^{B_2} \frac{\partial \bar{F}_{\mathbf{X}}((B_1,x_2),t_k|(B_1,y),t_\rho)}{\partial x_2} \hat{f}_{(X_2^a,T_1)}(y,t_\rho)\, dy \\
& + r_1 \sum_{\rho=0}^{k} \sum_{u_1=0}^{m_1} \frac{\partial \bar{F}_{\mathbf{X}}((B_1,x_2),t_k|(y_{u_1},B_2),t_\rho)}{\partial x_2} \tilde{f}_{(X_1^a,T_2)}(y_{u_1},t_\rho) \\
& \left. + r_2 \sum_{u_2=0}^{m_2} \frac{\partial \bar{F}_{\mathbf{X}}((B_1,x_2),t_k|(B_1,y_{u_2}),t_\rho)}{\partial x_2} \tilde{f}_{(X_2^a,T_1)}(y_{u_2},t_\rho) \right] = 0, \qquad (5.5b)
\end{aligned}
$$

due to conditions (4.2). Then, the thesis follows subtracting (5.5) from (5.4) and setting $x_i = y_{u_i}$, for $i = 1, 2$. □

The following theorem gives the convergence of the proposed algorithm.

THEOREM 5.2. *For* $i, j = 1, 2, i \neq j, k = 1, \ldots, N, \rho = 0, \ldots, k-1, u_i = 0, \ldots, m_i,$
if conditions

(i) $K_{i,k,\rho}((a,b),(c,y))\hat{f}_{(X_j^a,T_i)}(y,t_\rho)$ *and* $K_{i,k,\rho}((a,b),(y,d))\hat{f}_{(X_i^a,T_j)}(y,t_\rho)$ *are ultimately monotonic in* y;

(ii) $f_{(X_i^a,T_j)}(y,t_\rho)$ *is bounded, belongs to* L^1 *and there exist positive functions* $C_{i,1}(y) \in L^1$, $C_{i,2}(y) \in L^1$, *with* $x \in (-\infty, B_1)$ *and* $y \in (-\infty, B_2)$, *such that*

$$|K_{i,k,\rho}((a,b),(y,d))| \leq h C_{i,1}(y);$$
$$|K_{i,k,\rho}((a,b),(c,y))| \leq h C_{i,2}(y),$$

and $C_{i,1}(0)$ *and* $C_{i,2}(0)$ *are bounded;*

(iii) *for* $l = 1, 2$

$$\int_{-\infty}^{B_i - m_i(r_i)r_i} C_{l,i}(y) \left| \hat{f}_{(X_i^a,T_j)}(y,t_\rho) \right| dy \leq \psi_{l,i} r_i, \tag{5.6}$$

as $r_i \to 0$ *and* $m_i(r_i)r_i \to \infty$, *where* $\psi_{l,i}$ *are positive constant;*

(iv) *for* $l = 1, 2$, *there exist constants* $Q_{l,i}$ *such that*

$$\left| \int_{-\infty}^{B_i} \frac{\partial}{\partial t} \left[C_{l,i}(y) f_{(X_i^a,T_j)}(y,t_\rho) \right] dy \right| \leq Q_{l,i}; \tag{5.7}$$

(v) *for* $l = 1, 2$, $\mathbf{z}_1 = (y_{u_1}, B_2)$ *and* $\mathbf{z}_2 = (B_1, y_{u_2})$,

$$\frac{\partial}{\partial t} \left[\bar{F}_{\mathbf{X}}(\mathbf{z}_l, t_\rho | (B_1, y), t) f_{(X_2^a,T^1)}(y,t) \right] |_{t=\tau} \in L^1 \ in \ y \in (-\infty, B_2);$$

$$\frac{\partial}{\partial t} \left[\bar{F}_{\mathbf{X}}(\mathbf{z}_l, t_\rho | (y, B_2), t) f_{(X_1^a,T^2)}(y,t) \right] |_{t=\tau} \in L^1 \ in \ y \in (-\infty, B_1);$$

$$\frac{\partial}{\partial y_{u_l}} \frac{\partial}{\partial t} \left[\bar{F}_{\mathbf{X}}(\mathbf{z_1}, t_\rho | (B_1, y), t) f_{(X_2^a,T^1)}(y,t) \right] |_{t=\tau} \in L^1 \ in \ y \in (-\infty, B_2);$$

$$\frac{\partial}{\partial y_{u_l}} \frac{\partial}{\partial t} \left[\bar{F}_{\mathbf{X}}(\mathbf{z}_l, t_\rho | (y, B_2), t) f_{(X_1^a,T^2)}(y,t) \right] |_{t=\tau} \in L^1 \ in \ y \in (-\infty, B_1).$$

are satisfied, then

$$E^{(i)}(y_{u_i}, t_k) = O(h) + O(r), \tag{5.8}$$

where $r = max(r_1, r_2)$.

Proof. At first, we study the error $E^{(i)}_{k,u_i}$ due to the spatial discretization. It can be decomposed as

$$E^{(i)}_{k,u_i} = A^{(i)}_{k,u_i} - B^{(i)}_{k,u_i}, \qquad k = 1, \ldots, N. \tag{5.9}$$

Here, $A_{k,u_i}^{(i)}$ has the same expression of $E_{k,u_i}^{(i)}$ in (5.2), replacing $\tilde{f}_{(X_i^a,T_j)}(y,t_j)$ with $\hat{f}_{(X_i^a,T_j)}(y,t_j)$. Moreover, $B_{k,u_i}^{(i)}$ is defined by

$$B_{k,u_1}^{(1)} = \sum_{\rho=0}^{k-1}\left[r_1\sum_{v_1=0}^{m_1}K_{1,k,\rho}((y_{u_1},B_2),(y_{v_1},B_2))E_{\rho,v_1}^{(1)}\right.$$
$$\left.+r_2\sum_{v_2=0}^{m_2}K_{1,k,\rho}((y_{u_1},B_2),(B_1,y_{v_2}))E_{\rho,v_2}^{(2)}\right], \qquad (5.10a)$$

$$B_{k,u_2}^{(2)} = \sum_{\rho=0}^{k-1}\left[r_1\sum_{v_1=0}^{m_1}K_{2,k,\rho}((B_1,y_{u_2}),(y_{v_1},B_2))E_{\rho,v_1}^{(1)}\right.$$
$$\left.+r_2\sum_{v_2=0}^{m_2}K_{2,k,\rho}((B_1,y_{u_2}),(B_1,y_{v_2}))E_{\rho,v_2}^{(2)}\right]. \qquad (5.10b)$$

The term $A_{k,u_i}^{(i)}$ accounts for the approximation of the spatial integrals with finite sums. Hence we can split it into a first term $A_{k,u_i}^{(i,a)}$ accounting for the discretization procedure and a second $A_{k,u_i}^{(i,b)}$ for the truncation of the series.

By definition of $A_{k,u_i}^{(i,a)}$, we have

$$|A_{k,u_1}^{(1,a)}| = \left|\sum_{\rho=0}^{k-1}\left\{\left[\int_{-\infty}^{B_1}K_{1,k,\rho}((y_{u_1},B_2),(y,B_2))\hat{f}_{(X_1^a,T_2)}(y,t_\rho)dy\right.\right.\right.$$
$$\left.-r_1\sum_{v_1=0}^{\infty}K_{1,k,\rho}((y_{u_1},B_2),(y_{v_1},B_2))\hat{f}_{(X_1^a,T_2)}(y_{v_1},t_\rho)\right]$$
$$+\left[\int_{-\infty}^{B_2}K_{1,k,\rho}((y_{u_1},B_2),(B_1,y))\hat{f}_{(X_2^a,T_1)}(y,t_\rho)\,dy\right.$$
$$\left.\left.\left.-r_2\sum_{v_2=0}^{\infty}K_{1,k,\rho}((y_{u_1},B_2),(B_1,y_{v_2}))\hat{f}_{(X_2^a,T_1)}(y_{v_2},t_\rho)\right]\right\}\right|; \qquad (5.11a)$$

$$|A_{k,u_2}^{(2,a)}| = \left|\sum_{\rho=0}^{k-1}\left\{\left[\int_{-\infty}^{B_1}K_{2,k,\rho}((B_1,y_{u_2}),(y,B_2))\hat{f}_{(X_1^a,T_2)}(y,t_\rho)dy\right.\right.\right.$$
$$\left.-r_1\sum_{v_1=0}^{\infty}K_{2,k,\rho}((B_1,y_{u_2}),(y_{v_1},B_2))\hat{f}_{(X_1^a,T_2)}(y_{v_1},t_\rho)\right]$$
$$+\left[\int_{-\infty}^{B_2}K_{2,k,\rho}((B_1,y_{u_2}),(B_1,y))\hat{f}_{(X_2^a,T_1)}(y,t_\rho)\,dy\right.$$
$$\left.\left.\left.-r_2\sum_{v_2=0}^{\infty}K_{2,k,\rho}((B_1,y_{u_2}),(B_1,y_{v_2}))\hat{f}_{(X_2^a,T_1)}(y_{v_2},t_\rho)\right]\right\}\right|. \qquad (5.11b)$$

Let us focus on the terms in the first square brackets in (5.11a). It holds

$$\left| \int_{-\infty}^{B_1} K_{1,k,\rho}((y_{u_1}, B_2), (y, B_2)) \hat{f}_{(X_1^a, T_2)}(y, t_\rho) dy \right.$$

$$\left. - r_1 \sum_{v_1=0}^{\infty} K_{1,k,\rho}((y_{u_1}, B_2), (y_{v_1}, B_2)) \hat{f}_{(X_1^a, T_2)}(y_{v_1}, t_\rho) \right|$$

$$\leq \left| \int_{B_1-r_1}^{B_1} K_{1,k,\rho}((y_{u_1}, B_2), (y, B_2)) \hat{f}_{(X_1^a, T_2)}(y, t_\rho) dy \right|$$

$$\leq h \int_{B_1-r_1}^{B_1} C_{1,1}(y) \left| \hat{f}_{(X_1^a, T_2)}(y, t_\rho) \right| dy$$

$$\leq h r_1 \eta_{1,1}, \tag{5.12}$$

where we used condtion (i) and eq. (3.4.5) in [9] in the first inequality and condition (ii) in the second. Note that the numerical approximations $\hat{f}_{(X_j^a, T_i)}(y, t_\rho)$ can be rewritten as a function of $f_{(X_j^a, T_i)}(y, t_\rho)$ and $K_{i,k,\rho}(a, b, c, d)$, as shown in Remark 2 in [7]. Then, thanks to condition (ii), it follows that $\hat{f}_{(X_j^a, T_i)}(y, t_\rho)$ is bounded. Moreover, the integrable function $C_{1,1}(y)$ on the compact interval $[B_1 - r_1, B_1]$ is bounded. Thus $C_{1,1}(y) || \hat{f}_{(X_1^a, T_2)}(y, t_\rho)| \leq \eta_{1,1}$ for a positive constant η_1, which yields (5.12). A similar procedure can be done for the terms in the second square brackets in (5.11a) and for those in (5.11b), obtaining

$$|A_{k,u_1}^{(1,a)}| \leq (r_1 \eta_{1,1} + r_2 \eta_{1,2}) \sum_{\rho=0}^{k-1} h = (r_1 \eta_{1,1} + r_2 \eta_{1,2}) t_{k-1}; \tag{5.13a}$$

$$|A_{k,u_2}^{(2,a)}| \leq (r_1 \eta_{2,1} + r_2 \eta_{2,2}) \sum_{\rho=0}^{k-1} h = (r_1 \eta_{2,1} + r_2 \eta_{2,2}) t_{k-1}. \tag{5.13b}$$

Here $\eta_{i,l}$ are positive constant given by

$$C_{l,i}(y) f_{(X_i^a, T_j)}(y, t_\rho) \leq \eta_{l,i},$$

for $i, j, l = 1, 2, i \neq j$. Let us now consider the error $A_{k,u_i}^{(i,b)}$. Using condition (i), eq. (3.4.5) in [9] and then conditions (ii), (iii) in sequence, we get

$$|A_{k,u_1}^{(1,b)}| = \left| \sum_{\rho=0}^{k-1} \left[r_1 \sum_{v_1=m_1+1}^{\infty} K_{1,k,\rho}((y_{u_1}, B_2), (y_{v_1}, B_2)) \hat{f}_{(X_1^a, T_2)}(y_{v_1}, t_\rho) \right. \right.$$

$$\left. \left. + r_2 \sum_{v_2=m_2+1}^{\infty} K_{1,k,\rho}((y_{u_1}, B_2), (B_1, y_{v_2})) \hat{f}_{(X_2^a, T_1)}(y_{v_2}, t_\rho) \right] \right|$$

$$\leq \left| \sum_{\rho=0}^{k-1} h \left[\int_{-\infty}^{B_1-m_1 r_1} C_{1,1}(y) \hat{f}_{(X_1^a, T_2)}(y, t_\rho) dy \right. \right.$$

$$\left. \left. + \int_{-\infty}^{B_2-m_2 r_2} C_{1,2}(y) \hat{f}_{(X_2^a, T_1)}(y, t_\rho) dy \right] \right|$$

$$\leq (\psi_{1,1} r_1 + \psi_{1,2} r_2) t_k; \tag{5.14a}$$

$$|A_{k,u_2}^{(2,b)}| \leq (\psi_{2,1} r_1 + \psi_{2,2} r_2) t_k, \tag{5.14b}$$

where (5.14b) is obtained as (5.14a).

From (5.13), (5.14) and $r = \max(r_1, r_2)$, we get $|A_{k,u_i}^{(i)}| \leq rG_i t_k$, where G_i, $i = 1, 2$ are positive suitable constants. Using these bounds in (5.9) and observing that $B_{k,u_i}^{(i)}$ in (5.10) involves the errors $E_{\rho,v_i}^{(i)}$ for $0 \leq \rho \leq k - 1$, we get a system of inequalities

$$
|E_{k,u_1}^{(1)}| \leq G_1 r t_k + r \sum_{\rho=0}^{k-1} \left[\sum_{v_1=0}^{m_1} |K_{1,k,\rho}((y_{u_1}, B_2), (y_{v_1}, B_2))||E_{\rho,v_1}^{(1)}| \right.
$$
$$
\left. + \sum_{v_2=0}^{m_2} |K_{1,k,\rho}((y_{u_1}, B_2), (B_1, y_{v_2}))||E_{\rho,v_2}^{(2)}| \right] \tag{5.15a}
$$

$$
|E_{k,u_2}^{(2)}| \leq G_2 r t_k + r \sum_{\rho=0}^{k-1} \left[\sum_{v_1=0}^{m_1} |K_{2,k,\rho}((B_1, y_{u_2}), (y_{v_1}, B_2))||E_{\rho,v_1}^{(1)}| \right.
$$
$$
\left. + \sum_{v_2=0}^{m_2} |K_{2,k,\rho}((B_1, y_{u_2}), (B_1, y_{v_2}))||E_{\rho,v_2}^{(2)}| \right]. \tag{5.15b}
$$

We extend the method proposed in [7] to the system (5.15), that we solve iteratively as follows:

$$
|E_{0,u_i}^{(i)}| = 0 := r p_0^{(i)};
$$
$$
|E_{1,u_i}^{(i)}| \leq G_i r t_1 =: r p_1^{(i)};
$$
$$
|E_{2,u_1}^{(1)}| \leq G_1 r t_2 + r \left[r p_1^{(1)} \sum_{v_1=0}^{m_1} |K_{1,k,\rho}((y_{u_1}, B_2), (y_{v_1}, B_2))| \right.
$$
$$
\left. + r p_1^{(2)} \sum_{v_2=0}^{m_2} |K_{1,k,\rho}((y_{u_1}, B_2), (B_1, y_{v_2}))| \right]
$$
$$
\leq r \left[G_1 t_2 + r \beta_1^1 p_1^{(1)} + r \beta_2^1 p_1^{(2)} \right] =: r p_2^{(1)}; \tag{5.16}
$$
$$
|E_{2,u_2}^{(2)}| \leq r \left[G_2 t_2 + r \beta_1^2 p_1^{(1)} + r \beta_2^2 p_1^{(2)} \right] := r p_2^{(2)},
$$

where (5.16) holds due to condition (ii), eq. (3.4.5) in [9]. Here $\beta_l^i, i, l = 1, 2$ are suitable constants, which do not depend on r and h. Iterating this procedure, (5.15) becomes

$$
|E_{k,u_1}^{(1)}| \leq r \left[G_1 t_k + r \sum_{\rho=0}^{k-1} \left(\beta_1^1 p_\rho^{(1)} + \beta_2^1 p_\rho^{(2)} \right) \right] := r p_k^{(1)}; \tag{5.17a}
$$

$$
|E_{k,u_2}^{(2)}| \leq r \left[G_2 t_k + r \sum_{\rho=0}^{k-1} \left(\beta_1^2 p_\rho^{(1)} + \beta_2^2 p_\rho^{(2)} \right) \right] := r p_k^{(2)}. \tag{5.17b}
$$

Since $t_k \leq \Theta$, from (5.17) it follows

$$
p_k^{(i)} \leq G_i \Theta + r \sum_{\rho=0}^{k-1} \left(\beta_1^i p_\rho^{(1)} + \beta_2^i p_\rho^{(2)} \right), \qquad i = 1, 2.
$$

Then, by eq. (7.18) in [14], we get $p_k^{(i)} \leq G_i \Theta exp[(\beta_1^1 + \beta_2^2)rt_k]$. Therefore

$$|E_{k,u_1}^{(1)}| \leq rG_1\Theta \exp\left[(\beta_1^1 + \beta_2^1)rt_k\right]; \tag{5.18a}$$

$$|E_{k,u_2}^{(2)}| \leq rG_2\Theta \exp\left[(\beta_1^2 + \beta_2^2)rt_k\right], \tag{5.18b}$$

implying $|E_{k,u_i}^{(i)}| = \mathrm{O}(r)$.

Now, we focus on the time discretization error $e_k^{(i)}(y_{u_i})$. The error formulas for the Euler method are

$$\delta_{1,1,k}(h) = \frac{ht_k}{2} \int_{-\infty}^{B_1} \frac{\partial}{\partial t} \bar{F}_\mathbf{X}((y_{u_1}, B_2), t_k|(y, B_2), t) f_{(X_1^a, T_2)}(y, t)\, dy \bigg|_{t=\tau}; \tag{5.19}$$

$$\delta_{1,2,k}(h) = \frac{ht_k}{2} \int_{-\infty}^{B_2} \frac{\partial}{\partial t} \bar{F}_\mathbf{X}((y_{u_1}, B_2), t_k|(B_1, y), t) f_{(X_2^a, T_1)}(y, t)\, dy \bigg|_{t=\tau};$$

$$\delta_{2,1,k}(h) = \frac{ht_k}{2} \int_{-\infty}^{B_1} \frac{\partial}{\partial t} \bar{F}_\mathbf{X}((B_1, y_{u_2}), t_k|(y, B_2), t) f_{(X_1^a, T_2)}(y, t)\, dy \bigg|_{t=\tau};$$

$$\delta_{2,2,k}(h) = \frac{ht_k}{2} \int_{-\infty}^{B_2} \frac{\partial}{\partial t} \bar{F}_\mathbf{X}((B_1, y_{u_2}), t_k|(B_1, y), t) f_{(X_2^a, T_1)}(y, t)\, dy \bigg|_{t=\tau},$$

where $\tau \in (0, \Theta)$ and we used $t_k = hk$. Rewriting (4.1) with the corresponding residuals and evaluating it in $x_i = y_{u_i}$, $i = 1, 2$ respectively, we get

$$\bar{F}_\mathbf{X}((y_{u_1}, B_2), t_k) = h\sum_{\rho=0}^{k} \int_{-\infty}^{B_1} \bar{F}_\mathbf{X}((y_{u_1}, B_2), t_k|(y, B_2), t_\rho) f_{(X_1^a, T_2)}(y, t_\rho)\, dy$$

$$+ h\sum_{\rho=0}^{k} \int_{-\infty}^{B_2} \bar{F}_\mathbf{X}((y_{u_1}, B_2), t_k|(B_1, y), t_\rho) f_{(X_2^a, T_1)}(y, t_\rho)\, dy$$

$$+ \delta_{1,1,k}(h) + \delta_{1,2,k}(h); \tag{5.20a}$$

$$\bar{F}_\mathbf{X}((B_1, y_{u_2}), t_k) = +h\sum_{\rho=0}^{k} \int_{-\infty}^{B_1} \bar{F}_\mathbf{X}((B_1, y_{u_2}), t_k|(y, B_2), t_\rho) f_{(X_1^a, T_2)}(y, t_\rho)\, dy$$

$$+ h\sum_{\rho=0}^{k} \int_{-\infty}^{B_2} \bar{F}_\mathbf{X}((B_1, y_{u_2}), t_k|(B_1, y), t_\rho) f_{(X_2^a, T_1)}(y, t_\rho)\, dy$$

$$+ \delta_{2,1,k}(h) + \delta_{2,2,k}(h). \tag{5.20b}$$

Subtracting (4.1) from (5.20) and differentiating with respect to y_{u_i}, we get a system of integral equations for $e_\rho^{(i)}(y)$ given by

$$-\frac{\partial}{\partial y_{u_1}}[\delta_{1,1,k}(h) + \delta_{1,2,k}(h)] = \left\{ h\sum_{\rho=0}^{k}\left[\frac{\partial}{\partial y_{u_1}} \int_{-\infty}^{B_1} \bar{F}_\mathbf{X}((y_{u_1}, B_2), t_k|(y, B_2), t_\rho) e_\rho^{(1)}(y) dy\right.\right.$$

$$+ \frac{\partial}{\partial y_{u_1}} \int_{-\infty}^{B_2} \bar{F}_\mathbf{X}((y_{u_1}, B_2), t_k|(B_1, y), t_\rho) e_\rho^{(2)}(y) dy\bigg]\bigg\}; \tag{5.21a}$$

$$-\frac{\partial}{\partial y_{u_2}}[\delta_{2,1,k}(h) + \delta_{2,2,k}(h)] = \left\{ h\sum_{\rho=0}^{k}\left[\frac{\partial}{\partial y_{u_2}} \int_{-\infty}^{B_1} \bar{F}_\mathbf{X}((B_1, y_{u_2}), t_k|(y, B_2), t_\rho) e_\rho^{(1)}(y) dy\right.\right.$$

$$+ \frac{\partial}{\partial y_{u_2}} \int_{-\infty}^{B_2} \bar{F}_\mathbf{X}((B_1, y_{u_2}), t_k|(B_1, y), t_\rho) e_\rho^{(2)}(y) dy\bigg]\bigg\}. \tag{5.21b}$$

Rewriting (5.21) with respect to $k-1$, subtracting it from (5.21) and using (4.2), we obtain

$$
e_k^{(1)}(y_{u_1}) - \sum_{\rho=0}^{k-1} \left[\int_{-\infty}^{B_1} K_{1,k,\rho}((y_{u_1}, B_2), (y, B_2)) e_\rho^{(1)}(y) dy \right.
$$

$$
\left. + \int_{-\infty}^{B_2} K_{1,k,\rho}((y_{u_1}, B_2), (B_1, y)) e_\rho^{(2)}(y) dy \right]
$$

$$
= \frac{\partial}{\partial y_{u_1}} \left[\frac{(\delta_{1,1,k}(h) - \delta_{1,1,k-1}(h)) + (\delta_{1,2,k}(h) - \delta_{1,2,k-1}(h))}{h} \right]; \qquad (5.22a)
$$

$$
e_k^{(2)}(y_{u_2}) - \sum_{\rho=0}^{k-1} \left[\int_{-\infty}^{B_1} K_{2,k,\rho}((B_1, y_{u_2}), (y, B_2)) e_\rho^{(1)}(y) dy \right.
$$

$$
\left. + \int_{-\infty}^{B_2} K_{2,k,\rho}((B_1, y_{u_2}), (B_1, y)) e_\rho^{(2)}(y) dy \right]
$$

$$
= \frac{\partial}{\partial y_{u_2}} \left[\frac{(\delta_{2,1,k}(h) - \delta_{2,1,k-1}(h)) + (\delta_{2,2,k}(h) - \delta_{2,2,k-1}(h))}{h} \right]. \qquad (5.22b)
$$

Using (5.3), (5.19) and condition (v), and since $t_{k-1} = t_k - h$, we have

$$
\frac{\partial}{\partial y_{u_1}} |\delta_{1,1,k}(h) - \delta_{1,1,k-1}(h)|
$$

$$
\leq \frac{h t_k}{2} \int_{-\infty}^{B_1} \frac{\partial}{\partial t} \left[|K_{1,k,t}((y_{u_1}, B_2), (y, B_2))| |f_{(X_1^a, T_2)}(y, t)| dy \right] \Big|_{t=\tau}
$$

$$
+ \frac{h^2}{2} \left| \frac{\partial}{\partial y_{u_1}} \int_{-\infty}^{B_1} \frac{\partial}{\partial t} \left[\bar{F}_{\mathbf{X}}((y_{u_1}, B_2), t_{k-1}|(y, B_2), t) f_{(X_1^a, T_2)}(y, t) dy \right] \Big|_{t=\tau} \right|
$$

$$
\leq \frac{h^2}{2} [t_k Q_{1,1} + S_{1,1}] := \frac{h^2}{2} \alpha_{1,1}.
$$

The last inequality holds applying conditions (ii) and (iv) on the first term, and condition (v) on the second term, for a suitable positive constant $S_{1,1}$. Similarly

$$
\frac{\partial}{\partial y_{u_l}} |\delta_{l,i,k}(h) - \delta_{l,i,k-1}(h)| \leq \frac{h^2}{2} [t_k Q_{l,i} + S_{l,i}] := \frac{h^2}{2} \alpha_{l,i},
$$

for $i, l = 1, 2$ and suitable positive constants $S_{l,i}$ obtained from condition (v). Then

(5.22) becomes

$$|e_k^{(1)}(y_{u_1})| \le \frac{(\alpha_{1,1}+\alpha_{1,2})ht_k}{2} + \sum_{\rho=0}^{k-1}\left[\int_{-\infty}^{B_1}\left|K_{1,k,\rho}((y_{u_1},B_2),(y,B_2))e_\rho^{(1)}(y)\right|dy\right.$$

$$\tag{5.23a}$$

$$\left.+\int_{-\infty}^{B_2}\left|K_{1,k,\rho}((y_{u_1},B_2),(B_1,y))e_\rho^{(2)}(y)\right|dy\right];$$

$$|e_k^{(2)}(y_{u_2})| \le \frac{(\alpha_{2,1}+\alpha_{2,2})ht_k}{2} + \sum_{\rho=0}^{k-1}\left[\int_{-\infty}^{B_1}\left|K_{2,k,\rho}((B_1,y_{u_2}),(y,B_2))e_\rho^{(1)}(y)\right|dy\right.$$

$$\tag{5.23b}$$

$$\left.+\int_{-\infty}^{B_2}\left|K_{2,k,\rho}((B_1,y_{u_2}),(B_1,y))e_\rho^{(2)}(y)\right|dy\right].$$

Setting $\gamma_l = \max\{\alpha_{l,1},\alpha_{l,2}\}$, for $l=1,2$, we can write the system (5.23) iteratively for $k \ge 0$, obtaining

$$|e_0^{(i)}| = 0 := hq_0^{(i)};$$

$$|e_1^{(i)}| \le \gamma_i ht_1 := hq_1^{(i)};$$

$$|e_2^{(1)}| \le \gamma_1 ht_2 + hq_1^{(1)}\int_{-\infty}^{B_1}|K_{1,k,\rho}((y_{u_1},B_2),(y,B_2))|dy + hq_1^{(2)}\int_{-\infty}^{B_2}|K_{1,k,\rho}((y_{u_1},B_2),(B_1,y))|dy$$

$$\le h\left(\gamma_1 t_2 + h\xi_1^1 q_1^{(1)} + h\xi_2^1 q_1^{(2)}\right) := hq_2^{(1)};$$

$$|e_2^{(2)}| \le h\left(\gamma_2 t_2 + h\xi_1^2 q_1^{(1)} + h\xi_2^2 q_1^{(2)}\right) := hq_2^{(2)},$$

where we used condition (ii) to bound $e_2^{(i)}$. Here ξ_i^j are suitable constants independent on h and r. In general

$$|e_k^{(1)}(y_{u_1})| \le h\left[\gamma_1 t_k + h\left(\xi_1^1\sum_{\rho=0}^{k-1}q_\rho^{(1)} + \xi_2^1\sum_{\rho=0}^{k-1}q_\rho^{(2)}\right)\right] := hq_k^{(1)}; \tag{5.24a}$$

$$|e_k^{(2)}(y_{u_2})| \le h\left[\gamma_2 t_k + h\left(\xi_1^2\sum_{\rho=0}^{k-1}q_\rho^{(1)} + \xi_2^2\sum_{\rho=0}^{k-1}q_\rho^{(2)}\right)\right] := hq_k^{(2)}. \tag{5.24b}$$

Since $t_k \le \Theta$, from (5.24) it follows

$$q_k^{(i)} \le \gamma_i\Theta + h\left(\xi_1^i\sum_{\rho=0}^{k-1}q_\rho^{(1)} + \xi_2^i\sum_{\rho=0}^{k-1}q_\rho^2\right), \qquad i=1,2,$$

and applying eq. (7.18) in [14], we get $q_k^{(i)} \le \gamma_i\Theta exp[(\xi_1^i+\xi_2^i)t_k]$ and thus

$$|e_k^{(1)}(y_{u_1})| \le h\gamma_1\Theta\exp\left[(\xi_1^1+\xi_2^1)t_k\right]; \tag{5.25a}$$

$$|e_k^{(2)}(y_{u_2})| \le h\gamma_2\Theta\exp\left[(\xi_1^2+\xi_1^2)t_k\right]. \tag{5.25b}$$

The thesis follows noting that $|e_k^{(i)}(y_{u_i})| = O(h)$. $\square$

REMARK 4. *The numerical approximations $\hat{f}_{(X_j^a,T_i)}(y,t_\rho)$ can be rewritten such that they depend only on $f_{(X_j^a,T_i)}(y,t_\rho)$ and $K_{i,k,\rho}(a,b,c,d)$, as shown in Remark 2 in [7]. Therefore, conditions (i) and (iii) are in fact assumptions on f and K.*

6. Joint distribution of (T_1, T_2) for a bivariate Wiener process. Consider a bivariate Wiener process $\mathbf{X}$ solving (2.1) with constant drift $\boldsymbol{\mu}(\mathbf{X}(t)) = (\mu_1, \mu_2) \in \mathbb{R}^2$ and positive-definite covariance matrix

$$\boldsymbol{\Sigma}(t) = \begin{pmatrix} \sigma_1 & 0 \\ \rho\sigma_2 & \sigma_2\sqrt{1-\rho^2} \end{pmatrix},$$

for $\rho \in (-1, 1)$. Then $\boldsymbol{X}$ is a bivariate Wiener process with null drift and covariance matrix

$$\widetilde{\boldsymbol{\Sigma}} = \begin{pmatrix} \sigma_1^2 & \rho\sigma_1\sigma_2 \\ \rho\sigma_1\sigma_2 & \sigma_2^2 \end{pmatrix}.$$

That is, each component is marginally a Wiener process with drift μ_i, diffusion coefficient $\sigma_i > 0, i = 1, 2$ and ρ is the correlation of the bivariate Wiener process, e.g. $\rho = 0$ corresponds to have independent components. For the Wiener process, the densities $f_{\mathbf{X}}$, $f_{X_i^a}$ and $g_{T_i}, i, j = 1, 2, i \neq j$ are known [8]. Then, to determine the joint FPT distribution using Theorem 3.1, the unknown conditional density $f_{X_i^a | T_j}$ has to be derived. The first step is to calculate the unknown transition density $f_{\mathbf{X}^a}$, which solves the two-dimensional Kolmogorov forward equation

$$\frac{\partial f_{\mathbf{X}^a}(\mathbf{x}, t)}{\partial t} = \frac{\sigma_1^2}{2} \frac{\partial^2 f_{\mathbf{X}^a}(\mathbf{x}, t)}{\partial x_1^2} + \frac{\sigma_2^2}{2} \frac{\partial^2 f_{\mathbf{X}^a}(\mathbf{x}, t)}{\partial x_2^2} + \sigma_1\sigma_2\rho \frac{\partial^2 f_{\mathbf{X}^a}(\mathbf{x}, t)}{\partial x_1 \partial x_2}$$
$$- \mu_1 \frac{\partial f_{\mathbf{X}^a}(\mathbf{x}, t)}{\partial x_1} - \mu_2 \frac{\partial f_{\mathbf{X}^a}(\mathbf{x}, t)}{\partial x_2}, \tag{6.1}$$

with initial, boundary and absorbing conditions given by

$$\lim_{t \to 0} f_{\mathbf{X}^a}(\mathbf{x}, t) = \delta(x_1 - x_{01})\delta(x_2 - x_{02}); \tag{6.2}$$

$$\lim_{x_1 \to -\infty} f_{\mathbf{X}^a}(\mathbf{x}, t) = \lim_{x_2 \to -\infty} f_{\mathbf{X}^a}(\mathbf{x}, t) = 0; \tag{6.3}$$

$$f_{\mathbf{X}^a}(\mathbf{x}, t)|_{x_1 = B_1} = f_{\mathbf{X}^a}(\mathbf{x}, t)|_{x_2 = B_2} = 0, \tag{6.4}$$

respectively, where we set $t_0 = 0$. The solution provided in [11] does not fulfill (6.2) when $(\mu_1, \mu_2) \neq (0, 0)$. Following their proof, we noted that the normalizing factor

$$\exp\left(-\frac{(\mu_2\rho\sigma_1\sigma_2 - \mu_1\sigma_2^2) B_1 + (\mu_1\rho\sigma_1\sigma_2 - \mu_2\sigma_1^2) B_2}{(1-\rho^2)\sigma_1^2\sigma_2^2}\right) \tag{6.5}$$

was missing. Since (6.5) is equal to 1 when $(\mu_1, \mu_2) = (0, 0)$, the results in [11] are correct for the driftless case. In presence of drift, it holds

LEMMA 6.1. *The density $f_{\mathbf{X}^a}$ that the process never reaches the boundary $\mathbf{B}$ in $(0, t)$ is given by*

$$f_{\mathbf{X}^a}(\mathbf{x}, t) = \frac{2}{\alpha K_3 t} \exp\{K_1(B_1 - x_{01}) + K_2(B_2 - x_{02})\}$$
$$\times \exp\left(-\frac{\sigma_1^2\mu_2^2 - 2\mu_1\mu_2\sigma_1\sigma_2\rho + \sigma_2^2\mu_1^2}{2K_3^2} t - \frac{\bar{r}^2 + \bar{r}_0^2}{2K_3^2 t}\right) H(\bar{r}, \bar{r}_0, \phi, \phi_0, t), \tag{6.6}$$

where $\bar{r} := \bar{r}(x_1, x_2) \in (0, \infty), \phi := \phi(x_1, x_2) \in (0, \alpha)$ and

$$\bar{r} = \sqrt{\sigma_1^2(B_2 - x_2)^2 + \sigma_2^2(B_1 - x_1)^2 - 2\sigma_1\sigma_2\rho(B_1 - x_1)(B_2 - x_2)};$$

$$\bar{r}\cos(\phi) = \sigma_2(B_1 - x_1) - \sigma_1\rho(B_2 - x_2), \quad \bar{r}\sin(\phi) = \sigma_1\sqrt{1 - \rho^2}(B_2 - x_2);$$

$$\bar{r}_0 = \bar{r}_{|x_1=x_{01};x_2=x_{02}};$$

$$\phi_0 = \phi_{0|x_1=x_{01};x_2=x_{02}};$$

$$K_1 = \frac{\sigma_2\mu_1 - \sigma_1\mu_2\rho}{\sigma_1^2\sigma_2(1 - \rho^2)}, \qquad K_2 = \frac{\sigma_1\mu_2 - \sigma_2\mu_1\rho}{\sigma_1\sigma_2^2(1 - \rho^2)}, \qquad K_3 = \sigma_1\sigma_2\sqrt{1 - \rho^2};$$

$$\alpha = \arctan\left(-\frac{\sqrt{1 - \rho^2}}{\rho}\right) \in (0, \pi);$$

$$H(\bar{r}, \bar{r}_0, \phi, \phi_0, t) = \sum_{n=1}^{\infty} \sin(\frac{n\pi\phi_0}{\alpha})\sin(\frac{n\pi\phi}{\alpha})I_{n\pi/\alpha}\left(\frac{\bar{r}\bar{r}_0}{K_3^2 t}\right).$$

Here $(\bar{r}, \phi)$ are functions of (x_1, x_2) and are obtained through a suitable change of variables in [11]. In (6.6) we use them instead of (x_1, x_2) to simplify the notation. To compare our results with those in [11], one should introduce the transformation $r = \bar{r}/\sigma_1$ and $r_0 = \bar{r}_0/\sigma_1$, since they use different constant terms.

REMARK 5. *The distribution of the first exit time of the process from the strip* $(-\infty, B_1) \times (-\infty, B_2)$ *is given by*

$$\mathbb{P}\left(\min(T_1, T_2) < t\right) = 1 - \int_{-\infty}^{B_1} \int_{-\infty}^{B_2} f_{\mathbf{X}^a}(\mathbf{x}, t)dx_1 dx_2,$$

and it can be computed multiplying eq. (32) in [11] with the missing factor (6.5).

COROLLARY 6.2. *The conditional density $f_{X_i^a|X_j^a}(x_i, t|x_j, t)$, for $i, j = 1, 2$; $i \neq j$ is given by*

$$f_{X_i^a|X_j^a}(x_i, t|x_j, t) = \frac{2\sigma_j\sqrt{2\pi t}}{\alpha K_3 t} \exp\left(-K_i\left[\frac{\sigma_i}{\sigma_j}(x_j - x_{0j})\rho - (x_i - x_{0i})\right]\right)$$

$$\times \exp\left(-K_i t N_j - \frac{\bar{r}^2 + \bar{r}_0^2 - (x_j - x_{0j})^2\sigma_i^2(1 - \rho^2)}{2K_3^2 t}\right)$$

$$\times \left[1 - \exp\left(\frac{2(B_j - x_{0j})(x_j - B_j)}{\sigma_j^2 t}\right)\right]^{-1} H(\bar{r}, \bar{r}_0, \phi, \phi_0, t), \qquad (6.7)$$

with

$$N_1 = \frac{\sigma_1\mu_2 - \sigma_2\mu_1\rho}{2\sigma_1}, \qquad N_2 = \frac{\sigma_2\mu_1 - \sigma_1\mu_2\rho}{2\sigma_2}.$$

Proof. The conditional density is given by

$$f_{X_i^a|X_j^a}(x_i, t, |x_j, t; \mathbf{y}, s) = \frac{f_{\mathbf{X}^a}(\mathbf{x}, t|\mathbf{y}, s)}{f_{X_j^a}(x_j, t|y_j, s)}, \qquad (6.8)$$

and the thesis follows plugging $f_{X_j^a}$ given in [20] and (6.6) into (6.8). $\square$

Then, we can introduce the following

LEMMA 6.3. *The conditional density $f_{X_i^a|T_j}(x_i|t)$ for $i, j = 1, 2$ $i \neq j$ is given by*

$$f_{X_i^a|T_j}(x_i|t) = \frac{\sigma_j \pi \sqrt{2\pi t}}{\alpha^2 (B_i - x_i)(B_j - x_{0j})} \exp\left(-K_i \left[\frac{\sigma_i}{\sigma_j}(B_j - x_{0j})\rho - (x_i - x_{0i})\right]\right)$$
$$\times \exp\left(-K_i t N_j - \frac{[\rho\sigma_i(B_j - x_{0j}) - \sigma_j(B_i - x_{0i})]^2 + \sigma_j^2(B_i - x_i)^2}{2K_3^2 t}\right) G_{ij}(\bar{r}_0, \phi_0, x_i, t),$$
(6.9)

where

$$G_{ij}(\bar{r}_0, \phi_0, x_i, t) = \sum_{n=1}^{\infty} \delta_i n \sin\left(\frac{n\pi\phi_0}{\alpha}\right) I_{\frac{n\pi}{\alpha}}\left(\frac{\sigma_j(B_i - x_i)\bar{r}_0}{K_3^2 t}\right),$$

with $\delta_1 = 1$ and $\delta_2 = (-1)^{n+1}$.

Proof. When $x_j \to B_j$, both $f_{X_j^a}$ and $f_{\mathbf{X}^a}$ go to zero, due to the boundary condition (6.4). Therefore $f_{X_i^a|X_j^a}$ is indefinite, as noticed from (6.8). From the definition of ϕ, we have that $\phi \to \alpha$ when $x_1 \to B_1$ and $\phi \to 0$ when $x_2 \to B_2$. In both cases, $\sin(n\pi\phi/\alpha) \to 0$ and thus $H(\bar{r}, \bar{r}_0, \phi, \phi_0, t) \to 0$. Moreover,

$$\left[1 - \exp\left(\frac{2(B_j - x_{0j})(x_j - B_j)}{\sigma_j^2 t}\right)\right] \to 0,$$

when $x_j \to B_j$. Hence, the last two terms in (6.7) produce an indefinite form. Applying l'Hópital's rule, we obtain

$$\lim_{x_j \to B_j} \frac{\sin\left(\frac{n\pi\phi}{\alpha}\right)}{1 - \exp\left(\frac{2(B_j - x_{0j})(x_j - B_j)}{\sigma_j^2 t}\right)} = \frac{\sigma_i \sigma_j \pi \sqrt{1 - \rho^2} t}{2\alpha(B_i - x_i)(B_j - x_{0j})} n\delta_i,$$

with $\delta_1 = 1, \delta_2 = (-1)^{n+1}$, depending on whether $\phi \to \alpha$ or $\phi \to 0$, respectively. The thesis follows plugging in this ratio into (6.7). □

Finally, the joint distribution of the FPTs can be explicitly calculated:

THEOREM 6.4. *The joint distribution of (T_1, T_2) is given by*

$$\mathbb{P}(T_1 < t_1, T_2 < t_2) = \sum_{i,j=1; i \neq j}^{2} \frac{\sqrt{2\pi}}{2\alpha^2 \sigma_j} \exp\left(K_i(B_i - x_{0i}) - K_j x_{0j} + \frac{\mu_j B_j}{\sigma_j^2}\right)$$
$$\times \int_0^{t_i} \int_{-\infty}^{B_j} \int_{s_i}^{t_j} \frac{1}{s_i \sqrt{(s_j - s_i)^3}} \exp\left(-K_i \rho \frac{\sigma_i}{\sigma_j} x_j - K_i N_j s_i\right)$$
(6.10)
$$\times \exp\left(-\frac{\bar{r}_0^2 + \sigma_i^2(B_j - x_j)^2}{2s_i K_3^2} - \frac{(B_j - x_j)^2}{2\sigma_j^2(s_j - s_i)} - \frac{\mu_j^2 s_j}{2\sigma_j^2}\right) G_{ji}(\bar{r}_0, \phi_0, x_j, s_i) ds_j dx_j ds_i.$$

Proof. It follows plugging g_{T_i} given in [20] and (6.9) into (3.1), and then simplifying the resulting expression. □

6.1. Driftless Wiener process. For the driftless case, it holds

THEOREM 6.5. *The joint density of (T_1, T_2) is given by*

$$\mathbb{P}(T_1 \in dt_1, T_2 \in dt_2) = \sum_{i,j=1; i \neq j}^{2} \frac{\pi \sqrt{1 - \rho^2}}{2\alpha^2 \sqrt{t_i(t_j - t_i\rho^2)(t_j - t_i)}} \exp\left(-\frac{\bar{r}_0^2[t_j + t_i(1 - 2\rho^2)]}{4K_3^2 t_i(t_j - t_i\rho^2)}\right)$$
(6.11)
$$\times \sum_{n=1}^{\infty} \delta_j n \sin\left(\frac{n\pi\phi_0}{\alpha}\right) I_{\frac{n\pi}{2\alpha}}\left(\frac{\bar{r}_0^2(t_j - t_i)}{4K_3^2 t_i(t_j - t_i\rho^2)}\right) dt_i dt_j.$$

Proof. Since $\mu_1 = \mu_2 = 0$, it follows that $K_1 = K_2 = 0$. Deriving (6.10) with respect to t_1 and t_2, we have

$$\mathbb{P}(T_1 \in dt_1, T_2 \in dt_2)$$

$$= \sum_{i,j=1; i \neq j}^{2} \int_{-\infty}^{B_j} \left[\frac{\sqrt{2\pi}}{2\alpha^2 \sigma_j t_i \sqrt{(t_j - t_i)^3}} \exp\left(-\frac{\bar{r}_0^2 + \sigma_i^2 (B_j - x_j)^2}{2t_i K_3^2} - \frac{(B_j - x_j)^2}{2\sigma_j^2 (t_j - t_i)} \right) \right.$$

$$\left. \times G_{ji}(\bar{r}_0, \phi_0, x_j, t_i) \right] dx_j dt_i dt_j$$

$$= \sum_{i,j=1; i \neq j}^{2} \frac{\sqrt{2\pi} \exp\left\{ -\frac{\bar{r}_0^2}{2t_i K_3^2} \right\}}{2\alpha^2 \sigma_j t_i \sqrt{(t_j - t_i)^3}} \sum_{n=1}^{\infty} \delta_j n \sin\left(\frac{n\pi \phi_0}{\alpha} \right)$$

$$\times \int_{-\infty}^{B_j} \exp\left(-\frac{\sigma_i^2 (B_j - x_j)^2 (t_j - t_i \rho^2)}{2K_3^2 t_i (t_j - t_i)} \right) I_{\frac{n\pi}{\alpha}}\left(\frac{\sigma_i (B_j - x_j) \bar{r}_0}{K_3^2 t_i} \right) dx_j dt_i dt_j$$

$$= \sum_{i,j=1; i \neq j}^{2} \frac{\sqrt{2\pi} \exp\left(-\frac{\bar{r}_0^2}{2t_i K_3^2} \right)}{2\alpha^2 \sigma_i \sigma_j t_i \sqrt{(t_j - t_i)^3}} \sum_{n=1}^{\infty} \delta_j n \sin\left(\frac{n\pi \phi_0}{\alpha} \right)$$

$$\times \int_0^{\infty} \exp\left(-\frac{h^2 (t_j - t_i \rho^2)}{2K_3^2 t_i (t_j - t_i)} \right) I_{\frac{n\pi}{\alpha}}\left(\frac{h \bar{r}_0}{K_3^2 t_i} \right) dh dt_i dt_j, \tag{6.12}$$

where the last equality is obtained through a change of coordinate, namely $h = \sigma_i (B_j - x_j)$. The integral in (6.12) can be solved using the identity [15]

$$\int_0^{\infty} e^{-\beta^2 h^2} I_\nu(\gamma h) dh = \frac{\sqrt{\pi}}{2\beta} \exp\left(\frac{\gamma^2}{8\beta^2} \right) I_{\nu/2}\left(\frac{\gamma^2}{8\beta^2} \right), \tag{6.13}$$

setting $\beta^2 = (t_j - t_i \rho^2) / (2K_3^2 t_i (t_j - t_i))$, $\gamma = \bar{r}_0 / (K_3^2 t_i)$ and $\nu = n\pi/\alpha$. The thesis follows after some computations. $\square$

When $t_1 = t_2$, we have the following

COROLLARY 6.6. *The joint FPT density when $t_1 = t_2 = t$ is*

$$\mathbb{P}(T_1 \in dt, T_2 \in dt) = \begin{cases} 0 dt^2 & \text{if } \rho \in (-1, 0) \\ \infty dt^2 & \text{if } \rho \in (0, 1) \\ \frac{(B_1 - x_{01})(B_2 - x_{02})}{2\pi \sigma_i \sigma_j t^3} e^{-\frac{\sigma_2^2 (B_1 - x_{01})^2 + \sigma_1^2 (B_2 - x_{02})^2}{2\sigma_1^2 \sigma_2^2 t}} dt^2 & \text{if } \rho = 0 \end{cases}$$

Proof. If $t_i < t_j$, set $z = t_j - t_i, i, j = 1, 2, i \neq j$. When $z \to 0$, the limit of (6.11) is indefinite, being of the form $I_\nu(z)/z$, with $\nu = n\pi/(2\alpha)$. Using the fact that $I_\nu(z) \sim (z/2)^\nu / \Gamma(\nu + 1)$ [2], we get

$$\lim_{z \to 0} \frac{I_\nu(z)}{z} = \frac{1}{2^\nu \Gamma(\nu + 1)} z^{\nu - 1} = \begin{cases} 0 & \text{if } \nu > 1 \\ \infty & \text{if } \nu < 1 \\ \frac{1}{2} & \text{if } \nu = 0 \end{cases} \tag{6.14}$$

Since $\alpha \in (0, \pi)$, then $\nu > 1$ for $n > 2$, and thus all addends in the series in (6.11) vanish for $n > 2$. For $n = 2$, $\delta_1 = 1, \delta_2 = -1$ and thus the term in (6.11) is null, being the two densities symmetric. Finally, when $n = 1$, from (6.14), definitions of ν and ρ, it follows that $\nu < 1 \Leftrightarrow \alpha \in (0, \pi/2) \Leftrightarrow \rho \in (-1, 0)$; $\nu = 1 \Leftrightarrow \alpha = \pi/2 \Leftrightarrow \rho = 0$

and $\nu > 1 \Leftrightarrow \alpha \in (\pi/2, \pi) \Leftrightarrow \rho \in (0, 1)$, where $\Leftrightarrow$ denotes *if and only if*. The thesis follows plugging the resulting expression for (6.14) in (6.11). $\square$

REMARK 6.   *To compare* (6.11) *with the corresponding expression in [12] for* $s = t_1 < t_2 = t$, *we set*

$$\tilde{r}_0 = \frac{\bar{r}_0}{K_3},$$

since different transformations are used. Since

$$\sqrt{1 - \rho^2} = \sin \alpha, \qquad \rho^2 = \cos^2 \alpha, \qquad 2(t - s\rho^2) = (t - s) + (t - s \cos 2\alpha),$$

we obtain

$$\mathbb{P}(T_1 \in ds, T_2 \in dt, s < t)$$

$$= \frac{\pi \sin \alpha}{2\alpha^2 \sqrt{s(t - s\cos^2 \alpha)}(t - s)} \exp\left(-\frac{\tilde{r}_0^2(t - s\cos 2\alpha)}{2s[(t - s) + (t - s\cos 2\alpha)]}\right)$$

$$\times \sum_{n=1}^{\infty} (-1)^{n+1} n \sin(\frac{n\pi\phi_0}{\alpha}) I_{\frac{n\pi}{2\alpha}}\left(\frac{\tilde{r}_0^2(t - s)}{2s[(t - s) + (t - s\cos 2\alpha)]}\right) ds dt.$$

The result differs from that in [12], that uses an incorrect identity for (6.13), *as already discussed in [11].*

7. Examples. Denote $f_{\boldsymbol{T}}$ the theoretical joint density of (T_1, T_2) and $\hat{f}_{\boldsymbol{T}}$ its numerical approximation obtained applying the proposed algorithm. Here we report a brief illustration for two-dimensional Wiener and OU processes in presence of absorbing boundaries. For a bivariate Wiener, the theoretical joint density $f_{\boldsymbol{T}}$ is given by (6.11) for the driftless case, and is derived from (6.10) when the drift is not null. To compare $f_{\boldsymbol{T}}$ and $\hat{f}_{\boldsymbol{T}}$, throughout we consider the mean square error (MSE), which is defined by

$$\text{MSE}(f_{\boldsymbol{T}}) = \frac{1}{nm} \sum_{i=1}^{n} \sum_{j=1}^{m} \left(f_{\boldsymbol{T}}(t_i, t_j) - \hat{f}_{\boldsymbol{T}}(t_i, t_j) \right)^2.$$

7.1. Bivariate Wiener process. First, consider a symmetric bivariate Wiener process with null drifts, parameters $\sigma_1 = \sigma_2 = 1$, $\rho = 0.5$ and boundaries $B_1 = B_2 = 1$. The theoretical joint density and its contour plot are reported in the top panels of Fig.7.1. The numerical approximations are not shown, since they are indistinguishable from those theoretical. Indeed, choosing a space discretization step $r = 0.05$ and time discretization step $h = 0.01$ (resp. $h = 0.05$), we obtain $\text{MSE}(f_{\boldsymbol{T}}) = 3.5859 \cdot 10^{-5}$ (resp. $\text{MSE}(f_{\boldsymbol{T}}) = 4.8607 \cdot 10^{-4}$). This confirms the reliability of the algorithm, as expected from the convergence results of the error, proved in Theorem 5.2. Not surprisingly, also the joint FPT density the contour plots are symmetric, and the probability mass is concentrated in the area close to the diagonal $t_1 = t_2$, representing simultaneous FPTs, i.e. $T_1 = T_2$.
Second, consider a non-symmetric bivariate Wiener process with parameters $\mu_1 = 1, \mu_2 = 2, \sigma_1 = \sigma_2 = 1$, $\rho = 0.5$ and boundaries $B_1 = B_2 = 10$. The joint density $f_{\boldsymbol{T}}$ and the contour plot are reported in the low panels of Fig.7.1. They are indistinguishable from those obtained applying the numerical algorithm (figures not shown). As expected, the joint FPT density is not symmetric and the probability mass is concentrated around the means of the FPTs and it is spread out according to the variance of the FPTs. Indeed, for this parameter choice, we have $\mathbb{E}[T_1] = 10, \mathbb{E}[T_2] = 5, V(T_1) = 10$ and $V(T_2) = 1.25$, see [20].
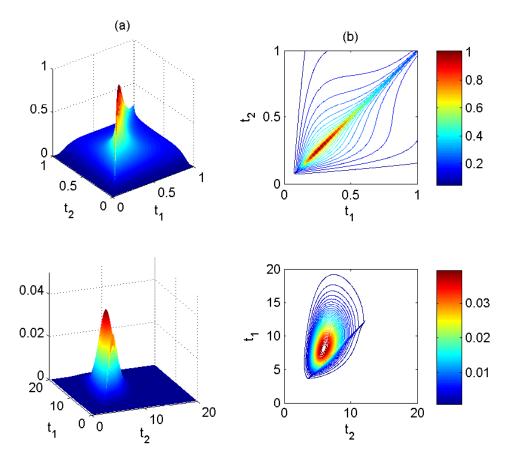
FIG. 7.1. *Theoretical joint densities and contour plots of (T_1, T_2) for two-dimensional Wiener processes. Parameter values common to all figures: $\sigma_1 = \sigma_2 = 1$, $\rho = 0.5$. Chosen drifts for the top figures: $\mu_1 = \mu_2 = 0, B_1 = B_2 = 1$ and time discretization step $h = 0.005$. Chosen drifts for the bottom figures: $\mu_1 = 1, \mu_2 = 1.5, B_1 = B_2 = 10$ and time discretization step $h = 0.05$. Panel (a): joint density of (T_1, T_2). Panel (b): contour plots of (T_1, T_2).*

7.2. Bivariate Ornstein-Uhlenbeck process. A bivariate OU process satisfies the stochastic differential equation (2.1) with

$$\mu(\mathbf{X}(t)) = \left(\begin{array}{c} \mu_1 - \frac{X_1(t)}{\theta} \\ \mu_2 - \frac{X_2(t)}{\theta} \end{array} \right), \ \boldsymbol{\Sigma}(t) = \boldsymbol{\Sigma} = \left(\begin{array}{cc} \sigma_{11} & \sigma_{12} \\ \sigma_{12} & \sigma_{22} \end{array} \right), \tag{7.1}$$

for $\mu_i \in \mathbb{R}, \sigma_{ij} > 0, 1 \le i, j \le 2, \sigma_{12} \in \mathbb{R}$ and $\boldsymbol{\Sigma}$ positive-definite matrix.

Throughout we fix $\theta = 10, \sigma_{12} = 1, \sigma_i = 2, B_i = 10$, for $i = 1, 2$. First, we consider a symmetric OU with $\mu_1 = \mu_2 = 1.5$. The approximated joint density $\hat{f}_{\boldsymbol{T}}$ and the contour plot of (T_1, T_2) are given in the top panels of Fig. 7.2. With this parameter choice, the asymptotic mean $\mu_i \theta$ of each component of the OU is above the boundary B_i. Also in this case, the probability mass is concentrated along the diagonal $t_1 = t_2$. Hence, the times when the components cross their boundary are similar.

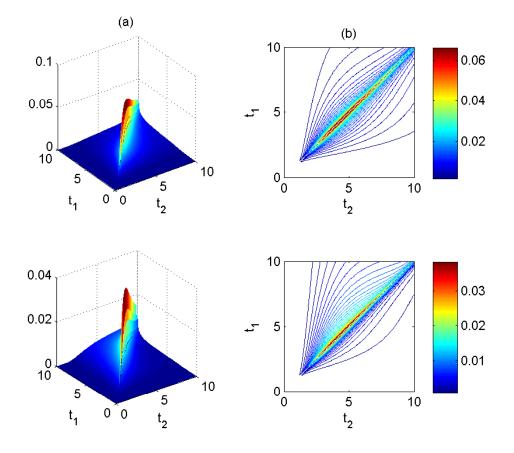Second, we consider a non-symmetric OU with drifts $\mu_1 = 0.95$ and $\mu_2 = 1.5$. The

FIG. 7.2. *Approximated joint densities and contour plots of (T_1, T_2) for bivariate OU processes. Parameter values common to all figures: $\sigma_{11} = \sigma_{22} = 2, \sigma_{12} = 1, B_1 = B_2 = 10$. Chosen drifts for the top figures: $\mu_1 = \mu_2 = 1.5$. Chosen drifts for the bottom figures: $\mu_1 = 0.95$ and $\mu_2 = 1.5$. Panel (a): joint density of (T_1, T_2). Panel (b): contour plots of (T_1, T_2).*

approximated joint density $\hat{f}_{\boldsymbol{T}}$ and the contour plot are reported in the bottom panels of Fig. 7.2. Note that the first component has asymptotic mean $\mu_1 \theta$ below B_1, and thus the noise determines the crossings of the boundary. As a consequence, the probabilistic mass is concentrate in the region $t_1 > t_2$.

8. Conclusion. We solve the FPT problem for a two-dimensional Wiener process with constant drifts and non-diagonal covariance matrix in presence of absorbing boundaries. In particular, we explicitly calculate the joint density of the FPTs and other relevant quantities, e.g. the first and second exit times from the strip, the transition density of the process under the boundary. For bivariate Gauss-Markov processes, explicit expressions of those densities are not available. Therefore, we suggest to use the proposed numerical method, which error is shown to converge. These results are also confirmed by our numerical examples for the Wiener case.

It can be discussed if is relevant for applications to assume absorbing boundaries and independent components after the first exit time from the strip. First, the proposed algorithm for the evaluation of $f_{(X_1^a, T_2)}$ and $f_{(X_2^a, T_1)}$ does not depend on

whether the boundaries are or not absorbed and thus it can be always used. Second, the assumption of absorbing boundaries simplifies the computations, but is not a shortcoming. Indeed, the proposed approach can be extended to non-absorbing boundaries, assuming either multivariate renewal or diffusion processes, as argued in Remark 2.

A generalization to the joint FPT distribution of a k-dimensional process would also be of interest. However, that study requests the knowledge of the solution of a k-dimensional Kolmogorov forward equation, when the process is a multivariate Wiener in presence of absorbing boundaries, or of a system of k Volterra-Fredholm first kind integral equations, when the process is Gauss-Markov.

REFERENCES

[1] M.A. ABDOU, *Fredholm-Volterra integral equation of the first kind and contact problem*, Appl. Math. Comput., 125 (2002), pp. 177–193.

[2] M. ABRAMOWITZ AND I.A. STEGUN, *Handbook of mathematical functions: with Formulas, Graphs and Mathematical Tables*, 1965.

[3] L. ALILI, P. PATIE, AND J.L. PEDERSEN, *Representation of the First Hitting Time Density of an Ornstein-Uhlenbeck process*, Stochastic Models, 21 (2005), pp. 967–980.

[4] L. ARNOLD, *Stochastic Differential Equations: Theory and Applications*, John Wiley & Sons, New York, 1974.

[5] P.G. BUCKHOLTZ AND M. T. WASAN, *First passage probabilities of a two dimensional Brownian motion in an anisotropic medium*, Sankhyā A, 41 (1979), pp. 198–206.

[6] A BUONOCORE, A.G. NOBILE, AND L.M. RICCIARDI, *A new integral equation for the evaluation of first-passage-time probability densities*, Adv. Appl. Prob., 19 (1987), pp. 784–800.

[7] A. CARDONE, E. MESSINA, AND A. VECCHIO, *An adaptive method for Volterra-Fredholm integral equations on the half line*, J. Comput. Appl. Math., 228 (2009), pp. 538–547.

[8] D.R. COX AND H.D. MILLER, *The Theory of Stochastic Processes*, John Wiley & Sons, New York, 1977.

[9] P.J. DAVIS AND P. RABINOWITZ, *Methods of Numerical Integration*, Academic Press, New York, 1984.

[10] S. DITLEVSEN AND P. LANSKY, *Estimation of the input parameters in the Ornstein-Uhlenbeck neuronal model*, Phys. Rev. An outline of theoretical and algorithmic approaches to first passageE, 71 (2005).

[11] M. DOMINÉ AND V. PIEPER, *First passage time distribution of a two-dimensional Wiener process with drift*, Prob. Eng. Inf. Sci., 7 (1993), pp. 545–555.

[12] S. IYENGAR, *Hitting line with two–dimensional Brownian motion*, SIAM J. Appl. Math., 45 (1985), pp. 983–989.

[13] M. JACOBSEN, *One-dimensional homogeneous diffusions*, in Stochastic Biomathematical Models with Application to Neuronal Modeling, vol. 2058 of Lecture notes in Mathematics, Springer, 2013.

[14] P. LINZ, *Analytical and numerical methods for Volterra equations*, SIAM, Philadelphia, 1985.

[15] W. MAGNUS, F. OBERHETTINGER, AND R. SONI, *Formulas and Theorems for the Special Functions of Mathematical Physics*, Springer–Verlag, Berlin, 1966.

[16] G. PESKIR, *Limit at zero of the Brownian first-passage density*, in Probability Theory and volume="124", Springer, 2002, pp. 100–111.

[17] S. REDNER, *A Guide to First-Passage Processes*, Cambridge University Press, Cambridge, 2001.

[18] L.M. RICCIARDI, A. DI CRESCENZO, V. GIORNO, AND A. NOBILE, *An outline of theoretical and algorithmic approaches to first passage time problems with applications to biological modeling*, Math. Japon., 50 (1999), pp. 247–321.

[19] L.M. RICCIARDI AND S. SATO, *Diffusion processes and first-passage-time problems*, in Lectures in Applied Mathematics and Informatics, Manchester University Press, Manchester, 1990,

ch. 5, pp. 206–285.

[20] L. Sacerdote and M.T. Giraudo, *Leaky Integrate and Fire models: a review on mathematical methods and their applications*, in Stochastic biomathematical models with applications to neuronal modeling, vol. 2058 of Lecture Notes in Mathematics, Springer, 2013, pp. 95 –148.

[21] L. Sacerdote, M. Tamborrino, and C. Zucca, *Detecting dependences between spike trains of pairs of neurons through copulas*, Brain Res., 1434 (2012), pp. 243–256.

[22] R.B. Stein, *A theoretical analysis of neuronal variability*, Biophys. J., 5 (1965), pp. 173–194.

[23] M. Tamborrino, L. Sacerdote, and M. Jacobsen, *Diffusion approximation and first passage time for multivariate jump processes*. Submitted.

[24] A.E.P. Villa, *Empirical Evidence about Temporal Structure in Multi-Unit Recordings*, in Time and the Brain, Harwood Acad, 2000, pp. 1–51.

[25] A.E.P. Villa and M. Abeles, *Evidence for spatiotemporal firing patterns within the auditory thalamus of the cat*, Brain Res., 509 (1990), pp. 325–327.

[26] A.E.P. Villa, A. Najem, J. Iglesias, I.V. Tetko, and J.L. Eriksson, *Spatio-temporal patterns of spike occurrences in freely-moving rats associated to perception of human vowels*, Soc. Neurosci. Abstr., 27 (2001), pp. 166–18.

[27] C. Zucca and L. Sacerdote, *On the inverse first-passage-time problem for a Wiener process*, Ann. Appl. Prob., 19 (2009), pp. 1319–1346.

IV

Identification of noisy response latency

Massimiliano Tamborrino
Department of Mathematical Sciences
University of Copenhagen

Susanne Ditlevsen
Department of Mathematical Sciences
University of Copenhagen

Petr Lansky
Institute of Physiology
Academy of Science of the Czech Republic

Publication details

Identification of noisy response latency

Massimiliano Tamborrino[*] and Susanne Ditlevsen[†]

Department of Mathematical Sciences, University of Copenhagen, Universitetsparken 5, DK 2100 Copenhagen, Denmark

Petr Lansky[‡]

Institute of Physiology, Academy of Sciences of the Czech Republic Videnska 1083, 142 20 Prague 4, Czech Republic

In many physical systems there is a time delay before an applied input (stimulation) has an impact on the output (response), and the quantification of this delay is of paramount interest. If the response can only be observed on top of an indistinguishable background signal, the estimation can be highly unreliable, unless the background signal is accounted for in the analysis. In fact, if the background signal is ignored, however small it is compared to the response and however large the delay is, the estimate of the time delay will go to zero for any reasonable estimator when increasing the number of observations. Here we propose a unified concept of response latency identification in event data corrupted by a background signal. It is done in the context of information transfer within a neural system, more specifically on spike trains from single neurons. The estimators are compared on simulated data and the most suitable for specific situations are recommended.

PACS number(s): 02.50.Tt, 02.50.Ey, 87.10.−e, 87.19.L−

I. INTRODUCTION

The formal representation of series of uniform events appearing randomly in time as a stochastic point process is common in several branches of physics [1]. Here we investigate one specific problem related to this representation and discuss it in a common application of the theory, namely, studies on information transfer in neural systems. However, the methodology is applicable in any other field in which the following scenario can be found. Assume a series of primary events observable for a period of time. At a known time instant, either controlled by an experimenter or induced by an external event, an additional stream of indistinguishable events is added to the original one. The question is what the waiting time is to the first event coming from the new source. Obviously, taking the time to the first event after the defined time instant may give a very biased answer. The problem is common in computational neuroscience and we use its terminology and reasoning.

The only way a neuron can transmit information about rapidly varying signals is by a series of all or none events: the action potentials (spikes or firings). An action potential is taken in the limit as a Dirac delta function and thus a spike train may be considered as a realization of a stochastic point process [2,3]. A characteristic of neuronal units of different types is the existence of so-called spontaneous activity, i.e., the generation of spikes without any (controlled) stimulation, usually with a low firing rate. It can, as a first approximation, be described by a Poisson process with constant intensity [3]. It is not possible to analyze the transfer of information within the nervous system without investigating the effect of changing conditions [4]. A common experimental approach, especially for studying the sensory systems, is the presentation of a stimulus and checking if and how the neuron responds to it. The general reason is that the information about the stimulus is encoded in the reaction. It has been shown experimentally and theoretically that the spike latency (vaguely described as the time between stimulation and neuronal response) contains important information in auditory, visual, olfactory, and somatosensory modalities [5–16]. In Ref. [17] the latency is studied experimentally and described by a mathematical function. Therefore, the precise definition and determination of the response latency appear as important problems.

An often applied technique for the stimulated neuronal activity involves estimates of the firing rate profile. The estimated latency to a response is the first instant following the stimulus onset in which the firing rate changes significantly. In statistical terminology, this is a change-point estimation in the intensity (firing rate) function. Three alternative latency estimation methods were provided in Ref. [18], all based on detecting the time at which the firing rate increases from the baseline. In Ref. [19] formal statistical tests for latency effects were proposed and a detailed study of statistical properties of estimation and testing methods was conducted. Also Ref. [20] discussed whether the first-spike latency could be a candidate neural code and an algorithm for detecting the first-spike latency for a single neuron was presented. It was based on detecting a change in the spontaneous discharge Poisson process model caused by evoked spikes. All of these methods are based on finding the point where the firing rate of the underlying point process has changed [21–25]. However, many behavioral responses are completed so fast that the underlying sensory processes cannot rely on estimation of the neural firing rate over an extended time window. Then the approach has to be based on finding the first spike that appeared due to the stimulation. Of course, this implicitly assumes that the response is excitatory.

Another often applied approach is based on assuming that the first spike after the stimulus onset is caused by the stimulus. In Ref. [26] the first-spike latency is defined as the time from the onset of a stimulus to the time of occurrence of the first-response spike. In neurons without spontaneous activity, the response latency can be easily determined. However, in

---

[*]mt@math.ku.dk
[†]susanne@math.ku.dk
[‡]lansky@biomed.cas.cz

neurons possessing spontaneous spiking, the assessment of the response latency is more complicated. The first spike after the stimulus may be caused by the spontaneous activity rather than the stimulus itself. In Ref. [27] shifts in the first-spike latencies in inferior colliculus neurons produced by iontophoretically applied serotonin were demonstrated. Neurons that showed spontaneous activity higher than a fixed firing rate were excluded from that study. In this way, the bias caused by the possibility that the first spike after the stimulation is spontaneous rather than evoked was avoided. An alternative to an estimator of the latency could be a constant deduced from the physical properties of the system under consideration [28].

As shown, the terminology of response latency is rather broad. In the literature, with a few exceptions, the response latency is identified with the first-spike latency or it is defined as the delay between the stimulus onset and the evoked modulation in neural activity. Our aim is to present a unified concept of the response latency, which includes two types of response latencies, absolute and relative. Furthermore, statistical procedures to deduce the properties of these quantities are proposed and compared in simulated experiments, extending the methods in Refs. [29,30].

II. CHARACTER OF EXPERIMENTAL DATA

In a typical neuronal recording session, a stimulus is presented and the spike generation times from the stimulus onset are recorded. Unfortunately, also the spontaneous activity (firing prior to the stimulation) is inevitably included in the record. The trials are repeated after a period of time ensuring that the effect of stimulation has disappeared. The situation is illustrated in Fig. 1 together with definitions of quantities that
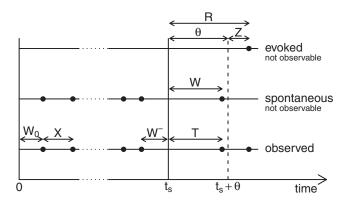

FIG. 1. Schematic description of the single experimental trial. Spikes are indicated with dots. At time 0 the measurements start and at time t_s a stimulus is applied. W (R) denotes the time to the first spontaneous (evoked) spike after t_s. For an observer, they cannot be distinguished. Here T represents the time to the first spike after the stimulus onset and is measured. In the presence of an *absolute response latency* θ, the response latency R is given by $\theta + Z$ and no evoked spikes can occur in $[t_s, t_s + \theta]$. In contrast, spontaneous spikes might occur in that time interval. The *relative response latency* Z denotes the time to the first evoked spike after $t_s + \theta$, the spontaneous ISIs are denoted by X, and the first spike after 0 is denoted by W_0. Finally, W^- corresponds to the backward recurrence time, defined as the time to the last spontaneous spike before t_s.

can be measured during the experiment and the ones we wish to deduce. The recorded spike train starts at time zero and is composed of spontaneously fired action potentials up to time t_s when the stimulation is presented. After that, the recorded spike train contains spontaneous spikes up to the moment of the first evoked spike. We assume that the spontaneous activity is not affected by the stimulus up to the first evoked spike. What happens after the first evoked spike is outside the scope of our study. The experiment is repeated n times and the recorded spike trains create n statistically indistinguishable trials.

In each trial we assume that there is at least a single spike prior to the stimulation, so there is an observable time interval W_0, defined as the time from 0 to the first spontaneous spike before t_s. Commonly, there is a set of complete interspike intervals (ISIs) between time 0 and t_s, denoted by X (see Fig. 1). In the theory of stochastic point processes, the quantity W_0 is called the forward recurrence time. The stimulation at time t_s divides the current interspike interval into two subintervals: the time from the last spontaneous spike to the instant of stimulation W^- (in the theory of stochastic point processes denoted as the backward recurrence time) and the time between the stimulation and the first spike after it, denoted by T. In most of the literature on stimulated neuronal activity, this time is called latency or response time or first-spike latency. However, imagine that the first spike after the stimulation onset is still not influenced or generated by the stimulation itself and would be there even in the absence of stimulation. Thus the spikes after the stimulation are either spontaneous or evoked, and for an observer these are indistinguishable. The situation is illustrated in Fig. 1. We denote the time to the evoked spike by R and call it *response latency*. We assume that the response latency is the sum of two components: *absolute* and *relative* response latency. The absolute response latency is denoted by θ and is defined as the time from the stimulation where no evoked spike can occur. The primary aim of the paper is to determine this delay. If the first spike after the stimulation is part of the prevailing spontaneous activity (which ends by the first evoked spike), this interval is denoted by W. Note that neither W nor R is observed, only their minimum T,

$$T = \min(R, W). \tag{1}$$

We assume that W and R are independent, i.e., the spontaneous and the stimulated activities are not related before the first evoked spike.

It follows from Eq. (1) and the independence of R and W that

$$\mathbb{P}(T > t) = \mathbb{P}[\min(R, W) > t] = \mathbb{P}(R > t)\mathbb{P}(W > t). \tag{2}$$

We are interested in understanding the role of the spontaneous activity in the response latency. In particular, we want to calculate the risk of failure when assuming $T = R$. This is the second aim of the paper. Consider therefore

$$p = \mathbb{P}(W < R) = \mathbb{P}(T = W), \tag{3}$$

i.e., the probability that the first observed spike after the stimulus onset is spontaneous. Obviously, $\mathbb{P}(T = R) = 1 - p$.

Throughout the paper, capital letters are used to stress that the quantities are random variables and lowercase

letters indicate their realizations. The cumulative distribution function (CDF) of a generic random variable Y is denoted by $F_Y(t) = P(Y \leqslant t)$, its survival function $1 - F_Y(t)$ by $\bar{F}_Y(t)$, its probability density function (PDF) by $f_Y(t)$, and the empirical CDF (ECDF) by $F_{Y;n}(t) = \frac{1}{n} \sum_{i=1}^{n} \mathbb{1}_{\{Y_i \leqslant t\}}$, where $\mathbb{1}_A$ is the indicator function of the set A. The average is denoted by $\bar{y} = \frac{1}{n} \sum_{i=1}^{n} y_i$. Finally, we use subindex i ($i = 1, \ldots, n$) for the serial number of the trial and subindex j ($j = 1, \ldots, m_i$) for the spontaneous ISIs in the time interval $[0, t_s]$ in the ith repetition.

III. MODEL

A. Spontaneous activity

If the spontaneous firing follows a renewal process model, the $X_{ij}(i = 1, \ldots, n; j = 1, \ldots, m_i)$ are independent and identically distributed random variables. Then the CDF of W is given by [31]

$$F_W(t) = \frac{\int_0^t [1 - F_X(x)]dx}{\mathbb{E}[X]} \tag{4}$$

and it follows that the mean of W is

$$\mathbb{E}[W] = \frac{\mathbb{E}[X^2]}{2\mathbb{E}[X]}. \tag{5}$$

In fact, Eq. (4) is also true under a less restrictive assumption. It is sufficient that the data are stationary, but when they are not independent, it can be difficult to estimate F_X. If the data are stationary, then the forward and the backward recurrence times W^- and W follow the same distribution [32]. Under this assumption, it is enough to know t_s and the involved pair of spikes in each trial. Even if the process is not stationary, it will be approximately true as long as the process is only slowly drifting.

Therefore, we consider two sampling strategies in the paper. Either all ISIs, i.e., the X_{ij}'s, prior to the stimulation enter in the statistical evaluation of the latency or only the time from the last spike prior to the stimulation, namely, W^-, can be used.

The simplest model to describe the spontaneous firing activity, often supported by experimental data [2,3], is a Poisson process and we will not consider other parametric models. Then X follows an exponential distribution with mean ISI equal to $1/\lambda > 0$ and PDF

$$f_X(t) = \lambda e^{-\lambda t}, \quad t > 0. \tag{6}$$

In this case, as directly follows from Eq. (4), $f_{W_0}(\cdot) = f_{W^-}(\cdot) = f_W(\cdot) = f_X(\cdot)$.

To summarize, throughout the paper we consider separately the following three assumptions about the distribution of the ISIs before stimulation: (a) the renewal assumption, using all data prior to the stimulation in the analysis; (b) the stationarity assumption (or only slowly drifting), using only the backward recurrence time W^- in the analysis; and (c) the parametric assumption, i.e., independent and exponentially distributed ISIs, using all data prior to the stimulation in the analysis.

B. Neural response to a stimulus

Let the absolute response latency $\theta \geqslant 0$ be a constant and assume that no evoked spike can occur before time $t_s + \theta$. Under the approach employed here, the total time from stimulation to the first evoked spike can be rewritten as

$$R = \theta + Z,$$

where the relative response latency Z is a random variable accounting for the time between the end of the delay and the first evoked spike. The primary aim of this article is to determine the absolute response latency θ.

By definition, F_R is a shifted distribution with delay (or shift) θ, i.e.,

$$F_R(t) = 0 \quad \text{if } t \in [0, \theta], \quad F_R(t) > 0 \quad \text{if } t > \theta.$$

The presence of the absolute response latency implies $\mathbb{P}(T > t) = \mathbb{P}(Z > t - \theta)\mathbb{P}(W > t)$ and the CDF of R becomes

$$F_R(t) = F_Z(t - \theta) = \begin{cases} 0 & \text{if } t \in [0, \theta] \\ 1 - \frac{1 - F_T(t)}{1 - F_W(t)} & \text{if } t > \theta. \end{cases}$$

Therefore, R follows a shifted distribution with shift θ and distribution family F_Z. Likewise, the CDF of T is

$$F_T(t) = 1 - [1 - F_Z(t - \theta)][1 - F_W(t)]$$

$$= \begin{cases} F_W(t) & \text{if } t \in [0, \theta] \\ F_W(t) + F_Z(t - \theta)[1 - F_W(t)] & \text{if } t > \theta. \end{cases} \tag{7}$$

Thus θ satisfies

$$\theta = \inf\{t > 0 : F_T(t) \neq F_W(t)\}, \tag{8}$$

which we will use to define a nonparametric estimator of θ. If it is reasonable to assume specific distributions, the following result will be useful to define parametric estimators of θ. For any (shifted or nonshifted) distribution family of R with $\theta \geqslant 0$, the nth moment of T is given by (see Appendix A)

$$\mathbb{E}[T^n] = \mathbb{E}[W^n] \left\{ 1 - e^{-\lambda \theta} \sum_{j=0}^{n-1} \frac{\lambda^j}{j!} \sum_{h=0}^{j} \binom{j-h}{h} \theta^h \mathcal{L}_Z^{(j-h)}(\lambda) \right\}. \tag{9}$$

Here $\mathcal{L}_Z(s)$ denotes the Laplace transform of f_Z, i.e., $\mathcal{L}_Z(s) = \mathbb{E}[e^{-sZ}] = \int_0^\infty e^{-st} f_Z(t)dt$. The kth derivative is denoted by $\mathcal{L}_Z^{(k)}(\cdot)$. In particular, the first two moments are

$$\mathbb{E}[T] = \mathbb{E}[W][1 - e^{-\lambda \theta} \mathcal{L}_Z(\lambda)], \tag{10}$$

$$\mathbb{E}[T^2] = \mathbb{E}[W^2]\{1 - e^{-\lambda \theta}[(1 + \lambda \theta)\mathcal{L}_Z(\lambda) + \lambda \mathcal{L}_Z^{(1)}(\lambda)]\}. \tag{11}$$

The second aim of this paper is to estimate the probability p, given by Eq. (3). In Appendix B it is shown that

$$p = 1 - e^{-\lambda \theta} \mathcal{L}_Z(\lambda) = \frac{\mathbb{E}[T]}{\mathbb{E}[W]}, \tag{12}$$

where the last equality follows from Eq. (10). Note that trivially $p \geqslant P(W \leqslant \theta) = 1 - e^{-\lambda \theta}$ and we therefore always have

$$\theta \leqslant -\frac{\ln(1 - p)}{\lambda} \tag{13}$$

with equality if and only if $\mathbb{P}(R = \theta) = 1$. This can also be seen from Eq. (12) since the Laplace transform of a degenerate variable in 0 equals 1 and otherwise is strictly smaller than 1.

In contrast to the spontaneous activity, we have no experimental evidence about the distribution of R. A commonly applied model to describe spike data is the gamma distribution [33,34] and we apply it to describe the relative response latency. Thus $Z \sim \Gamma(\alpha, \beta)$ and therefore R follows a shifted gamma distribution $R \sim \Gamma_{\text{sh}}(\theta, \alpha, \beta)$. The gamma distribution has the PDF

$$f_{Z;\Gamma}(t) = \frac{1}{\alpha^\beta \Gamma(\beta)} t^{\beta-1} e^{-t/\alpha}, \quad t > 0 \qquad (14)$$

and mean $\mathbb{E}[Z] = \alpha\beta$, implying $\mathbb{E}[R] = \theta + \alpha\beta$. Here $\beta > 0$ and $\alpha > 0$ denote the shape and the scale parameters, respectively, and $\Gamma(\beta)$ denotes the gamma function. In particular, the exponential distribution $R \sim \exp_{\text{sh}}(\theta, \omega)$ can be obtained as a special case if in Eq. (14) $\beta = 1$ and $\omega = 1/\alpha$. Then ω reflects the firing frequency. Other distributions, such as the inverse Gaussian, Weibull, or log-normal, can also be employed. For many distributions, $\mathcal{L}_Z^{(1)}(\cdot) = g_Z(\cdot)\mathcal{L}_Z(\cdot)$ for a function g_Z. In particular, for the gamma distribution

$$\mathcal{L}_Z(\lambda) = (1 + \lambda\alpha)^{-\beta}, \quad g_Z(\lambda) = \frac{\alpha\beta}{1 + \lambda\alpha}. \qquad (15)$$

IV. PARAMETER IDENTIFICATION

The aim of this paper is the estimation of θ and p. Note that whereas θ is a parameter of the model, p is not. Indeed, p is a probability characterizing the properties of the model, in particular, giving information about the risk of failure when assuming $T = R$.

A. Estimation of the probability that the first spike after stimulus onset is spontaneous

To estimate p expressed by Eq. (12) we need estimators of $\mathbb{E}[T]$ and $\mathbb{E}[W]$. Since T is observed, we simply estimate $\mathbb{E}[T]$ by $\bar{t}$. Under the stationarity assumption when the spontaneous ISIs cannot be used for the statistical evaluation, $\mathbb{E}[W]$ can be estimated by the empirical mean of W^-, $\overline{w^-}$. Under the renewal assumption the X_{ij}'s can be used, but first we make no assumptions about the parametric form of F_X. Using Eq. (5), the mean of W might be estimated from the empirical moments of X, namely, $\bar{x}$ and $\overline{x^2}$. However, due to the predefined finite sampling interval $[0, t_s]$, $\bar{x}$ underestimates $\mathbb{E}[X]$, since only ISIs shorter than t_s can be observed, and the density function

is proportional to the observation length t_s. The bias can be very large if t_s is not large compared to the mean of X, as can be confirmed by simulations (results not shown; see Ref. [33]). The density of the distribution of the sampled ISIs is $\eta^{-1}(t_s - t)f_X(t)$ for $t \in [0, t_s]$ and 0 otherwise, where $\eta = \int_0^{t_s}(t_s - t)f_X(t)dt = \int_0^{t_s} F_X(t)dt$ is the normalizing constant [33]. Therefore, the following sample averages have approximate means $\mathbb{E}[\bar{X}] \approx \eta^{-1}(t_s\mathbb{E}[X] - \mathbb{E}[X^2])$ and $\mathbb{E}[\overline{X^2/(t_s - X)}] \approx \eta^{-1}\mathbb{E}[X^2]$, where we have assumed t_s large enough to use the approximation $\int_0^{t_s} tf_X(t)dt \approx \int_0^\infty tf_X(t)dt = \mathbb{E}[X]$. Isolating $\mathbb{E}[X^2]$ and $\mathbb{E}[X]$ we obtain the estimators

$$\tilde{x^2} = \eta \frac{1}{\sum_{i=1}^n m_i} \sum_{i=1}^n \sum_{j=1}^{m_i} \frac{x_{ij}^2}{t_s - x_{ij}}, \quad \tilde{x} = \eta \frac{\bar{x} + \tilde{x^2}}{t_s}$$

and $\mathbb{E}[W]$ can be estimated by $\tilde{x^2}/2\tilde{x}$. Note that the normalizing constant η cancels out. When $t_s \to \infty$, the estimator converges to the usual empirical estimator. If the parametric approach is applied, i.e., X follows Eq. (6), then the likelihood estimator of λ is [35]

$$\hat{\lambda} = \frac{\sum_{i=1}^n(m_i + 1)}{nt_s}. \qquad (16)$$

To summarize, we have the following estimators of p:

$$\hat{p}_a = \frac{2\tilde{x}\bar{t}}{\tilde{x^2}}, \quad \hat{p}_b = \frac{\bar{t}}{\overline{w^-}}, \quad \hat{p}_c = \bar{t}\hat{\lambda}, \qquad (17)$$

under the renewal, the stationarity, and the parametric assumptions, respectively.

B. Estimation of the absolute response latency

We propose several estimators for the absolute response latency θ. The first group makes no assumptions about the distribution of the time to the first evoked spike. One estimator is based on the identification of θ with one of the measured times to the first spike after stimulation. Taking the shortest of them indirectly assumes that there is no spontaneous spike after stimulation. Those that are larger takes into account that there are also some spontaneous spikes mixed with the evoked activity and should depend on n, as will be shown. Another employs Eq. (8) for a nonparametric identification of θ. The other group of estimators assumes that the parametric forms of the distributions of W and R are known, i.e., the method of moments and maximum likelihood inference. The proposed estimators and their assumptions are summarized in Table I.

TABLE I. Proposed estimators of the absolute response latency θ under different assumptions for the spontaneous and evoked activities.

Estimator	Method	Assumption on W	Assumption on R
$\hat{\theta}_1$	$\hat{\theta}_1 = \min\{t_1, \ldots, t_n\}$	model free	model free
$\hat{\theta}_2$	$\hat{\theta}_2 = t^{(k)}, k = \lfloor n\hat{p} \rfloor + 1$	$\hat{\theta}_{2a}$, renewal; $\hat{\theta}_{2b}$, stationary; $\hat{\theta}_{2c}$, F_W known	model free
$\hat{\theta}_3$	based on CDFs	$\hat{\theta}_{3a}$, renewal; $\hat{\theta}_{3b}$, stationary; $\hat{\theta}_{3c}$, F_W known	model free
$\hat{\theta}_4$	maximum likelihood	F_W known	F_R known
$\hat{\theta}_5$	moment estimation	F_W known	F_R known
$\hat{\theta}_6$	maximum likelihood	F_W known	$R \sim \exp_{\text{sh}}(\theta, \omega)$

1. Naive estimator of θ

The first estimator $\hat{\theta}_1$ is defined as

$$\hat{\theta}_1 = \min\{t_1, \ldots, t_n\}.$$

It represents a simple estimator that can be used in a preliminary analysis, ignoring the presence of spontaneous activity, i.e., assuming $T = R$. Any other estimator should improve the performance by including the spontaneous activity in the analysis.

Note that any estimator that is defined as the kth-order statistic of $(t_1, \ldots, t_n)$, denoted by $t^{(k)}$ (e.g., $\hat{\theta}_1 = t^{(1)}$), will necessarily go to zero for any fixed k when the sample size increases since the number of spontaneous spikes before time $t_s + \theta$ in the sample will increase with n. In particular, if $Z \sim \exp(\omega)$ the mean of $\hat{\theta}_1$ is given by

$$\mathbb{E}[\hat{\theta}_1] = -\theta e^{-n\lambda\theta} + \frac{1}{n}(1 - e^{-n\lambda\theta}) + \frac{n}{n+1}\theta e^{-(n+1)\lambda\theta - \omega\theta}$$
$$+ \frac{n}{(n+1)(n+2)(\lambda+\omega)} e^{-(n+2)\lambda\theta - 2\omega\theta} \quad (18)$$

(see Appendix C). Note that it goes to zero as $n \to \infty$ independently of the value of θ and therefore it is not consistent. Thus any estimator based on an order statistic should depend on n.

2. Estimator of θ based on the proportion of spontaneous spikes in the sample

To improve $\hat{\theta}_1$, we propose an order statistic estimator depending on n and taking into account the presence of spontaneous activity. The probability that the first spike after the stimulus onset is spontaneous, $\mathbb{P}(T = W) = p$, is the expected proportion of spontaneous spikes. We therefore expect np spontaneous spikes and $n(1 - p)$ evoked spikes in a sample of size n. Thus we propose to estimate θ as the kth-order statistic given by

$$\hat{\theta}_2 = t^{(k)}, \quad k = \lfloor n\hat{p} \rfloor + 1, \quad (19)$$

where $\lfloor x \rfloor$ denotes the integer part of x and $\hat{p}$ is any of the estimators of p. This corresponds to assuming that all the observations $t_i < t^{(k)}$ are spontaneous and all $t_i \geqslant t^{(k)}$ are evoked, while in fact the two distributions overlap, especially if θ is small. Consequently, we expect θ to be overestimated with decreasing bias as θ increases and also not consistent.

3. Estimator of θ based on cumulative distribution functions

A different approach to the estimation of the absolute response latency is to use Eq. (8). Obviously, the estimated distributions are different and we need to define a criterion to distinguish between statistical fluctuation and systematic difference. We propose to use the standard deviation of the difference between $\hat{F}_T(t)$ and $\hat{F}_W(t)$ when $t \leqslant \theta$, denoted by $\sigma(t)$, as a measure of the statistical fluctuation. On $[0, \theta]$, no evoked activity is present and therefore $\sigma(t)$ does not depend on R. Then we estimate θ as the maximum time such that the difference between the two distributions is smaller than the statistical fluctuation $\sigma(t)$, i.e., $\hat{F}_T(t)$ and $\hat{F}_W(t)$ cannot be statistically distinguished. Thus $\hat{\theta}_3$ is defined as

$$\hat{\theta}_3 = \max\{t \in [0, \tilde{t}] : [\hat{F}_T(t) - \hat{F}_W(t)] \leqslant \hat{\sigma}(t)\}, \quad (20)$$

where $\tilde{t}$ is chosen as the time that maximizes the distance between $\hat{F}_T(t)$ and $\hat{F}_W(t)$, i.e.,

$$\tilde{t} = \arg\max_{t \in [0, t^{(n)}]} [\hat{F}_T(t) - \hat{F}_W(t)],$$

and $t^{(n)} = \max(t_1, \ldots, t_n)$. We estimate F_T by the ECDF $F_{T;n}(t)$. The choice of $\hat{F}_W(t)$ depends on the underlying assumptions and determines $\sigma(t)$. To obtain closed and manageable expressions for the level $\sigma(t)$, we will assume that W is exponential and then under this assumption find the distribution of $\sigma(t)$ for the different estimators of λ. In Appendix D it is shown that $\sigma(t)$ is estimated by

$$\sigma_b(t) = \sqrt{\frac{2}{n} e^{-t/\overline{w}}(1 - e^{-t/\overline{w}})}, \quad (21)$$

$$\sigma_c(t) = \sqrt{\frac{1}{n} e^{-\hat{\lambda}t}(1 - e^{-\hat{\lambda}t}) + e^{\hat{\lambda}nt_s(e^{-2t/nt_s}-1)} - e^{2\hat{\lambda}nt_s(e^{-t/nt_s}-1)}}$$
$$(22)$$

under the stationarity and parametric assumptions, respectively. Under the renewal assumption, the calculation of $\sigma(t)$ becomes more complicated. We therefore approximate $\sigma(t)$ by $\sigma_c(t)$, estimating λ by $2\tilde{x}/\tilde{x}^2$. We expect $\hat{\theta}_3$ to be consistent, as observed from simulations, since $\hat{F}_{T;n}$ and $\hat{F}_W$ converge to the true distributions F_T and F_W and σ_b and σ_c go to zero as $n \to \infty$.

4. Parametric approach: Maximum likelihood estimation of θ

The density of the distribution of T derived from Eq. (7) assuming $F_W(t) = 1 - e^{-\lambda t}$ is

$$f_T(t) = e^{-\lambda t} f_Z(t - \theta)\mathbb{1}_{\{t > \theta\}} + \lambda e^{-\lambda t}[1 - F_Z(t - \theta)\mathbb{1}_{\{t > \theta\}}], \quad (23)$$

where we have introduced the indicator function in the expression to emphasize the allowed values of t, which will be useful when evaluating the log-likelihood function $\sum_{i=1}^n \ln f_T(t_i)$ at the sampled values. The presence of θ complicates the inference because the likelihood function is not differentiable with respect to θ. Therefore, we should maximize directly the log-likelihood function to obtain an estimator of θ. We denote by $\hat{\theta}_4$ the maximum likelihood estimator (MLE) of θ.

Assume $R \sim \exp_{sh}(\theta, \omega)$ and thus $Z \sim \exp(\omega)$. The likelihood equation for ω is

$$0 = \sum_{i=1}^n \frac{1 - (\lambda + \omega)(t_i - \theta)}{\lambda + \omega} \mathbb{1}_{\{t_i > \theta\}}. \quad (24)$$

Note that from Eq. (24), only the sum $\lambda + \omega$ can be estimated. Estimate λ by Eq. (16) and obtain $\hat{\omega}$ as the solution of Eq. (24) for fixed θ as

$$\widehat{\omega + \lambda} = \frac{\sum_{i=1}^n \mathbb{1}_{\{t_i > \theta\}}}{\sum_{i=1}^n (t_i - \theta)\mathbb{1}_{\{t_i > \theta\}}}, \quad \hat{\omega} = \widehat{\omega + \lambda} - \hat{\lambda}.$$

The profile likelihood becomes

$$\tilde{l}_t(\theta) = -\hat{\lambda} \sum_{i=1}^{n} t_i + \sum_{i=1}^{n} [\hat{\lambda}(t_i - \theta) - 1] \mathbb{1}_{\{t_i > \theta\}}$$
$$+ \sum_{i=1}^{n} \ln(\widehat{\omega} \mathbb{1}_{\{t_i > \theta\}} + \hat{\lambda}).$$

Since $\tilde{l}_t(\theta)$ is strictly increasing for $\theta \in (t_i, t_{i+1})$, with $i = 1, \ldots, n-1$, it follows that θ can be estimated as the time $t_i - \epsilon$ maximizing $l_t(\theta)$, with $\epsilon > 0$ small enough, which can be maximized numerically to obtain $\hat{\theta}$.

Now assume $R \sim \Gamma_{\text{sh}}(\theta, \alpha, \beta)$ and thus $Z \sim \Gamma(\alpha, \beta)$. The log-likelihood function becomes

$$l_t(\theta, \alpha, \beta) = -\hat{\lambda} \sum_{i=1}^{n} t_i + \sum_{i=1}^{n} \ln\{ f_{Z;\Gamma}(t_i - \theta) \mathbb{1}_{\{t_i > \theta\}}$$
$$+ \hat{\lambda}[1 - F_{Z;\Gamma}(t_i - \theta) \mathbb{1}_{\{t_i > \theta\}}]\},$$

which can be maximized numerically to obtain the unknown parameters θ, α, and β. Here $F_{Z;\Gamma}(t) = \gamma(\beta, t/\alpha)/\Gamma(\beta)$, where $\gamma(\beta, t/\alpha)$ is the lower incomplete gamma function. Even if the likelihood function is not differentiable with respect to θ, we expect that the MLE is consistent, as observed from simulations.

5. *Parametric approach: Moment estimator of θ*

A different approach when $X \sim \exp(\lambda)$ and the distribution family of R is given consists in equating the theoretical moments of T given by Eq. (9) with the empirical moments. In particular, we solve a system of equations given by the first two or three moments in the two or three unknown parameters, namely, (θ, ω) when $Z \sim \exp(\omega)$ or (θ, α, β) when $Z \sim \Gamma(\alpha, \beta)$. We denote by $\hat{\theta}_5$ the moment estimator (ME) of θ.

Assume $R \sim \exp_{\text{sh}}(\theta, \omega)$ and estimate λ by Eq. (16). From Eqs. (10), (11), (15), and (E3) for $\beta = 1$ and $\alpha = 1/\omega$ we obtain

$$\theta = \frac{p - \frac{\mathbb{E}[T^2]}{\mathbb{E}[W^2]}}{\lambda(1-p)} - \frac{1}{\lambda + \omega}, \quad 1 - p - e^{-\lambda\theta}\frac{\omega}{\omega + \lambda} = 0.$$

Replacing $p, \mathbb{E}[T^2], \lambda$, and $\mathbb{E}[W^2]$ by $\hat{p}, \overline{t^2}, \hat{\lambda}$, and $2/\hat{\lambda}^2$ we can solve the system with respect to ω and θ.

Now assume $R \sim \Gamma_{\text{sh}}(\theta, \alpha, \beta)$. From Eqs. (10) and (15) we get

$$\beta = -\frac{\ln(1-p) + \lambda\theta}{\ln(1 + \lambda\alpha)}.$$

Plugging β into Eq. (11) we get

$$\theta = \frac{\left(p - \frac{\mathbb{E}[T^2]}{\mathbb{E}[W^2]}\right)(1 + \lambda\alpha)\ln(1 + \lambda\alpha) + \lambda\alpha(1-p)\ln(1-p)}{\lambda(1-p)[(1 + \lambda\alpha)\ln(1 + \lambda\alpha) - \lambda\alpha]}.$$

Substituting β and θ into Eq. (9) for $n = 3$, we obtain an equation in α that can be solved numerically.

Unfortunately, the moment equations do not always have a solution with positive parameters for a given sample. This is

due to the following inequality, which is shown in Appendix E:

$$\frac{\mathbb{E}[T^2]}{\mathbb{E}[W^2]} > p + (1-p)\ln(1-p). \quad (25)$$

It is always fulfilled from a theoretical point of view, but, as we will see later, the empirical counterpart might not be satisfied in a particular sample, especially if n is small or θ is large, in which case the moment estimator is not well defined. From the law of large numbers, the ME is consistent since it is expressed as a differentiable function of averages.

V. SIMULATION STUDY

A. Setup

We simulated a spontaneous spike train following a Poisson process with firing rate $\lambda = 1\text{s}^{-1}$ for a time period up to the first spike after 10s and thus $\mathbb{E}[W] = 1\text{s}$. At time $t_s = 10\text{s}$, the evoked activity was simulated by shifted exponentially ($\omega = 10\text{s}^{-1}$) or gamma distributed ($\alpha = 0.05\text{s}$ and $\beta = 2$) random variables R such that $\mathbb{E}[Z] = 0.1\text{s}$. Then we obtained a realization of T using Eq. (1). The empirical data end with the first spike after stimulus and therefore the recording of spikes ended at T. This was repeated to obtain samples of size n, where n varied between 10 and 150 in steps of 10, and each sample was repeated for different values of θ between 0.05 and 0.4 in steps of 0.025. For these values of θ, p was varying from 0.14 to 0.39. Finally, for each value of n and θ, we repeated this procedure 10 000 times, obtaining 10 000 statistically indistinguishable and independent trials.

We denote by $\hat{\theta}_a, \hat{\theta}_b$, and $\hat{\theta}_c$ the estimators of θ under the renewal, the stationarity, and the parametric assumptions and likewise for p. It is also of interest to evaluate how a misspecification of the model influences the statistical inference. We denote by $\hat{\theta}_6$ the misspecified estimator of θ, computed as $\hat{\theta}_4$ under the wrong assumption $Z \sim \exp(\omega)$, when in fact it is gamma distributed, $Z \sim \Gamma(\alpha, \beta)$.

To compare different estimators, we use the relative mean error R_{ME} to evaluate the bias and the relative mean square error R_{MSE}, which incorporates both the variance and the bias. They are defined as the average over the 10 000 repetitions of the quantities

$$E_{\text{rel}}(\hat{\theta}) = \frac{\hat{\theta} - \theta}{\theta}, \qquad E_{\text{rel sq}}(\hat{\theta}) = \frac{(\hat{\theta} - \theta)^2}{\theta^2}$$

and likewise for p.

B. Results for p

In Fig. 2 we report the $R_{\text{ME}}(\hat{p})$ and $R_{\text{MSE}}(\hat{p})$ when R is shifted exponential or gamma distributed with $\mathbb{E}[Z] = 0.1\text{s}$ for different values of n and θ. As expected, all $R_{\text{ME}}(\hat{p})$ and $R_{\text{MSE}}(\hat{p})$ decrease as n increases. For fixed n, $R_{\text{ME}}(\hat{p})$ is approximately constant, i.e., the performance of $\hat{p}$ does not depend on θ. This is expected because the bias is primarily due to the estimator of λ, which does not depend on θ. Also the $R_{\text{MSE}}(\hat{p})$ is approximately constant for fixed n, which is explained by the mean of T that is changing with θ, and estimated by a simple average and thus unbiased. The variance is primarily determined by the sample size and is only slowly varying with θ. The parametric estimator $\hat{p}_c$ largely
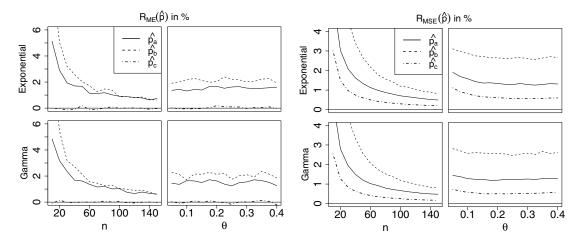
FIG. 2. Dependence of $R_{ME}(\hat{p})$ and $R_{MSE}(\hat{p})$ (average over 10 000 simulations) on the number of observations and the absolute response latency when W is exponential with rate $\lambda = 1\text{s}^{-1}$. Top panels: Z is exponential with rate $\omega = 10\text{s}^{-1}$. Bottom panels: Z is gamma with $\alpha = 0.05\text{s}$ and $\beta = 2$. In both cases $\mathbb{E}[Z] = 0.1\text{s}$. Left panels: Different values of n for fixed $\theta = 0.2\text{s}$, with $p \approx 0.26$. Right panels: Different values of θ for fixed $n = 50$. Here p varies between 0.14 and 0.39. Also shown are the estimators of p under the renewal assumption $\hat{p}_a$ (solid line), the stationarity assumption $\hat{p}_b$ (dashed line), and the parametric assumption $\hat{p}_c$ (dot-dashed line), given by Eq. (17).

outperforms the other two, it has no bias, and R_{MSE} is less than 1%, even for a sample size as small as $n = 30$. The other two overestimate p, which is also expected, since they are ratios of positive estimators, which tend to have heavy right tails. Furthermore, $\hat{p}_a$ performs better than $\hat{p}_b$ with respect to both R_{ME} and R_{MSE}. This happens because $\hat{p}_a$ and $\hat{p}_c$ use all ISIs sampled before the stimulation, whereas $\hat{p}_b$ uses only the time from the last spike before stimulation, W^-. Thus $\hat{p}_a$ and $\hat{p}_c$ are based on a larger sample size, reducing the estimation error, compared to $\hat{p}_b$. To conclude, with only a sample size of $n = 50$ the error is less than 3% and p appears to be well estimated by any of the proposed estimators, even for small sample sizes.

C. Results for θ

It follows from Eq. (18) that $\hat{\theta}_1$ has an R_{ME} between -70% and -100% when R belongs to a shifted exponential distribution family with $\theta \in (0,0.4]$ and n between 10 and 150. This is confirmed in simulations (results not shown) and emphasizes the importance of not ignoring the spontaneous activity in the analysis. Since the other estimators take the spontaneous activity into account, we expect that $|R_{ME}(\hat{\theta})| \leqslant |R_{ME}(\hat{\theta}_1)|$ and we do not consider $\hat{\theta}_1$ further.

Figure 3 shows $R_{ME}(\hat{\theta})$ and Fig. 4 shows $R_{MSE}(\hat{\theta})$, focusing only on those estimators, which have errors less than 10%. For this reason, the ME of the gamma distribution is not shown. Indeed, it performs better than $\hat{\theta}_1$, but is still unacceptable, probably due to the large number of samples where the estimator is not well defined (see below). Considerable improvement is observed with $\hat{\theta}_2$, which is the best nonparametric estimator when n is small or θ is large and always has a smaller variance than $\hat{\theta}_3$. When n increases, $R_{ME}(\hat{\theta}_2)$ reaches an asymptotic level away from 0 that depends on how much the distributions F_W and F_R overlap. This is due to the assumption that all the spontaneous spikes come before the evoked spikes. A good feature of $\hat{\theta}_2$ is that it does not seem to depend on the underlying assumption for F_W since the R_{ME} and R_{MSE} of

$\hat{\theta}_{2;a}$, $\hat{\theta}_{2;b}$, and $\hat{\theta}_{2;c}$ are almost identical. When n is large or θ is small $\hat{\theta}_3$ is the best nonparametric estimator. Simulations show that it depends only slightly on the underlying assumptions for
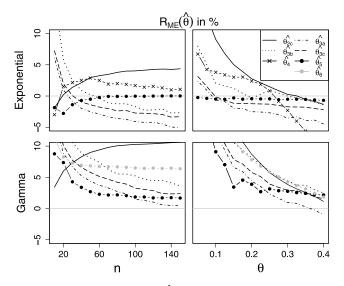

FIG. 3. Dependence of $R_{ME}(\hat{\theta})$ (average over 10 000 simulations) on the number of observations and the absolute response latency when W is exponential with rate $\lambda = 1\text{s}^{-1}$ for estimators with errors less than 10%. Top panels: Z is exponential with rate $\omega = 10\text{s}^{-1}$. Bottom panels: Z is gamma with $\alpha = 0.05\text{s}$ and $\beta = 2$. In both cases $\mathbb{E}[Z] = 0.1\text{s}$. Left panels: Different values of n and $\theta = 0.2\text{s}$. Right panels: Different values of θ and $n = 50$. The following estimators are shown: the p estimator $\hat{\theta}_{2;c}$ under the parametric assumption (solid line); the CDF estimators $\hat{\theta}_3$ under the renewal assumption (dot-dashed line), the stationarity assumption (dotted line), or the parametric assumption (long-dashed line); the MLE $\hat{\theta}_4$ (circles); the ME $\hat{\theta}_5$ (crosses) (only in the top panels); and the misspecified estimator $\hat{\theta}_6$ (gray circles) (only in the bottom panels). The estimators $\hat{\theta}_2$ under the renewal and stationarity assumptions $\hat{\theta}_{2;a}$ and $\hat{\theta}_{2;b}$ are not reported since they are almost identical to $\hat{\theta}_{2;c}$.
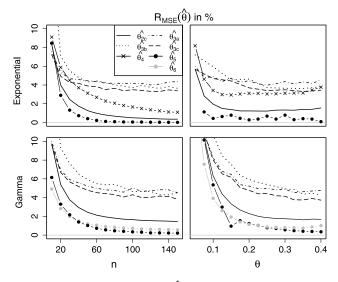
FIG. 4. Dependence of $R_{MSE}(\hat{\theta})$ (average over 10 000 simulations) on the number of observations and the absolute response latency when W is exponential with rate $\lambda = 1\mathrm{s}^{-1}$ for estimators with errors less than 10%. Top panels: Z is exponential with rate $\omega = 10\mathrm{s}^{-1}$. Bottom panels: Z is gamma with $\alpha = 0.05\mathrm{s}$ and $\beta = 2$. Left panels: Different values of n and $\theta = 0.2\mathrm{s}$. Right panels: Different values of θ and $n = 50$. The following estimators are shown: the p estimator $\hat{\theta}_{2;c}$ under the parametric assumption (solid line); the CDF estimators $\hat{\theta}_3$ under the renewal assumption (dot-dashed line), the stationarity assumption (dotted line), or the parametric assumption (long-dashed line); the MLE $\hat{\theta}_4$ (circles); the ME $\hat{\theta}_5$ (crosses) (only in the top panels); and the misspecified estimator $\hat{\theta}_6$ (gray circles) (only in the bottom panels). The estimators $\hat{\theta}_2$ under the renewal and stationarity assumptions $\hat{\theta}_{2;a}$ and $\hat{\theta}_{2;b}$ are not reported since they are almost identical to $\hat{\theta}_{2;c}$.

F_W. The error is in all cases small even for moderate sample sizes.

As expected, the MLE provides the best estimates of θ. The ME is acceptable only when Z follows an exponential distribution. The MLE is more reliable than the ME approach, as is usually observed comparing MEs and MLEs. In particular, for $n = 50$ fixed the $R_{ME}(\hat{\theta}_5)$ gets worse for large θ. This is probably due to the fact that the estimator is defined only if the parameter condition (25) is satisfied, which is often not the case, especially for large θ or small n. The percentages of the simulated samples where the estimator is undefined are reported in Fig. 5. Note that the right-hand side of Eq. (25) is increasing in p. Therefore an estimate $\hat{p}$ much larger than the true p tends to violate condition (25) and the ME is not defined.

Interestingly, the misspecified $\hat{\theta}_6$ that wrongly assumes Z exponentially distributed when $R \sim \Gamma_{sh}(\theta,\alpha,\beta)$ gives acceptable estimates of θ, even if more biased, but with approximately the same R_{MSE} as the correct MLE. This would of course not be the case for the other parameters α and β.

The results might depend on the particular choice of the distribution for Z and its parameter values. Simulations were also conducted for the inverse Gaussian distribution and for $\beta = 0.8$ and 10 in the gamma distribution (results not shown). The results for the estimation of θ are similar, though a larger sample size is needed when $\beta = 10$.
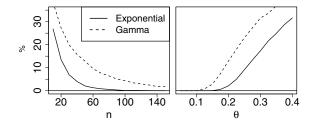

FIG. 5. Percentage of repetitions out of 10 000 that do not fulfill condition (25). For these data sets, the ME $\hat{\theta}_5$ cannot be evaluated. Here W is exponential with rate $\lambda = 1\mathrm{s}^{-1}$; Z is exponential with rate $\omega = 10\mathrm{s}^{-1}$ (solid line) or Z is gamma with $\alpha = 0.05\mathrm{s}$ and $\beta = 2$ (dashed line). Left panels: Different values of n for fixed $\theta = 0.2\mathrm{s}$. Right panels: Different values of θ for fixed $n = 50$.

VI. CONCLUSION

It can be discussed if the model in this paper reflects the biology correctly, more specifically, whether the spontaneous and the evoked activity can be distinguished once the stimulus is applied, since both are being produced by the same neuron. First, during the absolute latency no spike is influenced by the stimulus and the activity is thus well described by the spontaneous spikes. Second, during the response latency, our aim is simply to estimate how the time dynamics of spikes is changed by the stimulus. Further, the model can be considered a more general model. Assume that the observed output comes from a cluster of processing units, e.g., neurons, and some of these are changed by the stimulus and others are not, but they cannot be distinguished. This scenario would originate an observed response as described by our model.

A shortcoming of the analysis is the limitation of using only the first spike after the stimulus onset, ignoring the possible information carried by the entire spike train. The approach pursued here of first-spike coding is an alternative to the frequency coding principle. It would be interesting to extend the methods developed in this paper over the entire spike train after stimulus onset.

To conclude, numerical simulations emphasize the importance of taking into account the spontaneous activity W when estimating θ in order to avoid a serious bias. We suggest choosing the MLE if it is reasonable to assume that the evoked activity follows an exponential or gamma distribution, leading to a parametric estimation of θ. If no information about the distribution of R is available, we suggest applying the p estimator $\hat{\theta}_2$, which always estimates θ reasonably well, is easy to compute, and gives the same performance for any of the underlying assumptions for F_W. For simplicity, or from lack of knowledge of R, we also suggest using the misspecified estimator $\hat{\theta}_6$, assuming an evoked activity exponential, which does not appear to introduce a large error in the estimation of θ.

APPENDIX A: MOMENTS OF T

Assume that $X \sim \exp(\lambda)$ and R belongs to a shifted distribution family. Then the nth moment of T can be calculated using Eq. (23) as follows:

$$
\begin{aligned}
\mathbb{E}[T^n] &= \int_0^\infty t^n f_T(t)dt = \int_0^\theta t^n f_W(t)dt + \int_\theta^\infty t^n\{f_Z(t-\theta)[1-F_W(t)] + f_W(t)[1-F_Z(t-\theta)]\}dt\, dt \\
&= \int_0^\infty t^n f_W(t)dt - \int_0^\infty (y+\theta)^n f_W(y+\theta)F_Z(y)dy + \int_0^\infty (y+\theta)^n f_Z(y)[1-F_W(y+\theta)]dt \\
&= \mathbb{E}[W^n] - \int_0^\infty (y+\theta)^n \lambda e^{-\lambda(y+\theta)} F_Z(y)dy + \int_0^\infty (y+\theta)^n f_Z(y)e^{-\lambda(y+\theta)}.
\end{aligned}
\tag{A1}
$$

The second term can be solved by integration by parts:

$$
\begin{aligned}
&\int_0^\infty (y+\theta)^n \lambda e^{-\lambda(y+\theta)} F_Z(y)dy \\
&= \sum_{k=0}^n \frac{n!}{(n-k)!}\frac{1}{\lambda^k}\int_0^\infty (y+\theta)^{n-k} f_Z(y)e^{-\lambda(y+\theta)}dy.
\end{aligned}
\tag{A2}
$$

Using the binomial theorem, the $(n-k)$th power of $(y+\theta)$ can be expanded as

$$
(y+\theta)^{n-k} = \sum_{h=0}^{n-k}\binom{n-k}{h}y^{n-k-h}\theta^h.
$$

Therefore, the integral in Eq. (A2) becomes

$$
\begin{aligned}
&\int_0^\infty (y+\theta)^{n-k} f_Z(y)e^{-\lambda(y+\theta)} \\
&= e^{-\lambda\theta}\sum_{h=0}^{n-k}\binom{n-k}{h}\theta^h \int_0^\infty y^{n-k-h}e^{-\lambda y} f_Z(y)dy \\
&= e^{-\lambda\theta}\sum_{h=0}^{n-k}\binom{n-k}{h}\theta^h \mathcal{L}_Z^{(n-k-h)}(\lambda),
\end{aligned}
\tag{A3}
$$

where $\mathcal{L}_Z^{(j)}(\lambda)$ is the jth derivative of the Laplace transform of Z evaluated in λ. By plugging Eq. (A3) into Eq. (A2) and then into Eq. (A1), noting that the term for $k=0$ cancels out with the last integral in Eq. (A1), we finally obtain

$$
\begin{aligned}
\mathbb{E}[T^n] = \mathbb{E}[W^n]&\Bigg\{1 - e^{-\lambda\theta}\sum_{k=1}^n \frac{\lambda^{n-k}}{(n-k)!}\sum_{h=0}^{n-k}\binom{n-k}{h} \\
&\times \theta^h \mathcal{L}_Z^{(n-k-h)}(\lambda)\Bigg\},
\end{aligned}
$$

where we have used that $\mathbb{E}[W^n] = n!/\lambda^n$. The final expression (9) is obtained by the change of index $j = n-k$.

APPENDIX B: CALCULATION OF p

Assume that X follows Eq. (6) and R belongs to a shifted distribution family. To compute the probability p that the first spike after the stimulus onset is spontaneous, we proceed as follows. Define $U = R + (-W)$. Then

$$
p = \mathbb{P}(W < R) = \mathbb{P}(U > 0) = \int_0^\infty f_U(t)dt,
$$

where f_U is the convolution of f_R and $f_{(-W)}$. Here $f_{(-W)}$ is defined by

$$
f_{(-W)}(s) = f_W(-s)\mathbb{1}_{\{s\leqslant 0\}} = \lambda e^{\lambda s}\mathbb{1}_{\{s\leqslant 0\}}
$$

and $f_R(t) = f_Z(t-\theta)\mathbb{1}_{\{t\geqslant 0\}}$. Then the density f_U is given by

$$
\begin{aligned}
f_U(t) &= \int_{-\infty}^\infty f_R(u)f_{(-W)}(t-u)du \\
&= \int_t^\infty f_Z(u-\theta)\mathbb{1}_{\{u>\theta\}}\lambda e^{\lambda(t-u)}du \\
&= \lambda e^{\lambda t - \lambda\theta}\left[\mathcal{L}_Z(\lambda)\mathbb{1}_{\{0\leqslant t\leqslant\theta\}} + \mathbb{1}_{\{t>\theta\}}\int_{t-\theta}^\infty f_Z(x)e^{-\lambda x}dx\right]
\end{aligned}
$$

and therefore p becomes

$$
\begin{aligned}
p &= \lambda e^{-\lambda\theta}\mathcal{L}_Z(\lambda)\int_0^\theta e^{\lambda t}dt + \lambda e^{-\lambda\theta}\int_\theta^\infty\int_{t-\theta}^\infty e^{\lambda(t-u)}f_Z(u)du\,dt \\
&= (1-e^{-\lambda\theta})\mathcal{L}_Z(\lambda) + e^{-\lambda\theta}\int_0^\infty\left(\int_\theta^{u+\theta}\lambda e^{\lambda t}dt\right)e^{-\lambda u}f_Z(u)du \\
&= (1-e^{-\lambda\theta})\mathcal{L}_Z(\lambda) + \int_0^\infty (1-e^{-\lambda u})f_Z(u)du,
\end{aligned}
$$

which implies Eq. (12).

APPENDIX C: MEAN OF $\hat\theta_1$

Assume that X follows Eq. (6) and R belongs to a shifted exponential family. We have

$$
\begin{aligned}
\mathbb{P}(\hat\theta_1 > t) &= \mathbb{P}(t_1 > t, \ldots, t_n > t) \\
&= \prod_{i=1}^n [1-F_T(t)] = [1-F_T(t)]^n
\end{aligned}
$$

and therefore $\mathbb{P}(\hat\theta_1 \leqslant t) = 1 - [1-F_T(t)]^n$ with density $n[1-F_T(t)]^{n-1}f_T(t)$. From Eq. (7) we obtain

$$
\begin{aligned}
\mathbb{E}[\hat\theta_1] = &\int_0^\theta nt[1-F_W(t)]^{n-1}(t)f_W(t)dt \\
&+ \int_\theta^\infty nt[1-F_W(t)]^n[1-F_Z(t-\theta)]^{n-1}f_Z(t-\theta)dt \\
&+ \int_\theta^\infty nt[1-F_W(t)]^{n-1}[1-F_Z(t-\theta)]^n f_W(t)dt,
\end{aligned}
$$

which implies Eq. (18).

APPENDIX D: STATISTICAL FLUCTUATION OF $\hat{F}_T(t) - \hat{F}_W(t)$

Assume $t \in [0,\theta]$. The variance of the difference between $\hat{F}_T(t)$ and $\hat{F}_W(t)$, denoted by $\sigma^2(t)$, is defined as

$$\sigma^2(t) = \text{Var}[\hat{F}_T(t) - \hat{F}_W(t)]$$
$$= \text{Var}[\hat{F}_T(t)] + \text{Var}[\hat{F}_W(t)] - 2\,\text{Cov}[\hat{F}_T(t), \hat{F}_W(t)]. \tag{D1}$$

Define $A_{n;t} = \sum_{i=1}^{n} \mathbb{1}_{\{t_i \leqslant t\}}$; then $\hat{F}_{T;n} = A_{n;t}/n$. Here $A_{n;t}$ counts the number of observations $t_i \leqslant t$. Under the stationarity assumption $\hat{F}_W(t) = \hat{F}_{W^-;n}(t) = B_{n;t}/n$, where $B_{n;t} = \mathbb{1}_{\{w_i^- \leqslant t\}}$. Since $F_T(t) = F_{W^-}(t)$ for all $t \in [0,\theta]$, it follows that $A_{n;t}$ and $B_{n;t}$ are identically distributed random variables with covariance given by

$$\text{Cov}(A_{n;t}, B_{n;t}) = \sum_{i=1}^{n} \sum_{j=1}^{n} \text{Cov}\left(\mathbb{1}_{\{t_i \leqslant t\}}, \mathbb{1}_{\{w_j^- \leqslant t\}}\right)$$
$$= n\,\text{Cov}\left(\mathbb{1}_{\{t_j \leqslant t\}}, \mathbb{1}_{\{w_j^- \leqslant t\}}\right)$$
$$= n[\mathbb{P}(W \leqslant t, W^- \leqslant t) - F_W(t)^2]. \tag{D2}$$

In the second equality we have used that t_i and w_j^- are independent for $i \neq j$. If X follows Eq. (6), then the joint PDF of W and W^- at time (r,s), denoted by $f_{W^-;W}(r,s)$, is given by $\lambda^2 e^{-\lambda(r+s)}$ [36]. Therefore,

$$\mathbb{P}(W^- \leqslant t, W \leqslant t) = \int_0^t \int_0^t f_{W^-;W}(r,s)dr\,ds$$
$$= \int_0^t \lambda e^{-\lambda r} dr \int_0^t \lambda e^{-\lambda s} ds = F_W(t)^2.$$

Thus, by Eq. (D2), $\text{Cov}(A_{n;t}, B_{n;t}) = 0$. Note that this is not generally true; it is due to the memoryless property of the exponential distribution. In general, the backward and the forward recurrence times are negatively correlated. Plugging $F_{T;n}(t)$ and $F_{W^-;n}(t)$ into Eq. (D1), we obtain

$$\sigma_b^2(t) = \text{Var}[F_{T;n}(t) - F_{W^-;n}(t)] = \frac{2}{n^2}\text{Var}(A_{n;t})$$
$$= \frac{2}{n}F_W(t)[1 - F_W(t)].$$

Then the standard deviation $\sigma_b(t)$ equals Eq. (21).

Under the parametric assumption $\hat{F}_W = 1 - e^{-\hat{\lambda}t}$. Then Eq. (D1) becomes

$$\sigma_c^2(t) = \frac{1}{n}F_W(t)[1 - F_W(t)] + \text{Var}(e^{-\hat{\lambda}t}) + \frac{2}{n}\text{Cov}(A_{n;t}, e^{-\hat{\lambda}t})$$
$$= \frac{1}{n}(1 - e^{-\lambda t})e^{-\lambda t} + \text{Var}(e^{-\hat{\lambda}t}), \tag{D3}$$

where the covariance is null because of the same reasons as above. Rewrite Eq. (16) as

$$\hat{\lambda} = \frac{\sum_{i=1}^{n} N_i(t_s)}{nt_s} = \frac{N(t_s)}{nt_s},$$

where $N_i(t_s)$ is the random variable counting the number of spontaneous spikes in $[0,t_s]$ in the ith trial. By assumption $N(t_s)$ follows a Poisson distribution with rate λnt_s. Therefore,

$$\text{Var}(e^{-\hat{\lambda}t}) = \mathbb{E}[e^{-N(t_s)(2t/nt_s)}] - \mathbb{E}[e^{-N(t_s)(t/nt_s)}]^2$$
$$= \mathcal{L}_{N(t_s)}\left(\frac{2t}{nt_s}\right) - \mathcal{L}_{N(t_s)}^2\left(\frac{t}{nt_s}\right)$$
$$= e^{\lambda nt_s(e^{-2t/nt_s}-1)} - e^{2\lambda nt_s(e^{-t/nt_s}-1)}, \tag{D4}$$

where $\mathcal{L}_{N(t_s)}$ denotes the Laplace transform of $f_{N(t_s)}$. Plugging Eq. (D4) into Eq. (D3) and taking the square root, we finally obtain Eq. (22).

APPENDIX E: CONDITIONS ON THE PARAMETERS OF R

From Eq. (12) we have that
$$e^{-\lambda\theta}\mathcal{L}_Z(\lambda) = 1 - p \tag{E1}$$

and it follows
$$\theta = -\frac{\ln(1-p)}{\lambda} + \frac{\ln\mathcal{L}_Z(\lambda)}{\lambda}. \tag{E2}$$

Assume $Z \sim \Gamma(\alpha,\beta)$ and write $\mathcal{L}_Z^{(1)}(\lambda) = g_Z(\lambda)\mathcal{L}_Z(\lambda)$ given by Eq. (15). Using Eq. (E1), rewrite Eq. (11) as
$$\frac{\mathbb{E}[T^2]}{\mathbb{E}[W^2]} = p - (1-p)\lambda[\theta + g_Z(\lambda)]. \tag{E3}$$

Plugging Eq. (E2) into Eq. (E3), we get
$$\frac{\mathbb{E}[T^2]}{\mathbb{E}[W^2]} = p + (1-p)\ln(1-p)$$
$$+ \frac{\beta(1-p)}{1+\lambda\alpha}[\ln(1+\lambda\alpha)(1+\lambda\alpha) - \lambda\alpha].$$

Condition (25) follows by noting that the expression in square brackets on the right-hand side is larger than 0.

[1] N. G. van Kampen, *Stochastic Processes in Physics and Chemistry* (North-Holland, Amsterdam, 2007).
[2] W. Gerstner and W. M. Kistler, *Spiking Neuron Models* (Cambridge University Press, Cambridge, 2002).
[3] H. C. Tuckwell, *Introduction to Theoretical Neurobiology, Vol. 2: Nonlinear and Stochastic Theories* (Cambridge University Press, Cambridge, 1988).
[4] F. Rieke, *Spikes: Exploring the Neural Code* (MIT Press, Cambridge, 1999).
[5] S. Furukawa and J. C. Middlebrooks, J. Neurophysiol. **87**, 1749 (2002).
[6] R. Guyonneau, R. VanRullen, and S. J. Thorpe, Neural Comput. **17**, 859 (2005).
[7] S. Kalluri and B. Delgutte, J. Comput. Neurosci. **14**, 71 (2003).
[8] S. Panzeri, R. S. Petersen, S. R. Schultz, M. Lebedev, and M. E. Diamond, Neuron **29**, 769 (2001).
[9] D. S. Reich, F. Mechler, and J. D. Victor, J. Neurophysiol. **85**, 1039 (2001).
[10] J. P. Rospars, P. Lansky, A. Duchamp, and P. Duchap-Viret, Eur. J. Neurosci. **18**, 1135 (2003).
[11] H. C. Tuckwell and F. Y. M. Wan, Physica A **351**, 427 (2005).

[12] G. Wainrib, M. Thieullen, and K. Pakdaman, Biol. Cybern. **103**, 43 (2010).

[13] B. S. Krishna, J. Comput. Neurosci. **13**, 71 (2002).

[14] B. D. Fulcher, A. J. K. Phillips, and P. A. Robinson, Phys. Rev. E **78**, 051920 (2008).

[15] J. Kwapien, S. Drozdz, and A. A. Ioannides, Phys. Rev. E **62**, 5557 (2000).

[16] M. Deger, M. Helias, S. Cardanobile, F. M. Atay, and S. Rotter, Phys. Rev. E **82**, 021129 (2010).

[17] A. Grémiaux, T. Nowotny, D. Martinez, P. Lucas, and J. Rospars, Brain Res. **1434**, 123 (2012).

[18] S. N. Baker and G. L. Gerstein, Neural Comput. **13**, 1351 (2001).

[19] V. Ventura, Neural Comput. **16**, 2323 (2004).

[20] S. M. Chase and E. D. Young, J. Neurophysiol. **99**, 1672 (2008).

[21] A. Berenyi, G. Benedek, and A. Nagy, Brain Res. **1178**, 141 (2007).

[22] D. Endres, J. Schindelin, P. Foldiák, and M. W. Oram, J. Physiol. Paris **104**, 128 (2010).

[23] J. Lee, H. R. Kim, and C. Lee, J. Neurophysiol. **104**, 2556 (2010).

[24] H. Kim, B. Richmond, and S. Shinomoto, J. Comput. Neurosci. **32**, 137 (2012).

[25] M. P. Nawrot, A. Aertsen, and S. Rotter, Biol. Cybern. **88**, 321 (2003).

[26] P. Heil, Curr. Opin. Neurobiol. **14**, 461 (2004).

[27] L. M. Hurley and G. D. Pollak, J. Neurosci. **25**, 7876 (2005).

[28] F. G. Lin and R. C. Liu, J. Neurophysiol. **104**, 3588 (2010).

[29] D. Hampel and P. Lansky, J. Neurosci. Methods **171**, 288 (2008).

[30] Z. Pawlas, L. B. Klebanov, V. Beneš, M. Prokešová, J. Popelář, and P. Lánský, Neural Comput. **22**, 1675 (2010).

[31] D. R. Cox and P. A. W. Lewis, *The Statistical Analysis of Series of Events* (Methuen, London, 1966), p. 62.

[32] J. A. McFadden, J. R. Stat. Soc. B **24**, 364 (1962).

[33] M. P. Nawrot, C. Boucsein, V. R. Molina, A. Riehle, A. Aertsen, and S. Rotter, J. Neurosc. Methods **169**, 374 (2008).

[34] T. Shimokawa, S. Koyama, and S. Shinomoto, J. Comput. Neurosc. **29**, 183 (2010).

[35] T. Martinussen and T. H. Scheike, *Dynamic Regression Models for Survival Data* (Springer, Berlin, 2010), p. 66.

[36] R. D. Gill and N. Keiding, Lifetime Data Anal. **16**, 571 (2010).

V

Parametric inference of neuronal response latency in presence of a background signal

Massimiliano Tamborrino
Department of Mathematical Sciences
University of Copenhagen

Susanne Ditlevsen
Department of Mathematical Sciences
University of Copenhagen

Petr Lansky
Institute of Physiology
Academy of Science of the Czech Republic

Parametric inference of neuronal response latency in presence of a background signal

M. Tamborrino[a,*], S. Ditlevsen[a], P. Lansky[b]

[a]*Department of Mathematical Sciences, University of Copenhagen, Universitetsparken 5, Copenhagen, Denmark*
[b] *Institute of Physiology, Institute of Physiology, Academy of Sciences of the Czech Republic, Videnska 1083, 14220 Prague 4, Czech Republic*

Abstract

Neurons are commonly characterized by spontaneous generation of action potentials (spikes), which appear without any apparent or controlled stimulation. When a stimulus is applied, the spontaneous firing may prevail and hamper identification of the effect of the stimulus. Therefore, for any rigorous analysis of evoked neuronal activity, the presence of spontaneous firing has to be taken into account. If the background signal is ignored, however small it is compared to the response activity, and however large is the delay, estimation of the response latency will be wrong, and the error will persist even when sample size is increasing. The first question is: what is the response latency to the stimulus? Answering this question becomes even more difficult if the latency is of a complex nature, for example composed of a physically implied deterministic part and a stochastic part. This scenario is considered here, where the response time is a sum of two components; the delay and the relative latency. Parametric estimators for the time delay and the response latency are derived. These estimators are evaluated on simulated data and their properties are discussed. Finally, we show that the mean of the response latency is always satisfactorily estimated, even assuming a wrong distribution for the response latency.

Keywords: Maximum likelihood estimation, extracellular recordings in neurons, spontaneous activity, evoked activity, interspike intervals, spike trains

1. Introduction

Neurons are information processing units and there is an everlasting effort to determine the code they use. During the years it has become obvious that there is no unique coding scheme valid for all systems and many alternatives have been proposed. The temporal codes constitute one category and the latency

---

*Corresponding author. Phone: +45 35320732. Fax: +45 35320704.
Email addresses: `mt@math.ku.dk` (M. Tamborrino), `susanne@math.ku.dk` (S. Ditlevsen), `lansky@biomed.cas.cz` (P. Lansky)
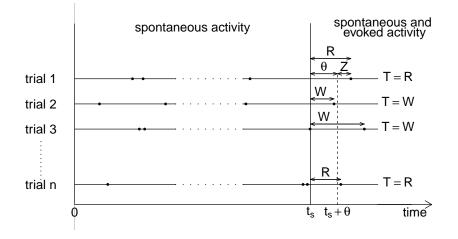
Figure 1: Schematic representation of an experiment with n trials. The spontaneous firing activity is measured between the beginning of the experiment, at time 0, up to the stimulus onset, at time t_s. After t_s, spontaneous and evoked activity are observed and they cannot be distinguished. The first spike after t_s is denoted T. If T is due to the spontaneous activity, then we say $T = W$. If T is due to the stimulus, then we say $T = R$. Neither R nor W are observed, but only T, representing the time to the first spike after t_s. In presence of a delay θ, no evoked activity can occur in $[t_s, t_s + \theta]$. Then the response latency is given by the sum of two components, namely θ and Z, where Z denotes the time to the first evoked spike after $t_s + \theta$. The measurement is stopped after time T and the neuron is permitted to relax for a period of time ensuring that the stimulus effect disappeared before the experiment is repeated. This leads to n independent and statistically indistinguishable trials.

code is one of the most prominent within this class. Despite the enormous interest in latency coding, formal treatment of experimental data of this type has only recently appeared in the literature (Gremiaux et al., 2012; Lin and Liu, 2010; Neubauer and Heil, 2008; Oran et al., 2011; Uzuntarla et al., 2012; Wainrib et al., 2010). In our previous work (Pawlas et al., 2010; Tamborrino et al., 2012), we suggested a formal statistical model of the latency experiments and proposed inference methods in presence of spontaneous spiking activity. Here we extend the previous efforts towards parametric analysis of data.

1.1. Model

An illustration of the character of experimental data and the description of the involved quantities is provided in Fig. 1. At time zero, the measurements start and spikes due to the spontaneous activity are recorded. At time t_s, a stimulus is applied and the measurements are stopped after the first spike following t_s, denoted by T. The experiment is then repeated n times, after a period of time long enough to ensure that the effect of stimulation has disappeared. This allows to obtain n independent and statistically indistinguishable trials of spike trains.

The spontaneous activity does not disappear after the stimulus onset and therefore the first spike T after t_s is not necessarily evoked. Moreover, an observer cannot distinguish whether T is due to spontaneous or evoked activity. Here we assume that the spontaneous activity is not influenced by the stimulus onset up to the first evoked spike.

The simplest model of the spontaneous firing activity, often supported by experimental data, is a Poisson process with intensity $\lambda > 0$ (Gerstner and Kistler, 2002; Tuckwell, 1988), and this will be assumed throughout the paper. Then the interspike intervals (ISIs) before t_s are exponentially distributed with mean ISI equal to $1/\lambda > 0$ and probability density function

$$f(t) = \lambda e^{-\lambda t} \qquad t > 0. \tag{1}$$

We denote W the time to the first spike which is part of the prevailing spontaneous activity, called spontaneous spike, after t_s. Due to the properties of the Poisson process, it holds that $W \sim exp(\lambda)$.

We denote R the time to the first spike which is due to the stimulation, called evoked spike, after the stimulus onset. Many experiments show that the response to a stimulus is not instantaneous. Let $\theta \geq 0$ be a constant and assume that no evoked spike can occur before time $t_s + \theta$. If $\theta > 0$, we call this quantity *delay* or *absolute response latency*. Under the approach employed here, the total time from stimulation to the first evoked spike can be rewritten as

$$R = \theta + Z,$$

where Z is a random variable accounting for the time between the end of the delay and the first evoked spike. We call Z the *relative response latency*. Thus, the response latency is a sum of two components: *absolute* and *relative response latency*. By definition, the distribution of R, denoted by F_R, is a shifted distribution with delay (or shift) θ, i.e.

$$F_R(t) = F_Z(t - \theta)\mathbb{1}_{\{t>\theta\}},$$

where $\mathbb{1}_A$ denotes the indicator function of a set A, and F_Z is the distribution function of Z.

Note that neither W nor R is observable, only their minimum T,

$$T = \min(W, R). \tag{2}$$

We assume that W and R are independent, and it follows that $\mathbb{P}(T > t) = \mathbb{P}(R > t)\mathbb{P}(W > t)$ and the cumulative distribution function of T becomes

$$\begin{aligned} F_T(t) &= 1 - (1 - F_R(t))(1 - F_W(t)) \\ &= F_W(t) + F_Z(t-\theta)\mathbb{1}_{\{t>\theta\}}\left(1 - F_W(t)\right), \end{aligned} \tag{3}$$

where F_W denotes the distribution function of W. The nth moment of T can be calculated for any θ and F_Z (Tamborrino et al., 2012).

3

We have no experimental evidence about the distribution of R. A commonly applied model to describe spike data is the gamma distribution (Nawrot et al., 2008; Shimokawa et al., 2010), and we apply it to describe the relative response latency. Thus, $Z \sim \Gamma(\alpha, \beta)$, and therefore R follows a shifted gamma distribution, $R \sim \Gamma_{\text{sh}}(\theta, \alpha, \beta)$. The gamma distribution has probability density function

$$f_\Gamma(t) = \frac{1}{\alpha^\beta \Gamma(\beta)} t^{\beta-1} e^{-t/\alpha}, \qquad t > 0, \tag{4}$$

mean $\mathbb{E}[Z] = \alpha\beta$ and variance $\text{Var}(Z) = \alpha^2\beta$, implying $\mathbb{E}[R] = \theta + \alpha\beta$ and $\text{Var}(R) = \beta\alpha^2$. Here, $\alpha, \beta > 0$ denote the scale and shape parameters, respectively, and $\Gamma(\beta)$ denotes the gamma function. In particular, the exponential distribution $exp(\omega)$, can be obtained as a special case if $\beta = 1$ and $\alpha = 1/\omega$ in (4). Then ω reflects the firing frequency.

Another common model of ISIs is the output from the Perfect Integrate-and-Fire model, leading to an inverse Gaussian distribution (IG) for Z. The probability density function is given by (Chhikara and Folks, 1989; Ditlevsen and Lansky, 2005)

$$f_{IG}(t) = \sqrt{\frac{\beta}{2\pi t^3}} \exp\left\{-\frac{\beta(t-\alpha)^2}{2\alpha^2 t}\right\}, \qquad t > 0, \tag{5}$$

with $\alpha, \beta > 0$, mean $\mathbb{E}[Z] = \alpha$ and variance $\text{Var}(Z) = \alpha^3/\beta$, implying $\mathbb{E}[R] = \theta + \alpha$ and $\text{Var}(R) = \alpha^3/\beta$. Other distributions, like Weibull or log-normal, can also be employed.

1.2. Identifiability of ϕ

In general, the distribution of R is determined uniquely by ϕ. However, we can find $\phi_0 = (0, \alpha_0, \beta_0)$ and $\phi = (\theta, \alpha, \beta)$ such that the mean and variance are the same. In particular, if Z belongs to the gamma distribution family and we set

$$\alpha_0 = \frac{\alpha^2\beta}{\theta + \alpha\beta} < \alpha, \qquad \beta_0 = \frac{(\theta + \alpha\beta)^2}{\alpha^2\beta} > \beta, \tag{6}$$

then $\mathbb{E}_{\phi_0}[R] = \alpha_0\beta_0 = \theta + \alpha\beta = \mathbb{E}_\phi[R]$ and $\text{Var}_{\phi_0}(R) = \alpha_0^2\beta_0 = \alpha^2\beta = \text{Var}_\phi(R)$. The skewnesses are different though: skewness $(\phi_0) = 2/\sqrt{\beta_0} = 2\alpha\sqrt{\beta}/(\theta + \alpha\beta) < 2/\sqrt{\beta} = $ skewness (ϕ) if $\beta > 1$.

Likewise, if Z belongs to the IG distribution family and

$$\alpha_0 = \alpha + \theta > \alpha, \qquad \beta_0 = \left(1 + \frac{\theta}{\alpha}\right)^3 \beta > \beta, \tag{7}$$

then the mean and variance are equal, while the skewness are different. Indeed, skewness $(\phi_0) = 3\sqrt{\alpha_0/\beta_0} = 3[\alpha/(\theta + \alpha)]\sqrt{\alpha/\beta} < 3\sqrt{\alpha/\beta} = $ skewness (ϕ). Plugging ϕ_0 and ϕ into the expression for $\mathbb{E}[T^n]$ provided in Tamborrino et al. (2012), we obtain $\mathbb{E}_{\phi_0}[T] \approx \mathbb{E}_\phi[T]$ and $\text{Var}_{\phi_0}(T) \approx \text{Var}_\phi(T)$.

In general, for fixed $\mathbb{E}[R]$ and $\mathrm{Var}(R)$, we can express α and β as a function of θ by setting

$$\alpha = \frac{\mathrm{Var}(R)}{\mathbb{E}[R] - \theta}, \qquad \beta = \frac{(\mathbb{E}[R] - \theta)^2}{\mathrm{Var}(R)}, \tag{8}$$

if $Z \sim \Gamma(\alpha, \beta)$ and

$$\alpha = \mathbb{E}[R] - \theta, \qquad \beta = \frac{(\mathbb{E}[R] - \theta)^3}{\mathrm{Var}(R)}, \tag{9}$$

if $Z \sim IG(\alpha, \beta)$. Therefore, there exists an infinite number of possible sets of parameter values ϕ yielding the same mean and variance. Thus, if $\theta > 0$, it might be difficult to statistically distinguish between sets of parameter values, unless the sample size is large.

2. Parameter estimation

The aim of this paper is parameter estimation of the response latency from a sample $\{t_i\}_{i=1}^n$ of n independent observations of T given in (2), and $\{N_i\}_{i=1}^n$, the random variables counting the number of spontaneous spikes in the n trials in the time interval $[0, t_s]$, assuming that the distribution family of W and R are known. That is, we want to estimate $\phi = (\theta, \omega)$ if R follows an exponential distribution (possibly shifted), or $\phi = (\theta, \alpha, \beta)$ if R follows a gamma or IG distribution (possibly shifted), assuming to know whether $\theta = 0$ or $\theta > 0$. We will use the maximum likelihood estimator (MLE).

2.1. Maximum likelihood estimation of λ

The MLE of λ is (Tamborrino et al., 2012)

$$\hat{\lambda} = \frac{\sum_{i=1}^n N_i}{n t_s}. \tag{10}$$

By assumption, N_i follows a Poisson distribution with rate λt_s. It follows that $n t_s \hat{\lambda} = \sum_{i=1}^n N_i \sim Poisson(n\lambda t_s)$. Therefore,

$$\mathbb{E}[\hat{\lambda}] = \lambda, \qquad \mathrm{Var}(\hat{\lambda}) = \frac{\lambda}{n t_s}.$$

2.2. Maximum likelihood estimation of ϕ

Since $F_W(t) = 1 - e^{-\lambda t}$, it follows from (3) that the density of T is

$$f_T(t) = e^{-\lambda t} f_Z(t - \theta) \mathbb{1}_{\{t > \theta\}} + \lambda e^{-\lambda t} \left(1 - F_Z(t - \theta) \mathbb{1}_{\{t > \theta\}}\right). \tag{11}$$

The observations are independent and identically distributed, and therefore the log-likelihood function is given by

$$l_t(\phi) = -\lambda \sum_{i=1}^n t_i + \sum_{i=1}^n \log\left[f_Z(t_i - \theta)\mathbb{1}_{\{t_i > \theta\}} + \lambda(1 - F_Z(t_i - \theta)\mathbb{1}_{\{t_i > \theta\}})\right]. \tag{12}$$

5

The first term in (12) does not depend on ϕ and can be ignored. The likelihood function is not differentiable with respect to θ, which complicates the inference. Therefore, we maximize (12) directly to obtain an estimator of ϕ. If the evoked activity is exponentially distributed, this can be slightly improved, see below. Explicit solutions to the likelihood equations are only available if Z is exponentially distributed and $\theta = 0$. It is not possible to obtain explicit estimators if R is gamma or IG distributed, because of the corruption from the spontaneous activity, and therefore (12) is maximized numerically.

2.2.1. Exponentially distributed evoked activity and instantaneous response: $\theta = 0$

Assume $R \sim exp(\omega)$. From (1) and (3) follows $F_T(t) = 1 - e^{-(\omega+\lambda)t}$ so $T \sim exp(\lambda + \omega)$. Therefore, the MLE is given by

$$\widehat{(\omega + \lambda)} = \frac{1}{\bar{t}} \tag{13}$$

where $\bar{t}$ is the average of $\{t_i\}_{i=1}^n$. From (13), only the sum $\lambda + \omega$ can be estimated. Therefore, we estimate λ by (10) and

$$\hat{\omega} = \frac{1}{\bar{t}} - \hat{\lambda}. \tag{14}$$

In particular, the mean and variance of $\hat{\omega}$ are

$$\mathbb{E}[\hat{\omega}] = \frac{n}{n-1}\omega + \frac{\lambda}{n-1}, \qquad \mathrm{Var}(\hat{\omega}) = \frac{n^2}{(n-1)^2(n-2)}(\lambda+\omega)^2 + \frac{\lambda}{nt_s}, \tag{15}$$

as shown in Appendix A.

2.2.2. Exponentially distributed evoked activity and delayed response: $\theta > 0$

Assume $R \sim exp_{\mathrm{sh}}(\theta, \omega)$. The likelihood equation for ω is

$$0 = \sum_{i=1}^n \frac{1 - (\lambda+\omega)(t_i - \theta)}{\lambda + \omega} \mathbb{1}_{\{t_i > \theta\}}. \tag{16}$$

Also here only $\lambda + \omega$ is identifiable, and therefore we estimate λ by (10), and obtain $\hat{\omega}$ as the solution of (16) for fixed θ as

$$\widehat{\omega + \lambda} = \frac{\sum_{i=1}^n \mathbb{1}_{\{t_i > \theta\}}}{\sum_{i=1}^n (t_i - \theta)\mathbb{1}_{\{t_i > \theta\}}}, \qquad \hat{\omega} = \widehat{\omega + \lambda} - \hat{\lambda}.$$

The profile likelihood of θ, i.e. the likelihood function where ω has been profiled out by maximizing the likelihood over ω as a function of θ, becomes

$$l_t(\theta) \propto \sum_{i=1}^n \left(\hat{\lambda}(t_i - \theta) - 1 \right) \mathbb{1}_{\{t_i > \theta\}} + \sum_{i=1}^n \log(\hat{\omega}\mathbb{1}_{\{t_i > \theta\}} + \hat{\lambda}).$$

Since $l_t(\theta)$ is strictly increasing for $\theta \in (t_i, t_{i+1})$, for $i = 1, \ldots, n-1$, it follows that θ can be estimated as the time $t_i - \epsilon$ maximizing $l_t(\theta)$, for $\epsilon > 0$ small enough.
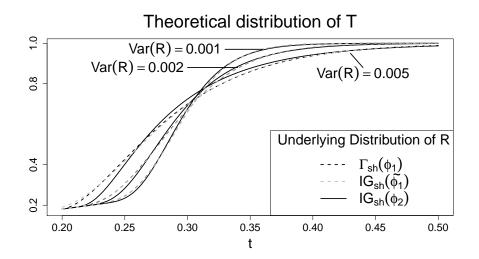
6

Figure 2: Theoretical distribution of T for underlying distributions R with different parameter values. Here, the three different sets of ϕ_1 and ϕ_2 values equal the sets of parameter values used in simulations if R is gamma or IG distributed, respectively, while $\tilde{\phi}_1$ is obtained from (17) such that mean, variance and skewness of the $\Gamma_{\mathrm{sh}}(\phi_1)$ and the $IG_{\mathrm{sh}}(\tilde{\phi}_1)$ distributions are equal. In particular: $R \sim \Gamma_{\mathrm{sh}}(\phi_1)$ (dashed lines), with $\phi_1 = (0.2, 0.05, 2)$ ($\mathrm{Var}(R) = 0.005$), $\phi_1 = (0.2, 0.2, 5)$ ($\mathrm{Var}(R) = 0.002$) or $\phi_1 = (0.2, 0.01, 10)$ ($\mathrm{Var}(R) = 0.001$); $R \sim IG_{\mathrm{sh}}(\tilde{\phi}_1)$ (dashed gray lines) and $R \sim IG_{\mathrm{sh}}(\phi_2)$ (full lines), with $\phi_2 = (0.2, 0.1, 0.2)$ ($\mathrm{Var}(R) = 0.005$), $\phi_2 = (0.2, 0.1, 0.5)$ ($\mathrm{Var}(R) = 0.002$) or $\phi_2 = (0.2, 0.1, 1)$ ($\mathrm{Var}(R) = 0.001$). Note that ϕ_1 and ϕ_2 satisfy (18), i.e. the delay θ, mean and variance of the $\Gamma_{\mathrm{sh}}(\phi_1)$ and the $IG_{\mathrm{sh}}(\phi_2)$ distributions are equal.
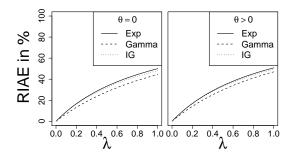

Figure 3: $R_{\mathrm{IAE}}(F_T)$ (in percentage) given by (20) if $W \sim exp(\lambda)$ for different values of λ, assuming instantaneous (left panel) or delayed (right panel) response. Distribution family of R: exponential (continuous line), gamma (dashed line) or IG (dotted line). Parameter values: $R \sim exp(1), R \sim \Gamma(1/2, 2), R \sim IG(1, 1)$ (left panel) and $\theta = 0.2, Z \sim exp(5/4), Z \sim \Gamma(2/5, 2), Z \sim IG(4/5, 1)$ (right panel). In all cases, $\mathbb{E}[R] = 1$s.

3. Model diagnostics

3.1. Model control

Denote $\hat{F}_T$ the parametric estimated cumulative distribution function of T obtained by plugging $\hat{\lambda}$ and $\hat{\phi}$ into (3). To check whether the data fits the statistical model, one could check whether $\hat{F}_T$ is close to the empirical cumulative distribution function $\sum_{i=1}^n \mathbb{1}_{\{t_i \leq t\}}/n$, e.g. by quantile-quantile plots.

3.2. Model selection

In general, the $\Gamma_{\mathrm{sh}}(\phi)$ and the $IG_{\mathrm{sh}}(\phi')$ distributions are different for any ϕ and ϕ', but it might still be difficult to statistically distinguish which of the two distributions have generated a given sample. Indeed, we can find $\phi = (\theta, \alpha, \beta)$ and $\phi' = (\theta', \alpha', \beta')$ such that the mean, variance and skewness of the $\Gamma_{\mathrm{sh}}(\phi)$ and the $IG_{\mathrm{sh}}(\phi')$ distributions are equal. If we choose

$$\theta' = \theta - \frac{1}{2}\alpha\beta, \qquad \alpha' = \frac{3}{2}\alpha\beta, \qquad \beta' = \left(\frac{3}{2}\right)^3 \alpha\beta^2, \tag{17}$$

the first three moments are equal. Finally, we can find two sets of parameters ϕ and ϕ' such that $\theta = \theta'$ and the mean and variance of the two distributions are the same, though the skewness are different, choosing

$$\alpha' = \alpha\beta, \qquad \beta' = \alpha\beta^2. \tag{18}$$

With this parameter choice, the $\Gamma_{\mathrm{sh}}(\phi)$ and the $IG_{\mathrm{sh}}(\phi')$ distributions are close, as well as the corresponding distributions of T. This can be observed in Fig. 2, where we show the theoretical distribution of T, if R is gamma or IG distributed, with parameter values satisfying (17) or (18). Thus, to statistically distinguish between two distribution families of R from the observations of T, the sample size has to be very large.

4. Error if spontaneous activity is ignored

To measure the error in the estimation of F_R, we consider the relative integrated absolute error (R_{IAE}) defined as

$$R_{\mathrm{IAE}}(\hat{F}_R) = \frac{\int_0^\infty |\hat{F}_R(t) - F_R(t)|dt}{\mathbb{E}[R]}. \tag{19}$$

Let R belong to any shifted distribution family. If we ignore the presence of spontaneous activity and estimate $F_R(t)$ by $F_T(t)$, then

$$R_{\mathrm{IAE}}(F_T) = 1 - \frac{\mathbb{E}[T]}{\mathbb{E}[R]}, \tag{20}$$

see Appendix B. Since $\mathbb{E}[T] \leq \mathbb{E}[R]$ with equality if and only if there is no spontaneous activity present, this error is zero only in this ideal case. In

particular, the error increases with λ, as shown in Fig. 3. Therefore, ignoring the presence of spontaneous activity introduces a considerable error.

In Table 1 we report the $R_{\text{IAE}}(F_T)$ when the parameters go to zero while keeping the other parameters fixed under the assumption that R belongs to any of the considered shifted distributions. When $\lambda \to \infty$ or $\alpha \to \infty$ for any distribution family, then $R_{\text{IAE}}(F_T) \to 1$. This also holds when $\beta \to \infty$ and $R \sim \Gamma_{\text{sh}}(\theta, \alpha, \beta)$. If $R \sim IG_{\text{sh}}(\theta, \alpha, \beta)$ and $\beta \to \infty$, then $R_{\text{IAE}}(F_T) \to 1 - [1 - e^{-\lambda(\alpha+\theta)}]/[\lambda(\alpha + \theta)]$. Note that some of these errors do not go to zero even when $\mathbb{E}[R] \to 0$, implying that the spontaneous activity always plays an important role and should not be ignored.

5. Simulation study

5.1. Set up

We simulated a spontaneous spike train following a Poisson process with firing rate $\lambda = 1s^{-1}$ for a time period up to the first spike after $10s$, and thus $\mathbb{E}[W] = 1s$. At time $t_s = 10s$, the evoked activity was simulated in seven different settings, either by shifted exponentially ($\omega = 10s^{-1}$), gamma ($(\alpha, \beta) = (0.05, 2), (0.02, 5), (0.01, 10)$) or IG ($(\alpha, \beta) = (0.1, 0.2), (0.1, 0.5),$ $(0.1, 1)$) distributed random variables R with θ between 0 and 0.3 in steps of 0.05. Thus, $\mathbb{E}[Z] = 0.1$s and $\text{Var}(Z) = 0.001, 0.002, 0.005$s^2 in the three settings for either gamma or IG distributions and $\text{Var}(Z) = 0.01$s^2 for the exponential case. Then, we obtained a realization of T using (2). This was repeated to obtain samples of size n, where n varied between 20 and 100, and each sample was repeated for different values of θ. Finally, for each set of values of n, θ, α and β, we repeated this procedure 1000 times, obtaining 1000

$\theta = 0$	$\alpha \to 0$	$\beta \to 0$
$R \sim \Gamma(\alpha, \beta)$	0	$1 - \dfrac{\ln(1 + \alpha\lambda)}{\alpha\lambda}$
$R \sim IG(\alpha, \beta)$	0	1

$\theta > 0$	$\alpha \to 0$	$\beta \to 0$
$R \sim \Gamma_{\text{sh}}(\theta, \alpha, \beta)$	$1 - \dfrac{\left(1 - e^{-\lambda\theta}\right)}{\lambda\theta}$	$1 - \dfrac{\left(1 - e^{-\lambda\theta}\right)}{\lambda\theta}$
$R \sim IG_{\text{sh}}(\theta, \alpha, \beta)$	$1 - \dfrac{\left(1 - e^{-\lambda\theta}\right)}{\lambda\theta}$	$1 - \dfrac{\left(1 - e^{-\lambda\theta}\right)}{\lambda(\theta + \alpha)}$

Table 1: $R_{\text{IAE}}(F_T)$ when α or β go to zero keeping the other parameters fixed, assuming $R \sim \Gamma_{\text{sh}}(\theta, \alpha, \beta)$ or $R \sim IG_{\text{sh}}(\theta, \alpha, \beta)$. When $\lambda \to 0$, i.e. $\mathbb{E}[W] \to \infty$, the $R_{\text{IAE}}(F_T) \to 0$, since the spontaneous activity becomes negligible. The exponential case can be obtained from $R \sim \Gamma_{sh}(\theta, \alpha, \beta)$ by setting $\omega = 1/\alpha$ and $\beta = 1$.

9

statistically indistinguishable and independent trials. For the considered sets of parameters and fixed θ, the mean and variance of the distribution of R for gamma and IG are equal, as follows from (18).

We use boxplots to compare the performance of the MLEs of ϕ and $\mathbb{E}[R]$ for different F_R, n and ϕ. The boxes contain the estimates between the $1st$ and the $3rd$ quartiles, while the $2nd$ quartile, i.e. the median of the estimates, is marked with the black horizontal line. The bars show the range of the estimates, except the outliers, defined to be the points outside the bars that are more than 1.5 times the interquartile range from the box. Only results for the exponential and the gamma cases are shown in the boxplots, since results from the IG case are similar to the gamma case. To evaluate the percentage of $\hat{\theta}$ underestimating θ more than 20%, we consider the relative error defined by

$$E_{\mathrm{rel}}(\hat{\theta}) = \frac{\hat{\theta} - \theta}{\theta}.$$

5.2. Instantaneous response: $\theta = 0$

In Fig. 4 are reported the boxplots of $\hat{\phi}$ if R is exponentially or gamma distributed for different values of n and ϕ. As expected, the MLE performs better when n increases.

If $R \sim exp(\omega)$, ω is well estimated, as anticipated from the theoretical mean and variance of $\hat{\omega}$ given by (15). In the other cases, the scale parameter α is estimated better than the shape parameter β. As expected, for fixed α, the performance of the estimator $\hat{\alpha}$ improves when β increases, i.e. when the variance decreases.

Single parameters might be difficult to estimate, whereas means are often easier to estimate. In Fig. 5 we report the boxplots of $\widehat{\mathbb{E}[R]}$ and the $R_{\mathrm{IAE}}(\hat{F}_R)$. As expected, the performance of the estimators of $\mathbb{E}[R]$ and F_R improves when the variance of R decreases. For fixed mean and variance, the estimation of $\mathbb{E}[R]$ and F_R is similar for different distribution families, as also observed in Fig. 2 and argued in Section 3.2. Note that $\widehat{\mathbb{E}[R]}$ has no bias and performs much better than the estimators of the single parameters, even for a sample size as small as $n = 20$. To conclude, different distribution families for R provides similar R_{IAE} and good estimates of the mean of the response latency, even for small sample sizes. For the estimation of ϕ, a larger sample size is needed.

5.3. Delayed response: $\theta > 0$

The boxplots of ϕ if R is shifted exponentially or gamma distributed for $n = 100$ and different values of ϕ are reported in Fig. 6. As expected, all estimators improve as n increases (results not shown).

In all cases, the absolute response latency θ is estimated better than the parameters of the relative response latency Z. Inference about the delay θ, and consequently of ϕ, becomes more difficult when β increases. It might be counterintuitive that the estimator deteriorates for decreasing variance of R, but can be explained as follows. If the probability of small values of Z is small, the
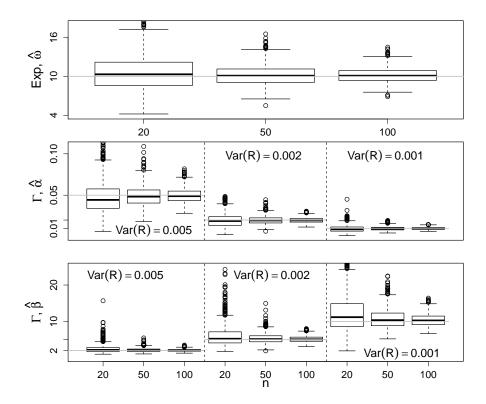
Figure 4: Boxplots of estimated ϕ (1000 estimates) for different number of observations and parameter values ϕ if W is exponential with rate $\lambda = 1\mathrm{s}^{-1}$ and the absolute response latency is null. Top panel: estimates of ω, R is exponential with rate $\omega = 10\mathrm{s}^{-1}$. Central panel: estimates of α. Bottom panel: estimates of β. R is gamma with $(\alpha, \beta) = (0.05, 2), (0.02, 5)$, or $(0.01, 10)$ and thus $\mathrm{Var}(R) = 0.005, 0.002$, or $0.001\mathrm{s}^2$. In all cases, $\mathbb{E}[R] = 0.1\mathrm{s}$. Gray lines are true values used in the simulations. For graphical reasons we do not report some large estimates of ω (1.6%), of α (less than 1%) and of β (less than 4.6%), all for $n = 20$.
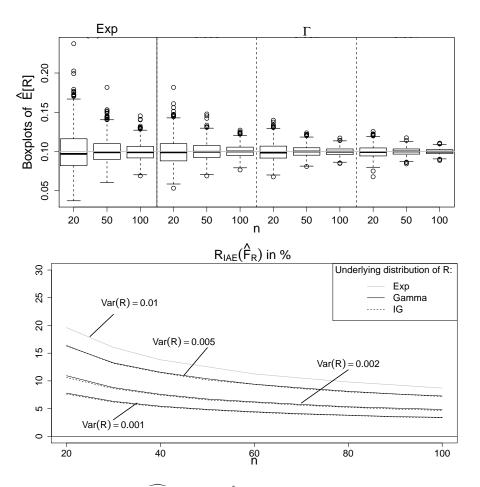
11

Figure 5: Dependence of $\widehat{\mathbb{E}[R]}$ and $R_{\mathrm{IAE}}(\hat{F}_R)$ on the number of observations and on the parameter ϕ if W is exponential with rate $\lambda = 1\mathrm{s}^{-1}$ and the absolute response latency is null. Top figure: boxplots of estimated $\mathbb{E}[R]$ (1000 estimates) with $\mathbb{E}[R] = 0.1\mathrm{s}$; $\mathrm{Var}(R) = 0.01\mathrm{s}^2$ if $R \sim exp(10)$, $\mathrm{Var}(R) = 0.005\mathrm{s}^2$ if $R \sim \Gamma(0.05, 2)$; $\mathrm{Var}(R) = 0.002\mathrm{s}^2$ if $R \sim \Gamma(0.02, 5)$ and $\mathrm{Var}(R) = 0.001\mathrm{s}^2$ if $R \sim \Gamma(0.01, 10)$. Gray line is true value used in the simulations. Bottom figure: $R_{\mathrm{IAE}}(\hat{F}_R)$ (average over 10,000 simulations) if R is exponentially (full gray line), Gamma (full lines) or IG (dashed lines) distributed, with variance of R decreasing from the top to the bottom lines.
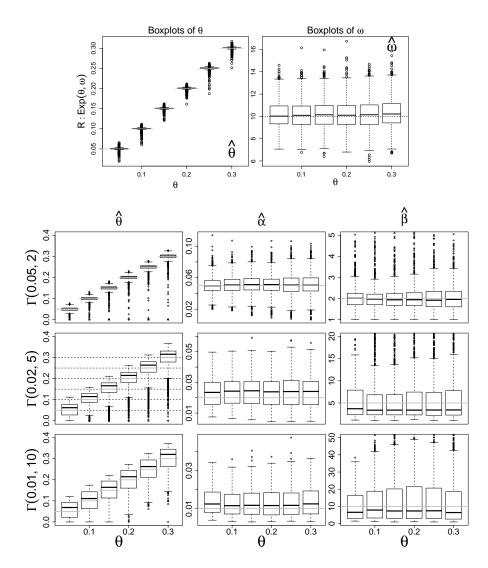
12

Figure 6: Boxplots of estimated ϕ (1000 estimates) for $n = 100$ and different values θ if W is exponential with rate $\lambda = 1\mathrm{s}^{-1}$ and the absolute response latency is not null: $\theta > 0$. Top figure: Z is exponential with rate $\omega = 10\mathrm{s}^{-1}$. Bottom figure: Z is gamma with $(\alpha, \beta) = (0.05, 2), (0.02, 5)$, or $(0.01, 10)$ and thus $\mathrm{Var}(Z) = 0.005, 0.002$, or $0.001\mathrm{s}^2$. Gray lines are true values used in the simulations. For graphical reasons we do not report some large estimates of α (less than 0.7%) and of β (less than 11.3%).
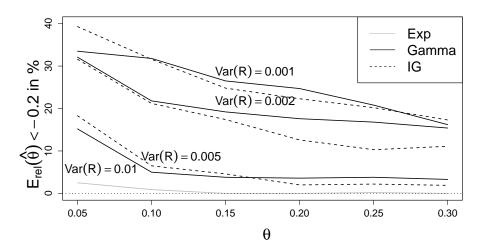
13

Figure 7: Percentage of samples where the estimated θ are underestimated with a relative error larger than 20% if W is exponential with rate $\lambda = 1\text{s}^{-1}$ and $n = 100$. The following cases are considered: Z is exponential with $\text{Var}(R) = 0.01\text{s}^2$ (grey full line), Γ with $\text{Var}(R) = 0.005\text{s}^2$ (bottom full line), 0.002s^2 (central full line), 0.001s^2 (top full line) and IG with $\text{Var}(R) = 0.005\text{s}^2$ (bottom dashed line), 0.002s^2 (central dashed line) and 0.001s^2 (top dashed line).

distribution of R is more peaked away from θ, and it is difficult to statistically distinguish between absolute and relative latency.

To understand the presence of outliers in the estimation of ϕ, the percentage of estimated θ that are underestimated with a relative error larger than 20% is plotted in Fig. 7. The percentage increases when β increases and decreases when θ increases. Most of these outliers underestimate θ (see Fig. 6). This can also be seen from the dependence of α and β on θ, assuming that $\mathbb{E}[R]$ and $\text{Var}(R)$ are correctly estimated, as shown in (8) and (9). Figure 8 shows scatterplots of $(\hat{\theta}, \hat{\alpha})$ and $(\hat{\theta}, \hat{\beta})$ if $\theta = 0.3\text{s}$, illustrating that the estimators are not independent. It is clear that mean and variance of R are well estimated, even if the single parameters are not. Results are similar for other values of θ (figures not shown). If $\hat{\theta} \approx 0$, then $\hat{\alpha} \ll \alpha$ and $\hat{\beta} \gg \beta$ for the gamma case and $\hat{\alpha} \gg \alpha$ and $\hat{\beta} \gg \beta$ for the IG case. This happens because $\hat{\alpha}$ and $\hat{\beta}$ are estimated as α_0 and β_0, respectively, as follows from (6) and (7).

Figure 9 shows boxplots of $\widehat{\mathbb{E}[R]}$ and the $R_{\text{IAE}}(\hat{F}_R)$ for different θ. As expected from Section 1.2, the mean of R is always well estimated, being $\widehat{\mathbb{E}[R]}$ unbiased and with a small variance. Furthermore, for fixed mean, it performs better when β increases and thus $\text{Var}(R)$ decreases. For the same reason, $R_{\text{IAE}}(\hat{F}_R)$ decreases when β increases. Moreover, the performance of $\hat{F}_R$ improves when θ increases and no significant differences are observed between the gamma and IG cases.

To conclude, the MLE can be used to estimate well the mean of the response latency, its distribution and reasonably well the absolute response latency θ. The estimation of the single parameters of Z is reliable only if n is large, as
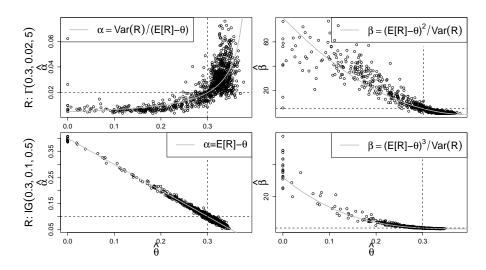
14

Figure 8: Plots of $(\hat{\theta}, \hat{\alpha})$ and $(\hat{\theta}, \hat{\beta})$ if W is exponential with rate $\lambda = 1\mathrm{s}^{-1}$, $n = 100$ and delay $\theta = 0.3\mathrm{s}$. Top panels: Z is gamma with $\alpha = 0.02\mathrm{s}$, $\beta = 5$. Bottom panels: Z is IG with $\alpha = 0.1\mathrm{s}$ and $\beta = 0.5$. In both cases, $\mathbb{E}[R] = 0.1\mathrm{s}$ and $\mathrm{Var}(R) = 0.002\mathrm{s}^2$. The gray lines are given in (8) and (9) and are obtained such that, for each estimate $\hat{\theta}$, the estimated mean and variance of R are equal to the true values.

observed in Fig. 10, where the boxplots of $\hat{\phi}$ are reported for $n = 100, 500$ and 1000. Thus, numerical simulations suggest that the MLE of ϕ is asymptotically unbiased.

6. Conclusion

If there is no spontaneous activity corrupting the response to the stimulus, i.e. R is directly observable, parameter estimation in models (4) or (5) is reasonably solved, also in presence of absolute latency (Hampel and Lansky, 2008). In the model we consider, statistical inference is complicated by the presence of spontaneous activity. If the absolute response latency θ is null, non-parametric and semi-parametric estimators for $F_R(t)$ were developed in Pawlas et al. (2010). Here we consider parametric estimators. The mean of the response latency can be well estimated even for small sample sizes. For the estimation of the single parameters, larger sample sizes are needed.

Even in absence of spontaneous activity, there is no experimental evidence about the distribution of the response latency. Therefore it can be discussed if it is realistic to assume F_R known. First, model diagnostics could be performed to evaluate the data fit. Second, mean and variance of the response latency, as well as its cumulative distribution function, can be well estimated even assuming a wrong distribution family for R. However, a right choice of F_R can guarantee a reasonable estimation of θ for a sample size if $n = 100$.
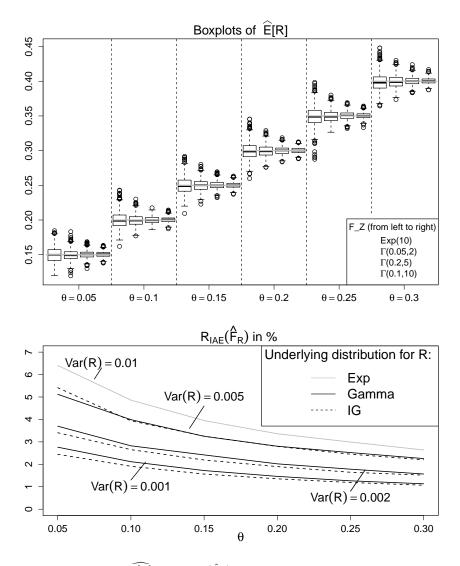
15

Figure 9: Dependence of $\widehat{\mathbb{E}[R]}$ and $R_{\mathrm{IAE}}(\hat{F}_R)$ on the absolute response latency θ if W is exponential with rate $\lambda = 1\mathrm{s}^{-1}$ and $n = 100$. Top figure: boxplots of $\widehat{\mathbb{E}[R]}$ (1000 estimates) with $\mathbb{E}[Z] = 0.1\mathrm{s}$. For each θ, the underlying distributions are: $Z \sim exp(10)$ (1st boxplots from the left) and $Z \sim \Gamma(0.05, 2), \Gamma(0.02, 5)$, and $\Gamma(0.1, 10)$ (2nd, 3rd and 4th boxplots from the left respectively). Gray lines are true values used in the simulations. Bottom figure: $R_{\mathrm{IAE}}(\hat{F}_R)$ (average over 1000 simulations) if R is exponentially (full gray line), Gamma (full lines) and IG (dashed lines) distributed, with variance of R decreasing from the top to the bottom lines.
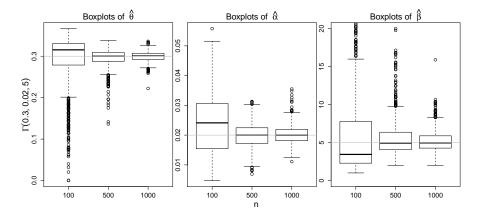
16

Figure 10: Dependence of $\hat{\phi}$ on the number of observations if W is exponential with rate $\lambda = 1\text{s}^{-1}$ and Z is gamma with $\theta = 0.3\text{s}, \alpha = 0.01\text{s}$ and $\beta = 10$ and thus $\mathbb{E}[R] = 0.4\text{s}$. Gray lines are true values used in the simulations. For graphical reasons we do not report some large estimates of β (less than 11.4%), all for $n = 100$.

Theoretical results and numerical simulations emphasize the difficulty in the estimation of the single parameters, especially α and β, unless $\theta = 0$ or the sample size is very large. An improvement in the estimation of ϕ might be obtained considering not only the first spike following the stimulus onset, but the entire spike train. A method to distinguish the evoked from the spontaneous spikes should then be provided.

Acknowledgments

References

References

Chhikara, R.S., Folks, J.L., 1989. The inverse Gaussian distribution: theory, methodology, and applications. Marcel Dekker, New York.

Ditlevsen, S., Lansky, P., 2005. Estimation of the input parameters in the Ornstein-Uhlenbeck neuronal model. Physical Review E 71, 011907.

Gerstner, W., Kistler, W.M., 2002. Spiking Neuron Models. Cambridge University Press.

Gremiaux, A., Nowotny, T., Martinez, D., Lucas, P., Rospars, J., 2012. Modelling the signal delivered by a population of first-order neurons in a moth olfactory system. Brain Research 1434, 123–135.

Hampel, D., Lansky, P., 2008. On the estimation of refractory period. J. Neurosci. Meth. 171, 288–295.

Lin, F.G., Liu, R.C., 2010. Subset of thin spike cortical neurons preserve the peripheral encoding of stimulus onsets. J. Neurophysiol. 104, 3588–3599.

Nawrot, M.P., Boucsein, C., Molina, V.R., Riehle, A., Aertsen, A., Rotter, S., 2008. Measurement of variability dynamics in cortical spike trains. J. Neurosci. Meth. 169, 374–390.

Neubauer, H., Heil, P., 2008. A physiological model for the stimulus dependence of first-spike latency of auditory-nerve fibers. Brain research 1220, 208–223.

Oran, Z., Shackleton, T., Nelken, I., Palmer, A., Shamir, M., 2011. First spike latency code for interaural phase difference discrimination in the guinea pig inferior colliculus. J. Neurosci. 31, 9192–9204.

Pawlas, Z., Klebanov, L.B., Beneš, V., Prokešová, M., Popelář, J., Lánský, P., 2010. First-spike latency in the presence of spontaneous activity. Neural Computation 22, 1675–1697.

Shimokawa, T., Koyama, S., Shinomoto, S., 2010. A characterization of the time-rescaled gamma process as a model for spike trains. J. Comput. Neurosci. 29, 183–191.

Tamborrino, M., Ditlevsen, S., Lansky, P., 2012. Investigation of noisy response latency. Physical Review E 86, 021128.

Tuckwell, H.C., 1988. Introduction to Theoretical Neurobiology, Vol.2: Nonlinear and Stochastic Theories. Cambridge Univ. Press, Cambridge.

Uzuntarla, M., Ozer, M., Guo, D., 2012. Controlling the first-spike latency response of a single neuron via unreliable synaptic transmission. Eur. Phys. J. B 85, 282.

Wainrib, G., Thieullen, M., Pakdaman, K., 2010. Intrinsic variability of latency to first-spike. Biol. Cybern. 103, 43–56.

Appendix A. Mean and variance of $\hat{\omega}$ if $\theta = 0$

Let $\bar{T}$ be the random variable defined by $\bar{T} = \sum_{i=1}^{n} T_i/n$. If $W \sim exp(\lambda)$ and $R \sim exp(\omega)$ then $T_i \sim exp(\lambda + \omega)$ and $T_i/n \sim exp(n(\omega + \lambda))$, while $\bar{T}$ is gamma distributed with parameters $\alpha = 1/n(\lambda + \omega)$ and $\beta = n$. Therefore, the probability density function of T is given by

$$f_{\bar{T}}(t) = \frac{[n(\lambda + \omega)]^n e^{-n(\lambda+\omega)y} y^{n-1}}{(n-1)!} dy,$$

18

with mean and variance given by

$$\mathbb{E}[\bar{T}] = \frac{1}{\lambda + \omega} \qquad Var(\bar{T}) = \frac{1}{n(\lambda + \omega)^2}.$$

Then,

$$
\begin{aligned}
\mathbb{E}[\frac{1}{\bar{T}}] &= \int_0^\infty \frac{1}{y} f_{\bar{T}}(y) dy \\
&= \int_0^\infty \frac{[n(\lambda + \omega)]^n e^{-n(\lambda + \omega)y} y^{n-2}}{(n-1)!} dy \\
&= \frac{n(\lambda + \omega)}{n-1}
\end{aligned}
$$

and the mean of $\hat{\omega}$ follows by (13), noting that $\mathbb{E}[\hat{\lambda}] = \lambda$.

Similarly,

$$
\begin{aligned}
\mathbb{E}[\frac{1}{\bar{T}^2}] &= \int_0^\infty \frac{[n(\lambda + \omega)]^n e^{-n(\lambda + \omega)y} y^{n-3}}{(n-1)!} dy \\
&= \frac{n^2(\lambda + \omega)^2}{(n-1)(n-2)}.
\end{aligned}
$$

Since the spontaneous activity follows a renewal Poisson process, $1/\bar{T}$ and $\hat{\lambda}$ are independent, due to the memoryless property of the exponential distribution. Therefore,

$$
\begin{aligned}
\text{Var}(\hat{\omega}) &= \text{Var}(\frac{1}{\bar{T}}) + \text{Var}(\hat{\lambda}) \\
&= \frac{n^2(\lambda + \omega)^2}{(n-1)(n-2)} - \frac{n^2(\lambda + \omega)^2}{(n-1)^2} + \frac{\lambda}{nt_s},
\end{aligned}
$$

and (15) follows.

Appendix B. RIAE

Let R belong to a shifted distribution family with the restriction that $t(1 - F_R(t)) \to 0$ when $t \to \infty$. A sufficient condition is that the variance of R is finite, and is thus fulfilled for the gamma and IG distributions. To calculate

$R_{\text{IAE}}(F_T)$, we estimate F_R by F_T given by (3) and obtain

$$
\begin{aligned}
R_{\text{IAE}}(F_T) &= \int_0^\infty \frac{|F_W(1 - F_R(t))|}{\mathbb{E}[R]} dt \\
&= \frac{1}{\mathbb{E}[R]} \int_0^\infty (1 - e^{-\lambda t})(1 - F_Z(t - \theta)\mathbb{1}_{\{t > \theta\}})dt \\
&= \frac{1}{\mathbb{E}[R]} \left[\int_0^\theta (1 - e^{-\lambda t})dt + \int_\theta^\infty (1 - e^{-\lambda t})(1 - F_Z(t - \theta))dt \right] \\
&= \frac{1}{\mathbb{E}[R]} \left[\theta + \frac{1}{\lambda}e^{-\lambda\theta} - \frac{1}{\lambda} + \int_0^\infty (1 - e^{-\lambda(u+\theta)})(1 - F_Z(u))du \right] \\
&= \frac{1}{\mathbb{E}[R]} \left\{ \theta + \frac{1}{\lambda}e^{-\lambda\theta} - \frac{1}{\lambda} + \left[(u + \frac{1}{\lambda}e^{-\lambda(u+\theta)})(1 - F_Z(u)) \right]_0^\infty \right. \\
&\quad + \left. \int_0^\infty u f_Z(u)du + \frac{1}{\lambda}e^{-\lambda\theta} \int_0^\infty e^{-\lambda u} f_Z(u)du \right\} \\
&= 1 - \frac{\mathbb{E}[W]}{\mathbb{E}[R]} \left(1 - e^{-\lambda\theta} M_Z(-\lambda) \right),
\end{aligned}
$$

where integration by parts has been used and $M_Z(s)$ denotes the moment generating function of Z, i.e. $M_Z(s) = \mathbb{E}[e^{sZ}] = \int_0^\infty e^{st} f_Z(t)dt$. Finally, (20) follows from the theoretical mean of T, $\mathbb{E}[T] = \mathbb{E}[W]\left(1 - e^{-\lambda\theta} M_Z(-\lambda)\right)$, see Tamborrino et al. (2012).